ISSN 0911-5730
UVSOR-19
March 1992

UVSOR
ACTIVITY REPORT
1991

Ultraviolet Synchrotron Orbital Radiation Facility
Institute for Molecular Science

CONTENTS

APPENDIX

Preface

It is a great pleasure for me to publish the 1991 UVSOR Activity Report which presents a number of recent synchrotron radiation studies carried out with our UVSOR Facility as well as the recent situation of the Facility.

During the last year, in the UVSOR ring we have installed a new computer control system to control the operation of our storage ring, and carried out various testing experiments controlling the bunch length. We have also remodelled our conventional transverse undulator into an optical klystron, with which FEL (free electron laser) gain measurements have been successfully carried out.

Our UVSOR synchrotron radiation source has been regularly operated with an electron energy of 750 MeV and at an initial ring current of 200 mA. The nine well-established beam lines (BL1B, BL2B1, BL3A1, BL3A2, BL6A1, BL7A, BL7B, BL8A, and BL8B1) have been provided for general users. On the other hand, the eight beam lines (BL1A, BL2A, BL2B2, BL3B, BL4A, BL4B, and BL6B) have been used by the in-house groups. Another beam line (BL5B) which belongs to the National Institute for Fusion Science has been used for calibration.

The various joint programs operating at UVSOR throughout in the 1991 fiscal year can be classified as followed; 3 Special-Project Programs, 27 Cooperative-Research Programs, and 114 Use-of-Facility Programs. Furthermore, two synchrotron radiation symposia were held at this Institute; One was a users' meeting, and the other was a workshop on synchrotron light sources.

I would like to express my thanks to all the UVSOR staff for their great efforts and contributions to the UVSOR Facility and its activity. I would also like to thank all the users for their kind cooperation.

February 1992

Katsumi Kimura
Professor
Director of UVSOR

LIGHT SOURCE & BEAMLINES

Control of bunch length of the UVSOR storage ring

Hiroyuki HAMA, Shiro TAKANO and Goro ISOYAMA
UVSOR Facility, Institute for Molecular Science, 38 Myodaiji, Okazaki 444

An extremely short bunched beam realized in an electron storage ring would give various advantages to experimental studies with synchrotron radiation. The short bunched beam extends a region of study in time-resolved experiments, and gain of a free electron laser on a storage ring increases due to a high peak current in such a beam. Moreover, emission of coherent synchrotron radiation[1], which has not been reported on storage rings[2,3], would be hopefully detected. We have conducted an experiment to control bunch length by means of changing the momentum compaction factor α on the UVSOR storage ring at an electron energy of 600 MeV. The storage ring has been regularly operated at an operating point of Q_x=3.16 and Q_y=2.64 with α=0.035, where the natural bunch length is approximately 260 ps (2σ) at the energy of 600 MeV[4]. The bunch length is proportional to the square root of α, which can be varied by changing the dispersion function because it is proportional to an integral of the dispersion function in bending magnets. The UVSOR ring has the magnet lattice called as the double bend achromat. It is possible to vary the dispersion function while the horizontal and vertical betatron wave numbers are maintained at constant values. We can make the dispersion function negative in a part of a bending magnet such that α is reduced due to cancellation in the integral.

Relying on a model calculation with a computer program for linear lattice calculation, we carried out the experiment. Prior to the experiment, magnet parameters of the model were adjusted to reproduce the measured α and the betatron numbers at the injection point. According to the calculation, the momentum compaction factor can be varied as the dispersion function at the center of long straight section η^{cal}_{Lss} is changed. At the regular operating point, η^{cal}_{Lss} is estimated to be approximately +0.38 m. As η^{cal}_{Lss} become smaller, α decreases and becomes zero at η^{cal}_{Lss}=-0.825 m, which is the unstable point for the synchrotron oscillation. The beam was injected at η^{cal}_{Lss}=+0.3 m throughout the experiment, which is close to the regular operating point. The storage ring was operated in a single bunch operation in order to avoid any effects from coupled bunch

instability. After the injection, excitation currents of the quadrupole magnets were changed synchronousely to reduce α using the same procedure for beam accelaration, which is supported by a computer control system.

We measured the following three diffrerent parameters relevant to the bunch length and the momentum compaction factor. (1)Bunch length was measured by the single photon counting method using a photomultiplier consisted of micro-channel plates. Time spectra of synchrotron radiation emitted from a bending magnet were obtained with the standard technique using a time-to-amplitude converter and a pulse height analyzer. (2)A signal from a pickup electrode was processed by a spectrum analyzer, and the synchrotron oscillation frequency f_s was measured. Even at a small beam current, a collective synchrotron oscillation due to instability was observed as sidebands of the RF frequency signal in the frequency spectrum, though the intensity was very weak. (3)Horizontal beam displacement Δx of the beam was measured as a function of the RF frequency. Then α was obtained using a relation $\Delta x=\eta(\Delta p/p)=\eta\alpha^{-1}(-\Delta f/f)$, where η is the value of dispersion function at the position monitors and $\Delta p/p$ and $\Delta f/f$ are relative deviations of the momentum and the RF frequency from central values.

As shown in fig. 1, we successfully controlled the bunch length from 300 ps down to approximately 40 ps (twice the standard deviation). The bunch length estimated from f_s was in good agreement with the bunch length measured directly, and both of them were in agreement with the model calculation. We, however, observed a strong nonlinear dependence of Δx and also f_s on the RF frequency in the low α region. Such nonlinearity is considered to be due to an effect of second order term of $\Delta p/p$ in α, which probably originated from different focusing forces of Q-magnets given to off-momentum particles. Taking into account the second order term, we analyzed the data using relations $\Delta l/l=\alpha_1(\Delta p/p)+\alpha_2(\Delta p/p)^2$. We obtained the value of $\alpha_2=-0.15$ at the operating point with $\eta^{cal}_{Lss}=-0.8$ m, while an estimated value by the calculation was +0.52. This discrepancy can be explained by taking account of an effect of the sextupole magnetic field on the nonlinearity. In the experiment, the natural chromaticities were compensated with the sextupole magnets, but the second order term was probably overcorrected. Actually we could supress the nonlinearity by reducing the magnetic field of the focusing sextupoles.

Figure 2 shows the experimental results of α and calculated values, which are in

good agreement. By suppressing the second order term, we obtained he lowest α of 0.00025 from the measurement of f_s so far, which corresponds to the bunch length of 25 ps.

References

1) F. C. Michel, Phys. Rev. Lett. 48 (1982) 580.

2) J. Yarwood et al., Nature 312 (1984) 742.

3) G. P. Williams et al., Phys. Rev. Lett. 62 (1989) 261.

4) A. Lin et al., to be published in Jpn. J. Appl. Phys.

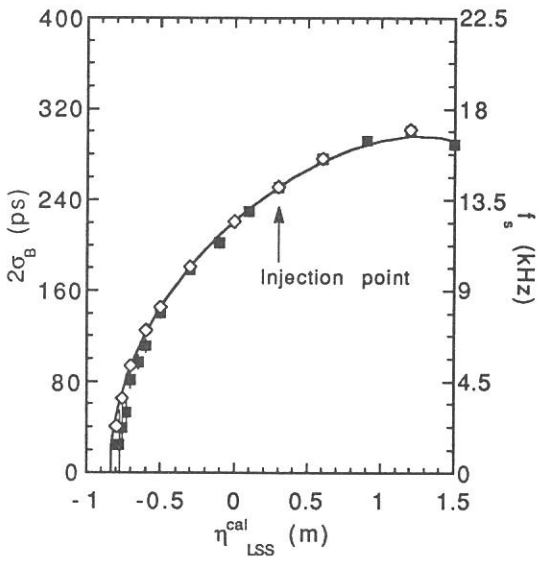

Fig. 1. Measured bunch lengths and synchrotron oscillation frequencies of several operating points, which are denoted by squares and diamonds. The right-han axis for f_s is normalized to be visible as same magnitude of bunch length. Theoretical bunch length is indicated by the line.

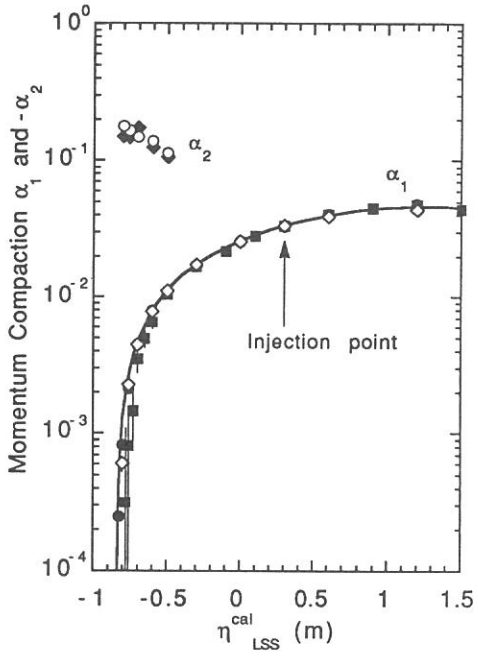

Fig. 2. Experimental result of momentum compaction factors. Values deduced from the data of bunch lengths are denoted by squares. Solid and open circles denote α_1 and α_2 deduced from the data of displacements. Diamonds represent those but from the data of synchrotron oscillation frequencies.

Free Electron Laser Experiment with an Optical Klystron on the UVSOR Storage Ring

Shiro TAKANO, Hiroyuki HAMA and Goro ISOYAMA

UVSOR Facility, Institute for Molecular Science,

Myodaiji, Okazaki 444

An experimental study of a free electron laser (FEL) in the visible region is in progress on the UVSOR storage ring. The present goal is to achieve lasing at a wavelength around 488 nm with the electron energy of 500 MeV. As the initial step of the project, an FEL gain was measured with a transverse undulator of nineteen periods with the period length of 11.1 cm made of permanent magnet.[1] The measured peak gain was 8×10^{-4} at the stored beam current of 10 mA/bunch, which was in good agreement with the theoretical calculation. It was concluded that the UVSOR storage ring had sufficient performance relevant to the FEL project.

In order to obtain an FEL gain as high as possible within the limitation imposed by length of a long straight section where the undulator was installed, we have remodeled the undulator to an optical klystron (OK).[2] The central three periods of the undulator have been removed and replaced by a three pole wiggler. The OK consists of two identical undulator sections of eight periods, called as an energy modulator and a radiator, respectively, separated by a dispersive section of 37 cm long, called as a buncher. The parameter N_d of the dispersive section, which is the number of optical wavelengths (488 nm) passing over electrons in the

dispersive section, can be changed in the range from 60 to 85 when the magnet gap of the dispersive section is varied.

The vertical magnetic field along the longitudinal axis of the OK is measured with a Hall probe. Figure 1 shows the measured magnetic field and the calculated electron trajectory in the horizontal plane. The magnetic field imperfection originating from magnetization errors in strength and in angle of magnet blocks is well compensated, so that there is no accumulated distortion of the orbit due to erroneous kick in angle when electrons travel along the OK. Figure 2 shows a spontaneous emission spectrum for N_d = 83 measured at a low beam current of less than 1 mA/bunch. The fine structure peculiar to radiation from an OK is evident, which arises from interference of radiation from the two undulator sections.

In order to check the performance of the OK, an FEL gain is measured by the method similar to that employed in the previous experiment with the conventional undulator.[1] The light at the wavelength of 488 nm from an Ar ion laser is modulated in polarization at a frequency of $f_{mod} \sim 2.8$ kHz by an Pockels' cell, injected into the OK, and detected with a PIN silicon photodiode after it interacts with the electron beam. As the storage ring is operated in single bunch mode, the gain signal appears at the combined frequency of the revolution frequency of the electrons f_{rev} and the modulation frequency f_{mod}. The signal is processed by a fast lock-in amplifier locked at $f_{rev}+f_{mod}$. The measured gain is shown in Fig. 3 as a function of N_d. The measured peak gain is about 0.4 % for the average beam current of 10 mA/bunch, which is

in agreement with calculation. The gain of the OK is about five times larger than that of the conventional undulator.

An optical resonator of 13.3 m long is installed for oscillation experiment. Radii of curvature of the front and rear mirrors are 8 m and 6 m, respectively. An oscillation experiment is now in preparation.

References

1) S. Takano, H. Hama, G. Isoyama and A. Lin: UVSOR activity Report 1990, p.4; S. Takano, H. Hama, G. Isoyama, A. Lin and N. A. Vinokurov: submitted to Jpn. J. Appl. Phys.

2) N. A. Vinokurov and A. N. Skrinsky: preprint 77-59 of the Institute of Nuclear Physics, Novosibirsk, 1977.

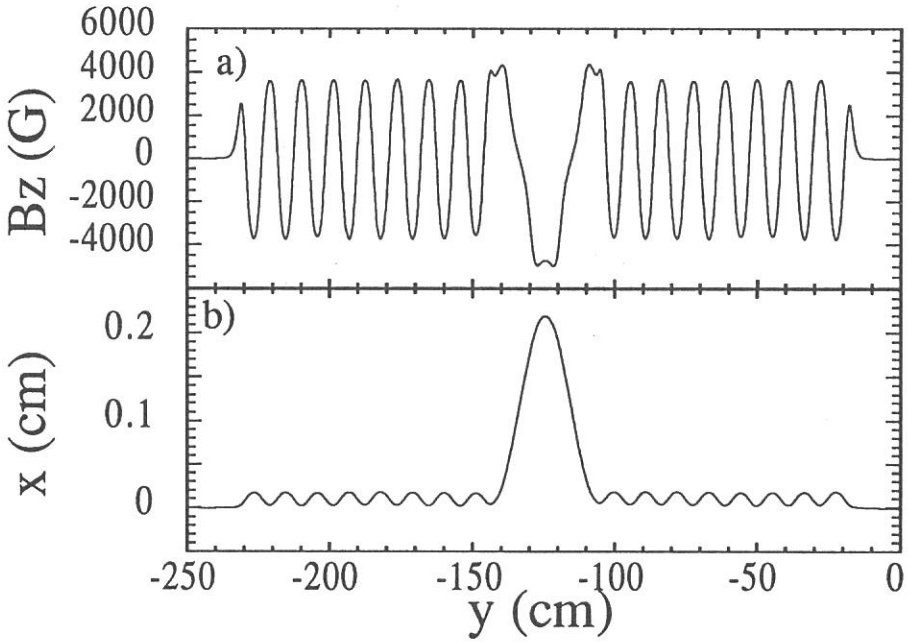

Fig.1 a) Vertical magnetic field in the optical klystron.
b) Calculated electron orbit in the horizontal plane.

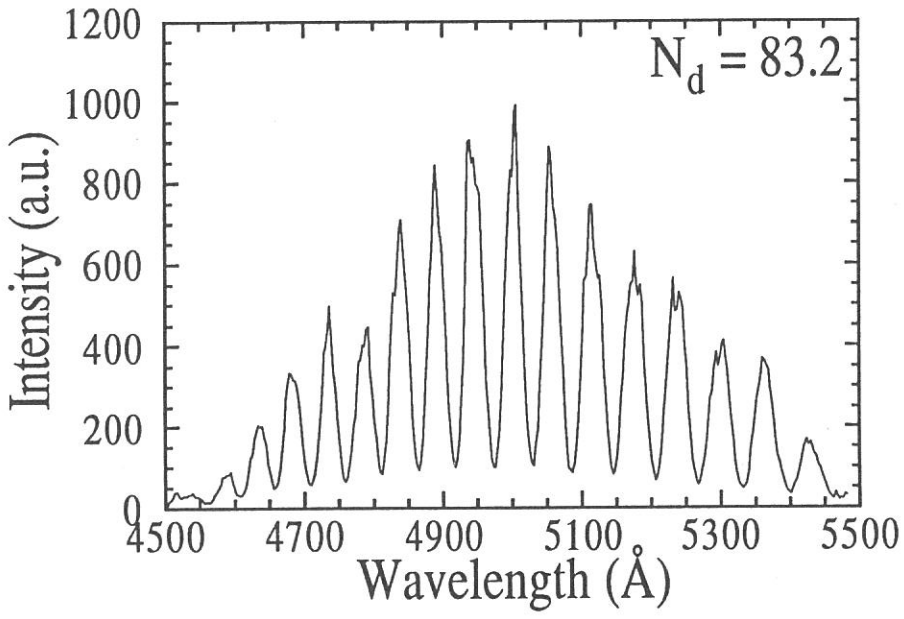

Fig. 2. Spontaneous emission spectrum of the optical klystron.

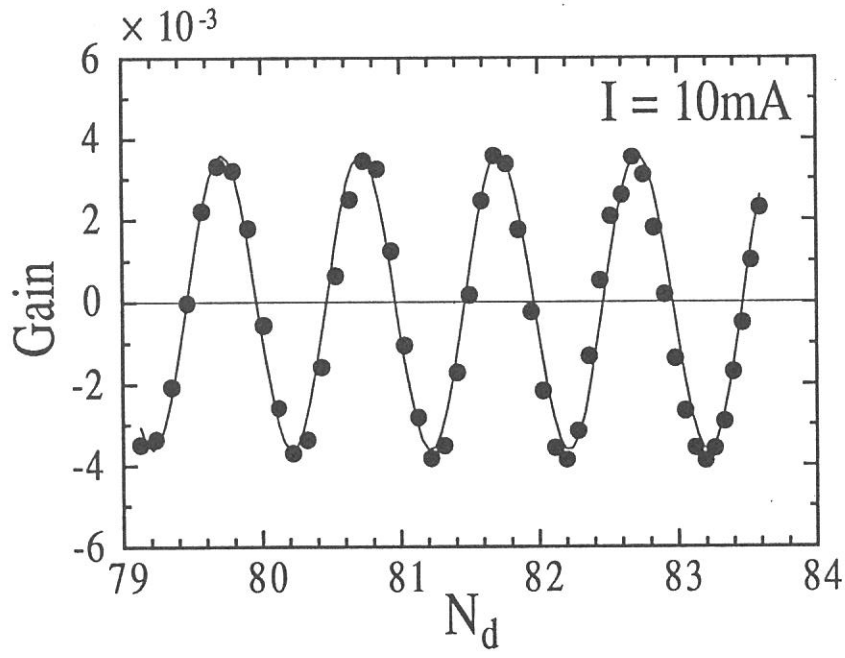

Fig. 3. Gain of the optical klystron as a function of N_d.

Computer Control System for the UVSOR Storage Ring

Noriichi KANAYA*, Hiroyuki HAMA, Jun-ichiro YAMAZAKI,
Osamu MATSUDO and Goro ISOYAMA

** Photon Factory, National Laboratory for High Energy Physics, 1-1 Oho, Tsukuba 305*
Institute for Molecular Science, 38 Myodaiji, Okazaki 444

Since the construction of the UVSOR accelerator system, the storage ring as well as the booster synchrotron had been operated by a manual control system. We sometimes met difficulties with the control system to improve the performance, especially, of the storage ring. In order to overcome the difficulties, a new control system based on mini-computers was recently installed for a part of the accelerator system, that is, for the storage ring and the beam transport line from the synchrotron. We employed Micro VAXs with the VMS operating system as the computers for control and mainly the CAMAC interface for connecting components of the accelerator system with the computers The new system has been working quite well.

The computer system consists of two min-computers (Micro VAX 3400) with four shared hard disks, which are used for communication between the computers, two work stations (VAX Station 3100) for operator's terminals and seven CRTs for status monitors, which are connected to the computers by a local network (DECNET) through two terminal servers (DEC Servers) They constitute a local cluster structure via the network. One of the mini-computers is used for control of the storage ring, and the other for the beam transport line. The latter computer will be also used for control of the synchrotron and the injector linac in the future. If one of the min-computers malfunctions due to a system failure, it is possible to control all the system by the other computer though the response time of the system is degraded.

The main interface between computers and accelerator components we adopted is CAMAC. There are six crates for the storage ring and two crates for the beam transport line, which are connected serially to each computer by an optical link. We mainly use parallel input and output modules to control devices; 24-bit change-of-state input register modules (Kinetic Systems 3473), 24-bit isolated input gate modules (3471), 48-bit digital output register modules (3072) and 16-bit input gate/output register modules (3063). Additionally, we use 32-channel 16-bit scanning analogue-to-digital converter modules (3516) for analogue inputs. Status data are read by the 3473 modules, though an interruption function (LAM) is not used for the moment, and numerical data are read by the 3471 modules. They are read or

written in the BCD format. Since approximately 70 DC power supplies with relatively small output capacity are necessary for steerings, sextupoles, skew quadrupoles and correction coils of bending magnets and quadrupole magnets, we employed the 3063 modules which can be connected to the power supplies directly by single cables. The CAMAC modules are electrically isolated from controlled devices. Some devices are connected to the computers by GPIB interface or RS232C interface.

In order to use most of the existing power supplies which were controlled by remote control boxes in the control room, interface boxes were made and inserted between the power supplies and the CAMAC interface. Since we use the same electrical and logical levels for the CAMAC modules, those of each power supply are converted to the standard ones for the CAMAC modules in the interface box. An exception is the DC power supplies for small magnets and coils, which are directly connected to the CAMAC modules one to one. They were newly built and replaced old ones.

The control program was made by Digital Equipment Corporation Japan. The standard tools of the X-window (DEC-Window) are used for the man-machine interface, which runs on the workstations. The control screen has a hierarchical structure. The main control window is a summary screen, on which operational and error status of the accelerator system is displayed, routine operations of the system such as starting-up, injection, acceleration, and so on are conducted, and sub-summary screens of the lower level such as for the magnet power supplies and the RF system of the storage ring are called. From a sub-summary screen, we can get access to control screens for individual devices. It is also possible on the sub-summary screen to set numerical values to the devices. Any of the screens can be displayed on the CRTs, the program for which is written by GKS.

The routine operations of the system are defined in the form of files, which consists of conduct files and data files. When one of the routine operations is selected by an operator, the program first reads a conduct file, in which names of data files are written, and then reads the data files written in the conduct file. In a data file, names and setting values of devices are written. The data file has a sub-structure called as pages, which is divided by the symbol of end of step (EOS). The control program reads commands written in a page, successively performs them, and waits till all the commands are completed. Then it proceeds to the next page. It is possible to write any numbers of data files in a conduct file. Owing to this control file system, it is possible to change operation modes without changing the control program.

Since the UVSOR accelerator system is running for user experiments, the control system was replaced stepwise during relatively short shutdown periods in 1991. The longest one was four weeks. In order to avoid unscheduled shutdown due to the new control system, the special care was taken so that anytime we could go back to the old control system if a malfunction of the new control system happened. Fortunately, there was no such an accident. We will extend the system to cover all of the accelerators in the future.

CONSTRUCTION OF BL-4A BEAM LINE AND ITS FACILITIES

Shinri SATO, Yuji UKISU, Eiken NAKAMURA, Toshio KINOSHITA, Atsunari HIRAYA, and Makoto WATANABE

Institute for Molecular Science, Myodaiji, Okazaki 444, Japan

In recent years, VUV surface photochemistry, especially SOR photochemistry has received increasing attention because of its potential applications to microelectronics, e.g., photo-CVD, microlithography, photo-etching, etc. Fundamental researches on VUV surface photochemistry are, however, far behind its technological researches due partly to lack of suitable light source. BL-4A beam line was constructed for the fundamental study on photochemistry of solid surfaces and of adsorbed molecules.

Figure 1 shows a schematic diagram of BL-4A beam line. The SOR light is focused by a prefocusing mirror onto a sample in a reaction and analysis chamber (RAC). Unfocused light is also available. Although the beam line has no spectrometer, wavelength region of the SOR light can be selected by a thin metal-film or a glass cut-off filter. RAC is equipped with some surface-science facilities; polarization-modulation reflection absorption FTIR spectroscopy (PM-IRAS) for molecular structure analysis of adsorbed species, a quadrupole mass spectrometer for gas analysis, Auger electron spectroscopy (AES), X-ray photoelectron spectroscopy (XPS) for surface chemical analysis, an ion sputtering gun for sample cleaning, a gas-handling system, and a sample load lock for a quick exchange of sample. RAC is pumped by a turbo molecular pump and an ion pump, and its base pressure is less than 1×10^{-9} torr. A sample holder attached to an XYZT precision manipulator can be cooled with liquid nitrogen and heated by electric heater. The temperature of the sample can be elevated at a constant rate for temperature-programmed desorption (TPD) technique.

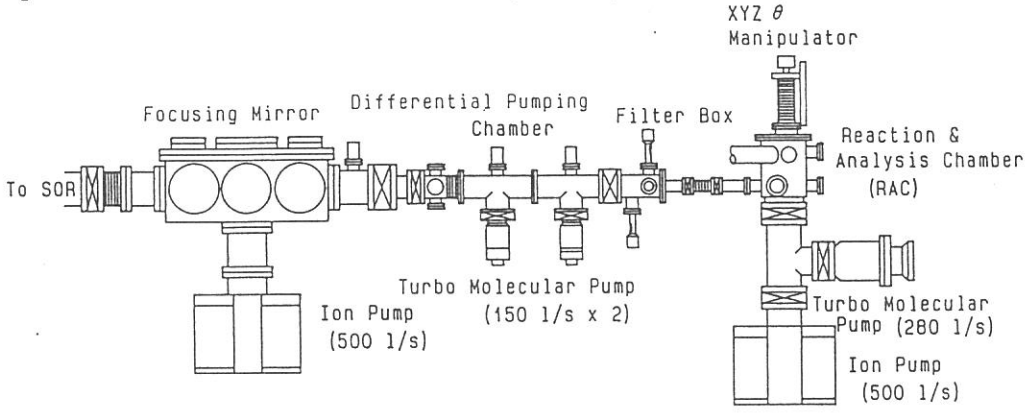

Figure 1. Schematic diagram of BL-4A beam line.

Figure 2 shows a schematic diagram of PM-IRAS which is carried out at the level of SOR beam. When P-polarized IR beam is incident to sample surface (metal surface in principle) at a high incident angle nearly 90°, the beam interacts efficiently with molecular vibration perpendicular to the surface, while S-polarized IR beam not. Therefore, PM-IRAS gives information of surface species alone even if gas-phase species are present, and serves for improvement in S/N ratio. In this system, PM is carried out at 64 KHz by a wire-grid polarizer and a photoelastic modulator.

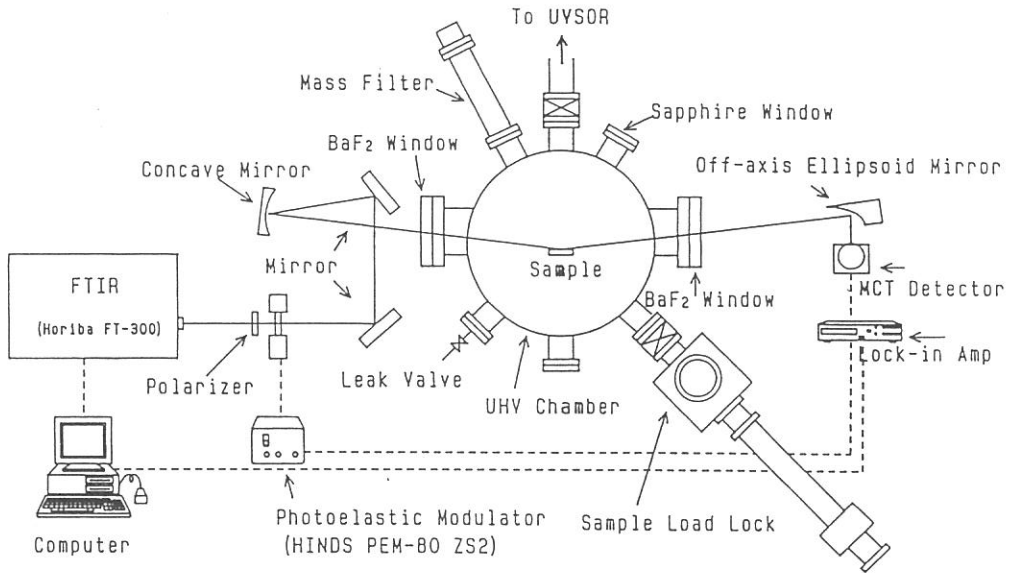

Figure 2. Schematic diagram of PM-IRAS system at the lower level of RAC.

Reflected IR beam from the sample is detected by a HgCdTe (MCT) detector cooled with liquid itrogen. A difference signal between P- and S-polarized beams is amplified by a lock-in amplifier and subjected to Fourier-transform calculation, while a reference spectrum is recorded without the lock-in amplifier. BaF_2 windows of RAC were specially made for IR spectroscopy in an ultra high XPS, AES, and sample cleaning are carried out at the upper level of RAC, to which the sample is transferred by the manipulator. A schematic diagram of the upper level system is shown in Fig. 3. An X-ray gun has dual anodes of Mg and Al, and an electron analyzer is VSW CLASS 150, specification of which is as follows: Energy range, 10 - 5000eV; Detector, Mulch-channel detector (Resistive anode PSD); Noise, 50meV (peak to peak); Sensitivity, 450Kcps at 0.9eV FWHM (Ag $3d_{5/2}$).

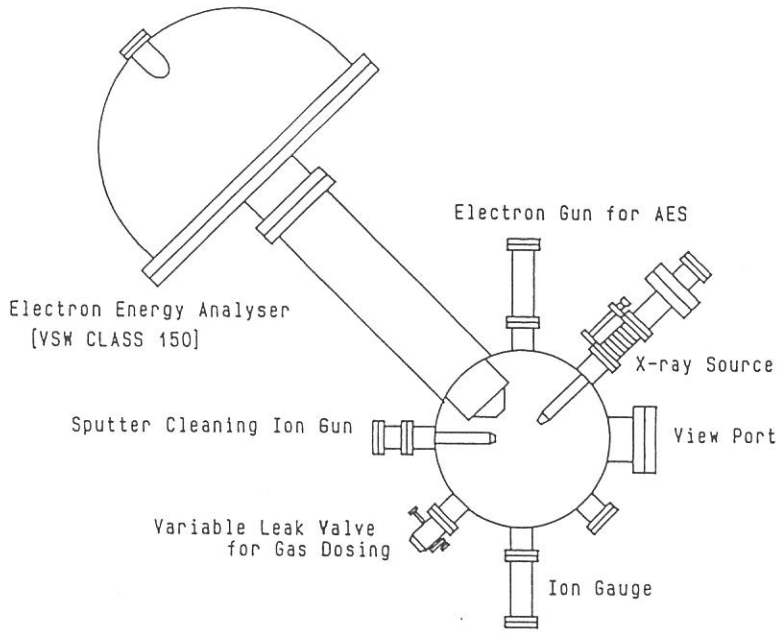

Figure 3. Schematic diagram of the upper level of RAC.

Design of an Instrument for Far-Infrared Microspectroscopy using a SR Source

A. Ugawa, H. Ishii,† K. Yakushi, H. Okamoto, T. Mitani, M. Watanabe, K. Sakai, K. Suzui, and S. Kato.

Institute for Molecular Science, Okazaki 444 Japan.

†Department of Chemistry, Faculty of Science, The University of Tokyo, Bunkyo-ku, Tokyo 113 Japan.

A design of a microspectro-photometric system using a synchrotron radiation (SR) source are described. The system covers the wide spectral range of 50-13000 cm^{-1}, being under construction at the UVSOR BL6B beam-line. The optical system, which is designed mainly for reflectance measurement, is schematically drawn in Fig. 1. The optical system constitutes of four components: 1) *Beam Line Optics (BL6B)* in ultra-high vacuum with interchangeable four windows, 2) *Fourier-Transform Interferometer* of vacuum type, 3) *Infrared Microscope* Spectra-Tech IR-PLAN, which will be placed in dry and CO_2 free atmosphere, and 4) *Si Bolometer* cooled by liquid helium. Preliminary experiments in the mid-infrared region (500-5000 cm^{-1}), as shown in Fig. 2, have qualitatively confirmed the theoretical calculation that the synchrotron radiation is more intense than a blackbody (T = 1200 K) when a microspectro-photomeric technique is applied, which is due to natural collimation and high brilliance of SR source. The SR as an infrared source exhibits its advantage on measuring the spectra of small single crystals especially in the far-infrared region.

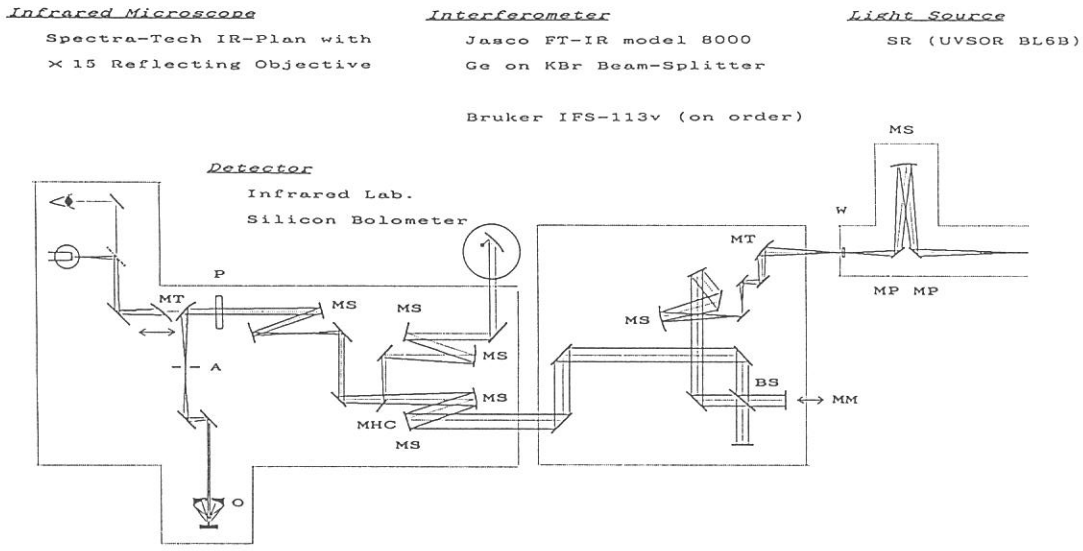

Fig. 1. Schematic drawing of the optical system.

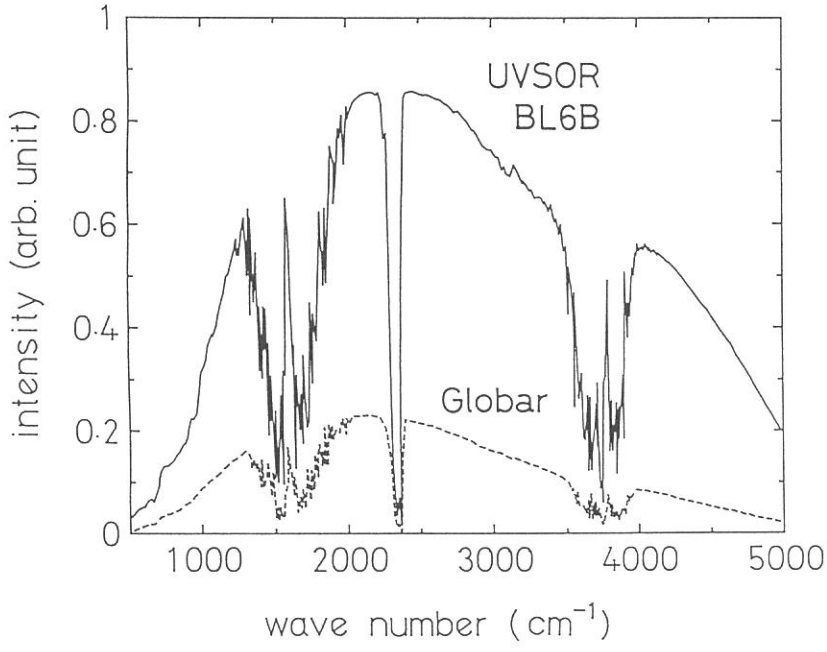

Fig. 2. Power spectrum of the SR (BL6B) and black body.

CONSTRUCTION OF AN APPARATUS FOR STUDIES OF SURFACE PHOTOCHEMICAL PROCESSES, III ON BL4B

Haruhiko OHASHI,* Eiken NAKAMURA, Toshio KINOSHITA, Atsunari HIRAYA, Makoto WATANABE, and Kosuke SHOBATAKE

Institute for Molecular Science, Myodaiji, Okazaki 444 Japan

** Visiting Student from Toyohashi Univ. of Technology, Toyohashi, 440 Japan*

An apparatus has been constructed on for studies of surface photochemical processes of semiconductor materials. The processes to be studied are synchrotron radiation-excited etching of semiconductor material surfaces and epitaxial growth of crystalline semiconductor film at low temperatures. A long focusing mirror (550 mm x 30 mm) was installed 2.31 m downstream from the source point and the focussed synchrotron radiation, which is deflected by 4°, is irradiated upon a sample surface 4.50 m downstream from the center of the mirror. It would be worth to describe the characteristics of the mirror installed here. From ray tracing calculations it was shown that the focussing behavior is improved quite a lot by using an elliptically bent cylindrical mirror.[1] Therefore the mirror surface is shaped to be circular in the vertical direction (radius: R_v =11.1 cm) and elliptical in the horizontal direction. Mechanically a long cylindrical mirror was bent by pressing it on an elliptically machined surface.

The beamline was designed such that one can also carry out experiments with unfocussed SR as it is directly radiated from the source point, despite of the low intensity levels compared with the focussed SR, because its absolute intensity and spectral profile can be theoretically estimated. Furthermore since the focused SR beam crosses with the unfocussed beam 3.02 m downstream from the center of the focussing mirror, one has to only rotate apparatus around the crossing point and realign SR beam.

The schematics of the apparatus is shown in Figure 1. It consists of a reaction chamber, two differential pumping chambers, DPC-1 and DPC-2, and a light chopper chamber. To the reaction chamber are attached a differential pumping chamber, DPC-1 from its upstream side, a stock chamber which keeps samples on top of it, and an ESCA (VSW Scientific Instrum., Model Class 150) analyzer chamber from the side of the reaction chamber. The samples on the sample holder are inserted in the leak chamber, and transfered to the stock chamber after the leak chamber is pumped down to low enough pressure. Thus the stock chamber and reaction chamber are not exposed to air. The base pressure of the stock chamber is 2,0 x 10^{-10} Torr and that of the reaction chamber is at present 1.0 x 10^{-9} Torr without baking. The chambers are pumped with magnetically suspended turbomolecular pumps. It is planned that from the downstream side of the reaction chamber will be connected a molecular beam chemistry apparatus II (MBC-II) which is being modified to detect desorbed species from a SR-irradiated surface using a rotatable mass spectrometer detector with an electron bombardment ionizer. In the mean time experiment is underway to detect desorbed species from the irradiated surface in another reaction chamber using a mass spectrometer detector.

References

1. A. Hiraya, et. al., *Rev. Sci. Instrum.* **63**, 1264 (1992).

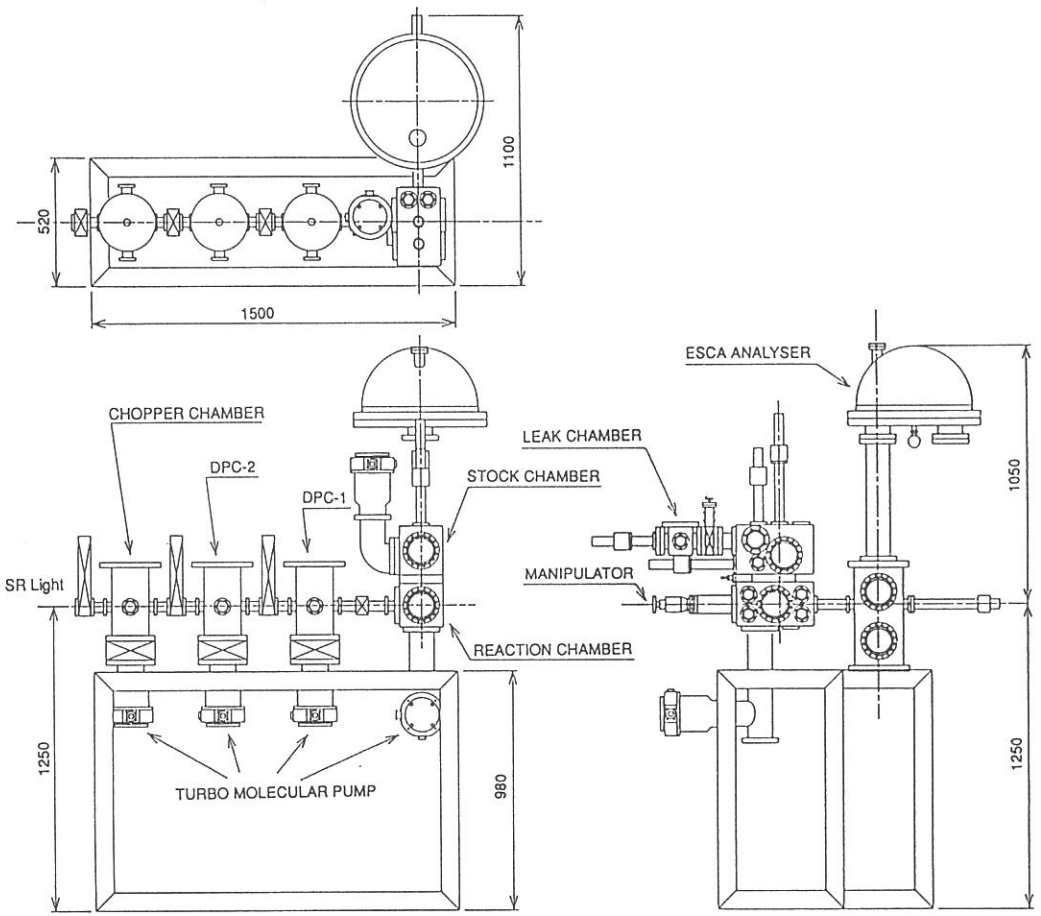

Figure 1. Schematic drawings of the apparatus constructed on Beamline BL4B for studies of surface photochemical processes. Top: downward view, bottom left: side view (note that the SR is radiated from the left), bottom right: side view facing the light beam source.

RESEARCH ACTIVITIES

PHOTOFRAGMENT EMISSIONS FROM CBr_4

Ikuo TOKUE, Kiyohiko Tabayashi* and Kosuke SHOBATAKE*

Department of Chemistry, Niigata University, Niigata 950-21

**Institute for Molecular Science, Myodaiji, Okazaki 444*

There has been only a little amount of information about photolysis of methyl bromides. In this report we focus on photolysis of CBr_4.

Fig. 1 shows the absorption and fluorescence cross sections of CBr_4 in the 105—175 nm region. The electronic configuration of n_{Br} is expressed as

$$(e)^2(t_2)^6(t_1)^6$$

and six IPs corresponding to these electrons have been determined [1]. Adopting these IP values a number of absorption peaks in Fig.1a have been assigned as the Rydberg transitions to *ns*, *np*, and *nd* levles.

The emission in the 540—930 nm range is 20—30 times as intense as that of 370—530 nm range. From thermochemical consideration, the emission was assigned as the $CBr_2(\tilde{A}^1B_1 - \tilde{X}^1A_1)$ transition [2]. CBr_2 is produced by the reaction $CBr_4 \rightarrow CBr_2(\tilde{A}) + 2Br$. The $\Delta H^o_{f,298}(CBr_2)$ value was evaluated to be 308 ± 4 kJ/mol on the basis of $\Delta H^o_{f,298}(CBr_4)$ = 50.2 kJ/mol from JANAF Table.

The decrease in the emission cross section at λ_{exc} < 140 nm is attributable to the decaying process forming CBr; its threshold is estimated to be 155 nm.

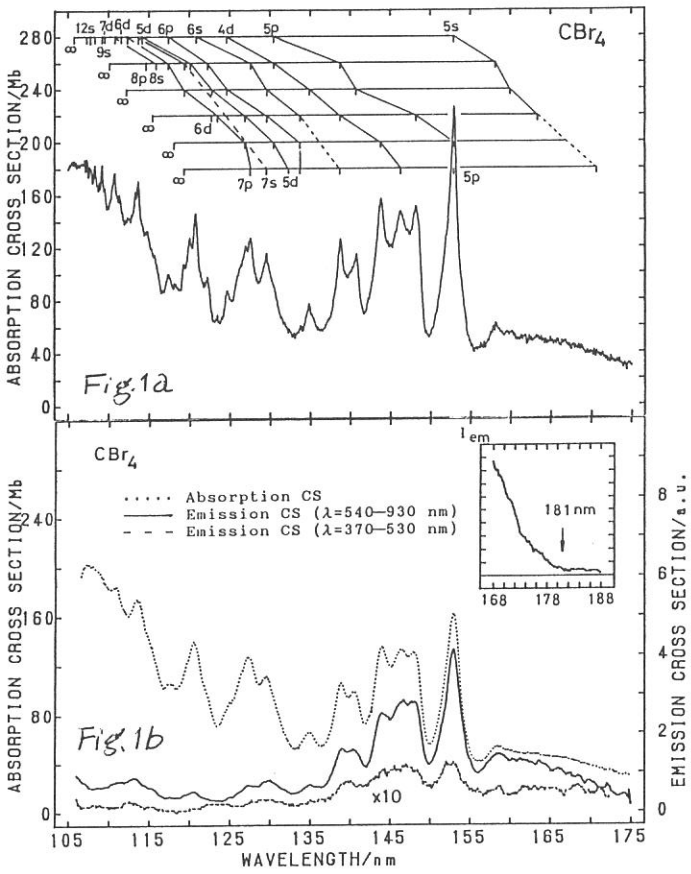

References

[1] A. W. Potts *et al.*, Phil. Trans. Roy. Soc. Lond. **A268**, 59(1970).

[2] V. E. Bondybey and J. H. English, J. Mol. Spectrosc. **79**, 416(1980).

OPTICAL SPECTRA OF $Sr_{1-x}La_xTiO_3$

Yuzo FUJISHIMA, Takahisa ARIMA, Shin-ya KOSHIHARA and
Yoshinori TOKURA

Department of Physics, University of Tokyo, Tokyo 113, Japan

We have started the title study with the aim at understanding a valence-dependent systematic change of electronic structures in a highly correlated electron system. In the present study, we have prepared and investigated the mixed crystal system, $Sr_{1-x}La_xTiO_3$, with perovskite-like structures, in which the Ti-valence (number of 3d electron per Ti-site) can be varied from +4 (0) to +3 (1). The reflectivity spectra of $Sr_{1-x}La_xTiO_3$ were measured on mechanically polished surfaces of the melt-grown samples at 300K in the photon energy range of 0.05-20eV, utilizing synchrotron radiation at UV-SOR for a light source in the VUV region.

In Fig.1 we show the reflectance spectra of $Sr_{1-x}La_xTiO_3$ at 300K. The spectral features are composed of two parts; plasma-like high reflectance bands below 1.5eV and interband transitions above 3eV. In the insulating x=0 ($SrTiO_3$) sample, some optical phonons show up as high reflectance bands in the infrared region, which should not be confused with the plasma-like photo-response. An apparent plasma edge is readily observed for the x=0.1 sample. The energy position of the plasma edge steadily shifts to higher energy with filling the d-band. However, the tendency seems to be saturated around x=0.5 and then the edge position rather shifts to lower energy.

We have deduced optical conductivity spectra (Fig.2) by Kramers-Kronig transformation of the reflectivity data. Conspicuous changes are seen in the spectra both for the infrared (Drude) region and visible-ultraviolet interband region with varying the filling parameter x. In the low-x samples, fine structures of the interband transitions are discernible above 3eV: Among them, lower-lying bands below 6 eV are assigned to the transitions form the O 2p valence bands to the Ti 3d bands. It is to be noted that the absorption edge due to these interband transitions are little changed with partially filling the d (t_{2g}) band. However, the lower-lying peak at ca. 5eV is considerably broadened with increasing x. This is perhaps because the final states involved in the transition are located near above the Fermi level of the metallic d-electron bands and subject to the strong screening effect.

On the other hand, a spectral weight in the infrared region below 1eV shows a large variation with filling the 3d band in accord with the above-mentioned observation on the position of the plasma edge: The infrared spectral weight increases monotonously with x up to ca.0.5, but rather decreases beyond x in spite

of apparent increase in number of d electrons. In particular, the samples with x close to the end (x=1.0) show a barely metallic photo-response with much reduced and non-Drude like optical conductivity. As far as the optical conductivity is concerned, the $Sr_{1-x}La_xTiO_3$ compound seems to be continuously transformed to an insulator with x approaching the integer filling (x=1). Our interpretation for this transitional behavior is that the effective d-electron mass near the Fermi level is critically enhanced on approaching the end (x=1) because of increasing importance of the electron correlation (or the so-called Hubbard U term).

The effect of Coulomb correlation in the narrow 3d band is thus quite filling(valence)-dependent. The detailed analysis of the present results and its significant implications will be published elsewhere.

This work was supported by the Joint Studies Program (1991) of the Institute for Molecular science and by Grant-In Aids from Ministry of Education, Science and Culture, Japan. We thank the staffs at UV-SOR for their help in VUV measurements.

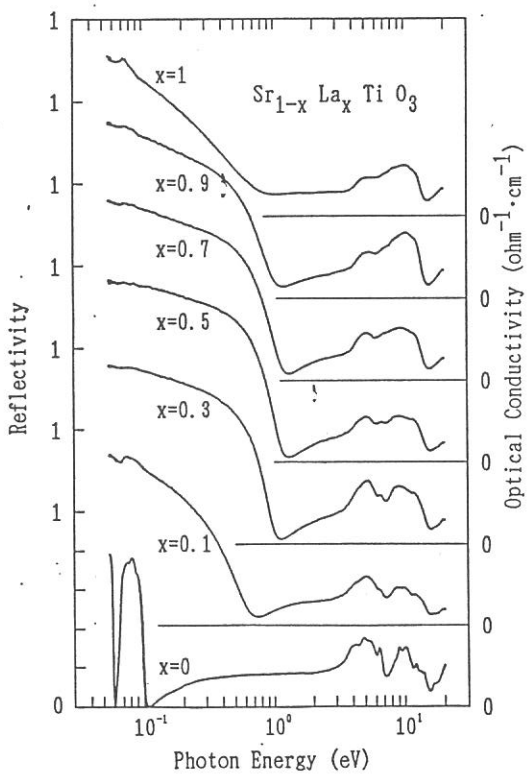

Fig.1: Reflectance spectra of $Sr_{1-x}La_xTiO_3$ at 300K.

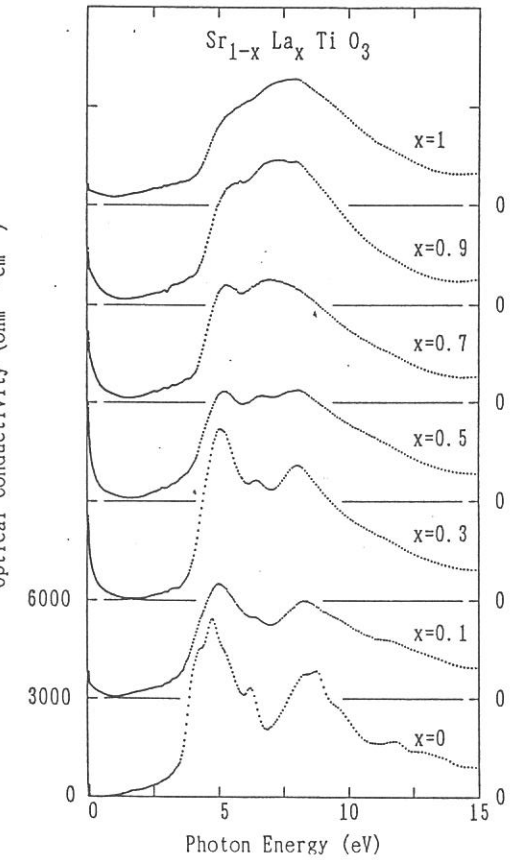

Fig.2: Optical conductivity spectra of $Sr_{1-x}La_xTiO_3$.

$N_{4,5}$ EMISSION SPECTRA OF SOME RARE-EARTH HEXABORIDES

Kouichi ICHIKAWA, Takashi UMEHARA, Katsuhito Aoki and Masao KAMADA*

College of Engineering, University of Osaka Prefecture, Mozu-Umemachi, Sakai 591
*Insitutute for Molecular Science, Myodaiji, Okazaki 444

There have been many studies on the absorption spectra and the photoemission spectra of rare-earths (RE) and their compounds in the region of 4d excitation because the 4d-4f interaction gives characterestic features in the spectra. The absorption spectra show weak lines with widths of several tenths of an electron volt and giant bands with 15-70 eV widths. The final states of the absorption decay radiatively and/or nonradiatively. The former process emits soft-x-rays in the region of 4d absorption and is distinct from ordinary x-ray emission.[1] The latter process ejects electrons with different kinetic energies corresponding to the various decay channels such as the Auger decay processes and the direct recombination of the excited electron and the 4d hole.[2,3] The observation of these phenomena is useful for understanding the electronic structure of RE compounds and the decay mechanism of the $4d^9 4f^{n+1}$ excited states, where n is a number of 4f electrons in the ground state.

In the present study we measured RE $N_{4,5}$ emission and photoelectron spectra of PrB_6, NdB_6, EuB_6 and GdB_6. Thin samples were prepeared in situ by evaporation to reduce intensity loss due to the self-absorption in the measurements of soft-x-ray emission. In the case of photoemission, polycrystalline samples were scraped in situ with a diamond file to obtaine clear surface.

The Eu $N_{4,5}$ emission spectra of EuB_6 with electron excitation mode were shown in Fig. 1 (a)-(c). Excitation voltage is indicated at a right hand side of each spectrum. The total yield spectrum measured with a plane-grating-monochromator at a beam line 6A2 was also shown at a bottom of Fig.

1. The intense peak A at about 110 eV in the emission spectrum is caused by the transition between Eu 5p and 4d inner-core levels, and thus spectra were normalized at this peak. The intensity of the peak D relative to the peak A increases with decreasing the incident electron energy. This result suggests that the emission spectra are affected by the self-absorption. In fact, strong absorption due to the transition from the 4d level to the empty 4f level is observed in this energy region as shown at the bottom of Fig. 1. In a common sense, ordinary x-ray emission cannot appear in the energy region where the absorption is observed. Thus, we think that the peak D in the emission spectra is caused by the radiative decay of the $4d^9 4f^{n+1}$ excited states as observed previously in LaB_6 and CeB_6.[1] In the present case, however, the emission feature does not agree well in shape with the absorption. Therefore, there is a possibility that the peak D is caused by the transition from $4d^9 4f^n$ states because of large 4d-4f interaction.

Similar results were obtained for other RE hexaborides. However, there are close resemblance in shape between the emission and absorption spectra with decreasing atomic number. Detailed analysis of the spectra is under way.

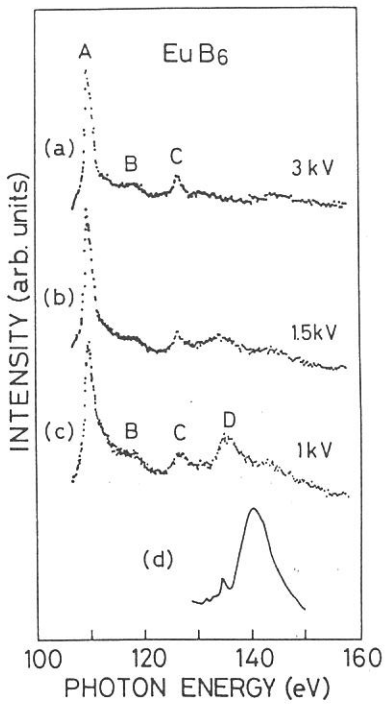

Fig. 1 Eu $N_{4,5}$ emission spectra (a)-(b), and total yield spectrum (d) of EuB_6. Emission spectra were obtained with the electron excitation mode and excitation voltage is indicated at a right hand side of each spectrum.

REFERENCES

1) K. Ichikawa, A. Nisawa and K. Tsutsumi, Phys. Rev. B 34 (1986) 6690.
2) J. W. Allen, L. I. Johansnon, I. Lindau and S. B. Hagstrom, Phys. Rev. B 21 (1980) 1335.
3) M. Aono, T. -C. Chiang, F. J. Himpsel and D. E. Eastman, Solid State Commun. 37 (1981) 471.

PERFORMANCE TEST OF CCD FOR DIRECT X-RAY DETECTION IN THE ENERGY RANGE OF 1~9 KEV AT UVSOR FACILITY

Hiroshi TSUNEMI, Shin'ichi KAWAI and Kiyoshi HAYASHIDA
Department of Physics, Faculty of Science, Osaka University
1-1 Machikaneyama, Toyonaka, Osaka 560

We performed a calibration of the charge-coupled device (CCD) in the direct X-ray detection method. The CCD chip is a product for optical use. It contains 1024×1024 pixels, each of which is 12×12 mm^2. When we use it in a frame-transfer mode, the image area contains 1024×512 pixels. The only difference in our system from the system for optical use is that the glass lid is removed for direct X-ray detection with the CCD. The CCD chip itself is cooled down to -60°C with a combination of a refrigerator and the Peltier cooler in order to reduce the thermal noise level for the photon counting mode. A mechanical shutter is placed in front of the CCD chip, which enables us to restrict the exposure time down to 1/125 s. A moving arm is also placed in front of the CCD chip, on which there are four kinds of X-ray filters made of aluminum foil or of plastic film to reduce the photon flux down to a reasonable level.

We performed an experiment using the beam line, BL-7A, in the UVSOR facility. Figure 1 shows the experimental setup in this study. The acceptable energy ranges as the 1st order are determined by the rotation angle of the crystal, and they are between 0.8 keV and 2.5 keV for beryl, between 2 keV and 6 keV for Ge(111) and between 3 keV and 9 keV for Ge(220).

We adjusted the position of the CCD camera system so that the X-ray beam was precisely in the center of the image area (6×12 mm^2). Figure 2 (a) shows the pulse height distribution of the pixel outputs at the X-ray energy of 2.45 keV. The highest peak on the left corresponds to the zero peak. Since the beam size is smaller than the image area, many pixels in the image area absorb no X-ray photons. These pixels form the zero peak. There are two peaks next to the zero peak; the higher one is two times higher than the lower one. These correspond to the n-fold of the 1st-order X-rays. The split events will produce pixels whose output is midway between the peaks.

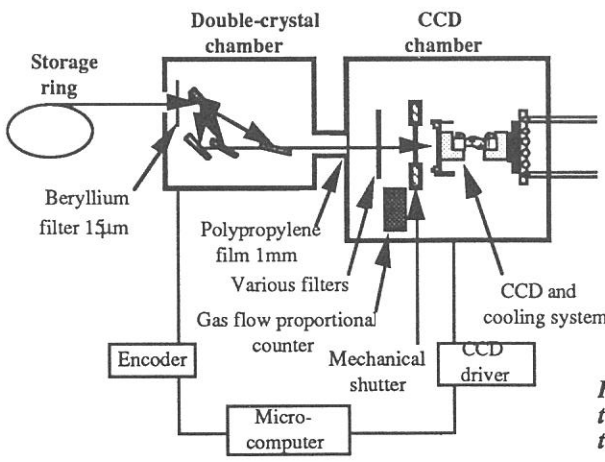

Fig. 1. Experimental setup to test the CCD performance in the UVSOR facility, BL-7A.

Figure 2 (b) shows the pulse height distribution of a single-pixel event. The single-pixel

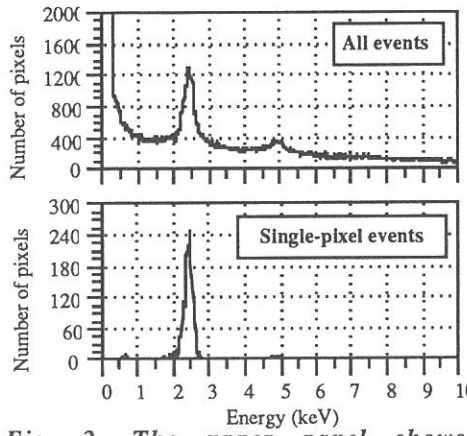

Fig. 2. The upper panel shows the pulse height spectrum of the outputs from the CCD. The increase towards zero (zero peak) is from the pixels which absorbed no X-rays. Single-pixel events form X-ray peaks while split events scatter among them. Lower panel shows the pulse height spectrum of the single-pixel events.

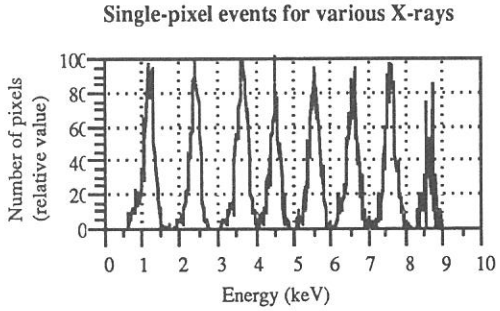

Fig. 3. The pulse height distribution of the single-pixel events for various X-ray energies ranging between 1 and 9 keV.

event is a pixel whose output is above the event threshold with the condition that its neighboring pixels are in the zero peak. Therefore, the photoelectrons produced through the photoabsorption were considered to gather into one pixel.

Figure 3 shows the pulse height distributions of the single-pixel events for various X-ray energies between 1 and 9 keV. The exposure time ranged from 8msecond to 15 second, depending on the beam intensity as well as the filter employed. The highest energy data shown in Fig. 3 were the weakest in intensity using Ge(220) at 8.56 keV, which were obtained with no filter with the exposure time of about 15 second. We obtained no X-ray photons above 9 keV from the statistical point of view. This is due to the upper limit of the X-ray energy available at the UVSOR facility rather than to the reduction of the detection efficiency of the CCD at high energy. The energy resolution (FWHM) obtained here ranges between 200 eV and 250 eV depending on the incident X-ray energy.

We irradiated the strong X-rays onto the CCD chip in order to measure the radiation damage effect. We selected the incident X-ray energy such that the mean absorption length of the X-ray became short enough to leave the maximum radiation damage on the CCD surface region. We left the CCD chip in this radiation field up to 10 minutes, keeping the bias voltage on the chip. The maximum dose of the CCD chip reached 10^4 rad. We measured the pulse height distribution of the single-pixel events as well as the charge transfer efficiency before and after the exposure at various parts of the chip. We found no difference between them from the statistical point of view. Therefore, we conclude that the direct X-ray detection system using this type of CCD can function in the standard measurement in the UVSOR beam line in the energy region of a few keV.

The details of our results are in H. Tsunemi, S. Kawai and K. Hayashida appeared in Jpn. J. Appl. Phys. **30** (1991) 1299.

Resonant Photoemission Study of an Al-Cu-Fe Icosahedral Phase

M. MORI, K. KAMIYA*, S. MATSUO, T. ISHIMASA, H. NAKANO, H. FUJIMOTO+ and H. INOKUCHI*

College of General Education, Nagoya University, Chikusa, Nagoya 464-01
*Institute for Molecular Science, Myodaiji, Okazaki 444
+The Graduate School of Science and Technology, Kumamoto University, 860

The discovery of an icosahedral phase (i-phase) by Shechtman et al., subsequently observed in many other alloys, has made a great surprise with the combination of forbidden symmetry and sharp diffraction spots. It has been known that an Al-Cu-Fe alloy system has a stable i-phase[1]. Two remarkable magnetic properties have been found on the i-phase[2]. One is that the magnetic susceptibility is proportional to T^2. Interpretation of this temperature dependence suggests existence of a sharp dip in DOS at E_F caused by the energy gap of the Brillouin zone. The other is that the Fe atoms have no localized magnetic moments. Recently, a dip-like anomaly in DOS near E_F was confirmed with the photoemission experiment[3]. But the study has left the role of Fe 3d states unclear.

A resonant photoemission study is useful to obtain direct information on a partial DOS. The principal purpose is to observe the resonant photoemission on the Al-Cu-Fe i-phase to discuss about the Friedel's suggestion on the role of the Fe 3d states on the i-phase stability.

The sample used in this study was an $Al_{65}Cu_{21}Fe_{14}$ i-phase ingot[3]. Photoemission studies were performed at BL8B2 of UVSOR. All measurements were carried out at room temperature. The specimen was so brittle that clean surfaces were easily obtained by filing in a vacuum of $3\text{-}7\times10^{-8}$ Pa, and the sample was transferred to the UPS experimental chamber in $0.5\text{-}3\times10^{-8}$ Pa. A spectral dependence was determined from a photoelectric yield of gold.

It is well known that an Fe 3d cross section increases like resonance at the photon energy corresponding to the Fe 3p core excitation. The width of Fe 3d bands can be estimated by using such a resonant phenomenon. The CIS spectra at several binding energies were measured as shown in Fig. 1. The CIS spectra A and B do not show a remarkable resonance effect in the observed photon energy region. Therefore, the electron states at the positions A and B can be assigned to be the states non-hybridized with Fe 3d orbitals, which mainly consist of the contribution from Al and Cu. On the other hand, an "anti-resonant" dip is observed in the spectra D and E at the energy region of the Fe 3p-3d core excitation. The electron states at these energies can be assigned to be the states hybridized with the Fe 3d orbitals which contains appreciable amounts of Fe 3d electrons. The spectrum C shows a small "anti-resonant" dip. The electron states at the binding energy 2eV are assigned to be the states hybridized with the Fe 3d orbitals which contains small amounts. The result leads to the interpretation that the Fe 3d bands are located in the region ranging from E_F to 2 - 2.5 eV in the binding energy. As the CIS intensity depends on the photon energy severely, we can not discuss the detailed resonant feature. The fitted spectrum was estimated from the non-resonant spectrum A as shown with the solid line on A

in Fig. 1. The relative spectrum A in Figure 2, defined with A in Fig. 1 divided by the fitted, indicates the validity of the fitting. The other spectra in Fig. 2 show the relative CIS curves given as the spectra C, D and E divided by the fitted. They have same asymmetric shape, in which the weak peak is on the lower photon energy side and the strong dip is on the higher. It is slightly difficult to determine the exact resonant energy, which seems to be around 52eV being slightly smaller than that of an Fe natural atom.

The presumption that the Fe 3d band is broader than 2eV may suggest two possibilities on the Fe 3d electron states. One is that the 3d electrons are not localized spatially like 3d electron bands in a usual transition metal. Another may be that the Fe atoms sit on various inequivalent sites. The 3d binding energy changes variously with sites in considering that the 3d electrons may be more or less localized. The 3d states are thus concluded to be located below E_F, which is not qualitatively inconsistent with the fact that the Fe atoms have almost no magnetic moments. But the energy position of 3d states is near E_F, and the validity of the interpretation[2] for the local moment formation seems to have to be examined quantitatively.

1) Ishimasa T, Fukano Y and Tsuchimori M, Phil. Mag. Lett. 58(1988)157
2) Matsuo S, Nakano H, Ishimasa T and Fukano Y, J. Phys.: Condens. Matter 1 (1989)6893
3) Mori M, Matsuo S, Ishimasa T, Matsuura T, Kamiya K, Inokuchi H and Matsukawa T, J. Phys.: Condens. Matter 3(1991)767

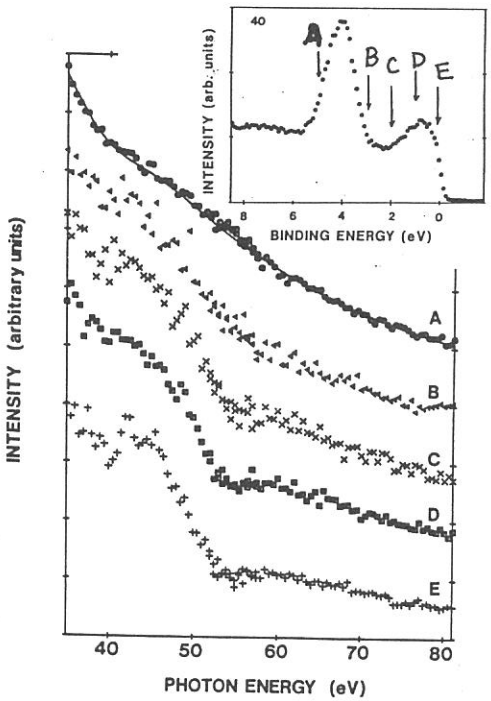

Fig. 1. CIS spectra for several binding energies. A, B, C, D and E corresponds to the spectrum at the binding energies 5eV, 3eV, 2eV, 1eV and 0.1eV, respectively.

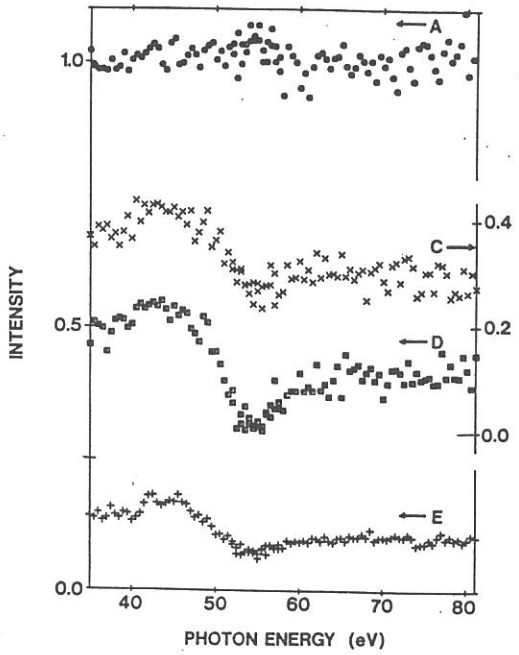

Fig. 2. Relative CIS spectra for several binding energies. The spectra A, C, D and E represent the CIS spectra of A, C, D and E, divided by the fitted spectrum, respectively.

IONIC FRAGMENTATION PROCESSES FOLLOWING Si:2p CORE LEVEL PHOTOEXCITATION OF 1,1,1-TRIMETHYLTRICHLORODISILANE ($Me_3SiSiCl_3$)

Shin-ichi NAGAOKA, Joji OHSHITA,* Mitsuo ISHIKAWA,*
Toshio MASUOKA,+ and Inosuke KOYANO#

Department of Chemistry, Faculty of Science, Ehime University, Matsuyama 790
*Department of Applied Chemistry, Faculty of Technology, Hiroshima University, Higashi-Hiroshima 724, Japan
+Department of Applied Physics, Osaka City University, Sumiyoshi, Osaka 558
#Department of Material Science, Faculty of Science, Himeji Institute of Technology, 1479-1 Kanaji, Kamigohri, Hyogo 678-12

In recent years, relaxation processes following core excitation in molecules have been a topic of much interest. We have investigated the dissociation processes following photoionization of 1,1,1-trimethyltrichlorodisilane (MCS) in the range of valence and Si:2p core-level ionization by means of the photoelectron-photoion and photoion-photoion coincidence methods (PEPICO and PIPICO methods, respectively). MCS has a structure given by $(CH_3)_3SiSiCl_3$ and the chemical environments of the two Si atoms are different from each other. Thus, we try to examine whether or not the site-specific fragmentation is observed in MCS.

The experiments were performed using a time-of-flight (TOF) spectrometer with variable path length, coupled to a constant-deviation grazing incidence monochromator installed on the BL3A2 beam line of the UVSOR synchrotron radiation facility in Okazaki.[1]

The total photoionizaion efficiency curve of MCS has two peaks near the 2p core-ionization threshold of the silicon atom bonded to three methyl groups (Si[Me]) (Fig. 1). One of these two peaks is assigned to the excitation of the Si[Me]:2p electron into an unoccupied orbital below the threshold. Autoionization

follows the excitation. The other peak is assigned to shape resonance coupled to the Si[Me]:2p continuum above the threshold. The excitation and ionization efficiency from the 2p core-level of the silicon atom bonded to three chlorine atoms (Si[Cl]) is very small.

Figure 2 shows an example of the TOF mass spectra in the PEPICO mode. The fragmentation scheme leading to the production of the ion pairs in MCS may be described as follows:

$$Me_3SiSiCl_3 + h\nu$$
$$\rightarrow Me_3SiSiCl_3^{+} + e \quad \text{(Si[Me]:2p ionization)}$$
$$\rightarrow Me_3SiSiCl_3^{2+} + e \quad \text{(LVV Auger)}$$
$$\rightarrow CH_m^{+} + C_2H_n^{+} \text{ (or } Si^{+}) + n.p.$$
$$\rightarrow H^{+} + CH_m^{+} + n.p.$$
$$\rightarrow H^{+} + SiCH_{m'}^{+} + n.p.$$

1. T. Masuoka, T. Horigome, and I. Koyano, Rev. Sci. Instr. 60, 2179 (1989); E. Ishiguro, M. Suzui, J. Yamazaki, E. Nakamura, K. Sakai, O. Matsudo, N. Mizutani, K. Fukui, and M. Watanabe, Rev. Sci. Instr. 60, 2105 (1989).

Fig. 1 (left-hand side) Total photoionization efficiency curve of MCS in the range 100-110 eV.
Fig. 2 (right-hand side) TOF mass spectrum of MCS taken by excitation at 105.5 eV in the PEPICO mode.

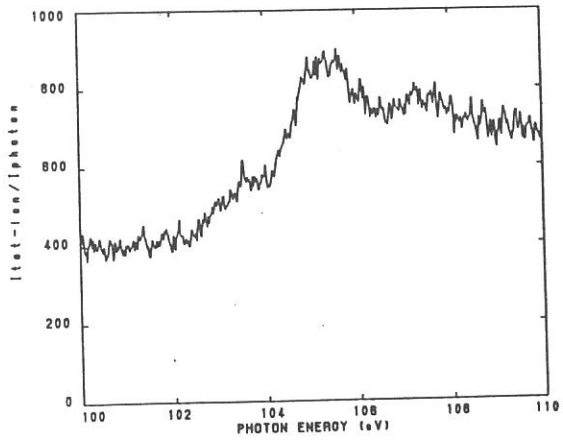

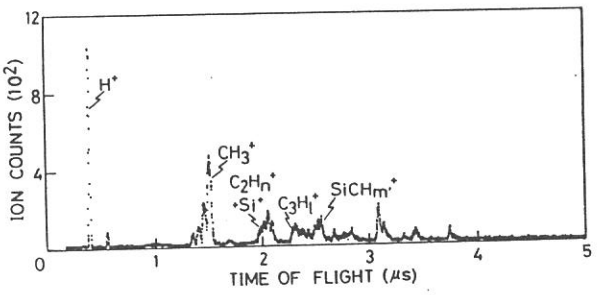

ENERGY PARTITIONING IN THE DISSOCIATION REACTION $Ar_3^+ \rightarrow Ar_2^+ + Ar$

Kenji FURUYA, Katsumi KIMURA, and Takato HIRAYAMA*

Institute for Molecular Science, Myodaiji, Okazaki 444

*Department of Physics, Gakushuin University, Toshima-ku, Tokyo 171

We have observed threshold-photoelectron photoion coincidence (TPEPICO) spectra of argon clusters in the region 82.00 - 85.00 nm. Figure 1 shows TPEPICO spectra observed at 83.00 nm and at stagnation pressures of 2620, 1970, and 1310 Torr. All the line shapes due to the Ar_2^+ ion appearing in the TPEPICO spectra have been appropriately simulated in terms of superposition of sharp and broad Gaussian functions , as shown in Fig. 2. The sharp Gaussian function corresponds to the ionization of the argon dimer, and the broad Gaussian function corresponds to the following reactions:

$$Ar_n + h\nu \rightarrow Ar_n^+ + e_{th}^- \rightarrow Ar_2^+ + Ar_{n-2}[\text{or}(n-2)Ar, \textit{etc.}] + e_{th}^-, \qquad (1)$$

where e_{th}^- means a threshold photoelectron. It should be noted that the Gaussian shape of the Ar_2^+ broad component is not caused by the contribution of the larger clusters than Ar_3, because the error of the simulation is independent of the stagnation pressure, as shown in Fig. 2. Therefore, we have found that the excess energy in the Ar_3 ionization and the successive dissociation of Ar_3^+ is thermally or quasi-thermally partitioned into the translational energies of the fragment species. The results reduced from the estimation of average kinetic energies of Ar_2^+ are summarized in Table I. We have found from Table I that the percentage of excess energy in Ar_3^+ that is partitioned into the total translational energy of the fragment species is dependent on the excitation energy and that the percentage is slightly less than the value (40%) predicted from the statistical theory. We have also found that complete dissociation of Ar_3^+ takes place in the excess energy range 0.3 - 1.1 eV.

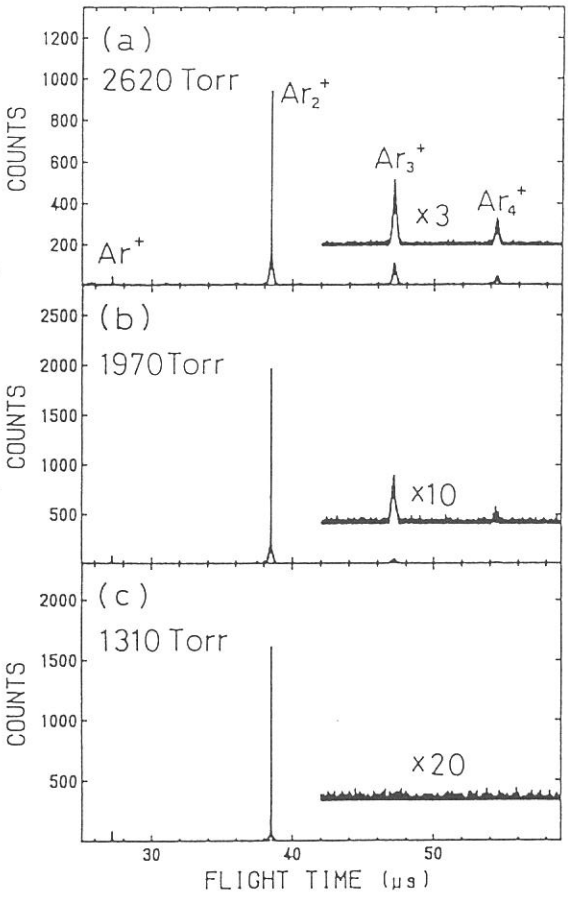

Figure 1. TPEPICO spectra of Ar clusters, observed at 83.00 nm and at stagnation pressures of (a) 2620 Torr, (b) 1970 Torr, and (c) 1310 Torr.

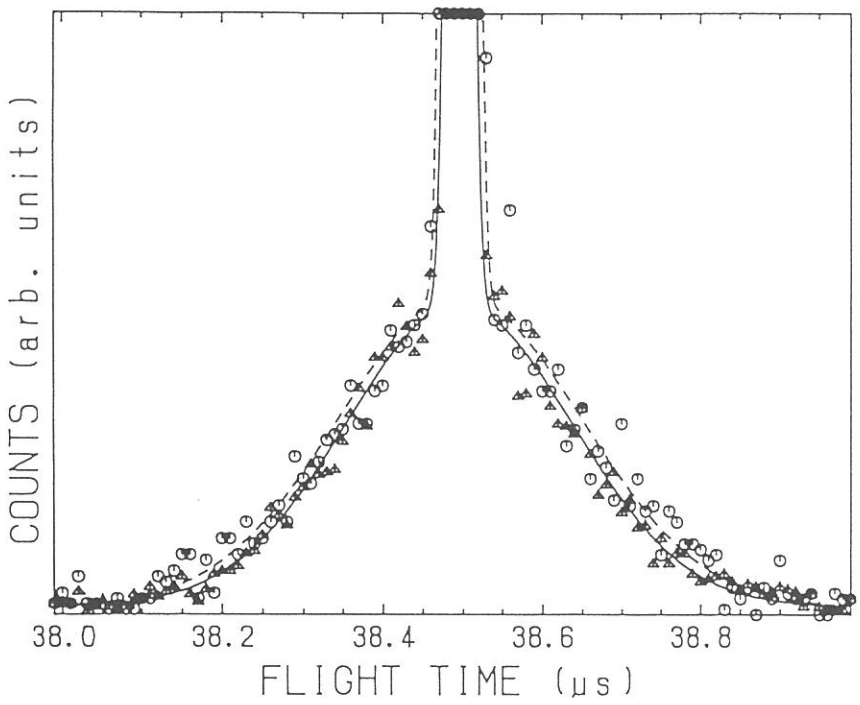

Figure 2. Ar_2^+ line shapes in Ar_n TPEPICO spectra observed at 83.00 nm and at stagnation pressures of 2620 Torr (triangles) and 1310 Torr (circles). The simulated spectra are indicated by solid and broken lines which correspond to triangles and circles, respectively. The simulated spectra have been normalized to the maximum of the broad bands.

Table I. Energy partitions obtained from TPEPICO spectra of Ar_2^+.

Wavelength (nm)	79.00	80.00	81.00	82.00	83.00
Energy (eV)	15.69	15.50	15.30	15.12	14.94
Excess energy (eV)[1]	1.117	0.921	0.730	0.543	0.361
Lower limit of FWHM (ns)[2,3]	584	555	457	410	375
Upper limit of FWHM (ns)[4]	656	635	505	468	409
Lower limit of Total KER (eV)[3]	0.332	0.300	0.203	0.163	0.136
Upper limit of Total KER (eV)[4]	0.420	0.393	0.248	0.213	0.162
Lower limit of KER/Excess energy (%)[3]	29.7	32.6	27.8	30.0	37.7
Upper limit of KER/Excess energy (%)[4]	37.6	42.7	34.0	39.2	44.9

[1]Estimated with IP(Ar_3) = 14.37 eV and D($Ar_3^+ \rightarrow Ar_2^+$) = 0.207 eV.

[2]The FWHM of the sharp Gaussian function is 26.5 ns.

[3]Observed at 1310 Torr.

[4]Extrapolated at 0 Torr.

A METHOD FOR TIME-RESOLVED MEASUREMENTS APPLIED ON INTRINSIC LUMINESCENCE IN ALKALI HALIDES

Tamao MATSUMOTO, Toshiya KAWATA, Akinori MIYAMOTO, Ken-ichi KAN'NO
Masami HASUMOTO* and Masao KAMADA*

Department of Physics, Kyoto University, Sakyo-ku, Kyoto 606
*Institute for Molecular Science, Myodaiji, Okazaki 444

Emission from different excited states which are characterized by different decay times may appear in a similar energy range, which results in a decay curve composed of more than one decay component. When decay times of the components differ appreciably each other, an appropriate spectrum of each component can be obtained by measuring the signal in a particular time range where the component is dominant. We report here a method of obtaining such time-resolved emission spectra applied under single-bunch operation of UVSOR.

In fig.1 is shown a schematic diagram of a detecting system. Signal pulses from an MCP photomultiplyer (Hamamatsu R2286U-06) are discriminated with a constant fraction discriminator (CFD) whose output signal is used as a start pulse for a time-to-amplitude converter (TAC). A stop pulse is taken from the RF signal synchronizing with the bunched light pulse. The positive output of the TAC, which would be stored in a multi-channel analyser (MCA) for obtaining decay curves, is divided into two channels of a quad single-channel analyser (SCA). Their upper levels and lower levels are adjusted to appropriate time ranges respectively, which are, for example, indicated as Δt_1 and Δt_2 in the figure. Outputs are stored in channel 2 and 3 of a quad counter for appropriate preset time (channel 1 is used as a time counter), and the counts are sent to a PC-98 personal computer through GPIB. The negative output of the TAC is directly stored in channel 4 of the counter, whose output gives the total count. Minimum window width of the quad SCA is 2mV, which corresponds to time duration of 36ps when gain of the TAC is set to convert 177.6ns (SR pulse interval) into 10V (maximum discriminater level of the SCA). Thus, if one scans photon energy of detecting the luminescence in an appropriate rate, two time-resolved emission spectra and a time-integrated spectrum are obtained simultaneously.

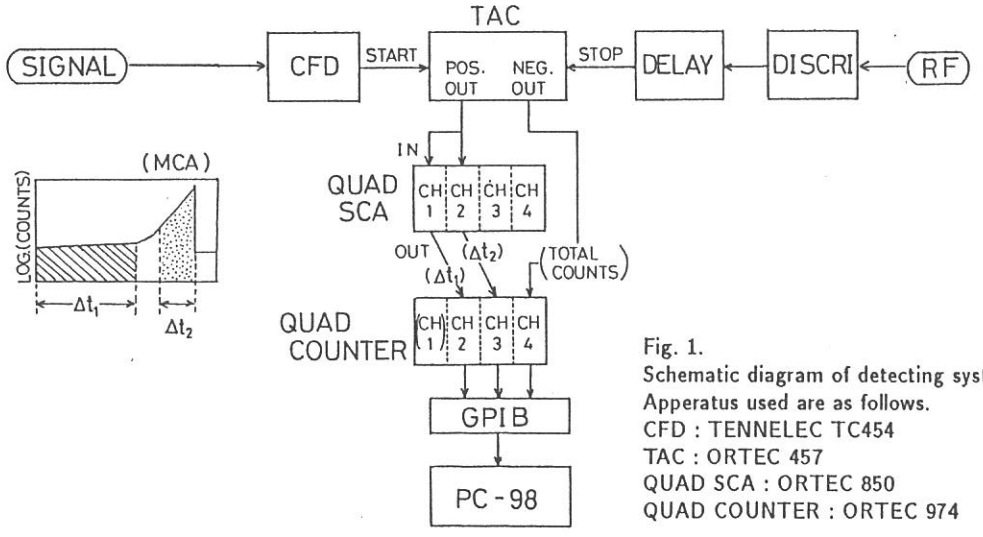

Fig. 1.
Schematic diagram of detecting system.
Apperatus used are as follows.
CFD : TENNELEC TC454
TAC : ORTEC 457
QUAD SCA : ORTEC 850
QUAD COUNTER : ORTEC 974

In fig.2 ~ fig.4 is shown an example of experimental results on intrinsic luminescenc in NaBr. Decay curve of this emission is shown in fig.2. It is composed of a fast decay component and a slow decay component. These components originate from the spin singlet level and the triplet one of the lowest excited state of self-trapped exciton respectively.[1] In fig.3 are shown its emission spectra obtained as mentioned above. Curve (a) represents total counts. Curve (b) represents counts in time range 30 ~ 130ns, which corresponds to hatched region in fig.2, where the triplet component is dominant. Curve (c) represents dotted region 0 ~ 5ns, where the singlet component is dominant. With scanning photon energy of SR pulses, time-resolved excitation spectra were also obtained (shown in fig.4). Curves (a) to (c) represent spectra of the same time ranges as fig.3. Interesting points made clear are as follows: 1) Lower peak energy of the singlet component than the triplet one (inset of fig.3), contrary to simple anticipation. 2) Less efficiency of stimulating the singlet component when the excitation is made into the higher energy tail of the lowest exciton absorption (~ 6.7eV). The latter is consistent with the previous result obtained by analysing decay curves.[2]

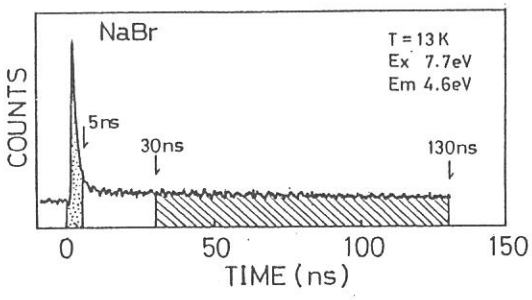

Fig. 2.
Decay curve of intrinsic emission in NaBr obtained under excitation into the interband transition with the 7.7eV light. Emission is detected at its peak energy of 4.6eV.

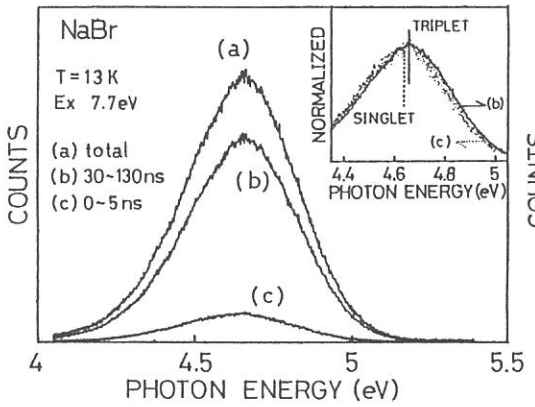

Fig. 3.
Time-integrated emission spectrum, (a), and time-resolved ones, (b) and (c), of NaBr excited at 7.7eV. In inset are shown (b), solid curve, and (c), dotted curve, normalized at their emission peaks.

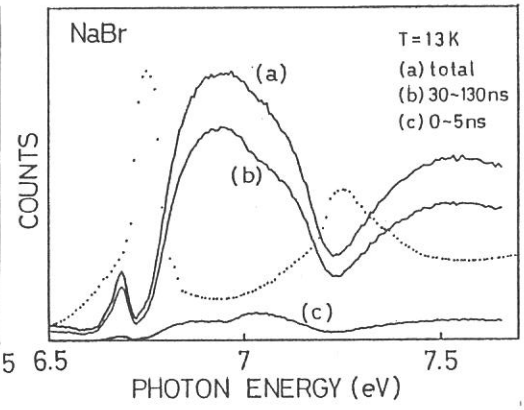

Fig. 4.
Time-integrated excitation spectrum, (a), and time-resolved ones, (b) and (c), for the STE luminescence of NaBr. Dotted curve is absorption spectrum reported by Teegarden and Baldini.[3]

REFERENCES

1) K.Kan'no, K.Tanaka and T.Hayashi : Rev. Solid State Science 4 (1990) 383.
2) K.Kan'no, K.Tanaka, H.Kosaka,Y.Nakai and K.Toyoda : UVSOR Activity Report (1989) 42.
3) K.Teegarden and G.Baldini : Phys. Rev. 155 (1967) 896.

DECAY PROFILE OF THE σ EMISSION BAND IN KBr

Tamao MATSUMOTO and Ken-ichi KAN'NO

Department of Physics, Kyoto University, Sakyo-ku, Kyoto 606

In the last few years, a new stage has been brought to understanding of self-trapped exciton (STE) luminescence in alkali halide crystals.[1] The most important point made clear is that the STE luminescence bands are classified into three types, I, II and III, irrespective of the traditional classification into two categories (σ and π bands).[2] This means that there appear, at most, three distinct local minima in the adiabatic potential energy surface (APES) of the singlet-triplet pair of the lowest energy. It will be important to see how the shape of the APES is, and how the population is fed into each minimum. In this connection, one of the urgent topics to be studied is the origin of the short lifetime singlet σ emission band, and its relation to the longer lifetime triplet π luminescent state.

We have studied precisely a decay profile of the σ emission band (4.4 eV) in KBr at $\sim$13K using TAC method under single-bunch operation of UVSOR (BL1B). Counting photons with a wide dynamic range over four orders of magnitude has revealed existence of a phosphorescent component piled-up with a lifetime ($\sim$ 500ns) longer than the time interval 177ns of SR pulses, in addition to the main fluorescent component of the short lifetime 3.3ns and the component of an intermediate lifetime around 20ns. In Fig. 1 is shown a typical result obtained under excitation with the 7.7 eV light, which falls into the band-to-band transition region. Dark counts of an MCP have already been carefully subtracted. Solid lines show the decomposition of the decay curve into the three exponentials. Percentage of the integrated intensity of each component to the total emission intensity is also given in the figure. The phosphorescent component was confirmed to have almost the same emission and excitation spectra as those of the fluorescent component by measuring time-resolved spectra with use of the method described in this issue.[3] Quite a similar situation has been confirmed also in the σ emission bands of NaCl, RbBr, KI, and RbI. Thus, it is most likely that the σ emission band is, in general, composed of not only the singlet decay component but also components originating from the triplet levels of type I configuration.

During the course of study, we found that the decay profile of the σ emission in KBr varies appreciably depending on exposure time of the excitation light. That is, the relative intensity ratio of the slow decay component to the main singlet component increases apparently after prolonged exposure. This is because of a partial quenching of the singlet component: As shown in Fig. 2, the decay time of the singlet component becomes short from 3.3ns to 2.9ns. Its integrated intensity decreases down to less than a half, while that of the slow decay component remains almost constant. These results suggest that defects formed affect the relaxation process into the lowest singlet STE level selectively.

References

1) W.B. Fowler and N. Itoh (editors), Rev. Solid State Sci. 4, 357-465 (1990).

2) K. Kan'no, K. Tanaka and T. Hayashi, Rev. Solid State Sci. 4, 383 (1990).

3) T. Matsumoto, T. Kawata, A. Miyamoto, K. Kan'no, M. Hasumoto and M. Kamada, UVSOR Activity Report (1991, this issue).

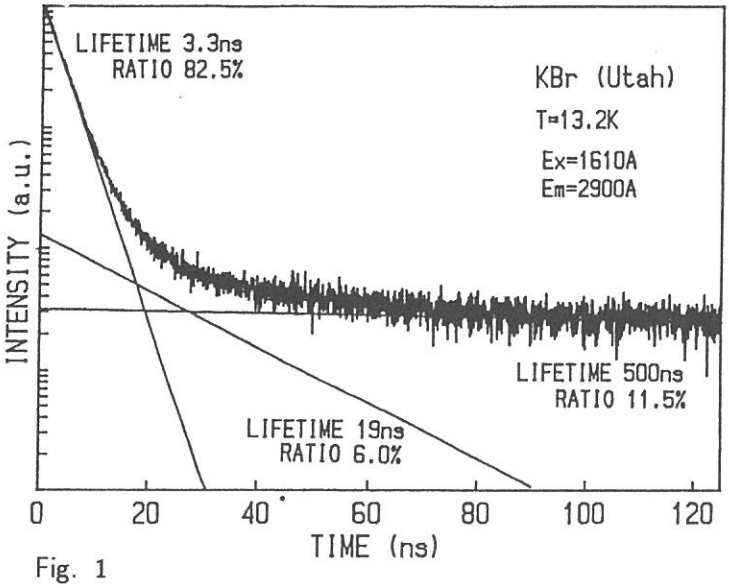
LIFETIME 3.3ns
RATIO 82.5%
KBr (Utah)
T=13.2K
Ex=1610A
Em=2900A
INTENSITY (a.u.)
LIFETIME 500ns
RATIO 11.5%
LIFETIME 19ns
RATIO 6.0%
0
20
40
60
80
100
120
TIME (ns)

Fig. 1

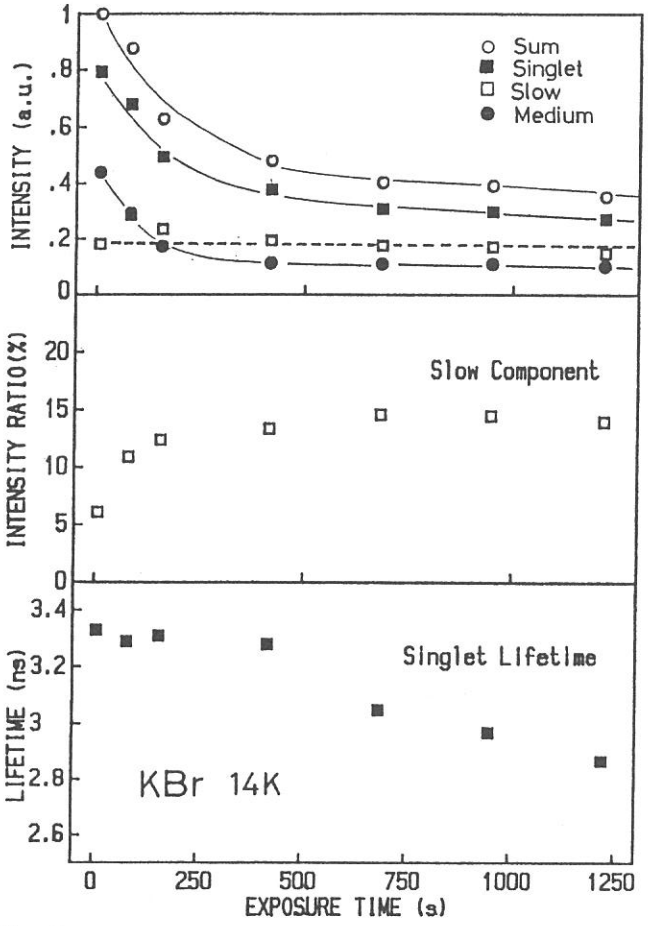
Sum
Singlet
Slow
Medium
INTENSITY (a.u.)
1
.8
.6
.4
.2
0
INTENSITY RATIO(%)
Slow Component
20
15
10
5
0
LIFETIME (ns)
Singlet Lifetime
3.4
3.2
3
2.8
2.6
KBr 14K
0
250
500
750
1000
1250
EXPOSURE TIME (s)

Fig. 2

ANGLE-RESOLVED PHOTOEMISSION STUDY OF $Bi_2Sr_2Ca_{1-x}Y_xCu_2O_8$ (x=0.0, 0.2, 0.4, 0.6) SINGLE CRYSTALS

Toshiaki KUSUKOKI[1], Takashi TAKAHASHI[1], Hiroshi KATAYAMA-YOSHIDA[1],
Koji KAMIYA[2] and Hiroo INOKUCHI[2]
[1]Department of Physics, Tohoku University, Sendai 980, Japan
[2]Institute for Molecular Science, Okazaki 444, Japan

The existence of the Fermi-liquid states in high-Tc superconductor has been well established by angle-resolved photoemission spectroscopy (ARPES)[1-4]. A next step to understand the high-Tc mechanism is to elucidate the process of formation of the Fermi-liquid states. We have already reported a comparative ARPES study of superconductive and non-superconductive $Bi_2Sr_2Ca_{1-x}Y_xCu_2O_8$(x=0.0 and 0.6)[5]. In this paper, we report a comprehensive ARPES study of a series of $Bi_2Sr_2Ca_{1-x}Y_xCu_2O_8$ (x=0.0, 0.2, 0.4, and 0.6) single crystals. In the course of study, we have paid a special attention to the change of the electronic structure in the vicinity of the Fermi level from non-superconductor to superconductor and from superconductor to normal metal.

Single crystals of $Bi_2Sr_2Ca_{1-x}Y_xCu_2O_8$ were grown with a self-flux method. The atomic ratio between Ca and Y was determined by EPMA (Electron-Probe-Micro-Analysis) and x-ray diffraction analysis of c-axis length[6]. The resistivity measurement of the crystals showed that the crystals of x=0.0 and 0.2 have Tc of 80K and 85 K, respectively. The non-doped crystal (x=0.0) is in so-called over-doped region. The crystal of x=0.6 did not show superconductivity even at 4K, while the crystal of x=0.4 showed an incomplete resistivity drop at 50K but again behaved like an insulator in the lower temperature.

Photoemission measurement was performed at BL8B2. The crystal was cleaved in the spectrometer to obtain a clean flat crystal surface and was kept at room temperature during the measurement. The spectrum was recorded at the energy resolution of about 0.15eV.

Figure 1 shows comparison of ARPES spectra in the vicinity of the Fermi level of $Bi_2Sr_2Ca_{1-x}Y_xCu_2O_8$ (x=0.0-0.6). The spectra were measured at the polar angle of emitted electrons of 0 , which represent the Γ point in the Brillouin zone. As shown in Fig.1, the intensity of spectrum at the Fermi level gradually increase with the hole-concentration, in other words with decreasing the Y content (x). This clearly shows that hole-doping does not necessarily cause a rigid shift of the density of states relative to the Fermi level but creates new electronic states in the vicinity of the Fermi level.

Figure 2 shows comparison of the whole valence band structure determined from ARPES measurement for these crystals of x=0.0 (open circles), 0.4 (triangles), and 0.6 (filled circles). It is noticed again that there are no dispersive bands near the Fermi level for an insulator (x=0.6). As for x=0.4, we find small structure near the Fermi level, but they do not touch apparently the Fermi level. It is remarked that band C is sensitively shifted by hole-doping from 2.3eV for x=0.6 to 1.4eV for x=0.0. In contrast with the remarkable change in the small-binding-energy region, such a large change is not found in the higher-binding-energy region (bands D-F), except for a slight energy shift of 0.2-0.3eV. These experimental results again show that the change of the electronic structure caused

by hole-doping in not a simple rigid shift of bands.

Figure 3 shows comparison of the experimental bands structure near the Fermi level between the crystals of x=0.0 (open circles) and x=0.2 (filled circles). As shown in Fig.3, the both crystals have two dispersive bands which cross the Fermi level, and the bands of x=0.2 are shifted as a whole toward the high binding energy direction by 0.1-0.2eV. This suggests that a rigid band picture may be recovered in the "over-doped" region.

In summary , the experimental result of a comprehensive angle-resolved photoemission study on a series of $Bi_2Sr_2Ca_{1-x}Y_xCu_2O_8$ (x=0.0-0.6) single crystals show that (1) hole-doping in an insulator (x=0.6) produces new electronic states in the charge-transfer gap and (2) a rigid-band picture may be recovered in the "over-doped" region (x=0.0, 0.2)

References

1. T.Takahashi et al., Nature 334 (1988) 691.
2. C.G. Olson et al., Science 245 (1989) 731.
3. T. Manzke et al., J. Euro. Phys. Lett. 9 (1989) 477.
4. J. C. Campuzano et al., Phys. Rev. Lett. 64 (1990) 2308.
5. T. Takahashi et al., Physica C 170 (1990) 416.
6. T. Tamegai et al., Jpn. J. Appl. Phys., 28 (1989) 112.
7. S. Massida et al., Physica C 152 (1988) 251.

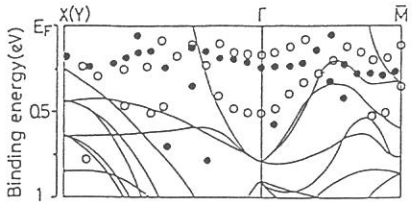

Figure 3

Comparison of the experimental band structure near the Fermi level of $Bi_2Sr_2Ca_{1-x}Y_xCu_2O_8$ [x=0.0 (open circles) and x=0.2 (filled circles)]. Note that dispersive bands of x=0.2 are shifted as a whole relative to those of x=0.0 toward the higher-binding-energy direction by 0.1-0.2eV.

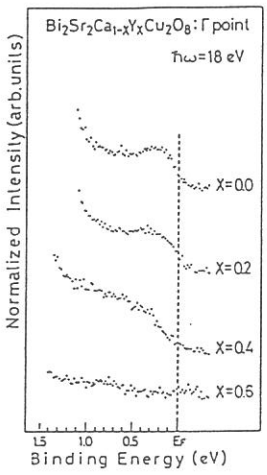

Figure 1

Comparison of angle-resolved photoemission spectra in the vicinity of the Fermi level for $Bi_2Sr_2Ca_{1-x}Y_xCu_2O_8$ (x=0.0-0.6). All spectra were measured at the polar angle of 0° , representing the Γ point in the Brillouin zone.

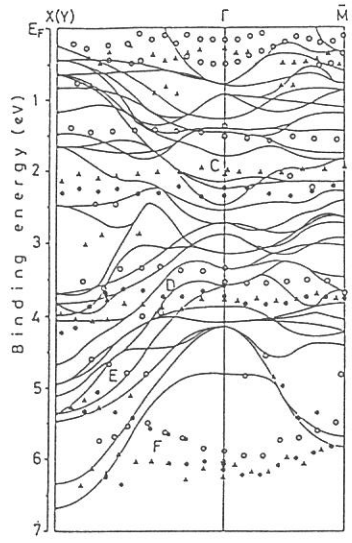

Figure 2

Comparison of whole valence band structure between $Bi_2Sr_2Ca_{1-x}Y_xCu_2O_8$, where x=0.0 (open circles), 0.4 (triangles), and x=0.6 (filled circles). A representative band structure calculation[7] is shown by this solid lines for comparison.

COPPER L_{III} ABSORPTION STUDY OF $La_{2-x}Sr_xCuO_4$ (x=0.0-0.5) AND NONSUPERCONDUCTIVE COPPER OXIDES

Satoru SUZUKI, Takashi TAKAHASHI, Shigeru SATO
and Hiroshi KATAYAMA-YOSHIDA
Department of Physics, Tohoku University, Sendai 980

We measured the copper L_{III} absorption spectra of $La_{2-x}Sr_xCuO_4$ in the wide range of the Sr content in order to study the change of the electronic structure from the insulator to the "normal" metal via the superconductor. We also measured the copper L_{III} absorption spectra of various nonsuperconductive copper oxides; $Sr_2CuO_2Cl_2$ (abbreviated by SCOC), $La_4BaCu_5O_{13}$ (LBCO) and $La_{1.9}Sr_{1.1}Cu_2O_6$ (LSCO) to study the reason why they do not show the superconductivity.

Copper L_{III} absorption spectra were measured at BL7A with the total-photoelectron-yield method at the energy resolution of about 0.3 eV. Samples were scraped with a diamond file in the vacuum chamber just before the measurement to obtain a fresh and clean surface.

Figure 1 shows a series of the copper LIII absorption spectra of $La_{2-x}Sr_xCuO_4$ (x=0.0 - 0.5). It is known that $La_{2-x}Sr_xCuO_4$ is an insulator at x=0.0, and becomes a superconductor by the Sr-doping with the highest superconducting transition temperature of 35K at x=0.15, then changes to a "normal" metal around x=0.3. In the spectra, we find two prominent structures at 930 eV and 932.5 eV, respectively. The former is ascribed to the $3d^{10}$ final state and the latter is due to the $3d^{10}\underline{L}$. It is found in the figure that the $3d^{10}\underline{L}$ state grows with the Sr-doping, which indicates that the doped holes are accommodated mainly in the oxygen 2p orbital. It is also found in the figure that there are no sudden changes from x=0.0 to 0.5. This means that there are no discontinuous changes in the electronic states at least in the copper site in $La_{2-x}Sr_xCuO_4$ even when they change from insulator to "normal" metal via superconductor. This is in good agreement with the oxygen K absorption measurement for the same compounds.[1)]

Figure 2 shows the copper L_{III} absorption spectra of the above-mentioned three nonsuperconductive copper oxides. It is known that SCOC is an insulator while the others (LBCO and LSCO) are metals. It is found in the figure that LBCO has a large weight of the $3d^{10}\underline{L}$ component comparable to that of $La_{2-x}Sr_xCuO_4$ at x=0.4. This suggests that LBCO is heavily doped and the over-doped holes prevent the appearance of superconductivity. The spectral shape of LSCO is similar to that of $La_{2-x}Sr_xCuO_4$ at x=0.1, so that the amount of the

doped holes may be appropriate for the appearance of the superconductivity. The absence of the superconductivity may be due to its inherent randomness of position of oxygen atoms connecting the CuO_2 sheets. The absence of superconductivity in SCOC is due to the lack of the $3d^9\underline{L}$ ground state as found in Fig. 2.

Reference

1. T. Takahashi, H. Matsuyama, T. Watanabe, H. Katayama-Yoshida, S. Sato, N. Kosugi, A. Yagishita, S. Shamoto, and M. Sato, Proc. 3rd Int. Symp. Superconductivity (Springer, 1991), p.75.

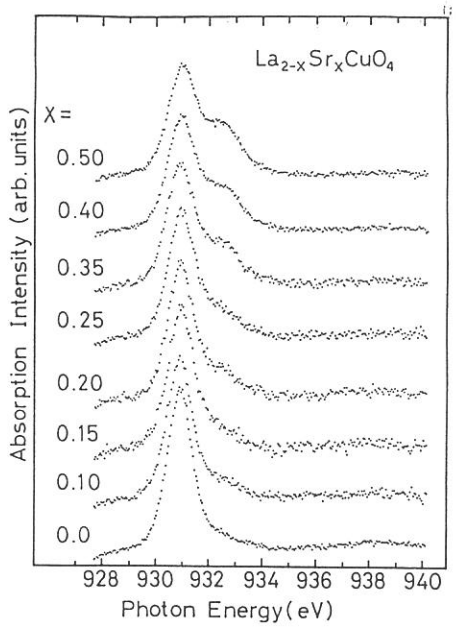

Figure 1
Copper L_{III} absorption spectra of $La_{2-x}Sr_xCuO_4$ (x=0.0 - 0.5)

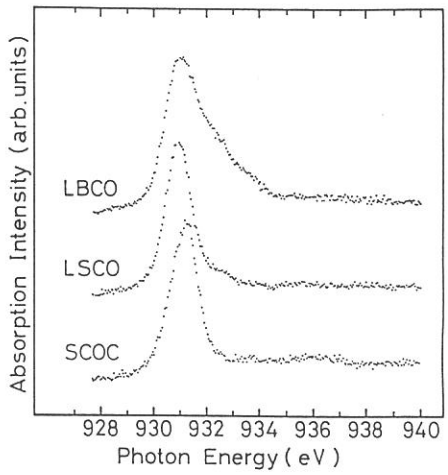

Figure 2
Copper L_{III} absorption spectra of $Sr_2CuO_2Cl_2$ (SCOC), $La_4BaCu_5O_{13}$ (LBCO) and $La_{1.9}Sr_{1.1}Cu_2O_6$ (LSCO)

PHOTOEMISSION STUDY OF C_{60} AND ITS ALKALI-METAL COMPOUNDS

Takashi TAKAHASHI[1], Takashi MORIKAWA[1], Hiroshi KATAYAMA-YOSHIDA[1], Kazuhiko SEKI[2], Hitoshi FUJIMOTO[3], Shojun HINO[4], Shinji HASEGAWA[5], Koji KAMIYA[5], Hiroo INOKUCHI[5], Koichi KIKUCHI[6], Shinzo SUZUKI[6], Kun IKEMOTO[6], and Yoji ACHIBA[6]

[1]Department of Physics, Tohoku University, Sendai 980
[2]Department of Chemistry, Nagoya University, Nagoya 464
[3]Department of Chemistry, Kumamoto University, Kumamoto 860
[4]Department of Image Science and Technology, Chiba University, Chiba 260
[5]Institute for Molecular Science, Okazaki 444
[6]Department of Chemistry, Tokyo Metropolitan University, Tokyo 192-03

A recent report of occurrence of superconductivity of solid C_{60}[1] doped with alkali metal (K[2], Tc=18K or Rb[3,4], Tc =28K) has provoked much interests in the electronic structure of C_{60} and its variation with alkali-metal doping. In this report, we present the first photoemission study of Rb-doped C_{60}, together with K-doped one for comparison.

C_{60} powders were produced by arc-discharge method with graphite rods and separated with high-pressure liquid chromatography. Photoemission measurement was done at BL8B. The photoemission spectrum was recorded with the energy resolution of about 0.15 eV. A thin film for photoemission measurement was prepared by in-situ vapor-deposition of C_{60} powder on a gold-coated molybdenum substrate and subsequent successive deposition of alkali metal with a SAES getter. In order to characterize the film thus prepared, we monitored the electrical resistivity of a film deposited on a quartz substrate placed just next to the photoemission sample by a van der Pauw method. The Fermi level of the sample was referred to that of gold deposited on the sample.

Figure 1 shows the variation of room-temperature resistivity of a C_{60} film upon a successive Rb-deposition. The resistivity drops rapidly with Rb-doping, reaches the minimum value five order smaller than that of pure C_{60}, and then increases with further doping. This behavior is consistent with a previous report.[5]

Figure 2 shows valence-band photoemission spectra of C_{60} and Rb_xC_{60} measured with photon energy of 20 eV. The Rb-doped film was prepared by 60 min-deposition and x is estimated to be 3-4 from the discussion below. The spectrum of a C_{60} film shows a rich structure reflecting its molecular nature and is in good agreement with a previous measurement with higher-photon energy.[6] The first band (HOMO band) located at 2.5 eV is ascribed to the five-fold degenerated h_u state and the second one to a composite of the h_g and g_g states.[7] We find that a new band appears near the Fermi level for the Rb-doped film.

Figure 3 shows the change of photoemission spectrum in the vicinity of the Fermi level upon successive Rb-doping. A slight addition of Rb (5- min deposition) to C_{60} causes a rigid shift of the valence band toward the high-binding-energy direction by 0.3 eV and at the same time a broad band having a clear Fermi edge appears between the Fermi level and the HOMO band. Further deposition increases the intensity of this broad band and it is remarked that this broad band has a doublet structure with the subbands at 0.3 and 0.9 eV, respectively. The appearance of a broad band with a doublet structure upon alkali-metal doping obviously contradicts a simple-band-filling model. It is remarked that further doping after 25 min increase the intensity of only the first subband closer to the Fermi level. The energy separation between this first subband and the HOMO band (about 1.7 eV) is very close to the energy separation between the HOMO and the LUMO band observed for C_{60}^- ion.[8] Rb-doping of 5 min to 45 min causes a gradual shift of the HOMO and the second bands toward the Fermi level. This direction is just opposite expected from a simple-band-filling model, suggesting again an overall reconstruction of the band structure by Rb-

doping. When the resistivity of the film shows the minimum (45 min-deposition in Fig. 1), the HOMO band approaches closest to the Fermi level and the density of states at the Fermi level shows the maximum. The composition of the film at this stage is estimated to be Rb_3C_{60}.[5] Further doping after 45 min causes a shift of the spectrum as a whole again toward the high-binding-energy direction and as a result the density of states at the Fermi level decreases and finally almost disappears, indicating that the film becomes less conductive. This behavior is in good agreement with the result of the resistivity measurement in Fig. 1. A quite similar result in photoemission spectrum and its correlation to the resistivity was obtained for K_xC_{60} , although a doublet structure in the broad band near the Fermi level is not well resolved in K_xC_{60}, suggesting a small difference in modifying the electronic structure of C_{60} between K and Rb .

References

1. W. Kratschmer et al., Nature 347 (1990) 354.
2. Hebard et al., Nature 350 (1991)600.
3. M.J. Rosseinsky et al., Phys. Rev. Lett. 66 (1991) 2830.
4. K. Holczer et al., Science 252 (1991) 1154.
5. R.C. Haddon et al., Nature 350 (1991) 320.
6. J.H. Weaver et al., Phys. Rev. Lett. 66 (1991) 1741.
7. S. Saito and A. Oshiyama, Phys. Rev. Lett. 66 (1991)2637.
8. R.F. Curl and R.E. Smalley, Science 242 (1988) 1022.

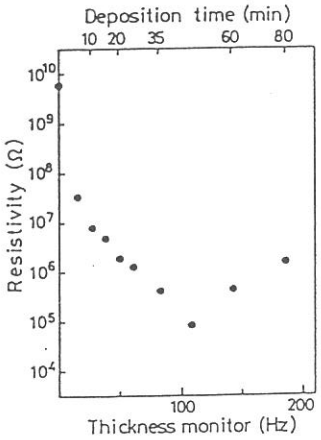

Fig. 1 Change of resistivity of a C60 film upon Rb-doping.

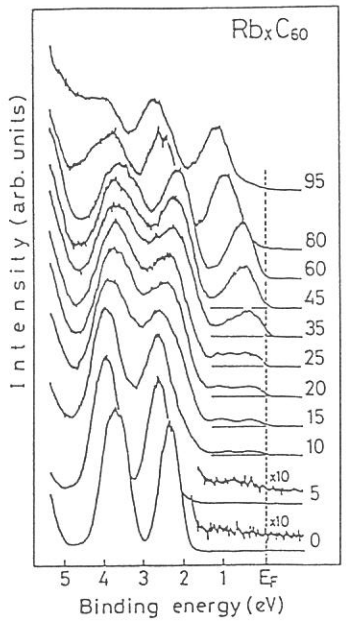

Fig. 3 Change of photoemission spectrum of a C60 film upon successive Rb-doping. Deposition time is indicated on each spectrum.

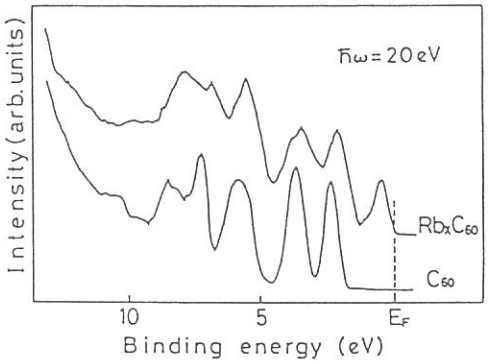

Fig. 2 Valence-band photoemission spectra of pure C60 and RbxC60 (x=3-4).

POLARIZED REFLECTION SPECTRA OF ORTHORHOMBIC $PbCl_2$ AND $PbBr_2$

Masami FUJITA, Hideyuki NAKAGAWA,[+] Kazutoshi FUKUI,[+]
Atsuhiko KASHINO,[+] Hiroaki MATSUMOTO,[+] Takeshi MIYANAGA[++]
and Makoto WATANABE[+++]

Maritime Safety Academy, Wakaba, Kure 737
[+]*Department of Electrical and Electronics Engineering,*
Faculty of Engineering, Fukui University, Fukui 910
[++]*Department of Physics, Faculty of Education,*
Wakayama University, Wakayama 640
[+++]*Institute for Molecular Science, Myodaiji, Okazaki 444*

$PbCl_2$ and $PbBr_2$ have the orthorhombic layered structures of D_{2h}^{16} (*Pmnb*) space group. In order to investigate the electronic states in these biaxial crystals, optical study using polarized light is necessary. In the present study,[1] polarized reflection spectra were measured up to 30 eV using the 1 m Seya-Namioka type monochromator at BL1B in UVSOR.

Figure 1 shows reflection spectra of cleaved surfaces of $PbCl_2$ at 45 K and $PbBr_2$ at 27 K for polarization parallel to the *a*-axis (*E//a*) or *b*-axis (*E//b*) below 12 eV. Sharp structures are observed clearly. The excitons in orthorhombic lead halides are regarded as Frenkel-type excitons corresponding to the $6s^2 \rightarrow 6s6p$ intraatomic excitation in Pb^{2+} ion. By comparison of the spectra of lead halides with those of Pb^{2+} doped alkali halides,[2] the first exciton band at 4.7 eV of $PbCl_2$ and at 3.9 eV of $PbBr_2$ are assigned to the $^1S_0 \rightarrow {}^3P_1$ transition in Pb^{2+} ion, and the prominent peak at 6.5 eV of $PbCl_2$ and the structures around 5.7 eV of $PbBr_2$ are attributed to the transition to the $^1P_1$ state. The peaks at 5.9 eV of $PbCl_2$ and at 4.9 eV of $PbBr_2$ observed for *E//b* are tentatively assigned to the transition to the $^3P_2$ state.

Three sharp peaks are found in the 20-25 eV region as shown in Fig. 2. They are ascribed to the Pb^{2+} 5*d* core exciton transition. Energy position and relative intensity of each peak depend only slightly on the polarization. Three transitions to the excited state of $^3P_1$, $^1P_1$ and $^3D_1$ are allowed from the $^1S_0$ ground state, in the intermediate coupling scheme of atomic excitation picture ($5d^{10}6s^2 \rightarrow 5d^9 6s^2 6p$). Relative intensities and energy

splittings of the observed peaks are explained well based on the atomic excitation model neglecting the crystal field effect.[1] This is in contrast to the case of Cd^{2+} $4d$ core exciton in cadmium halides.[3] The spectra of the Cd^{2+} $4d$ core exciton are explained in terms of spin-orbit splitting of the $4d$ core level and crystal field splittings of the $4d$ and $5p$ levels of Cd^{2+} ion.

References

1) M. Fujita, H. Nakagawa, K. Fukui, H. Matsumoto, T. Miyanaga and M. Watanabe: J. Phys. Soc. Jpn. 60(1991)4393.
2) A. Fukuda: Sci. Light 13(1964)64.
3) M. Fujita, H. Nakagawa, N. Kitagata, H. Matsumoto, T. Miyanaga, K. Fukui and M. Watanabe: J. Phys. Soc. Jpn. 60(1991)1792.

Fig. 1. Reflection spectra of $PbCl_2$ and $PbBr_2$ below 12 eV.

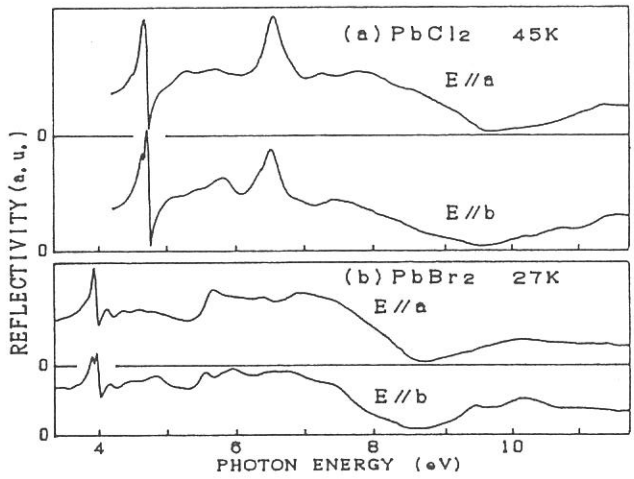

Fig. 2. Reflection spectra of $PbCl_2$ and $PbBr_2$ in the Pb^{2+} $5d$ core exciton region.

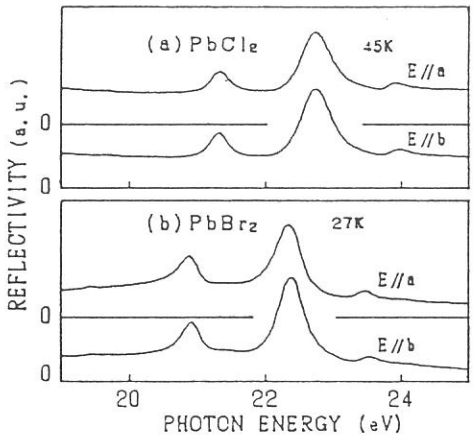

ABSORPTION AND LUMINESCENCE SPECTRA OF HIGH-PURITY SILICA GLASS

Yoshimichi OHKI, Takayuki SOTA, Hiroyuki NISHIKAWA,
and Ryuta NAKAMURA
Department of Electrical Engineering, Waseda University,
3-4-1 Ohkubo, Shinjuku-ku, Tokyo 169

Absorption and luminescence spectra were measured on high-purity silicas using synchrotron radiation from a storage ring installed in Institute of Molecular Science, Okazaki, Japan. The radiations were dispersed by a 1m Seya-Namioka type monochromator. Samples used in the experiments are high-purity silica glasses prepared by soot, plasma, and direct methods. The characteristics of the samples are listed in Table 1. Figure 1 shows the vacuum-ultraviolet absorption spectra of samples A to D. Each sample exhibits characteristic feature associated with various diamagnetic centers or impurities. Oxygen-deficient silica A shows a peak at 7.6 eV due to oxygen vacancy (≡Si-Si≡) [1,2]. The oxygen-surplus B shows a broad feature associated with oxygen-excess type defect (≡Si-O-O-Si≡) [1,2]. High-OH silica C produced with direct method exhibits absorption at about 8 eV, while silica D produced with soot shows no absorption bands even at 8 eV. Figure 2 shows luminescence spectra of oxygen-deficient silica A. Silica A exhibits a luminescence band at 4.3 eV. It is found that the 4.3-eV luminescence has an excitation peak at 5.0 and 6.7 eV. The 4.3-eV is considered to be correlated with the oxygen vacancy defect.

1. Imai et al. Phys. Rev. B 38, 12772 (1988).

2. Tohmon et al. Phys. Rev. B 39, 1337 (1989).

Table I. Sample list

Sample	Preparation method	Impurity (ppm) Cl	OH
A	Soot	0.3	free
B	$Ar+O_2$ plasma	370	0.46
C	Direct	free	1000
D	Soot	0.3	270

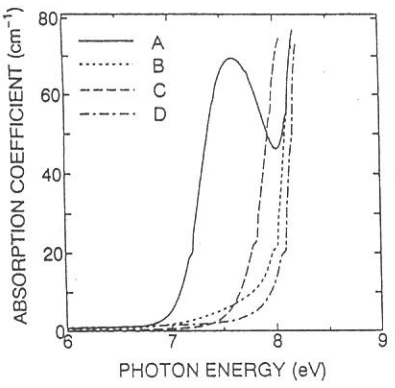

FIG.1 Absorption spectra of samples A(oxygen deficient), B(oxygen surplus), C(high-OH), and D(high-OH).

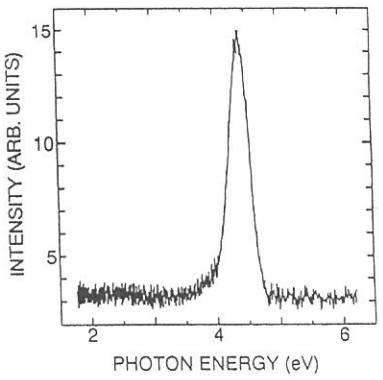

FIG.2 Luminescence spectra of oxygen-deficient sample A when excited at 6.7 eV (185 nm).

PHOTOLUMINESCENCE IN KBr THIN LAYERS DEPOSITED ON KCl AND LiF SUBSTRATE.

Arisato EJIRI, Akira HATANO and Kazumichi NAKAGAWA*

Dept. of Pure and Applied Sciences, University of Tokyo, 3-8-1 Komaba, Meguroku, Tokyo 153
*Faculty of Education, Kobe University, 3-11 Tsurukabuto, Nadaku, Kobe 659

Photoluminescence in alkali halide single crystals has been well investigated by several authors[1-3]. The present study intends to observe the behaviors of UV-excited carriers in the conduction band as well as in the valence band of alkali halide multilayers. As the first step of this intention, UV-excited luminescence in several KBr thin layers (20,10,5nm) deposited on KCl and LiF single crystal substrate is studied at 30k at BL-1B. Luminescence spectra are measured in the wavelength region from 200nm to 600nm by using a Jobin-Yvon grating monochromator. Luminescence in KCl, KBr and LiF single crystals is also measured for comparison. Observed absorption spectra of the KBr layers on KCl indicate the existence of weak interface mixture[4].

In these thin KBr layers, intrinsic luminescence σ band is first observed at about 280nm for UV-excitation at several wavelengths shorter than 181.6nm(6.83eV) which corresponds to the first exciton energy. In Fig 1, the σ bands in KBr(20nm) on KCl and in KBr(10nm) on LiF are shown together with the band in KBr single crystal. The band in KBr single crystal excited at 7,55eV, higher than the interband threshold energy, is at 4.43eV which is very close to the previous results 4.42eV[1,2]. The band of KBr on LiF excited at 8.37eV is, however, at 4.38eV and that of KBr on KCl excited at 7.8eV is at 4.53eV.

In the case of KBr on KCl, the energy position of the band excited by 7.8eV light significantly increases for decreasing of the KBr thickness as shown in Fig 2. These shifts are much larger than the blue shift of

absorption band of the first exciton observed. It is also found that the intensities of the band does not depend uniformly on the KBr thickness but on a different manner, where the band of KBr 10nm is significantly larger than others. These phenomena are not observed in the low-energy (7,2eV)-excited σ band in KBr on KCl, and also in KBr on LiF excited at 8.37eV which is much lower than the threshold energy of LiF.

As an origin of these phenomena, it can be imagined that the photoexcited carriers in the substrate (KCl) are diffused into the KBr layer and relaxed in the layer, because the KCl first exciton is excited at 7.8eV, whereas this cannot be excited at 7.2eV. The mechanism of the large blue shift of the σ band cannot be explained at this moment, however, it may be due to some influences of the KCl-KBr interface mixture.

Reference
1) M. V. Kabler; Phys. Rev. 30 (1964) 1296.
2) M. Ikezawa and T. Kojima; J. Phys. Soc. Jpn. 27 (1969) 1551.
3) M. Yanagihara, Y. Kondo and H. Kanzaki; J. Phys. Soc. Jpn. 52 (1983) 4937.
4) A. Ejiri, K. Nakagawa and A. Hatano; Physica Scripta 41 (1990) 95.

Fig. 1

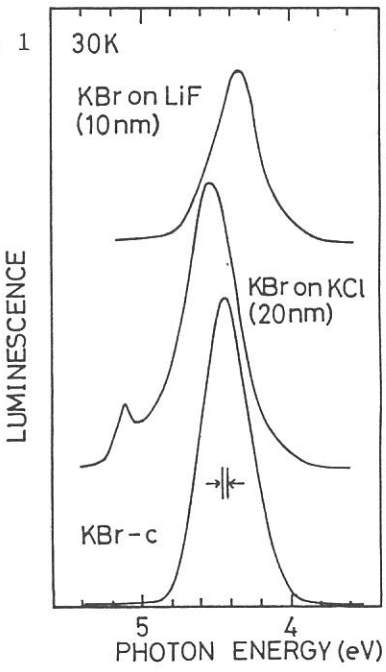

Fig. 2

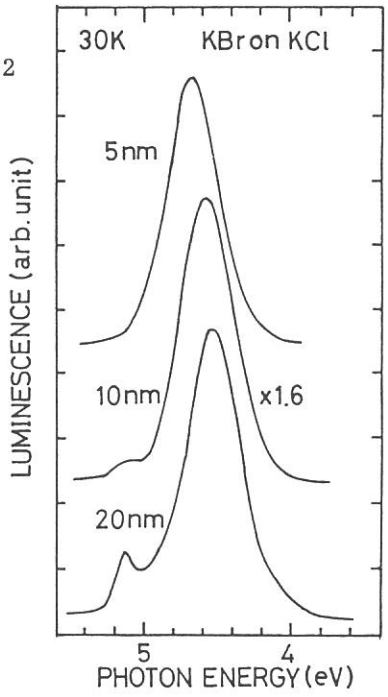

AUGER-FREE LUMINESCENCE IN RbF-CsF MIXED SYSTEM

M. ITOH, N. OHNO* and S. HASHIMOTO**

Faculty of Engineering, Shinshu University, Nagano 380

**Faculty of Engineering, Osaka Electro-Communication University, Neyagawa 572*

***Kyoto University of Education, Fushimi-ku, Kyoto 612*

Radiative transitions between the outermost core and valence bands of large band-gap materials are responsible for a new type of fundamental luminescence which is characterized by short decay time ($\sim 10^{-9}$ s) and high temperature stability. The observed emission bands are called "Auger-free (AF) luminescence".[1] In the present work, we have studied the AF luminescence in mixed $Rb_{1-x}Cs_xF$ crystals.

Figure 1 shows luminescence spectra obtained at 295 K under the core-band excitation at 21.0 eV; (a) "pure" RbF, (b) $x = 0.01$, (c) $x = 0.52$, and (d) pure CsF ($x = 1.0$). The "pure" RbF crystal used here contains small amounts of Cs^+ ions ($x = 0.0008$). In Fig. 1(a), an intense band peaking at 5.4 eV is assigned to the AF luminescence between the F^- $2p$ valence and Rb^+ $4p$ core bands. A weak band appears around 4.3 eV in the low-energy side of the 5.4 eV band. From Fig. 1 it is evident that the introduction of even small amounts of Cs^+ ions into RbF gives rise to a band at 3.1 eV coinciding with the AF luminescence band of pure CsF. Excitation spectra for the 3.1, 4.3 and 5.4 eV bands of "pure" RbF are depicted in Fig. 2. These three bands have the same excitation threshold, which corresponds to the interband transition from the Rb^+ $4p$ core band to the conduction band. The Cs^+ $5p$ core band is located 2-3 eV above the Rb^+ $4p$ core band. Therefore, the present results indicate strongly that the core hole created in the Rb^+ $4p$ band can move efficiently through the crystal, becoming trapped into the Cs^+ $5p$ state to emit the AF luminescence via a radiative recombination with an electron in the F^- $2p$ valence band.

Figure 3 shows decay behaviors of the 3.1, 4.3 and 5.4 eV bands in "pure" RbF, measured under the single-bunch operation. The 3.1 eV band has a decay time of 3.5 ns, in agreement with the value of AF luminescence in CsF. On the other hand, the decay time of the 4.3 eV band is 1.7 ns, which is the same as that of the 5.4 eV band. This fact, along with the result of Fig. 2, means that the 4.3 eV band is also linked to AF luminescence of RbF. If lattice relaxation is neglected, the AF luminescence of RbF is anticipated to appear at the energy between 5.2 and 6.8 eV from the band-structure

data.[2] Accordingly, the origin of the 4.3 eV band may be explained by introducing some relaxation of the outermost core-hole state and/or the valence-band state.

References

1) M. Itoh, S. Kubota, J. Ruan(Gen) and S. Hashimoto: Rev. Solid State Science 4 (1990) 467.

2) C.S. Inouye and W. Pong: Phys. Rev. B **15** (1977) 2265.

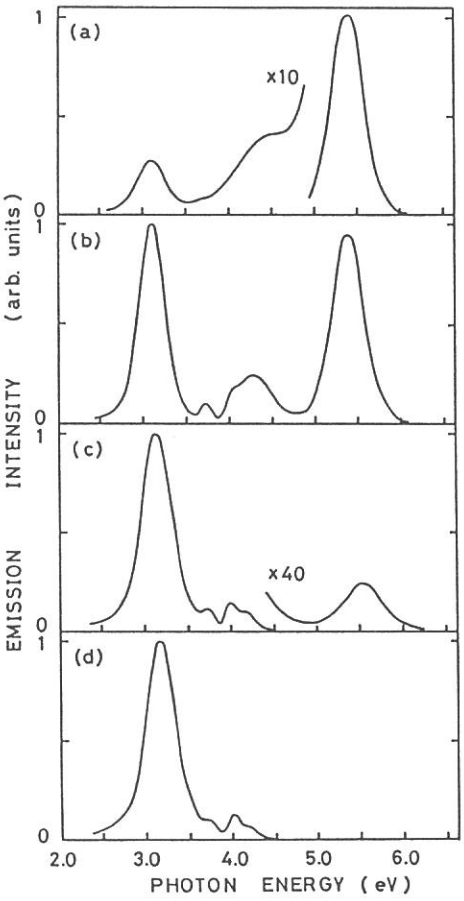

Fig. 1

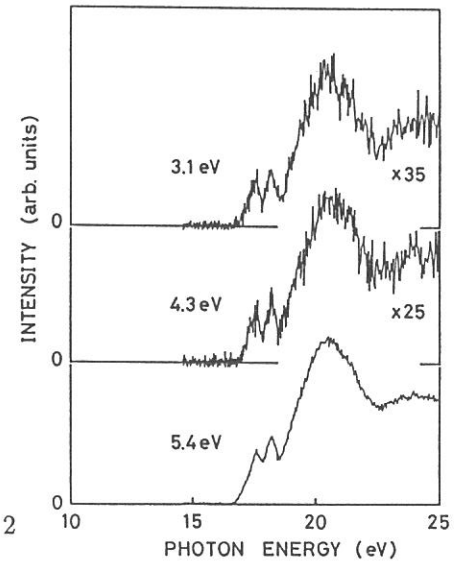

Fig. 2

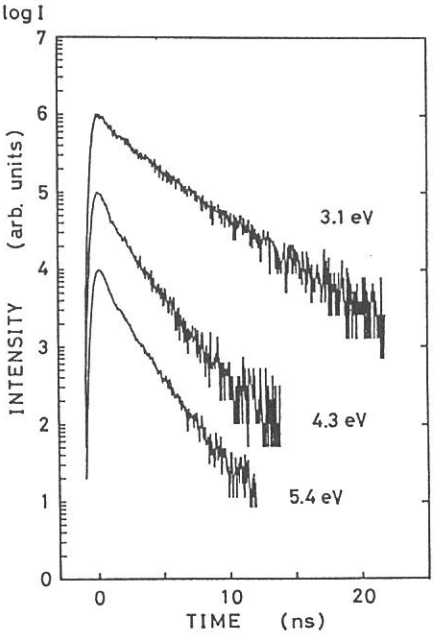

Fig. 3

DECAY-TIME MEASUREMENTS OF NH_4-HALIDE LUMINESCENCE UNDER SINGLE-BUNCH OPERATION

N. OHNO, M. ITOH* and S. HASHIMOTO**

Faculty of Engineering, Osaka Electro-Communication University, Neyagawa 572

**Faculty of Engineering, Shinshu University, Nagano 380*

***Kyoto University of Education, Fushimi-ku, Kyoto 612*

The self-trapped exciton (STE) in alkali halides has long been thought to consist of a self-trapped hole (V_K center) and a bound electron, both being centered on the midpoint between two nearest-neighbor halide sites in a relaxed configuration of D_{2h} symmetry. Song and his co-workers, however, have proposed that the STE in alkali halides is unstable in the state of D_{2h} symmetry, resulting in relaxation to an off-center configuration.

Ammonium halides (NH_4I, NH_4Br and NH_4Cl) are ionic crystals with the CsCl structure at low temperatures. The fundamental absorption spectra of these halide crystals have been found to resemble closely those of alkali halides. Therefore, ammonium halides will be a suitable system for the extension of investigations on the exciton relaxation done for alkali halides.

Figure 1 shows luminescence spectra of ammonium halides under the UV-light excitation into the interband transition at 10 K. A broad luminescence band appears at 3.74 eV for NH_4I, 4.18 eV for NH_4Br and 4.91 eV for NH_4Cl, arising from the radiative annihilation of the STE.[1-3] It is noteworthy that these halide crystals exhibit a single STE luminescence band with a rather small Stokes shift in the ultraviolet region. In Fig. 2 are shown decay profiles of the STE luminescence bands, measured under the single-bunch operation. The STE bands have two decay components; fast and slow. The fast decay time is 2-3 ns in the three cases. The slow component is longer in NH_4Br (700 ns) than that in NH_4I (200 ns).

The present results of ammonium halides indicate a close resemblance to those of NaI and NaBr. This fact strongly suggests that the STE in ammonium halides is situated in an on-center configuration as in NaI and NaBr. The initial state of the STE would be a pair of the triplet $^3\Sigma_u^+$ state and the singlet $^1\Sigma_u^+$ state, separated slightly by the exchange interaction. The tetrahedral structure of NH_4^+ ion would work as a restraint on the off-center displacement of the V_K core. The CsCl structure is more close-packed compared with the NaCl-type crystal, which may be another reason why the STE does not relax off

center. The stability of the on-center STE in ammonium halides is in accordance with the fact that no F center is produced in this system, although the V_K center does exist.

The short-lived component of the STE luminescence band increases in intensity in order of NH_4I, NH_4Br and NH_4Cl, while the long-lived component decreases. This is reasonably explained by considering that the spin-orbit interaction of the hole in V_K center decreases in this order, reducing the mixing of a higher excited $^1\Pi_u$ state into the lowest $^3\Sigma_u^+$ state.

References

1) M.J. Marrone and M.N. Kabler: Phys. Rev. **176** (1968) 1070.

2) M. Itoh: J. Phys. Soc. Jpn. **57** (1988) 372.

3) M. Itoh: J. Phys. Soc. Jpn. **58** (1989) 2994.

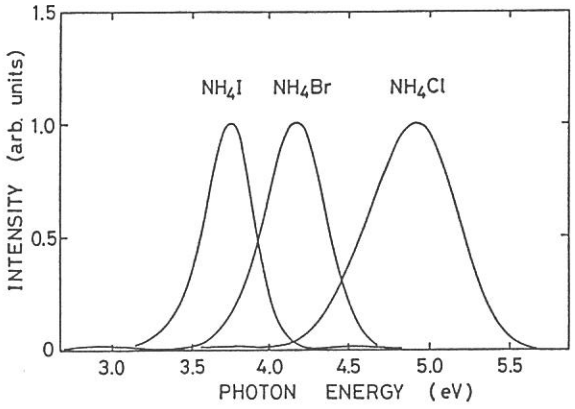

Fig. 1

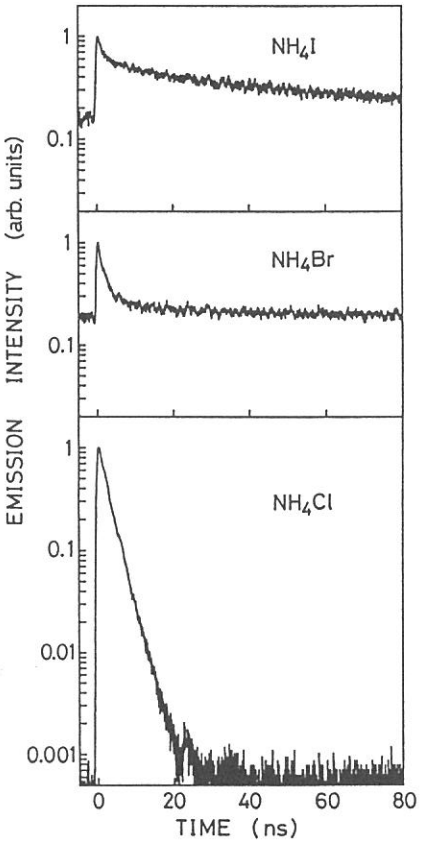

Fig. 2

Electronic Structure of Bis[1,2,5]thiadiazolo-*p*-quinobis(1,3-dithiole) (BTQBT) Studied by Ultraviolet Photoemission Spectroscopy

H. Fujimoto, K. Kamiya,[a,b] S. Tanaka,[a] T. Mori,[a] Y. Yamashita,[a] H. Inokuchi,[a] and K. Seki,[b]

Department of Environmental Science, the Graduate School of Science and Technology, Kumamoto University, Kumamoto 860

[a]*Institute for Molecular Science (IMS), Myodaiji, Okazaki 444*

[b]*Department of Chemistry, Faculty of Science, Nagoya University, Nagoya 464*

Ordinary organic compounds with single component tend to form a molecular solid in which molecules are bound only by weak van der Waals interaction. Reflecting this weak interaction, they are usually electric insulators. Recently, we designed and prepared a new heterocyclic compound bis[1,2,5]thiadiazolo-*p*-quinobis(1,3-dithiole) (BTQBT), which shows a high electric conductivity of 1.0×10^{-3} S/cm at room temperature.[1] The studies of the crystal structure and several physical properties[1] support the presence of intermolecular interaction as expected from the molecular structure of BTQBT shown in Fig.1.

In this study, we carried out a study of BTQBT by ultraviolet photoemission spectroscopy (UPS) to get further insight by carefully investigating the electronic structure of this novel organic semiconductor. The semiempirical MNDO molecular orbital calculation was performed to analyze the UPS spectral features. Moreover, the degree of the intermolecular interaction was deduced from the lowering of ionization threshold energy from gas to the solid state.

Two type of UPS systems were used in this study: a retarding-field-type and the angle-resolved-type (at the beamline 8B2 of UVSOR) systems. BTQBT was synthesized as reported[1] and purified by vacuum sublimation. Thin films of 50 nm thick on a copper substrate were prepared through *in situ* evaporation in both systems. MNDO calculations were performed on HITAC S-810/10 and HITAC M-680H computers at the Computer Center of IMS. The detailed experimental method will be published elsewhere.[2]

A typical photoemission spectra obtained by synchrotron radiation are shown in Fig.2 , which are measured with the Fermi energy (E_F) as the energy reference. The orbital energies obtained by the MNDO calculations are also shown in this figure by the vertical lines. For comparison with the observed UPS spectra, a simulated spectrum (the broken line in Fig.1) was calculated by assuming the Koopmans' theorem and convoluting delta functions located at each orbital energy with a Gaussian function of 0.6 eV width without correction for cross-section effects. To get the best fit between the observed and simulated spectra, the simulated spectrum was shifted down by about 7.1 eV. This shift of 7.1 eV arises mainly from the work function and the reduction of ionization energy from gas to solid state. The one-to-one correspondence between the observed and simulated spectra is not so good as in the case of the thiophene-based compounds.[3] These facts might suggest the possibility that the electronic structure of BTQBT in the solid state differs from that of the free molecule due to the strong intermolecular interaction.

From the UPS spectra obtained by the retarding-field-type system, the ionization threshold for the solid state is determined to be 4.5_7 eV, and the work function of BTQBT is found to be 4.3_1 eV. The ionization threshold is rather low as a sulfur-containing organic compounds. From the values of the work function and the ionization threshold, the energy difference between the Fermi level and the top of the valence band is determined to 0.3 eV, which is close to the

observed activation energy in the electric conduction measurements.[1)]

On the other hand, the ionization energy for the gas phase can be estimated to be 6.4 eV from the first ionization potential. Moreover, the preliminary band calculation using the transfer integrals showed that the valence band formed from the HOMOs of free molecules has a width of 0.7 eV. This is much larger than the value of ordinary organic solids (≤0.1 eV). Using this value, the polarization energy is estimated to be 1.5 eV. The electronic structure in the top region of the valence band described above is schematically summarized in Fig.3.

In the solid state of BTQBT, the low ionization energy is mainly due to two effects: the polarization effect and the band formation. In usual organic compounds, the effect of the band formation is small and of the order of 0.1 eV. However, BTQBT has a large value of this effect due to the strong intermolecular interaction through the short sulfur-sulfur distance between adjacent molecules. This should be partly responsible for the high conductivity of BTQBT through the effective carrier generation.

References

1)Y. Yamashita, S. Tanaka, K. Imaeda, and H. Inokuchi, *Chem. Lett.*, **1991**, 1213.

2)H. Fujimoto, K. Kamiya, S. Tanaka, T. Mori, Y. Yamashita, H. Inokuchi, and K. Seki, submitted to *Chem. Phys.*

3)H. Fujimoto, K. Seki, U. Nagashima, H. Nakahara, J. Nakayama, M. Hoshino, K. Fukuda, and H. Inokuchi, *UVSOR Activity Report*, **15**, 68 (1987); **16**, 102 (1988); **17**, 70 (1989).

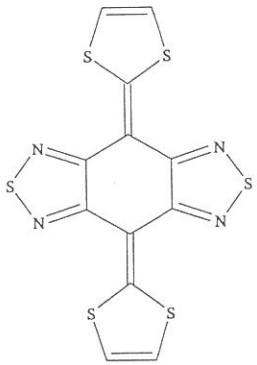

Fig.1 BTQBT

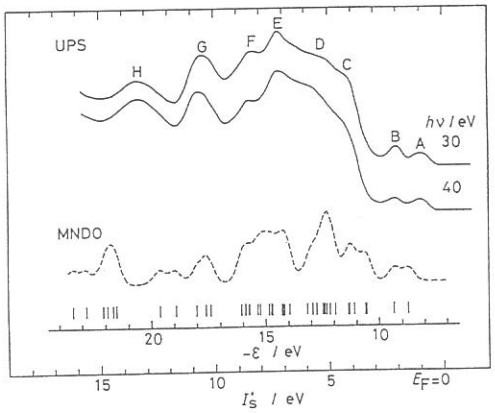

Fig.2 UPS spectra of BTQBT.

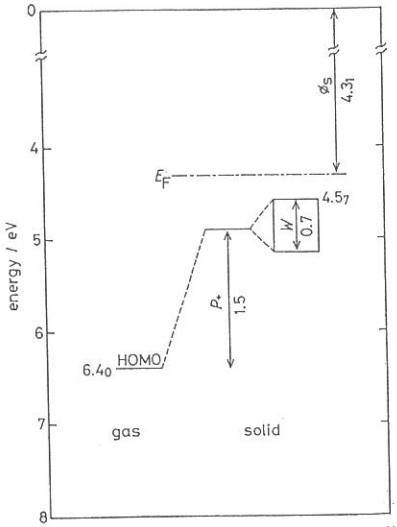

Fig.3 Electronic structure in the top region of the valence band of BTQBT.

LUMINESCENCE IN p-TERPHENYL CRYSTALS

S.Sato, M.Segawa and K.Uchida
Fukui Institute of Technology, Gakuen, Fukui 910

Y.Takahashi
Aichi Institute of Technology,Yakusa,Toyoda 590-02

E.Ishiguro
Department of Applied Physics,Osaka City University, Osaka 558

The molecule of p-terphanyl consists of three benzene rings joined by single bond. In the crystal, intermolecular force is of the same order than that of intramolecular force. Therefore, at room temperature, molecules appear like planar due to a large amplitude thermal motion of the central ring which rotated with relation to the long axis of the molecules[1,2]. At low temperature, p-terphenyl molecules become nonplanar with the angle about 16 degree from the plane formed by the two outer benzene rings. Accordingly, we measured fluorescence decay times of p-terphenyl crystals in order to clarify the effect of the libration of benzene rings molecular on luminescence processes.

Fluorescence decay times were measured by the time-correlated single photon counting system under the single bunch operation of UVSOR, using 1 m Seya-Namioka monochromator in BL7B beam line. A vacuum of a cryostat chamber was separated from the beam line by LiF window because vapor pressure of p-terphenyl crystals is very high.

In the figure 1, the decay curves of the 370 nm emission (a) and the 450nm emission (b) under the 300nm excitation are shown at room temperature. The decay curve in fig.1(a) has decay time of 2.9 ns. In fig.1(b) the decay curve consists of the fast decay component of 4.0 ns and of the slow decay component. The decay time of the slow component is the order of 100 ns. The emission intensity of slow component is weak at 410 nm, but this intensity increases as the observing wavelength is longer. Also, the slow component decreases in the intensity with decreasing the temperature. These indicate that the excimer emission is included in the region of the longer wavelength of the emission spectrum. The creation of The excimer emission would be able to be elucidated by the term of

the libration of benzene ring of p-terphenyl molecues. As the molecules get more planner with temperature, the intermolecular interaction become larger. So it is easy to create the excimer at higher temperature.

In the fig.2 (a), the wavelength dependence of the emission decay time under the 300 nm excitation is shown at room temperature. The decay times in the region from 350 nm to 380 nm are about 3.0 ns, and these above 380 nm become longer with wavelength. These results is attributed to the reabsoption of the emission in the region from 350 nm to 380 nm[3].

[1] P.J.L.Baudour and H.Cailleau, Acta Cryst. B33(1977)1773

[2] I.B.Berlman J.Phys.Chem. 74(1970)3085

[3] K.Uchida et al. J.Luminescence 48&49(1991)337

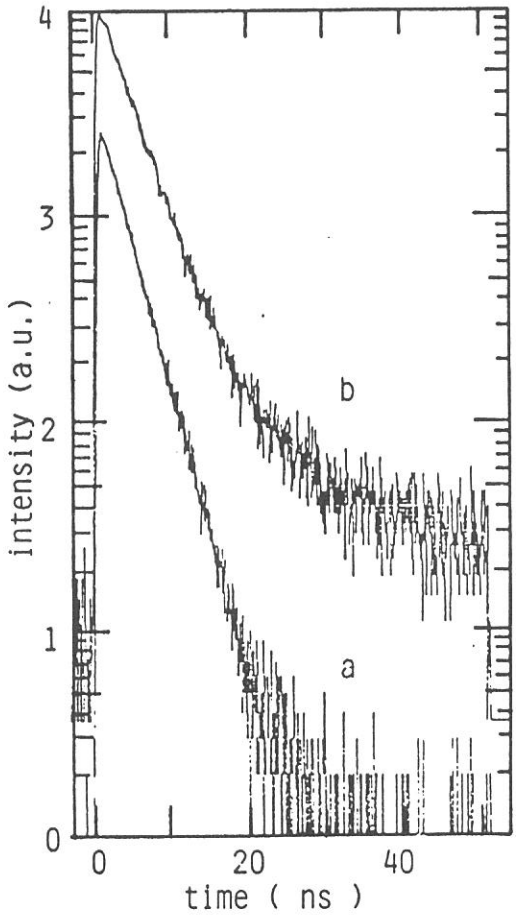

Fig.1 The emission decay curves at 370 nm (a) and 450 nm (b).

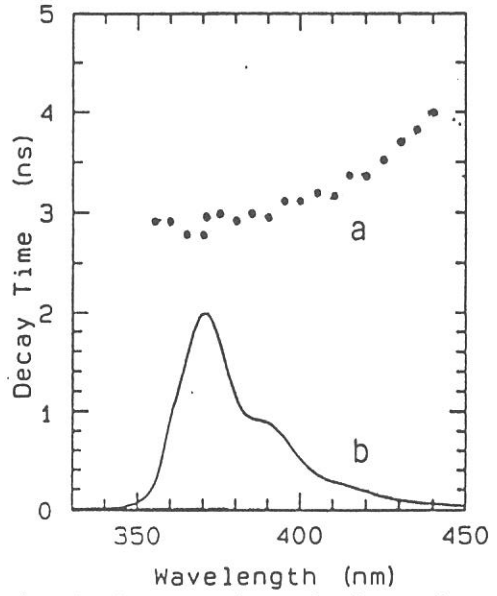

Fig.2 The wavelength dependence of the decay times(a) and the emission spectrum.

IONIC PLASMON IN SUPERIONIC CONDUCTORS

Teruyoshi AWANO, Takao NANBA* and Mikihiko IKEZAWA**

Department of Applied physics, Tohoku Gakuin University, Tagajo 985
*Department of physics, Kobe University, Kobe 657
**Research Institute for Scientific Measurements, Tohoku University, Sendai 980

An absorption band by diffusive motion of conduction ions in a superionic conductor is expected to appear in the spectral region of several wave numbers. But millimeter wave absorption spectra of these crystals and their temperature dependence have not been studied in detail because of experimental difficulties.

Volkov et al. studied conductivity spectra of a $RbAg_4I_5$ single crystal in the spectral range between 2 and 33 cm^{-1} [1,2]. In their model, the low frequency region was described by the sum of the Drude free electron and a Debye relaxator. But the origin of the Debye relaxator was not clear and the parameters of the Drude free carrier was too small comparing with the expected value from the mass ratio of the ion and electron. There is a shoulder peak near 7 cm^{-1} in their data and we think this structure is due to the ionic plasmon.

We have measured reflectivity spectra of single crystals of MAg_4I_5 (M=Rb, K and NH_4) in the spectral region from 3.5 to 250 cm^{-1} at temperatures between 15 K and 470 K. Optical constants were calculated by the Kramers-Kronig analysis. We also measured about $Rb_4Cu_{16}Cl_{13}I_7$ to compare with the case of copper ion conduction. This crystal has the same structure as MAg_4I_5.

Energy loss function spectra of KAg_4I_5 and $NH_4Ag_4I_5$ obtained from the reflectivity spectra are shown in fig. 1. We already reported spectra at various temperatures in superionic phase of $RbAg_4I_5$. There is a plateau in each spectrum in the spectral region near 10 cm^{-1} on the low energy side of the attempt frequency mode near 20 cm^{-1}. These structure of the spectra are analogous to that of electronic plasma oscillation in metals and possibly are interpreted as being due to ionic plasmon. In the Drude model, the plasma frequency ω_p is defined as

$$\omega_p^2 = \frac{4\pi N e^2}{m^* \varepsilon_\infty}$$

N is the number of the mobile ions and m* is effective mass of the ions. ε_∞ is the background dielectric constant from vibrational and electronic contribution.

Dashed curves were drown by the Drude model with the parameters of ω_p = 30 cm^{-1}, damping frequency γ = 75 cm^{-1} and ε_∞ = 7.8 for KAg_4I_5 and ω_p = 28 cm^{-1}, γ = 85 cm^{-1} and ε_∞ = 9.0 for $NH_4Ag_4I_5$.

Figure 2 shows energy loss function spectrum of $Rb_4Cu_{16}Cl_{13}I_7$ at 300 K. The dashed curve was fitted by the parameters of ω_p=41 cm^{-1}, γ = 75 cm^{-1} and ε_∞ = 10.

The conduction ions in superionic conductors feel coulomb repulsion from each other. This force probably cause the cooperative motion of conduction ions. Estimated plasma frequency using bare mass of conduction ions and dielectric constants by electronic contribution are 29 cm^{-1} for MAg_4I_5 and 38 cm^{-1} for $Rb_4Cu_{16}Cl_{13}I_7$. The observed value were 28 cm^{-1} and 41 cm^{-1} as described above and the agreement is very well. The root of the mass ratio of the silver and copper (1.3) agrees with the ratio of the plasma frequency observed in $RbAg_4I_5$ and $Rb_4Cu_{16}Cl_{13}I_7$ (1.7).

References
[1]A.A.Volkov,V.G.Goffman,G.V.Kozlov and G.I.Mirzoyants, Sov.Phys.Solid State 27 (1985) 1126.
[2]G.V.Kozlov,G.I.Mirzoyants,A.A.Volkov and V.G.Goffman, Phys.Lett. 22 (1984) 324.

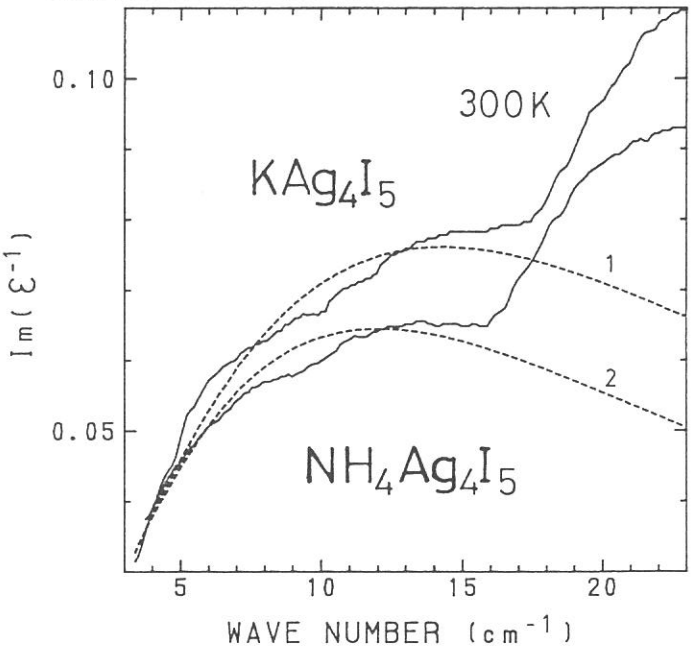

Fig. 1
Energy loss function spectra of KAg_4I_5 and $NH_4Ag_4I_5$ at 300 K. Dashed curves show the Drude model.

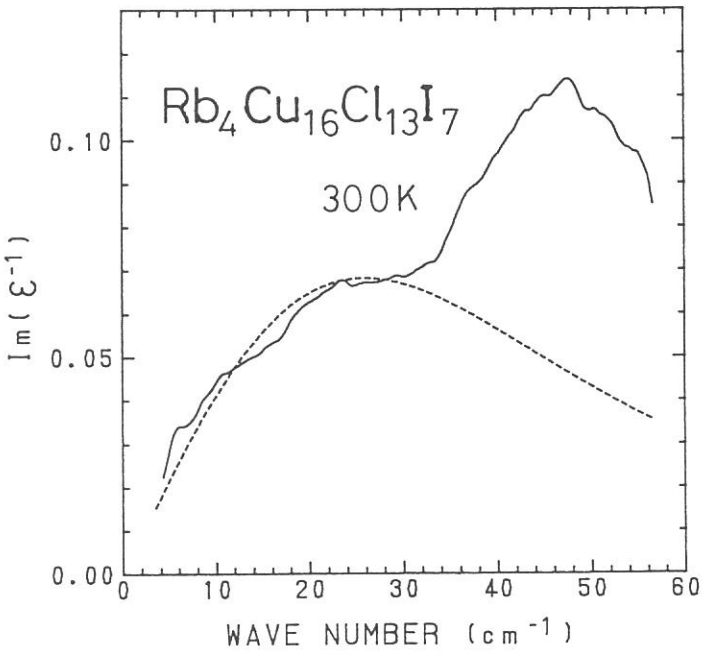

Fig. 2
Energy loss function spectrum of $Rb_4Cu_{16}Cl_{13}I_7$ at 300 K. The dashed curve was fitted by the parameters of ω_p = 41 cm^{-1}, γ = 75 cm^{-1} and ε_∞ = 10.

PHOTOIONIZATION POTENTIAL OF ANTHRACENE DOPED IN SUPERCRITICAL XENON: AN INTERPRETATION BASED ON A CLUSTER MODEL

Kazumichi NAKAGAWA, Kazuie KIMURA* and Arisato EJIRI+

Physics Division, Faculty of Education, Kobe University, Tsurukabuto, Nada-Ku, Kobe 657, Japan
*The Institute of Physical and Chemical Research(RIKEN), Wako, Saitama 351, Japan
+Department of Pure and Applied Sciences, University of Tokyo, 3-8-1 Komaba, Meguro-Ku, Tokyo 153, Japan

Supercritical rare gases are known to have fairly high solubility for aromatic hydrocarbons. It is easy to control the density of supercritical fluids over a wide range, which may offer us an opportunity to study the evolution of physical and chemical properties of guest molecules from isolated state to condensed phase. Optical ionization potential I_p of anthracene doped in supercritical xenon fluids were measured as a function of xenon density N and obtained results were reported in our previous paper[1]. A germinal idea of a cluster model was invoked to interpret the experimental I_p values at $N<7\times10^{21}cm^{-3}$ lower than those calculated with a continuous model (curve A in fig. 1). In this paper, we report a result of application of a cluster model in an attempt to reproduce the density dependence of I_p values quantitatively.

As the first approximation, we assumed that ionization potential of anthracene is reduced by D from I_g through an association of one xenon atom due to a polarization effect; I_g is the gas-phase ionization potential of anthracene. Thus I_p value of a Anthracene-$(Xe)_n$ cluster is approximated to be $I_p=I_g+nD$. This simple model is based on a work by Kajimoto et. al.[2]. They reported that the energy of S_0-S_1 transition of (N,N-dimethylamino)benzonitrile doped in supercritical CF_3H is reduced in proportional with n for small values of n. In supercritical fluids, size of clusters, thus magnitude of n, show a distribution determined by a fluid density N, e. g., distribution of large n is higher for higher N[3]. According to Kajjimoto et. al.[2], n is represented with N taking into account of an entropy effect via the Langmuire-type equilibrium; $n=(mN)/(N+N_1(m-1))$, where N_1 depicts the fluid density for n=1 and m is the maximum number of association.

Consequently, we can get an equation, $I_p(N)=I_g+(mND)/(N+N_1(m-1))$. Using this equation with two parameters of D and N_1, we calculated the best fit values of $I_p(N)$ to the experimental result. As seen from the curve B in fig. 1, experimental values of I_p for $0.03\times10^{21}cm^{-3}<N<8\times10^{21}cm^{-3}$ are well reproduced with value of I_g=7.40eV, m=6, D=-0.31eV and $N_1=8\times10^{20}cm^{-3}$. This value of m was estimated via an examination of microscopic structure of the cluster by a method of atom-atom pair potential[4].

We would like to thank professors M. Watanabe, H. Inokuchi and O. Kajimoto for encouragement. This work was supported by the joint study program of the Institute for Molecular Science, No. 61-E914 and 2-A806.

References [1]K. Nakagawa, A. Ejiri, K. Itoh and M. Nishikawa, Chem. Phys. Lett. 147, 557(1988). [2]O. Kajimoto, M. Futakami, T. Kobayashi and K. Yamasaki, J. Phys. Chem. 92, 1347(1988). [3]e. g. "Supercritical fluid Science and Technology", K. P. Johnston and J. M. L. Penninger eds., American Chemical Society, Washington DC, 1989. [4]M. J. Ondrechen, Z. Berkovich-Yellin and J. Jortner, J. Am. Chem. Soc. 103, 6586(1981).

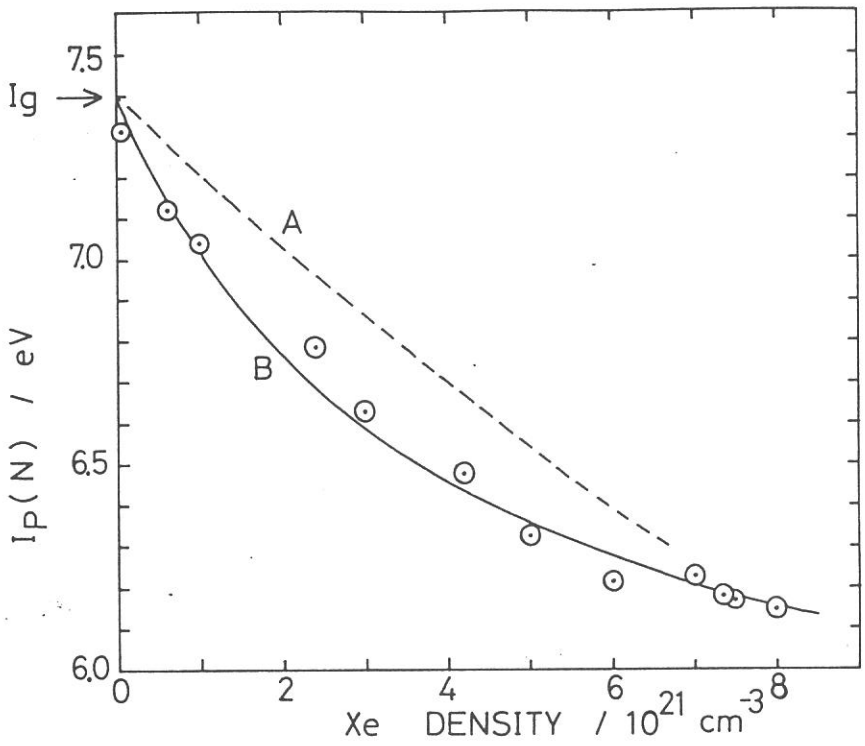

Fig. 1 Optical ionization potential Ip vs. xenon density N at 300K. ⊙: Experimental values[1], Curve A: Continuum model[1], Curve B: Cluster model (see text).

DISPERSED FLUORESCENCE OF O_2 EXCITED BY $h\nu$ = 70-280 eV

Toshio IBUKI,[a] Eiji ISHIGURO,[b] Shigeyoshi UMEMIYA,[b]
Muneo HITOMI,[b] Atsunari HIRAYA,[c] and Makoto WATANABE[c]

a Kyoto University of Education, Fushimi-ku, Kyoto 612
b Department of Applied Physics, Osaka City University, Sumiyoshi-ku, Osaka 558
c Institute for Molecular Science, Myodaiji, Okazaki 444

Emissions from electronically excited doubly charged molecular cations have been observed only in N_2^{2+} and NO^{2+} [1,2]. In the recent studies of oxygen *K* edge excitation of O_2 molecule, fluorescence observed in the range of 380-500 nm was first assigned as the $\tilde{B}^3\Pi_g \rightarrow \tilde{A}^3\Sigma_u^+$ transition in doubly charged O_2^{2+} ion [3.4]. The observed fluorescence spectra show three broad bands under the condition of a low spectral bandpass of about 20 nm for dispersing emission [3], and they have been assigned as a vibrational progression [3,4]. The potential energy level of the doubly charged ground state O_2^{2+} ion lies at 36.3 ± 0.5 eV.

In the present work, we excited oxygen molecule by using white light at BL8B1 station of UVSOR. The energy of the primary photon beam was spread over 70-280 eV, and the maximum intensity was at ~120 eV. A spectral resolution of 0.4 nm was employed for the fluorescence dispersion by using a Jobin-Yvon HR-320 monochromator with a cooled CCD detector. A part of spectra observed is given in Figure 1. All of the sharp bands in the region of 390-500 nm can be assigned as emissions from the excited O^+ fragment ion. No fluorescence attributed to O_2^{2+} double cation was observed. At $h\nu$ > 500 nm the $O_2^+(\tilde{b}^4\Sigma_g^- \rightarrow \tilde{a}^4\Pi_{ui})$ transition was observed as was in the soft X-ray excitation [3,4]. The recent *ab initio* calculation suggests the absence of a minimum in the potential energy curve for the $\tilde{A}^3\Sigma_u^+$ state [5]. Thus, the assignment of the visible emission observed in X-ray [3,4] remains an open question. We think the low bandpass of the monochromator used in the soft X-ray studies probably gave rise to three broad single bands which are composed of many sharp atomic O^+ lines as shown in figure 1.

In the region of 190-310 nm the $O_2^+(\tilde{A}^2\Pi_u \rightarrow \tilde{X}^2\Pi_g)$ transition was observed, which is not reported in the X-ray experiments.

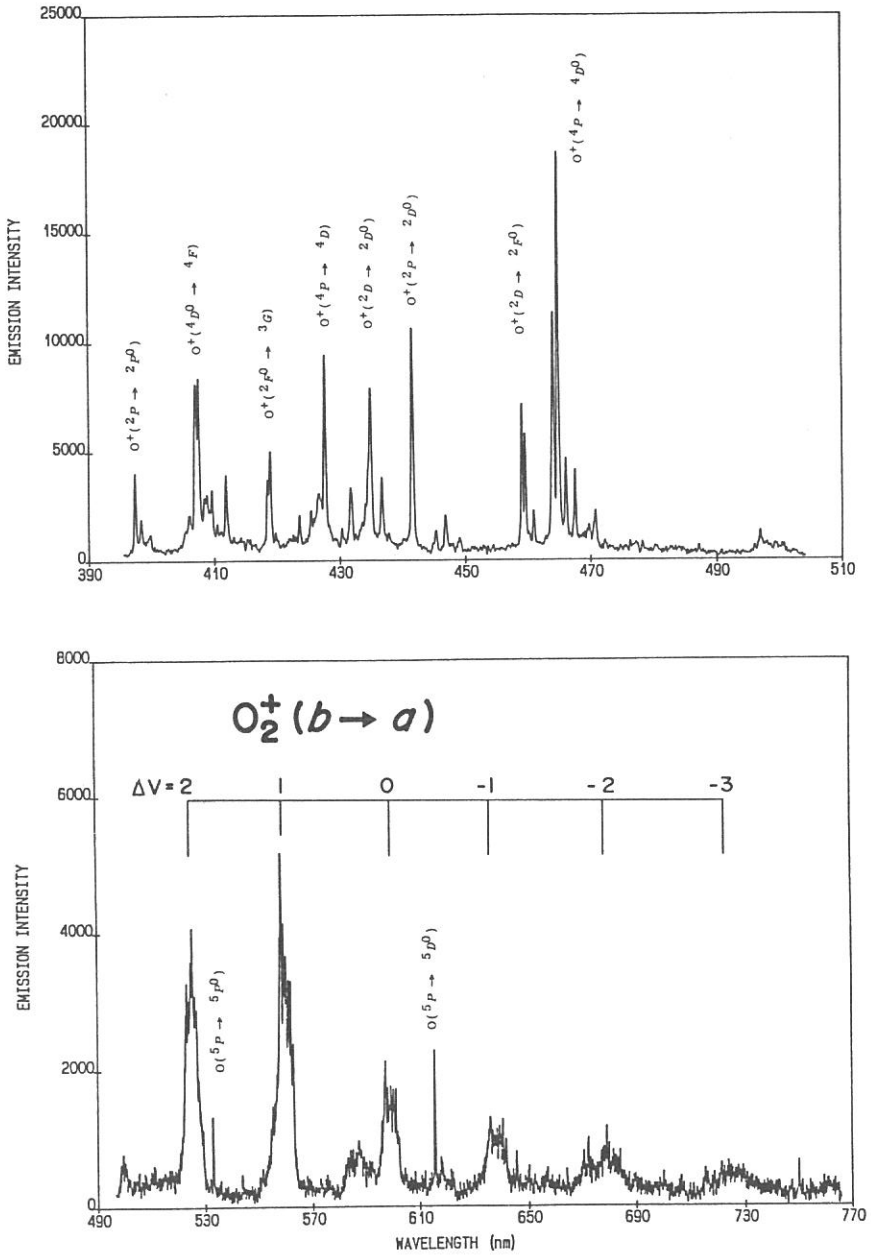

Figure 1. Dispersed fluorescence of O_2 excited by 70-280 eV.

REFERENCES

[1] B.J.Olsson et al. J. Chem. Phys. 88, 7501 (1988).

[2] M.J.Besnard et al. J. Chem. Phys. 85, 1316 (1986).

[3] K.Tohji et al. J. Chem. Phys. 85, 7492 (1986).

[4] B.X.Yang et al. J. Chem. Phys. 89, 1215 (1988).

[5] L.G.M.Pettersson and M.Larsson J. Chem. Phys. 94, 818 (1991).

UPS OF NEW TYPE PURE CIS AND TRANS POLYACETYLENE

Jiro TANAKA, Koji KAMIYA, Takayuki MIYAMAE, Masato OKU, Chizuko TANAKA, Kazuhiko SEKI and Hiroo INOKUCHI*

Department of Chemistry, Nagoya University, Chikusa, Nagoya 464-01
*Institute for Molecular Science, Myodaiji, Okazaki 444

Polyacetylene (CH)x is of primary inportant in the study of conducting polymer since high conductivity was obtaiined by the use of a doping technique for (CH)x.[1] Recentry Naarmann and Theophilou [2] and Tsukamoto [3] succeeded in preparing new type (CH)x, with conductivity over 10^5 S/cm. We studied UPS of new type pure cis and trans (CH)x.

We synthesized new type (CH)x film ($\sim$ 200 nm) on Mo plate by the method of Tsukamoto. Cis film was synthesized at -78℃ in agron and introduced to the pre-chamber of UPS system without exposing to the air by the use of vaccum type glove box. UPS were measured at the UVSOR Facility in IMS. The Fermi enegy (E_f) of the UPS system was determined by using the Fermi edge of gold film evaporated *in situ*. The UPS measurements were carried out with photon of 40eV energy by incident angle 50° and normal emission. An *ab initio* GAUSSIAN 86 SCF-MO calculation was carried out on a HITAC M-680H and S-820 computer at the IMS Computer Center. The simulated spectra were obtained by broadening the delta function without correction of cross section effect. The value of the Gaussian width is chosen to be 0.5eV.

Fig.1 and Fig.2 are UPS spectra of cis and trans (CH)x. By comparing the observed and simulated spectra, the bands observed at 4<Eb<9eV, 8<Eb<14eV and 14<Eb<16eV for cis (CH)x, 4<Eb<10eV, 10<Eb<14eV and about 15eV for trans (CH)x, are ascribed to the π, $\sigma(2p_x, 2p_y)$ and $\sigma(2s)$ bands. Cis and trans spectra are not very much different, but the densities of $2p_x+2p_y$ and 2s orbitals of trans (CH)x are higher than that

of cis (CH)x. The $2p_x+2p_y$ and 2s bands of trans (CH)x are observed more clealy than that of cis (CH)x. The band gap of cis and trans (CH)x estimated from the UPS spectra are 1.4eV and 1.8eV, respectivily. These value are good agreement with results of absorption spectra.

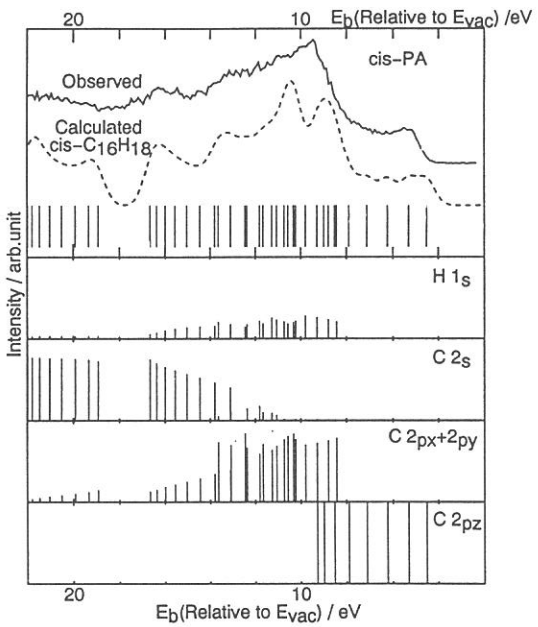

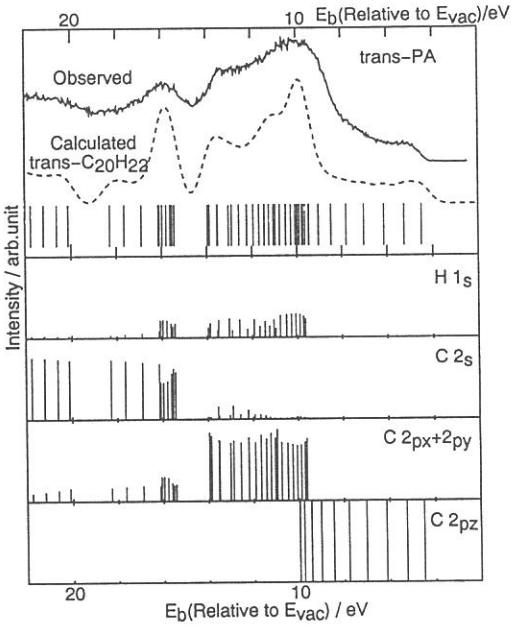

Fig.1 UPS of cis (CH)x. Fig.2 UPS of tran (CH)x.
Observed (solid line) and simulated (broken line) UPS spectra. The virtical lines indicate the orbital energies. The vacuum level (E_{vac}) is taken as the origin of the energy scale.

References

[1]T.Ito, H.Shirakawa and S. Ikeda, *J.Polym.Sci.Polym.Chem.Ed.*, **12**(1974)11.

[2]H.Naarmann and N.Theophilou, *Synth.Metals*, **22**(1987)1.

[3]J.Tsukamoto, A.Takahashi and K.Kawasaki, *Jpn.J.Appl.Phys.*, **29**(1990)125.

Far-Infrared Spectroscopy in High Pressure Phases of Ice

Michihiro KOBAYASHI, Shigeji MORITA, Toshimitsu NAKAI
Takao NANBA* and Masao KAMADA†

Faculty of Engineering Science, Osaka University, Toyonaka, Osaka 560
*Department of Science, Kobe University, Rokkodai, Kobe 657
†Institute for Molecular Science, Myodaiji, Okazaki 444

After the development of the diamond anvil cell, various kinds of optical measurements have been performed regarding almost whole classes of substance under the high pressure. However, only few researches [1,2] have been made at the far-infrared region because of the difficulty to attain sufficient light intensity after transmitting a small gasket hole.

Here we report far-infrared absorption spectra of high pressure phases on ice. According to Nanba and Watanabe [2], the synchrotron radiation at Institute for Molecular Science (beam line BL6A1) was used to conquer the weakness of usual light sources.

The far-infrared region is important to get direct information regarding the hydrogen bond, since the inter-molecular vibrational mode mediated by the hydrogen bond exists in this region.

Ice Ⅶ and Ⅷ have almost the same structure regarding arrangements of oxygen ions, while protons in Ⅶ and Ⅷ have disordered- and ordered structures, respectively. The order-disorder phase transition was observed by capacitance measurements [3]. We have expected to detect the order-disorder transition through the change of the far-infrared absorption spectra.

Figure 1 shows the absorption spectra for ice Ⅶ (dotted line) and Ⅷ (solid line) at 3.1 GPa, where α stands for the absorption coefficient and d expresses the sample thickness. The spectral shape of the dotted line remained almost unchanged above 277 K, while the shape of the solid line was maintained below 264 K. Whalley et al. [3] reported that the phase transition from Ⅶ to Ⅷ occurs at near 270 K. Therefore we can conclude that the spectral change shown at Fig. 1 originates from the order-disorder transition of protons in ice at high pressure.

A broad absorption band centered at near 130 cm^{-1} in ice Ⅷ is attributed

to the inter-molecular vibration having the translational symmetry $\nu_T E_u$ [4]. In ice Ⅶ whole the lattice vibrational modes over the entire Brillouin zone become optically active, since the orientation of electric dipole moment for each H_2O molecule is random [5]. In ice Ⅷ only the zone center mode is optically active, therefore the absorption intensity becomes weaker compared with ice Ⅶ.

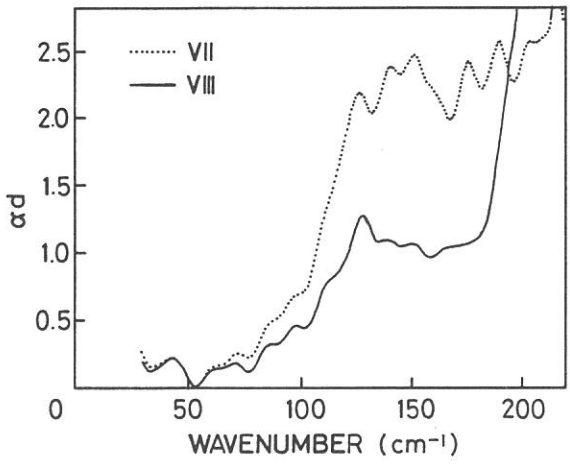

Fig. 1 Far-infrared absorption spectra of ice Ⅶ (dotted line) and Ⅷ (solid line) at 3.1 GPa.

It is interesting to note that the considerable amount of the randomness still remains in ice Ⅷ, because the absorption band has a long tail starting from 120 cm^{-1} toward the lower wavenumber, which is similar to ice Ⅶ, though the absolute intensity is about half.

REFERENCES

[1] W. A. Challener and J. D. Thompson, Appl. Spectrosc. 40 (1986) 298.

[2] T. Nanba and M. Watanabe, J. Phys. Soc. Jpn. 58 (1989) 1535.

[3] E. Whalley, D. W. Davidson and J. B. R. Heath, J. Chem. Phys. 45 (1966) 3976.

[4] S. P. Tay, D. D. Klug and E. Whalley, J. Chem. Phys. 83 (1985) 2708.

[5] E. Whalley and J. E. Bertie, J. Chem. Phys. 46 (1967) 1264.

NEGATIVE-ION MASS SPECTROMETRIC STUDY OF ION-PAIR FORMATION IN THE VACUUM ULTRAVIOLET. $CF_4 \longrightarrow F^- + CF_4^+$

Koichiro MITSUKE,[α] Shinzo SUZUKI,[β] Takashi IMAMURA,[γ] and Inosuke KOYANO[δ]

[α] Department of Vacuum UV Photoscience, Institute for Molecular Science, Myodaiji, Okazaki 444

[β] Department of Chemistry, Tokyo Metropolitan University, Minami-Osawa, Hachioji, Tokyo 192-03

[γ] Atmospheric Environment Division, National Institute for Environment Studies, Onogawa, Tsukuba, 305

[δ] Department of Material Science, Himeji Institute of Technology, 1479-1 Kanaji, Kamigohri, Hyogo 678-12

Photoexcitation of molecules to highly-excited states is often accompanied by dissociation into a pair of positive and negative ions in the photon energy range of 10 - 50 eV. The detection of negative ions produced by such ion-pair processes provides a sensitive probe to investigate the properties of Rydberg states lying in the vacuum ultraviolet. We have measured the negative-ion efficiency curves using synchrotron radiation and obtained basic spectroscopic data and cross sections for the photodissociation into ion pairs.

Figure 1 shows the photodissociation efficiency curve of F^- produced from CF_4.[1] The observed spectral features are identified as resonance peaks resulting from transitions to the Rydberg states converging to the five lowest ionic states of CF_4^+: $\tilde{X}\,^2T_1$, $\tilde{A}\,^2T_2$, $\tilde{B}\,^2E$, $\tilde{C}\,^2T_2$, and $\tilde{D}\,^2A_1$. Structureless peaks at photon energies of 13.62 (feature *F*1) and 13.90 eV (feature *F*2) are assigned to CF_4^{**} ($1t_1 \rightarrow 3pt_2\ ^1T_2$) and CF_4^{**} ($4t_2 \rightarrow 3sa_1\ ^1T_2$), respectively. The $^1A_1$ components of these Rydberg states directly dissociate into a pair of the ground state F atom and a radical in Rydberg states, CF_3^{**}. The CF_3^{**} radical thus formed is electronically excited and decays radiatively by emitting UV or visible fluorescence. The conversion to the ion-pair state occurs through avoided potential energy surface crossings between these repulsive CF_4^{**} states and the $^1A_1$ ion-pair state that dissociates into $F^-(^1S_g) + CF_3^+(\tilde{X}\,^1A_1')$. In contrast, the CF_4^{**} ($3t_2 \rightarrow npt_2\ ^1T_2$, $4 \leqq n \leqq 6$) Rydberg state converging to $CF_4^+(\tilde{C}\,^2T_2)$ shows a long series of the ν_1 vibrations in the F^- efficiency curve (features *F*6 and *F*7). The $4pt_2$ Rydberg state is considered to have radiative decay channels to the dissociative Rydberg states converging to the $\tilde{X}\,^2T_1$ and

$\tilde{A}\,^2T_2$ states, such as the $4t_2 \rightarrow 4pt_2\,^1A_1$ and $1t_1 \rightarrow 4pt_2\,^1T_2$ states. The system is then converted to the ion-pair state $F^-(^1S_g) + CF_3^+(\tilde{X}\,^1A_1')$ via avoided surface crossings along the CF_3—F dissociation coordinate.

1) K. Mitsuke, S. Suzuki, T. Imamura, and I. Koyano, J. Chem. Phys. **95,** 2398 (1991).

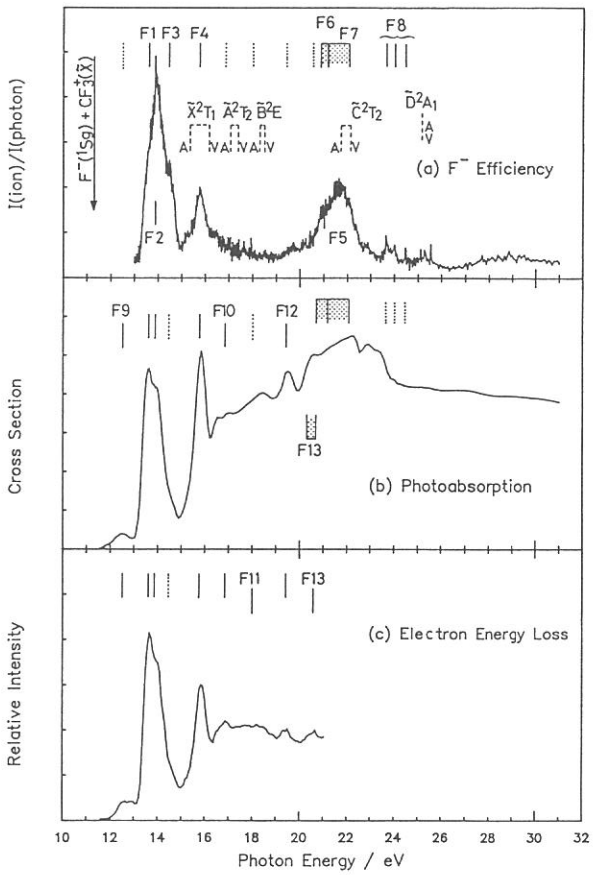

Figure 1. Comparison among (a) photodissociation efficiency curve of F^- produced from CF_4, (b) photoabsorption cross section curve of CF_4 (L. C. Lee et al.), and (c) electron-energy-loss spectrum of CF_4 (W. R. Harshbarger et al.). The adiabatic and vertical ionization potentials for the five lowest ionic states of CF_4^+ (C. R. Brundle et al.) are indicated by the dashed lines with marks *A* and *V*, respectively. The thermochemical threshold for the formation of $F^-(^1S_g) + CF_3^+(\tilde{X}\,^1A_1')$ is also indicated.

NEGATIVE-ION MASS SPECTROMETRIC STUDY OF ION-PAIR FORMATION IN THE VACUUM ULTRAVIOLET. $NO \longrightarrow O^- + N^+$ and $CO \longrightarrow O^- + C^+$

Koichiro MITSUKE,[α] Shinzo SUZUKI,[β] Takashi IMAMURA,[γ] and Inosuke KOYANO[δ]

[α] Department of Vacuum UV Photoscience, Institute for Molecular Science, Myodaiji, Okazaki 444

[β] Department of Chemistry, Tokyo Metropolitan University, Minami-Osawa, Hachioji, Tokyo 192-03

[γ] Atmospheric Environment Division, National Institute for Environment Studies, Onogawa, Tsukuba, 305

[δ] Department of Material Science, Himeji Institute of Technology, 1479-1 Kanaji, Kamigohri, Hyogo 678-12

Ionic states of NO and CO below 20 eV have been extensively studied by photoelectron spectroscopy by using discharge lamps and lasers. In contrast, there are complex and dubious experimental data for high-lying states above 20 eV, owing to a great number of undefined satellites in a photoelectron spectrum. Since photoexcitation with 20 - 50 eV energy allows ionization of electrons from inner valence orbitals in most molecules, subsequent relaxation of the hole states leads to multiple excitation of outer valence electrons into low-lying antibonding valence orbitals. In the case of CO, several two hole-one electron configurations (i.e. two-electron-excited ionic states) are predicted to exist from analysis of high resolution He II photoelectron spectra.[1] Some peaks observed in photoabsorption spectrum[2] are then assigned to transitions to the Rydberg states converging to these ionic states. On the other hand, multiply excited states have not been discussed yet for high-lying states of NO. In the present study, we measure the photodissociation efficiency curves of O^- produced from CO and NO by the ion-pair formation using synchrotron radiation and detect the Rydberg states converging to several two-electron-excited ionic states.

Figure 1 shows the efficiency curve of O^- produced from CO. It is evident that sharp peaks below 22.5 eV result from transitions to the Rydberg states converging to the three two-electron-excited ionic states, $(\pi 2p)^{-1}(\sigma 2p)^{-1}(\pi^* 2p)^1\, \tilde{C}\, ^2\Sigma^+$, $(\pi 2p)^{-2}(\pi^* 2p)^1\, \tilde{D}\, ^2\Pi$ and $(\pi 2p)^{-1}(\sigma 2p)^{-1}(\pi^* 2p)^1\, \tilde{E}\, ^2\Sigma^+$. The markedly stronger peaks are assigned to the Rydberg states $CO^{**}[(\pi 2p)^{-2}(\pi^* 2p)^1(np\pi)]$ converging to $CO^+(\tilde{D}\, ^2\Pi)$ and $CO^{**}[(\pi 2p)^{-1}(\sigma 2p)^{-1}(\pi^* 2p)^1(ns\sigma)]$ converging to $CO^+(\tilde{C}\, ^2\Sigma^+)$. In these assignments, we apply the gerade-ungerade dipole selection rule by assuming that the molecular orbitals of CO have similar distributions to those of N_2, an isoelectronic molecule of CO.

Figure 2 shows the efficiency curve of O^- produced from NO. Some of the spectral features are identified as resulting from transitions to the

$nd\pi$ and $nd\sigma$ Rydberg states converging to NO^+ ($\tilde{c}\,^3\Pi$) at the ionization potential of 21.72 eV. Assignments have been made on the basis of the results of photoabsorption spectra reported by Narayana and Price[3] and negative-ion efficiency curves by Oertel et al.[4] Above 22.5eV, there exist weak equally spaced peaks, which are probably ascribed to the Rydberg states converging to unknown two-electron-excited ionic states.

1) L. Åsbrink, C. Fridh, E. Lindholm, and K. Codling, Phys. Scr. **10,** 183 (1974).
2) K. Codling and A. W. Potts, J. Phys. **B7,** 163 (1974).
3) B. Narayana and W. C. Price, J. Phys. **B5,** 1784 (1972).
4) H. Oertel, H. Schenk, and H. Baumgärtel, Chem. Phys. **46,** 251 (1980).

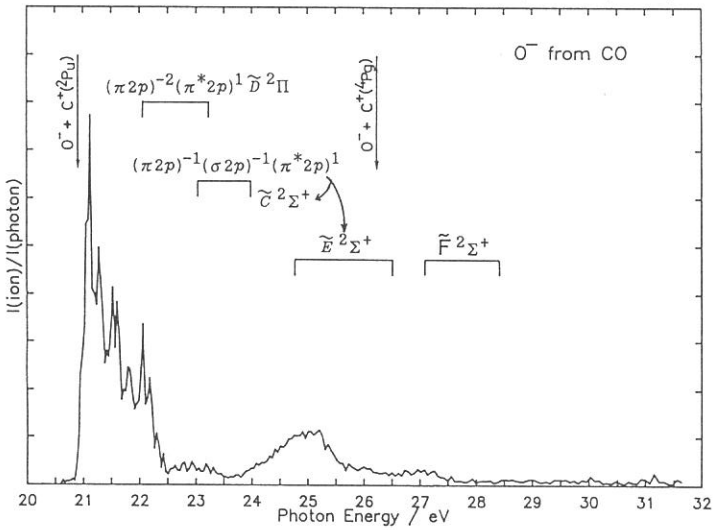

Figure 1. Photodissociation efficiency curve of O^- produced from CO. Regions of the vibrational progressions for the two-electron-excited ionic states are indicated.

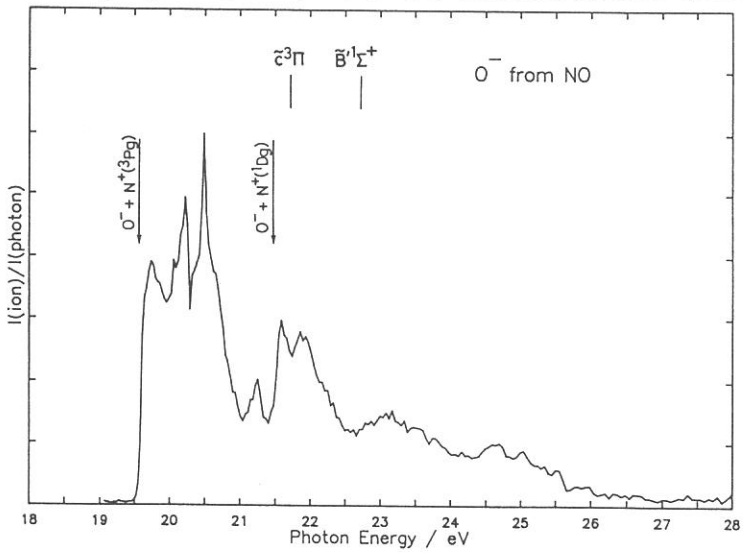

Figure 2. Photodissociation efficiency curve of O^- produced from NO. The adiabatic ionization potentials for NO^+ are indicated.

Carbon K-edge XANES spectra of C_{60} and C_{70}

K. Tohji and H. Shinohara*

Department of Resources Engineering, Tohoku University
Sendai 980, Japan
*Department of Chemistry for Materials, Mi'e University
Tsu 514, Japan

The very stable, nonreactive all-carbon fullerenes C_{60} and C_{70} have produced in macroscopic quantities by vaporization of graphite rods with contact arc. It is presumed that solid C_{60} and C_{70} exhibit unique and completely different electronic properties as compared with graphite and diamond. Perhaps most intriguing is the spherical shape of the non-planer conjugated pi-bond network of those fullerenes which is formally composed of sp^2 hybridized carbon atoms. Therefore, It is particularly important to shed light, experimentally, on the π and σ electronic structure of C_{60} and C_{70}. In general, XANES(X-ray absorption near-edge structure) features are sensitive to the local symmetry and the type of chemical bonding of the exciting atom and can be useful as fingerprints to distinguish structures.

The carbon K-edge XANES spectra of microcrystalline C_{60} and C_{70} at room temperature are displayed in Fig.1. Several band peaks and shoulders are clearly seen. The resonance labeled π^* corresponds to a transition to π^* antibonding orbitals. Between 290 and 310 eV, transitions to σ^* antibonding orbitals are observed. The XANES spectra of C_{60} and C_{70} resemble that of graphite in terms of the presence of an 1s -> π^* transition appearing at 284.8 eV, though the overall spectral features are entirely different. As expected, the carbon K-shell XANES features of the microcrystalline C_{60} and C_{70} are quite different from those of graphite and diamond.

The presence of the π^* resonance at 284.8eV is characteristic of unsaturated(sp^2 or sp) carbon bonds. Its prominent intensity in the C_{60} and C_{70} cluster therefore indicates the presence of unsaturated C-C bonds as in graphite and amorphous carbon (but in contrast to diamond). However, another prominent π^*peak is observed at 287.4 eV in the C_{60} spectrum. This is in marked contrast to the XANES spectra of the other forms of solid carbon. A similar fine structure is also observed in the C_{70} spectrum. In order to examine the angular dependence of the XANES features, the microcrystalline samples were rotated 20-80 degrees relative to the incident X-ray beam. No spectral changes were observed.

This guarantees that the present absorption spectra reflect the density-of-states of the unoccupied states of C_{60} and C_{70}.

These spectral features agree well with the recent theoretical studies done by Saito and Oshiyama[1,2]. In the light of their calculation, for example, the origin of the π^* band peaks at 285.5 and 287.4 eV can be assigned as the g_g -> t_{2u} and g_g -> h_u transitions, respectively. They found that most levels between -6 eV and +7 eV (HOMO = 0 eV) had considerable dispersions in the fcc crystal because of large intercluster overlaps of the bond spreads outside the clusters. Very recently, Terminello et al. have reported a high resolution XANES study on thin film C_{60} and C_{70}. Their XANES spectra show very strong peaks due to the 1s -> LUMO transitions, which are weak in our spectra.

In conclusion, the XANES spectra of C_{60} and C_{70} show fine structures in both of the resonances, and most of the spectral positions of the observed peaks are good agreement with a reported density-of-state calculation.

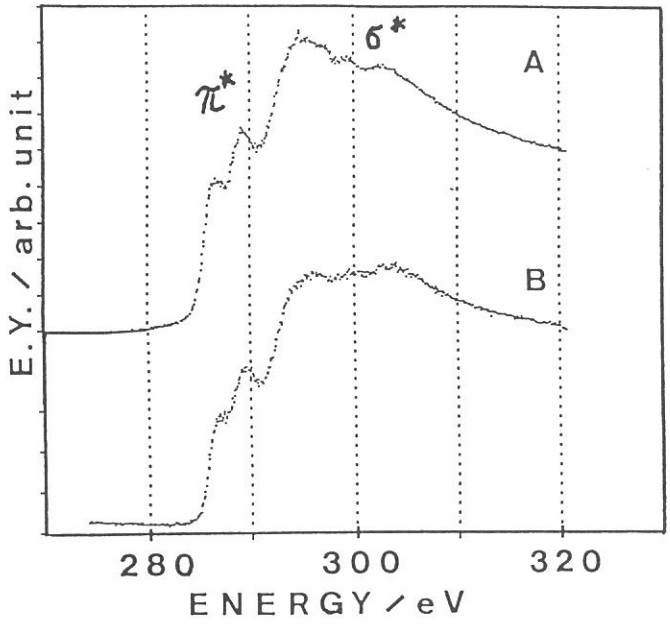

Fig.1 Carbon K-edge XANES spectra of microcrystalline (a) C_{60} and (b) C_{70}. Between 285 and 292 eV, transition to π^*antibonding orbitals are observed. The intensities of two spectra are normalized at 325.8 eV, so that a direct comparison of the absorption intensity is possible.

References

(1) S. Saito, A. Oshiyama, Phys. Rev. Lett., 66, 2637 (1991).
(2) S. Saito, A. Oshiyama, to be published.

WAVELENGTH-DEPENDENT RESPONSE FUNCTIONS OF PHOTOSTIMULABLE PHOSPHOR MATERIALS

Kou KUROSAWA, Masahito KATTO*, Ryusuke MATSUMOTO*, and Wataru SASAKI

Department of Electrical Engineering, University of Miyazaki, Gakuen-Kibanadai-Nishi, Miyazaki 889-21
*Department of Electronics, University of Osaka Prefecture, Mozu-Umemachi, Sakai, Osaka 591

Recently photostimulable phosphor materials have drawn special attention for two-dimensional recording media particularly in medical X-ray diagnostics and X-ray crystal structure analyses because of their advantages of high sensitivity, wide dynamic-range and easy data-acquisition when combined with a computer [1]. The materials emit in the photostimulation process with red light violet light, whose intensity is proportional to the absorbed X-ray photon numbers. The proposed energy diagram of the materials, in particular BaFBr:Eu^{2+}, suggests that it is usable for image recording in the vacuum ultraviolet (VUV) spectral range. In fact, we have obtained the sensitivity and linear response for pulsed ArF (193nm) and Ar_2 (126nm) excimer lasers [2]. The photostimulated luminescence (PSL) intensities were observed to saturate above $6x10^{16}$ photons/cm^2 and $4x10^{14}$ photons/cm^2 for ArF and Ar_2 excimer laser outputs, respectively. The next interesting points are (1) whether the response is different for pulsed and continuous radiation or not, and (2) wavelength range usable.

An imaging plate containing powdered BaFBr:Eu^{2+} was placed in the sample chamber in the beam line BL-1B of UVSOR. The storage was performed with irradiation by monochromatized UVSOR radiation and the absorbed photon numbers were changed by changing the exposure time. As for stimulation measurements, a He-Ne laser was used. The emission was detected by a photomultiplier tube through an optical filter. The PSL intensities for incident photon numbers at 193 and 126nm are shown in Fig. 1. They show good linear response below and saturate around $5x10^{12}$ photons/cm^2 at 193nm and $6x10^{11}$ photons/cm^2 at 126nm. The difference between the cases of the pulsed and quasi-continuous radiation is considered to be explained by the wavelength dependencies in the electron capture rate, halogen vacancy creation probability and absorption coefficient.

Figure 2 shows the wavelength dependence of the PSL intensity. The intensity increases around 200nm, where the absorption coefficient becomes low and the transition probability

high. At 248nm, the PSL intensity was confirmed to show the linear response to the exposed time and also to the pulse numbers from a KrF excimer laser.

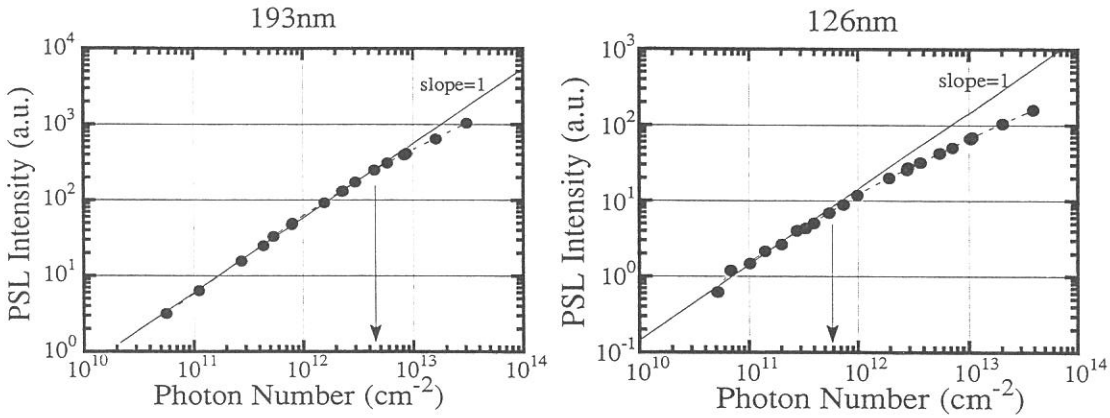

Fig. 1 PSL intensity plotted as a function of the exposure time at 193nm (a) and 126nm (b).

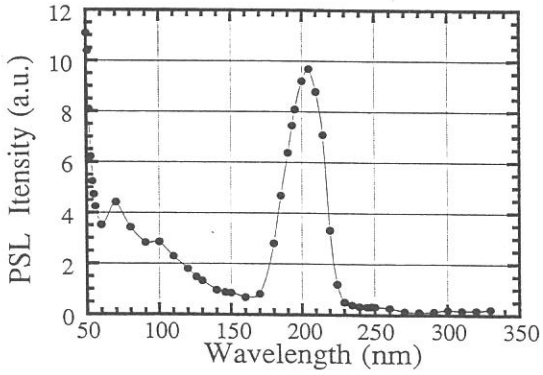

Fig. 2 Wavelength dependence of PSL intensity.

REFERENCES

[1] J.Miyahara, Y.Amemiya and T.Matsushita: Butsuri **45**(1990)398.
[2] M.Katto et al.: Jpn. J. Appl. Phys. **30**(1991)2806.

Soft X-Ray Microscope with Zone Plates II

Norio Watanabe[1], Yoshio Shimanuki[2], Mieko Taniguchi[1] and Hiroshi Kihara[3]

1)Department of Physics, Nagoya University, Nagoya 464
2)School of Dental Medicine, Tsurumi University, Yokohama 230
3)Jichi Medical School, School of Nursing, Tochigi 329-04

An imaging microscope with zone plates was constructed. Optical performance was evaluated at wavelengths of 3.1nm and 5.4nm in terms of modulation transfer functions. Bio-specimens such as diatom and muscle were observed. Wet bio-specimens were also observed using a wet cell at a wavelength of 4.6nm.

X-ray Microscope System

Fig.1 shows a schematic of the optical system of the x-ray microscope set up at BL8A. X-ray source size is defined by an upstream pinhole(UPH;100-400μmϕ). The x-ray from the UPH enters a condenser zone plate(CZP) through a filter(Ti,thickness: 315nm, support:90% transparent Ni mesh) and a mask(an 80% transparent Ni mesh of which the 750*750 μm^2 area is covered with paint). The CZP monochromatized and condensed at a properly placed pinhole(SPH;12μmϕ or 34μmϕ). A specimen, placed a little downstream from the SPH was imaged by an objective zone plate(OZP) on a microchannel plate(single layer). Table-1 shows characteristics of the CZP and the OZP. The magnification of the system is 176 (5.4nm), 148 (4.6nm) or 98.4 (3.1nm). The x-ray images are converted to the visible ones by a fluorescent plate and taken by a SIT camera.

The image data were digitized, accumulated(64 frames), subtracted the background data(accumulated records of the same number of frames without x-ray illumination), and then stored on floppy disks using an image processor.

Modulation Transfer Function(MTF)

The MTFs were measured at 3.1nm and 5.4nm using a zone plate as a specimen (Au, thichness: 0.5μm, diameter: 212μm, outermost zone width: 0.414μm). The zone plate images were stored on floppy disks, and its contrast was measured. Fig.2 shows one of the zone plate images; the outermost zone can be distinguished.

The experimental results had lower contrasts, compared with theoretical calculations. However, taking into account of the resolution of the MCP (FWHM:50μm), the results agree fairly well with the theoretical ones. Fig.3 compares the theoretical and experimental MTFs at 5.4nm.

Dry Bio-specimens

Dry bio-specimens (diatom, muscles of rabbit and crab, collagen, blood cell, human chromesome, magnetotactic bacterium and protoplast) were observed at 3.1nm and 5.4nm. Some of the images were shown in Figs. 4-5.

Wet Bio-specimen

Wet bio-specimens, keeping in a hydrated state and at atomospheric pressure, were observed with a wet cell of which windows are made of polypropylene foils of 4 μm thickness. Spicule of trepang, blood cell, muscle, diatom and protoplast were able to be monitored at 4.6 nm with good contrast. Fig. 6 shows an image of the spicule of trepang.

Acknowledgements
The authors are gratefull for the help and encouragements from Prof. M. Watanabe, O. Matsudo and other staffs of the Institute for Molecular Science. The authors are also grateful for making of the wet cell for Mrs. M. Sugiyama and A. Ohba of Hamamatsu Photonics K.K.

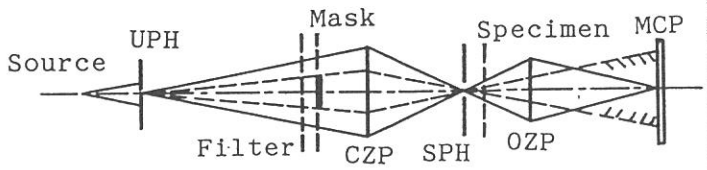

Fig.1 A Schematic of the Microscope.

Table-1 Characteristics of Zone Plates

	CZP	OZP
Diameter(μm)	2400	212
Outermost zone width(μm)	0.44	0.41
Zone number	1350	128
Focus(λ=4.5nm)(mm)	238	19.6
Material	Au	Ni
Manufacturer	Heidenhain	

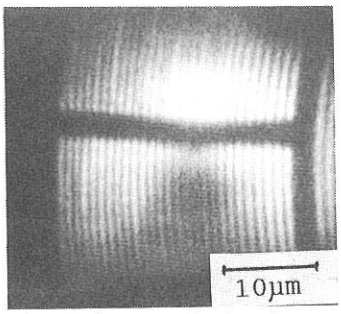

Fig.2 Zone plate image at 5.4nm

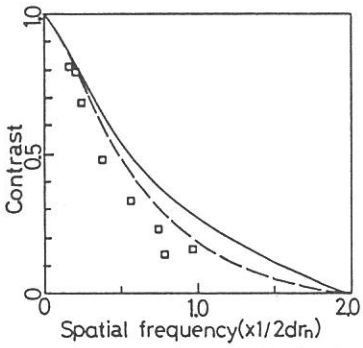

Fig.3 Experimentally obtained (▫) and calculated(solid line and dashed line) MTFs at 5.4nm(SPH:12μmϕ, λ / Δ λ=100). Dashed line:the resolution of the MCP is taken into account. dr_n=0.414μm

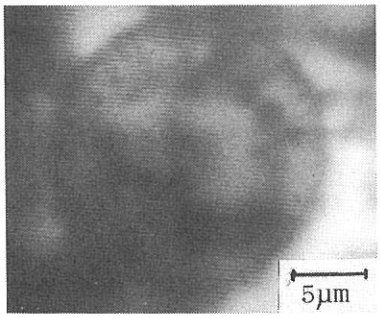

Fig.4 Diatom image at 5.4nm

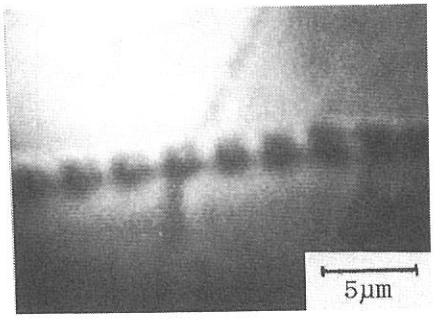

Fig.5 Rabbit muscle image at 5.4nm

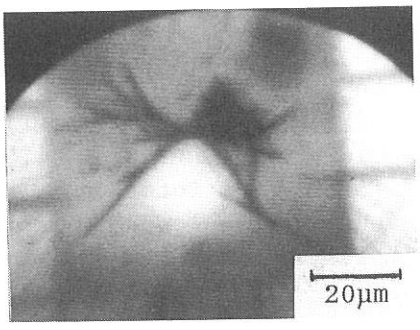

Fig.6 Wet spicule of trepang image at 4.6nm

Ultraviolet Photoelectron Spectra of C_{84} and K_xC_{84}

S. Hino, K. Matsumoto, S. Hasegawa[a], K. Kamiya[b], H. Inokuchi[a], T. Morikawa[c], T. Takahashi[c], K. Seki[b], K. Kikuchi[d], S. Suzuki[d], I. Ikemoto[d] and Y. Achiba[d]

Department of Image Science, Faculty of Engineering, Chiba University, Chiba 260 Japan.

a) IMS, Okazaki 444 Japan.
b) Dept. Chemistry, Nagoya University, Nagoya 464 Japan.
c) Dept. Physics, Tohoku University, Sendai 980 Japan.
d) Dept. Chemistry, Tokyo Metropolitan University, Tokyo 192-03 Japan.

Ultraviolet photoelectron spectra (UPS) of C_{84}, one of the fullerene family compounds, and potassium dosed C_{84} have been measured at BL8B2 of UVSOR. The spectra of C_{84} are compared with those of C_{60} and C_{70} (Fig.1). The photoemission spectral onset of C_{84} is 1.3 eV below the Fermi level, which is smaller by 0.5 eV than that of C_{60} or C_{70}. This indicates its small band gap, which has been expected from their absorption spectra [1]. The FWHM's of the first two bands in the C_{84} spectrum which are supposed to be derived from $C2p_z$ orbitals from the analogy of theoretical calculation of the C_{60} molecule [2] are about 1 eV and wider than those of C_{60}. This should be due to the difference of the symmetry and resultant degeneracy.

Figure 2 shows the photon energy dependence of the photoelectron spectra of C_{84}. The intensity ratio of the first band to the second band oscillates, and it varies from 0.88 ($h\nu$ = 40 eV) to 2.09 ($h\nu$ = 30 eV). This kind of oscillation is also observed in C_{60} [2,3] and C_{70} [4,5]. Except for this intensity oscillation, there is no sudden appearance or disappearance of the structure in the spectra, as has been often observed in the UPS of the strict k-vector conserved system.

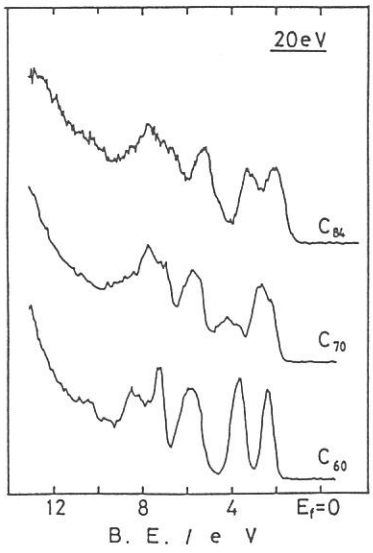

Fig. 1

Upon potassium dosing (Fig.3) a new band forms between the Fermi level and the HOMO band. This is supposed to be due to the filling of the LUMO of C_{84} by K4s electrons. The new band increases its intensity and its edge moves toward the Fermi level in accordance with potassium dosage. However it does not cross the Fermi level, which indicates that potassium dosed C_{84} is not metallic but semiconductive.

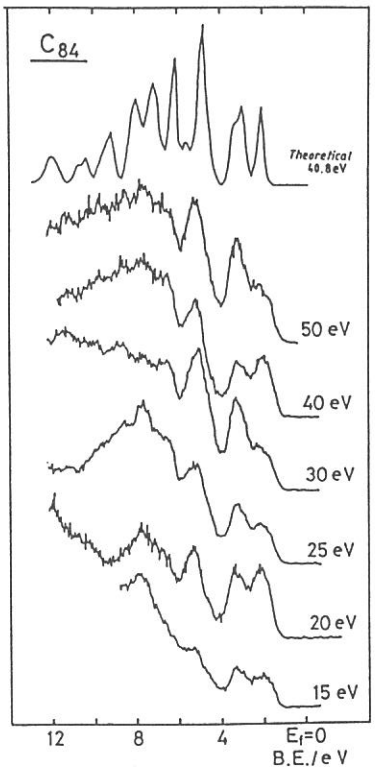

Fig. 2

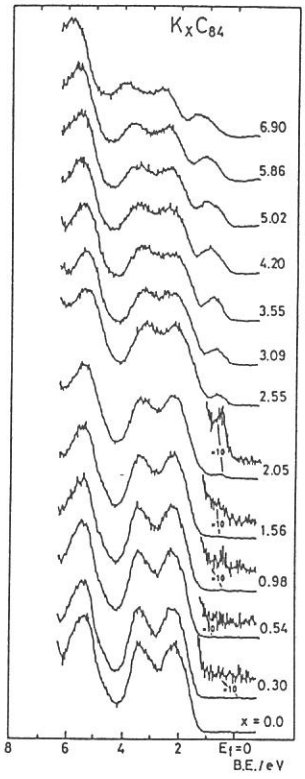

Fig. 3

REFERENCES

1 K. Kikuchi, Y. Nakayama, M. Honda, S. Suzuki, K. Saito, H. Shiromaru, K. Yamauchi, I. Ikemoto, T. Kuramochi, S.Hino, and Y. Achiba, Chem. Letts. 1991, 1607.

2 J. H. Weaver, J. L. Martins, T. Komeda, Y. Chen, T. R. Ohno, H. Knoll, N. Troullier, R. E. Haufler, and R. E. Smalley, Phys. Rev. Letts. 66, 1741 (1991).

3 P. J. Benning, D. M. Poirier, N. Toullier, J. L. Martins, J. H. Weaver, R. E. Haufler, L. P. F. Chibante and R. E. Smalley, Phys. Rev. B44, 1962 (1991).

4 T. Takahashi, T. Morikawa, S. Hasegawa, K. Kamiya, H.Fujimoto, S. Hino, K. Seki, H. K.-Yoshida, H. Inokuchi, K. Kikuchi, S. Suzuki, I. Ikemoto, and Y. Achiba, Physica C, in press.

5 M. B. Jost, P. J. Benning, D. M. Poirier, J. H. Weaver, L. P. F. Chibante and R. E. Smalley, Chem. Phys. Letts. 184, 423 (1991).

FIR ABSORPTION BY ELECTROLYTE SOLUTIONS

Taro DODO, Masao SUGAWA and Eiji NONAKA

Faculty of science, Ehime University, Matsuyama 790

The far infrared absorption spectra of aqueous solutions and methanol solutions of LiCl have been investigated in the frequency range 8 - 40 cm^{-1} at room temperature. In the low frequency range (8 - 20 cm^{-1}), the absorption is mainly controlled by Debye relaxation of the electric dipole rotation, and the absorption decreases as the concentration increases.

FIR absorption through aqueous solutions and methanol solutions of LiCl were investigated with the use of Fourier transform spectrometer. Far infrared radiation from a synchrotron orbit radiation source (UVSOR of the Institute for Molecular Science in Okazaki) is used for radiation source because the radiation intensity from UVSOR is stronger than that from the usual high pressure mercury lamp in the frequency range below 50 cm^{-1}.[1] The radiation power from SOR decreases with $\omega^{1/2}$ whereas that from the black body radiation (lamp) decreases with ω^2.

The first aim of this experiment is to detect the collective mode " plasma oscillation " $\omega_p = (ne^2/\varepsilon m)^{1/2}$ in a high density plasma (highly concentrated electrolyte solution), where n is the ion density, e the electronic charge, ε the dielectric constant of solvent, m the effective mass of the ion. If the numerical values of ω_p were obtained, the dielectric constant ε , which expresses the shielding of the Coulomb field of the ion by the solvent, and the effective mass, which is composed from the ion mass and the mass of solvents sticked to the ion, may be estimated. The existence of the plasma oscillation in high density plasma[2] (strongly coupled plasma k_BT < Coulomb energy) is not detected whereas the collective motion of ω_p is well known in ordinary collisionless plasma (k_BT >> Coulomb energy).

Our experimental results indicate that the plasma oscillation is

not detected. The transmitted radiation intensities through the electrolyte solutions are shown in Figs.1 and 2. The absorptions in concentrated solutions are smaller than that in pure water and alcohol in the frequency range 8 - 20 cm^{-1}. In the high frequency range (> 40 cm^{-1}), the absorption increases as the concentration increases. The authors consider that the absorption in low frequency range consists of mainly Debye relaxation of the electric dipole rotation. The dielectric constant of concentrated aqueous solution[3] is about 20 which is much lower than that of pure water 80. The contributions from Debye relaxation absorption with the use of the dielectric constant and the absorption by the electrical conductivity $\varepsilon_i = \sigma/\varepsilon_0\omega$ are shown in Fig.3 with the experimental value at the frequency 10 cm^{-1}.

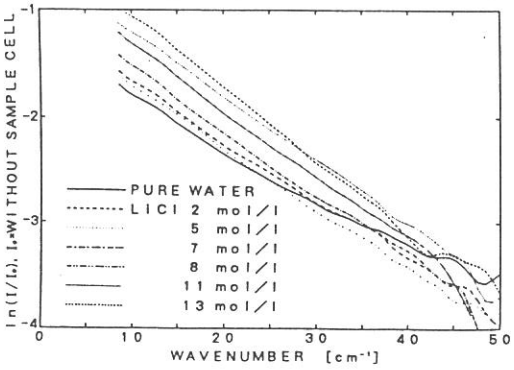

Fig.1 Transmitted FIR intensities through LiCl aqueous solutions normalized by the incident radiation spectrum at 26.5℃.

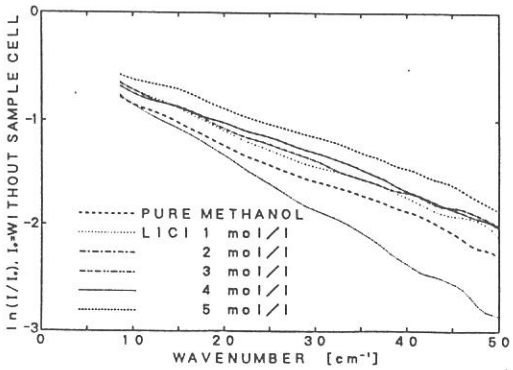

Fig.2 Transmitted FIR intensities through LiCl methanol solutions at 26.5℃.

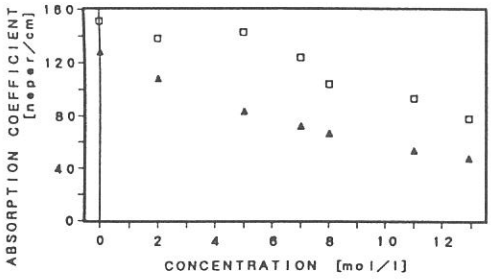

Fig.3 Absorption coefficients □ in LiCl aqueous solution as a function of concentration, deduced from the data in Fig.1 at 10cm^{-1}, in which the reflection loss at the vacuum - quartz window is subtracted. The calculated values from Debye relaxation and the conductivity are shown by the symbol ▲.

1) Takeo Namba ; Rev. Sci. Instruments 60(1989) 1680.
2) S.Tanaka and S.Ichimaru ; Phys. Rev. A 35(1987) 4743.
3) H.Behret, F.Schmithals and J.Barthel ; Z. für Physikalische Chemie N.F. 96(1975) 73.

FIR absorpti(on) electrol(yte) solution

DEFECTS IN HYDROGENATED AMORPHOUS SILICON FILMS INDUCED BY VACUUM ULTRA-VIOLET LIGHT

Yoji SAITO and **Akira YOSHIDA***
Toyohashi University of Technology, Toyohashi 441
*Institute for Molecular Science, Okazaki 444

We have studied[1,2] on the rapid degradation in hydrogenated amorphous silicon (a-Si:H) films induced by irradiation of soft-X ray from synchrotron radiation (SR). The defect creation kinetics by soft-X ray is different from those by visible light.[3] In this work, the defect creation mechanism are investigated through the dependence of the creation kinetics on the vacuum ultra-violet (VUV) light having a wavelength between 5 and 80 nm.

Undoped a-Si:H films with the thickness of about 400 nm were deposited onto glass substrates at 250 °C, using rf glow discharge technique. Aluminum contacts were made on the a-Si:H film for the electrical conductivity measurements.

The a-Si:H samples were irradiated by SR light (BL8B1) through a monochromator as shown in Fig.1. The photo-induced defect density, estimated from the photo-conductivity of the films, is proportional to the irradiation time regardless of the wavelength between 10 and 16 nm. This tendency is in agreement with that by soft-X ray light.[1] However, this defect creation mechanism can occur without an inner-shell excitation, because the 16 nm light cannot excite an inner-shell electron in Si.

The samples were irradiated with the 30-80 nm light which is filtered through a metal film (Al or In or Sn) and reflected by Au 45°mirror from undulator line (BL3A1) as shown in Fig.2. The appropriate filter and the mirror can efficiently cut the higher harmonic components of the undulator light. The proportional relation between the photo-induced defect density and the irradiation time is also obtained up to 50 nm. However, the defect creation is scarcely observed above 70 nm. The results are summarized in Fig.3.

The 10-50 nm light induced electrons have especially short mean free path[4] below 0.5 nm and can ionize the Si atoms. Therefore, the neighbor silicon atoms are likely ionized at the same time. The repulsive Coulomb's force between the positive ionized silicon atoms possibly breaks the Si-Si bonds.[5] The bond-breaking process will create the meta-stable defects because of the structural flexibility in

the a-Si:H system.

References

1. Y.Saito, K.Inoue, A.Yoshida, J.Appl.Phys.**65**, 2552(1989).
2. Y.Saito and A.Yoshida, UVSOR Activity Report 1989, **UVSOR-17**, 90 (1990).
3. M.Stutzmann, W.B.Jackson, C.C.Tsai, Phys.Rev.**B32**, 23(1985).
4. J.C.Riviere, Contemp.Phys.**14**, 513 (1973).
5. Y.Saito and A.Yoshida, Philos.Mag.**B**, submitted.

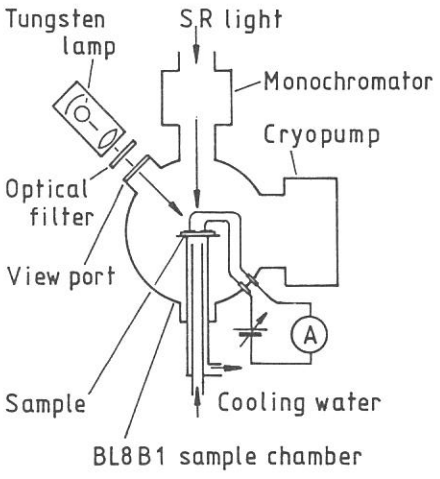

Fig.1 Irradiation apparatus for BL8B1 (10-16 nm)

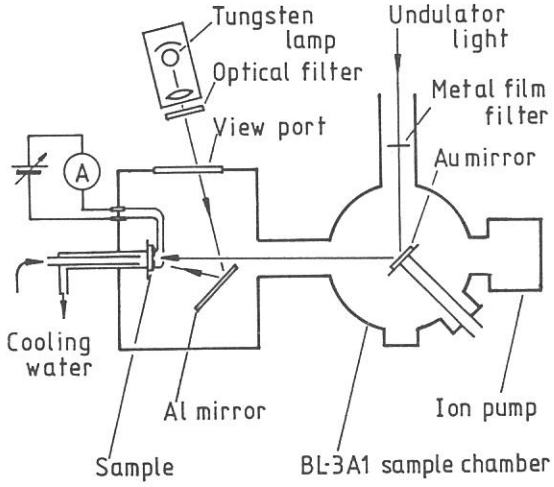

Fig.2 Irradiation apparatus for BL3A1 (30-80 nm)

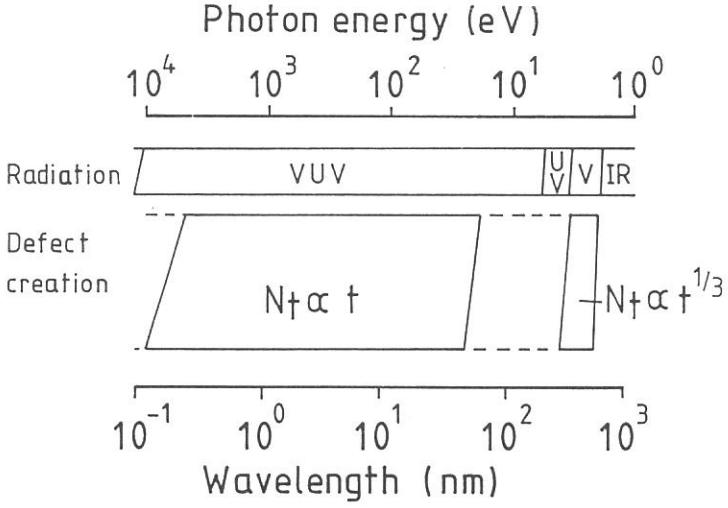

Fig.3 Dependence of defect creation kinetics on irradiation wavelength, where N_t and t are defect density and irradiation time, respectively.

THICKNESS DEPENDENCE OF ANGLE-RESOLVED PHOTOEMISSION SPECTRA FOR COPPER PHTHALOCYANINE ON GRAPHITE SURFACE

[a]N. Ueno, [a]K. Suzuki, [b]K. Kamiya, [b]M. Hasegawa, [c]M. Hara,
[d]K. Seki, [a]K. Sugita, [c]H. Sasabe and [b]H. Inokuchi

[a]Faculty of Engineering, Chiba University, Chiba 260

[b]Institute for Molecular Science, Okazaki 444

[c]Frontier Research Program,
The Institute of Physical and Chemical Research, Wako 351-01

[d]Faculty of Science, Nagoya University, Nagoya 464

The investigation of the molecular orientation and electronic structure of ultrathin films of organic molecules has become important in recent years. This is partly because organic molecules are very attractive as functional materials for new electronic devices. In general, molecular orientation in thin films is affected not only by intermolecular interaction but also the interaction between the molecules and substrate surface. This suggests that the molecular orientation depends on the film thickness. The phthalocyanine class of organic materials have been widely known as the most stable organic semiconductor. They can be sublimed to form high quality thin films [1]. The angle-resolved ultraviolet photoelectron spectroscopy (ARUPS) is powerful for investigating the electronic structure and molecular orientation of the ultrathin films of organic molecules [2].

We have measured ARUPS spectra of thin films of copper phthalocyanine (CuPc) evaporated on to a cleaved graphite (HOPG) surface as a function of the film thickness. The film thickness was measured by a quartz thickness monitor. The intensity of the monochromatized synchrotron radiation was reduced by introducing a nickel mesh of 50% nominal light transmission across the light path. The photon energy ($h\nu$) and incidence angle of photons (α) were fixed at 30 eV and 0°, respectively.

The ARUPS spectra for 9.1 Å and 52.4 Å films are shown in Figs. 1 and 2, respectively, as a function of the electron take-off angle θ, where the photoelectron intensity was normalized to the intensity of incidence photons. In Figs. 3 and 4, the intensities of peaks A and B are plotted as a function of θ for 9.1 Å and 52.4 Å films, respectively. For both films, the θ dependence of the intensity of peak A is sharper than that of peak B. This can be understood by an idea that peak A consists of single π state, while peak B involves many other states. It is notable that the θ dependence of peak A is much sharper for 9.1 Å film than that for 53.4 Å film. This result indicates that the degree of the molecular orientation of 9.1 Å film is better than that of 52.4 Å film.

References

[1] N. Ueno, T. Shinmura, and K. Sugita, Phys. Rev. B44, 6472 (1991).

[2] *Photoemission and the electronic properties of surfaces*, ed. by B. Feuerbacher, B. Fitton, and R. F. Willis, (John Wiley & Sons, New York, 1979).

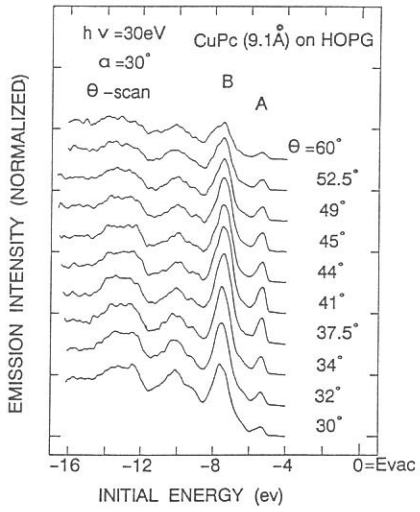

Fig. 1 θ dependence of ARUPS spectra for CuPc film (9.1Å) on HOPG graphite. The photon energy was 30 eV and the incidence angle was 0°.

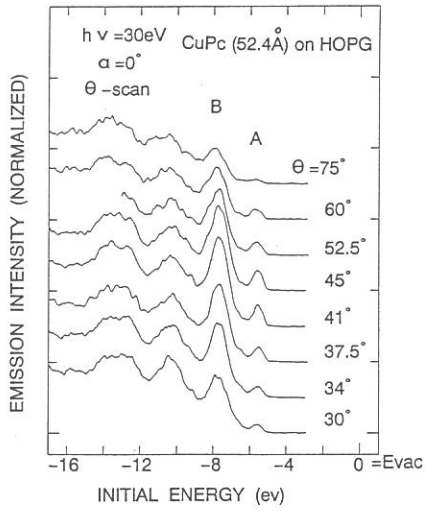

Fig. 2 θ dependence of ARUPS spectra for CuPc film (52.4Å) on HOPG graphite. The photon energy was 30 eV and the incidence angle was 0°.

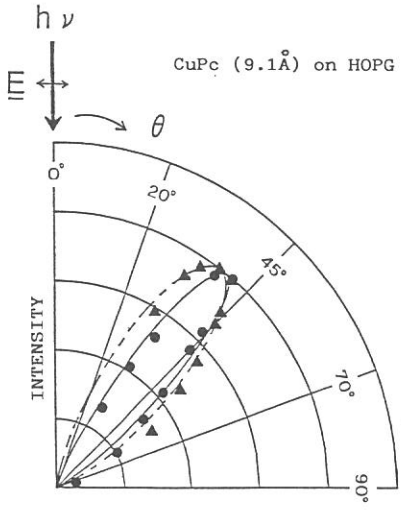

Fig. 3 θ dependence of the intensity of peaks A (●) and B (▲) for 9.1 Å film.

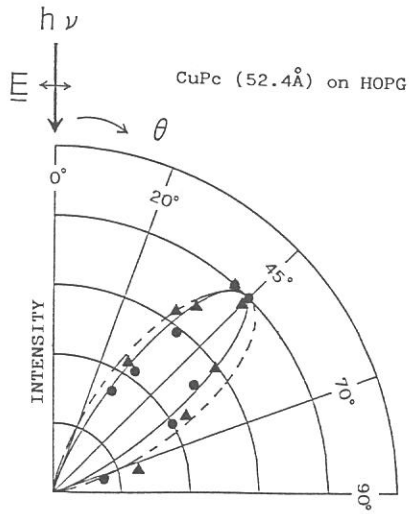

Fig. 4 θ dependence of the intensity of peaks A (●) and B (▲) for 52.4 Å film.

EXCITATION SPECTRUM OF CN($A^2\Pi_i$) AND CN($B^2\Sigma^+$) PRODUCED BY PHOTODISSOCIATION OF SIMPLE NITRILES IN THE 105 - 150 nm REGION

Kazuhiro KANDA, Syunji KATSUMATA,
Takashi NAGATA*, Tamotsu KONDOW*,
Atsunari HIRAYA**, Kiyohiko TABAYASHI** and Kosuke SHOBATAKE**

Department of Fundamental Science, College of Science and Engineering, Iwaki Meisei University, Iwaki 970
* Department of Chemistry, Faculty of Science, The University of Tokyo, Bunkyo-ku 113
** Institute for Molecular Science, Myodaiji, Okazaki 444

Vacuum ultraviolet (VUV) photodissociation of a cyanogen-containing molecule produces a CN radical in a variety of electronically excited states; the radical produced in $A^2\Pi_i$ and $B^2\Sigma^+$ states immediately fluorescences into the ground electronic state and a subsequent strong emission is observed. In the present study, VUV absorption spectra and fluorescence excitation spectra for the CN(A-X, B-X) emission of several nitriles were measured in the wavelength range of 105-150 nm. The fluorescence excitation spectrum was measured by monitoring the emission from the product CN radical through adequate optical filters as a function of excitation wavelength.

Figures 1(a) and 1(b) depict the observed VUV absorption spectrum and fluorescence excitation spectrum of CH_3CN, respectively. The band structure appearing in this wavelength region has been assigned to transitions into the Rydberg states converging to the first and the second ionization potentials, or to the transitions into high-lying valence states.[1,2] The absolute scale for the emission cross sections was determined by a comparison of the observed emission intensities with those in the photodissociation of HCN. The emission cross sections obtained in the present measurements correspond to the cross sections for the production of CN(A) and CN(B) radicals from the nitrile because no processes other than the radiative decay is expected for the $A^2\Pi_i$ and $B^2\Sigma^+$ states of CN.

As shown in Fig. 1(B), the fluorescence excitation curve for the CN(B-X) emission almost mimics that for the CN(A-X) emission, while the absolute cross

section is 2-3 times larger for the CN(A) production. This indicates that the CN(A) and CN(B) fragments are produced via identical precursor states of CH_3CN. The production of CN(A) is found to be enhanced via $2e \rightarrow np\sigma$ transitions around 125nm (see Fig. 1(c)). This observation can be explained by a simple molecular-orbital assignment as follows. The highest occupied molecular orbital of CH_3CN, $2e(\pi_{C-N})$ bonding orbital, correlates to the 1π orbital of CN radical. Hence, the $2e \rightarrow np\sigma$ transitions possibly gives rise to a hole in the 1π orbital of the incipient CN radical, which asymptotically correlates to a free CN fragment in $A^2\Pi_i$ state. The quantum yield for the production of the excited CN radicals reaches at most $\sim 8\%$ in the wavelength region studied. Most of the product CN seems to be formed in the ground electronic state as CN(X). The spectra for larger nitriles, such as C_2H_5CN and $n\text{-}C_3H_7CN$, display remarkably different features; only diffuse bands were observed.

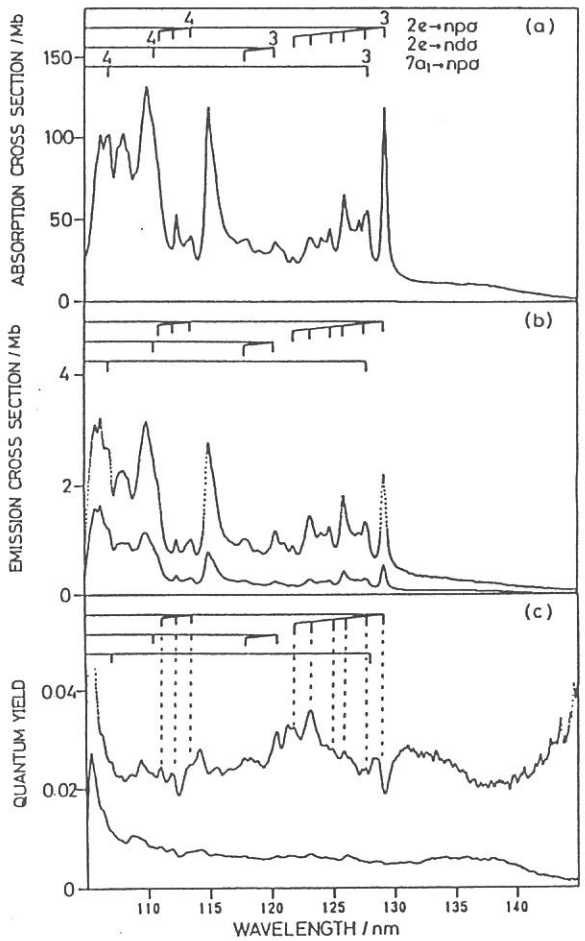

Figure 1. (a) Absorption spectrum of CH_3CN.
(b) Fluorescence excitation spectra for CN(A-X) (dotted line) and CN(B-X) (solid line).
(c) Quantum yield for the production of CN(A) (dotted line) and CN(B) (solid line).

references

[1] C. Fridh, J. Chem. Soc. Faraday Trans. II, *74*, 2193 (1978).

[2] J. A. Nuth and S. Glicker, J. Quant. Spectrosc. Transfer, *28*, 223 (1982).

Effect of pressure on the far-infrared collision-induced absorption of liquid benzene and hexafluorobenzene

Yoshitaka FUJITA, Takahiro CHO and Shun-ichi IKAWA

Department of Chemistry, Faculty of Science, Hokkaido University, Sapporo 060

Effect of pressure on the far-infrared collision-induced absorption(CIA) bands of non-polar liquids provides a clue to the local structure of the liquids and the intermolecular interactions. Previously, we measured the CIA bands of liquid CS_2 and CCl_4 under pressure and obtained the zeroth and second spectral moments as functions of pressure.[1] In the present study, the far-infrared CIA bands of liquid C_6H_6 and C_6F_6 have been measured at pressures in the 1-540 bar range. The experimental setup was described previously.[1),2] The resulting CIA bands of both liquids are shown in Fig. 1. For both liquids, with increasing pressure, the total intensities of the bands increase while the intensities of the low-frequency wing decrease. The zeroth and second moments were obtained from the curves fitted to the experimental intensity, which are shown by broken lines in Fig. 1. From the zeroth moment, an average magnitude of the collision-induced dipole moment $\sqrt{\langle\mu^2\rangle}$ is obtained by

$$\langle\mu^2\rangle = c\left(\frac{F}{\rho}\right)\int \nu^{-2}\alpha(\nu)\,d\nu$$

where c is a constant, F a correction factor for the internal-field effect, ρ the number density. The resulting values of $\sqrt{\langle\mu^2\rangle}$ and the second moment M_2 are plotted against pressure in Fig. 2. With increasing pressure, the second moments increase while $\sqrt{\langle\mu^2\rangle}$ decrease. The rate of decrease in $\sqrt{\langle\mu^2\rangle}$ with pressure is larger for C_6H_6 and C_6F_6 than for CS_2 and CCl_4, which indicates the larger cancellation effect due to the many-body interactions for the former liquids. The pressure dependence of $\sqrt{\langle\mu^2\rangle}$ can be estimated by

calculating the local electric field from surrounding molecules by use of the local structure model. In order to develop the above discussion, a molecular dynamics calculation is now in progress.

References
1) Y. Fujita, T. Ohba and S. Ikawa, Can.J.Chem., 69, No. 11 (1991).
2) Y. Fujita and S. Ikawa, UVSOR Activity Report 1991, p97.

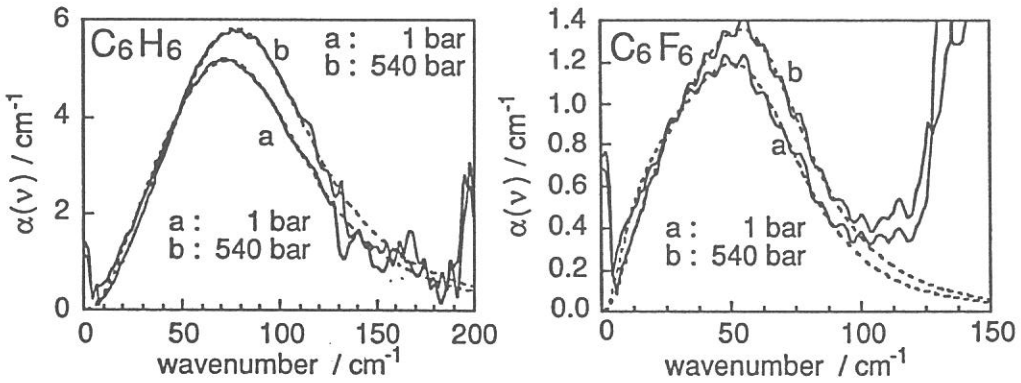

Fig. 1 Effect of pressure on the far-infrared spectra of liquid C_6H_6 and C_6F_6.

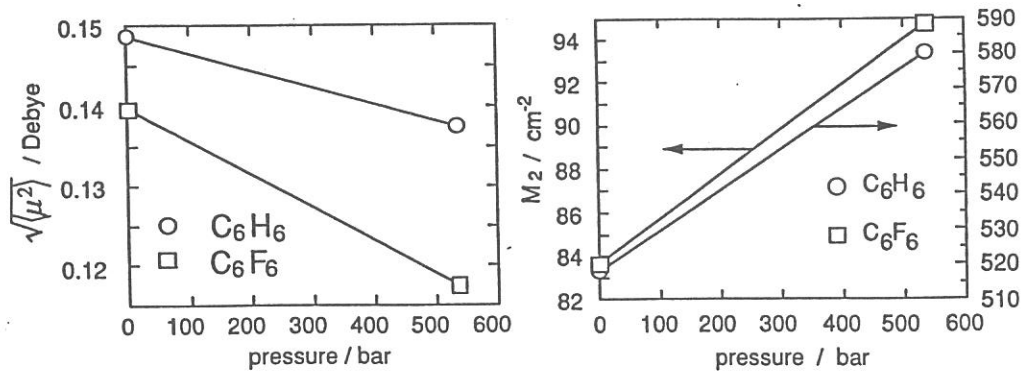

Fig. 2 The root-mean-square values of the induced dipole moments $\sqrt{\langle \mu^2 \rangle}$ and the second spectral moments $M_2 = \int \alpha(\nu)\, d\nu$ of liquid C_6H_6 and C_6F_6 plotted against pressures.

VUV Reflectivity Spectra of Rare-Earth Sesquioxides

Shin-ichi KIMURA, Fumitaka ARAI, Mikihiko IKEZAWA,
Yuki CHIBA and Mareo ISHIGAME
Research Institute for Scientific Measurements, Tohoku University,
Aoba-ku, Sendai 980

A series of rare-earth sesquioxide R_2O_3 is a typical insulator rare-earth compound. Over the past years, however, only a few studies have been made on the VUV reflectivity spectra of two kinds of rare-earth oxide, CeO_2 [1, 2] and Y_2O_3 [3], and no systematic optical study in the VUV region of R_2O_3 has ever been made. Then reflectivity spectra of four kinds of R_2O_3 (R = La, Nd, Gd and Y) single crystals were measured in the photon energy region between 2 eV and 35 eV at 300 K at the beamline BL7B. Our purpose is to investigate the fundamental electronic state of R_2O_3 including the mixing effect between rare-earth (R) 4*f* and oxygen (O) 2*p* states.

Single crystals of these materials were grown by a floating zone method using a Xe-arc lamp image furnace. We measured their reflectivity spectra using the cleavage surface of the crystals. The crystal structure of La_2O_3 and Nd_2O_3 is hexagonal and a layered structure, which is called A-type generally, and these crystals are easily cleaved along the c-plane. On the other hand, Gd_2O_3 and Y_2O_3 form bcc type crystal structures (C-type) and both of these materials are cleaved parallel to {111} - plane.

Figure 1 shows reflectivity spectra of all the materials. All of these spectra are almost similar to one another. This means that the origin of these structure is the transition from O-2*p* and R-5*p* to R-5*d*. The absorption edge of all these materials is located at around 6 eV. The detailed analysis is proceeded by using the optical conductivity spectra (Fig. 2), which are derived from the Kramers-Kronig transformation of the reflectivity spectra in Fig. 1. It is seen that the sharp rise of the structure is located at around 6 eV and two large peak structures are located at around 10 eV (now called a) and 30 eV (b). We can see that the sharp rising structure obviously shows the transition between the energy gap from the valence band (O-2*p*) to the conduction band (R-5*d*). Therefore the origin of the a-peak is the charge transfer excitation from the O-2*p* to the R-5*d*. The origin of b-peak is explained as follows. The systematic optical study of the rare-earth hexaboride VUV reflectivity spectra shows that the transition from 5*p* core state to 5*d* is seen at around 30 eV. [4] The same explanation applies to the R_2O_3 optical spectra, i. e., the origin of the b-peak is the intra-atomic transition from R-5*p* to R-5*d* states.

The detailed study about other rare-earth oxides and 2*p*-4*f* mixing and other effects will be continued.

References

[1] F. Marabelli and P. Wachter, Phys. Rev. **B36**, 1238 (1987).

[2] M. Niwano, S. Sato, T. Koide, T. Shidara, A. Fujimori, H. Fukutani, S. Shin and M. Ishigame, J. Phys. Soc. Jpn. **57**, 1489 (1988).
[3] T. Tomiki, J. Tamashiro, Y. Tanahara, A. Yamada, H. Fukutani, T. Miyahara, H. Kato, S. Shin and M. Ishigame, J. Phys. Soc. Jpn. **55**, 4543 (1986).
[4] S. Kimura, T. Nanba, S. Kunii and T. Kasuya, submitted to Phys. Rev. **B**.

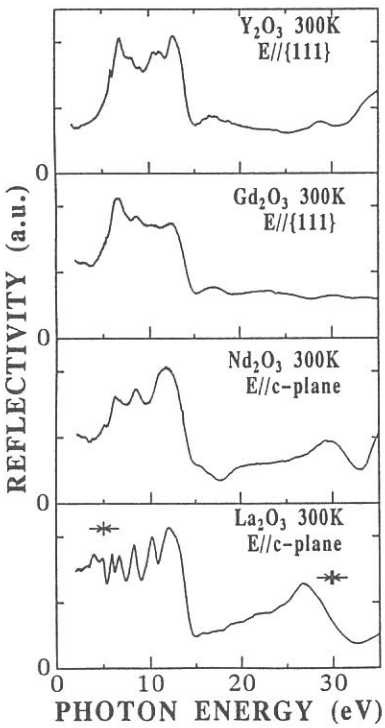

Fig. 1. Reflectivity spectra of R_2O_3 (R = La, Nd, Gd and Y) crystals in the photon energy region between 2 eV and 35 eV at 300 K.

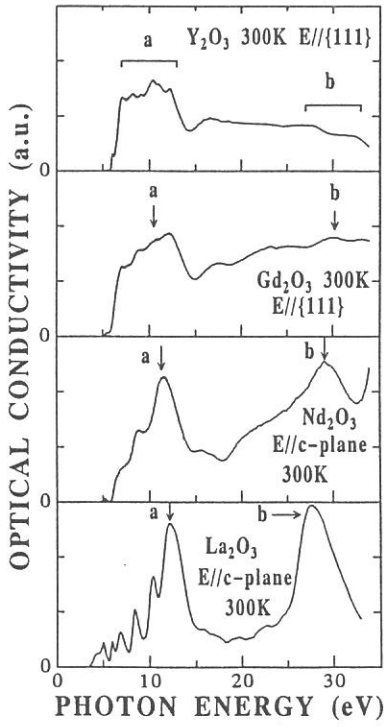

Fig. 2. Optical conductivity spectra of R_2O_3, which were derived from the Kramers–Kronig transformation of the reflectivity spectra in Fig. 1.

MASS SPECTROSCOPIC ANALYSIS IN SR PHOTO-CVD OF SiO_2 THIN FILM

Masanori OOKUYAMA Yuichi MATSUI, Takeshi KANASHIMA,
Junko IZUMITANI and Yoshihiro HAMAKAWA

Department of Electrical Engineering, Faculty of Engineering Science,
Osaka University, Toyonaka, Osaka, 560

Investigation of chemical reaction in SR-photo-CVD of SiO_2 thin film is very important for understanding the deposition mechanism and improving the film quality. The molecular and atomic species produced in vapor phase reaction were analyzed from the mass-spectroscopic measurement. Figure 1 shows top view of the measuring system of the mass spectrum[1]. Gate valve system, evacuation system and reaction chamber for the deposition are almost the same as that in the previous report[2]. Whole light beam from BL-8A of UVSOR was applied to the sample without any spectroscopic system. The substrates of n/n^+-Si(100) single crystals were set on a sample holder in the reaction chamber. The tube of a quadruple mass analyzer (ULVAC Co., QMA-400) was set to the deposition chamber through a stainless tube, which had a short tube of diameter 1/16 inch at its top. It has been confirmed from a viewing port of the deposition chamber that the top of the tube entered the area irradiated by SR. Signals from the mass-spectrometer were sent to the micro-computer. Si_2H_6 and O_2 gases were mixed at 0.2 Torr in the deposition chamber. Partial pressures of Si_2H_6 and O_2 were 0.01 Torr and 0.19 Torr, respectively. The SR was applied for 20 min and the ion currents were measured every minutes for m/e=1-102 with the assistance of a microcomputer. Amounts of various species increase because of decomposition of the reaction gases by the SR. However, as the total pressure is fixed at 0.2 Torr, the absolute increasing or decreasing in quantity of the species cannot be compared. Therefore, the relative increasing or decreasing was obtained by the ion current intensities of all mass number (m/e=1-102) normalized with that of Si_2H_6 (m/e=62). Figures 2 (a), (b) and (c) show the normalized ion current intensities of species Si_2H_x ($1 \leqq x \leqq 5$), SiH_y ($0 \leqq y \leqq 3$) and $SiOH_z$ ($0 \leqq z \leqq 4$), as a function of irradiation time, respectively. The Si_2H_x ($0 \leqq x \leqq 5$) are decreased a little by irradiation of the SR light. The SiH, SiH_2 and SiH_3 are increased a little, and the increase of the Si is rather larger than those of these species. Moreover, increasing of the SiO is rather larger than that of SiOH, but $SiOH_z$ ($2 \leqq z \leqq 4$) are very small in this work and show no change. The high

values of Si and SiO in the dark are caused N_2 and CO_2 contained in background, respectively. Inoue et al. pointed out from the mass spectroscopic analysis that precursor for SiO_2 film deposition is estimated to be Si_2OH_5 in the photo-CVD using D_2 lamp[3]. But, Si_2OH_5 and Si_2OH_6 are very small and are not changed by the SR irradiation. The precursor for the SiO_2 thin film deposition may be SiO and Si as only these species increase under the irradiation. Therefore, SR photo-CVD is very effective for making good SiO_2 thin films having low concentration of the Si-H and Si-OH bonds.

References

1) Y. Matsui, R. Nagayoshi, M. Nakamura, M. Okuyama and Y. Hamakawa: to be published in Jpn. J. Appl. Phys.

2) M. Okuyama, M. Nakamura and Y. Hamakawa: Solid State Electron. 33 Suppl. (1990) 149.

3) K. Inoue, Y. Nakatani, M. Okuyama and Y. Hamakawa: J.Appl.Phys. 64(1988)6496.

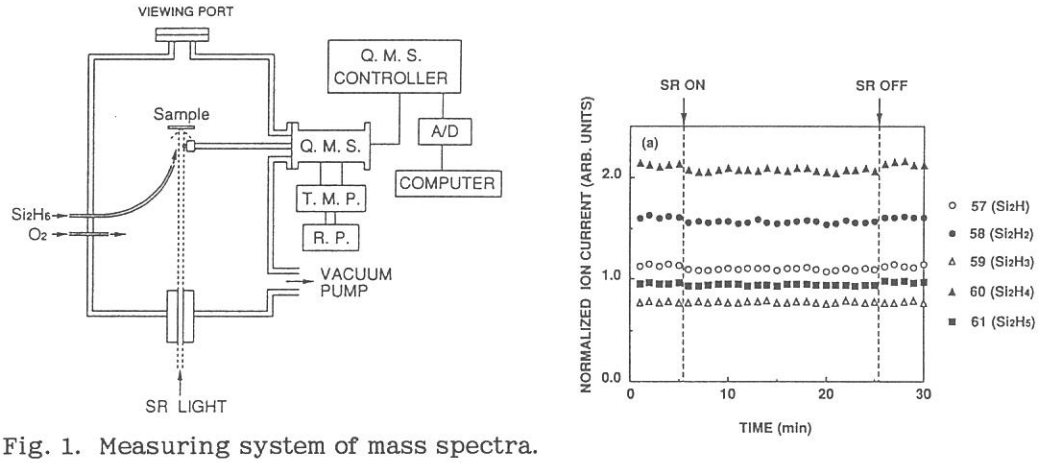

Fig. 1. Measuring system of mass spectra.

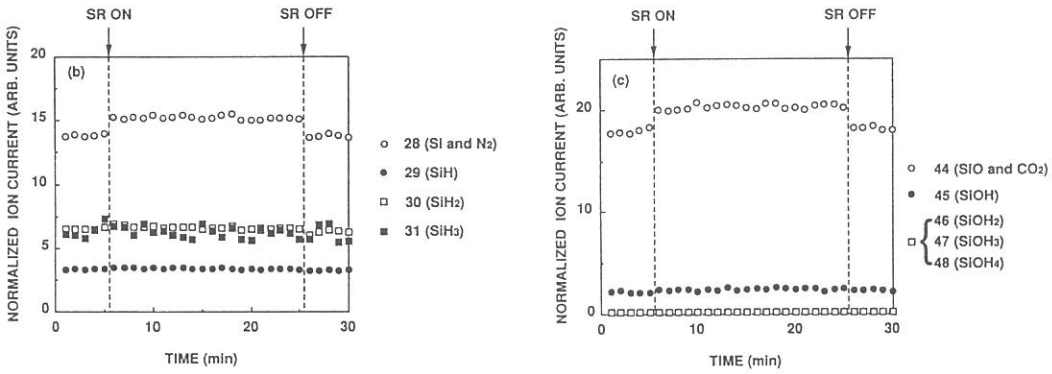

Fig. 2. Ion current of (a)Si_2H_x($1 \leqq x \leqq 5$) (m/e=57-62), (b)SiH_y($0 \leqq y \leqq 3$)(m/e=28-31) and (c)$SiOH_z$($0 \leqq z \leqq 4$) (m/e=44-48) normalized with that of Si_2H_6 (m/e=62) in Mass-spectroscopic measurement.

Far-infrared spectroscopy of hydorogen-banded ferroelectrics

Shinji SAITO, Shik SHIN[A], Yuki CHIBA,
Kiyoshi DEGUCHI[B], Mareo ISHIGAME

Resaerch Institute for Scientific Measurements,
Tohoku University, Sendai 980
[A]The Institute for Solid State Physics,
The University of Tokyo, Tokyo 188
[B]Department of Physics, Faculty of Science,
Hiroshima University, Hiroshima 730

There have been many investigations on potassium dihydorogen phosphate (KDP) and its isomorophs by means of infrared spectroscopy. We have already reported infrared reflectivity spectra of CDP and RDP[1]. In this report, we have measured the infrared reflectivity spectra of KDP , deuterated KDP (DKDP) and deuterated RDP (DRDP).

KDP type crystals are well known as the material showing the large isotope effect on the phase transition temperature. For instance, by the deuteration of KDP it increases by about 100K. However there are a lot of questions on these phase transition mechanism. Thus, it is important to find a real soft mode involving relaxation mode. Therefore we measured infrared reflectivity spectra by using synchrotron radiation (SR) as a light source in the low frequency region in which such a soft mode should be observed. SR is useful for far-infrared source, because it is brighter than the conventional light source in the low frequency region and it is polarized in horizontal plane.

The far-infrared reflectivity spectra were measured by the b-c surface of crystal with the configuration of polarization parallel to the crystallographic c-axis using Martin-Puplet interferometer in frequency region from 10 to 250 cm^{-1} at BL6A installed at UVSOR.

Figure 1 shows the temperature dependence of the reflectivity spectra of KDP, DKDP, RDP, and DRDP. It is found that each of these spectra shows a wing of the central peeks. In the deuterized crystal, the reflectivity of wings seems to decrease comparing with the non-deuterized sample.

These spectra are analyzed by the factorized form[1] of four-parameter dispersion formula. By this analysis,central peeks are found to consist of relaxation modes and overdamped modes which do not become soft toward Tc (figure 2). However, it is clear that relaxation modes show critical relaxation toward Tc (figure 3). It is concluded that the real soft mode is the relaxation mode. Moreover, it is clear that the reflectivity of overdamped modes are decreased by the deuteration as a result of the decrease of TO-LO splitting in both KDP and RDP. Since we have already showed[1] that the overdamped mode is not A_1 librational mode in RDP, it is believed that the overdamped mode is not A_1

librational mode in even KDP. However the origin of over-damped mode is not understood in this study. We tentatively claim that it is a proton mode which is suggested by Onodera et al[3].

References

1). S.Saito, S.Shin, Y.Chiba, and M.Ishigame, UVSOR Activity Report 1990 p.93 (1991).
2). P.Simon and F.Gervais, Phys. Rev. B 37, 1969 (1988).
3). Y.Onodera, Buturi 46, 23 (1991).

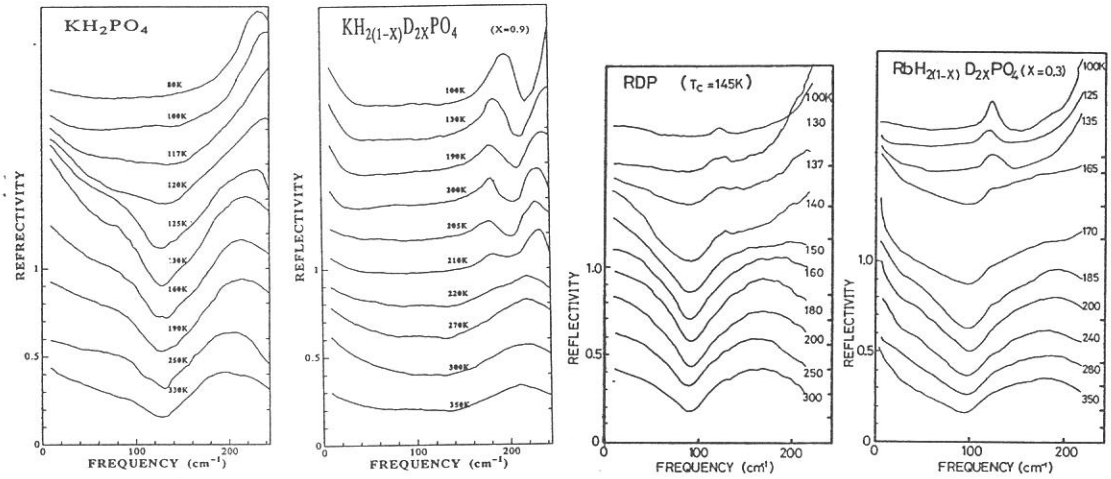

Fig. 1 The temperature dependence of the reflectance spectra of KDP,DKDP,RDP,and DRDP.

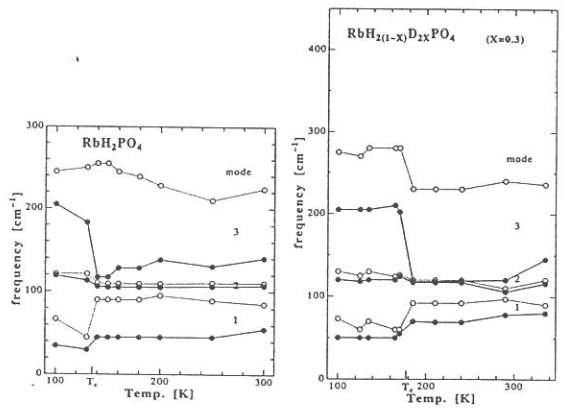

Fig. 2 The temperature dependence of external mode ferequencies. (open and full circles are LO and TO modes.)

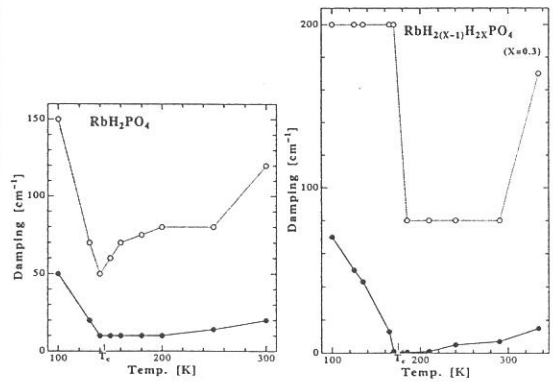

Fig. 3 The temperature dependence of dampping of the relaxaion modes. (open and full circles are LO and TO modes.)

ANGLE-RESOLVED PHOTOEMISSION FROM ORIENTED SEXIPHENYL

Satoru NARIOKA, Kunishige EDAMATSU, Hisao ISHII,[*]
Akira YUYAMA,[*] Koji KAMIYA,[*] Shinji HASEGAWA,[**]
Hiroo INOKUCHI,[**] Toshiaki OHTA, and Kazuhiko SEKI[*]

Department of Materials Science, Faculty of Science, Hiroshima University, Kagamiyama, Higashihiroshima 724
[*]Department of Chemistry, Faculty of Science, Nagoya University, Chikusaku, Nagoya 464
[**]Insitute for Molecular Science, Myodaiji, Okazaki 444

INTRODUCTION

Conjugated polymers with extended pi electron systems recently attract much attention for their potential practical applications and also for being suitable materials of basic understanding of the electronic properties. Poly(*p*-phenylene) (PPP) is one of such conjugated polymers. We have been studying its electronic structure using the technique of ultraviolet photoelectron spectroscopy (UPS) with the samples of PPP [1] and its model compounds *p*-phenylenes up to the hexamer *p*-sexiphenyl [2].

In our previous studies [1,2], only unoriented samples of PPP and oligomers could be prepared, and the obtained results mainly reflect the valence density of states of these materials. In this study we report more detailed study by the combination of oriented sample of sexiphenyl and synchrotron radiation.

EXPERIMENTAL

Oriented samples of sexiphenyl were prepared by vacuum deposition onto heated Ag substrate. Examination by X-ray diffraction and infrared reflection-absorption spectroscopy revealed that the molecules are oriented with their long molecular axis vertical to the substrate surface. The UPS spectra were measured on the angle-resolving UPS system at BL8B2 of UVSOR. Most of the spectra were recorded with the setup of normal emission, with the electron energy analyzer accepting the photoelectrons emitted vertical to the sample surface, and some spectra were measured also with the setup of off-normal setup.

RESULTS AND DISCUSSION

In Fig. 1 we show the normal emission UPS spectra of the uppermost pi states at several photon energies. The spectral features in this energy range are derived from the doubly degenerate HOMOs of benzene. One of them is not perturbed by forming sexiphenyl molecule due to the lack of electron density at the bridge-head carbons, while the other HOMO with pi electron density at these carbons interact strongly to split into six levels. The intense peak D in Fig. 1 corresponds to the unpertured state, while the features A and B correspond to the split levels. We note that the features A and B are clearly

observed at photon energy of 36 eV, while they are barely observable at 44 eV. The former photon energy corresponds to the excitation energy expected from the simple *k*-conservation rule in the intramolecular pi band, and the results in Fig. 1 may correspond to the first observation of the validity of such a selection rule for an extended pi electron system. More detailed studies at various photon energies including off-normal emission are underway.

References

[1] K. Seki, K. Edamatsu, S. Narioka, T. Ohta, K. Kamiya, H. Inokuchi, and T. Yamamoto, UVSOR Activity Rep. (1990) 71.
[2] K. Seki, U.O. Karlsson, R. Engelhardt, E.E. Koch, and W. Schmidt, Chem. Phys., 91 (1984) 2091.

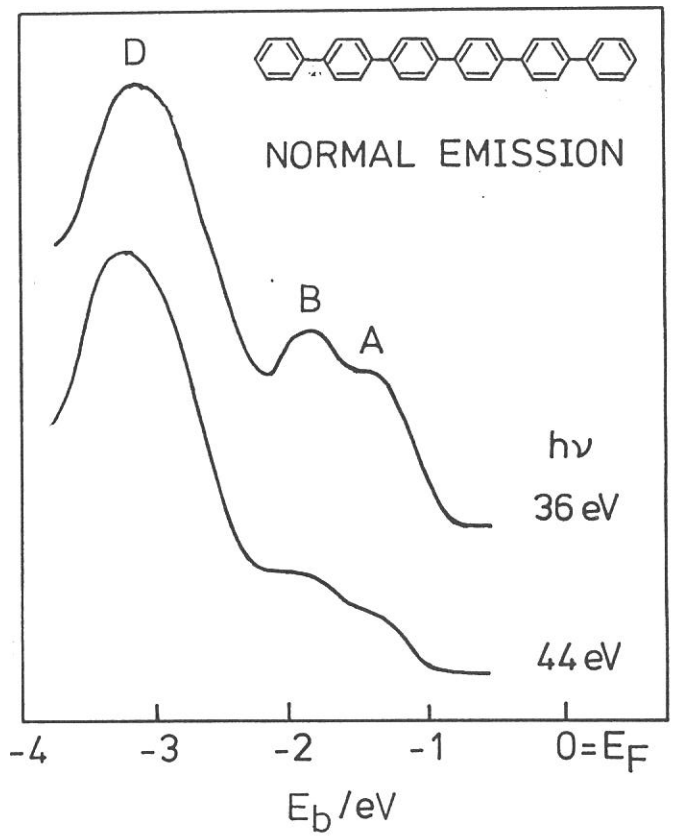

Fig. 1. Normal emission UPS spectra of *p*-sexiphenyl oriented with their long molecular axis vertical to the substrate.

X-Ray-Absorption Near-Edge Structure of Solid Rare Gases

Atsunari HIRAYA and Makoto WATANABE

Institute for Molecular Science, Myodaiji, Okazaki 444

X-ray absorption near-edge structure (XANES) spectra of solid rare gases were recorded for Ne *K*-edge, Ar *K*-edge, Kr *L*-edge, and Xe *M*-edge. Observed peak positions in XANES spectra are interpreted using a model proposed and applied to the sulfur $L_{2,3}$-edge and several edges of alkali halides by Kasray et al.[1] This model is based on the Natoli's theory,[2] in which XANES features are correlated with interatomic distances R, according to the equation $E_r = E_b + C/R^2$, where E_r is the energy of the peak, E_b is the energy of an excitonic resonance just before the onset of the continuum, and C is a constant for the absorbing material. Since all solid rare gases have the same crystal structure, studies on their XANES is interesting to check the applicability of this model.

The x-ray absorption spectra were measured, using transmission method, at BL7A and BL1A both equipped with a double crystal monochromator (DXM). As the monochromator crystal, beryl was used for Ne-*K*, Kr-*L*, Xe-*M* and germanium for Ar-*K*. Solid samples of rare gases were deposited on an Al foil (0.8 μm) which was supported on a sample holder at the cold end of a He-cryostat.

Figure 1(a) shows the *K*-edge XANES spectrum of solid Ne. The peak positions of XANES of Ne and other solid rare gases studied are given in Table I. Peak *a* of Ne *K*-absorption is a $1s \rightarrow 3p$ exciton band and peak *b* is a composite of the higher exciton band and continuum of the second conduction band having *p*-like character.[3] Figure 1(b) shows plots of R^{-2} versus photon energy, where values of R correspond to the second neighbor distance R_2 (peak *c*), the first neighbor distance R_1 (peak *d*), and d_{111} lattice spacing (peak *e*) in decreasing order. The d_{111} is included in the present analysis because it is known that the backscattering of photoelectrons which gives XANES peak occurs not only at atoms but also at crystal lattice planes.[1] Peaks are chosen so that the linear fitting

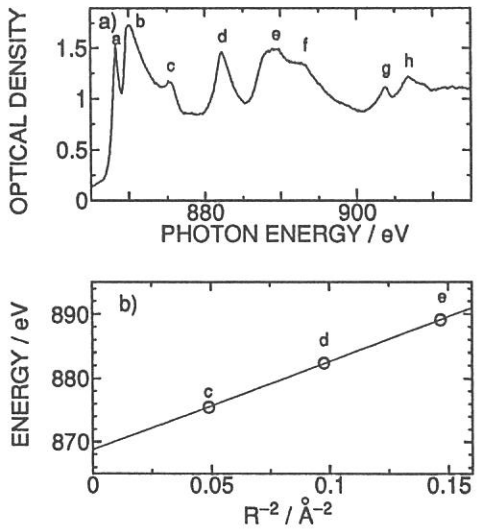

Figure 1. Ne *K*-edge XANES spectrum and correlation plot between energy and R^{-2}.

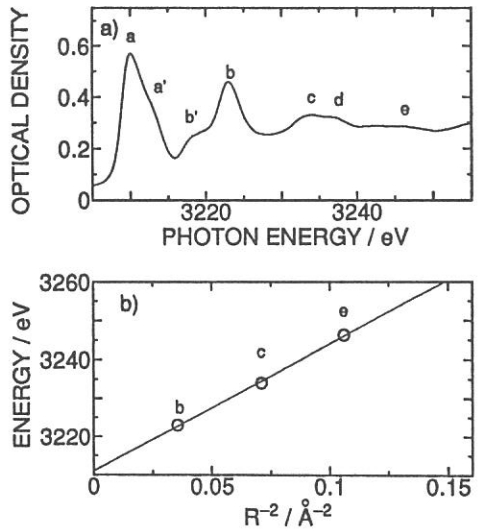

Figure 2. Ar *K*-edge XANES spectrum and correlation plot between energy and R^{-2}.

Table I. Positions of major peaks in XANES spectra of solid rare gases.

	a	b	c	d	e	f	g	h	i
Ne-*K*	868.3	870.1	875.5	882.4	889.1	893.2	903.8	907.0	
Ar-*K*	3210.0	3223.0	3234.0	3237.3	3246.3				
Kr-L_3	1678.6	1681.7	1686.8	1695.9	1706.0	1715.0			
Kr-L_2							1731.7	1739.5	1749.4
Xe-M_3	938.8	945.9	960.9	976.0					
Xe-M_2					1000.5	1008.2	1022.5	1036.4	

of the plots intersect with the energy axis at the energy nearest to the peak *a*, also with the least fitting error. The peaks *g* and *h* of Ne spectrum are not included in the present XANES analysis, but they are too sharp to assign as EXAFS feature. Therefore these peaks can be also attributed to the XANES feature correlating with the higher order lattice plane such as d_{120}. Figures 2(a) - 4(a) show the XANES spectra of Ar-*K*, Kr-$M_{2,3}$, Xe-$M_{2,3}$, respectively. The correlation plots for these XANES spectra are shown in figures 2(b) - 4(b). In these plots the same set of distances (R_2, R_1, d_{111}) are used as in that for Ne. As shown in the figures, the linearity is good for all the plots and all intersections coincide with the first peak position of each absorption edge within ±1 eV, except for those of Xe-M_2 and M_3 of which intersections are lower than the respective first peak positions by 6 and 8 eV. The values of *C* for Ne-*K*, Ar-*K*, Kr-$L_{2,3}$, and Xe-$M_{2,3}$ are 138.9, 330.0, 324.7, 290.6, 546.8, and 580.9 eV Å^2. By Karsay et al., difference in *C* values for different materials were attributed to a change in phase shift during backscattering. As a conclusion, for solid rare gases the XANES peaks have been correlated with the interatomic distances and lattice spacing based on the Natoli's theoretical model.

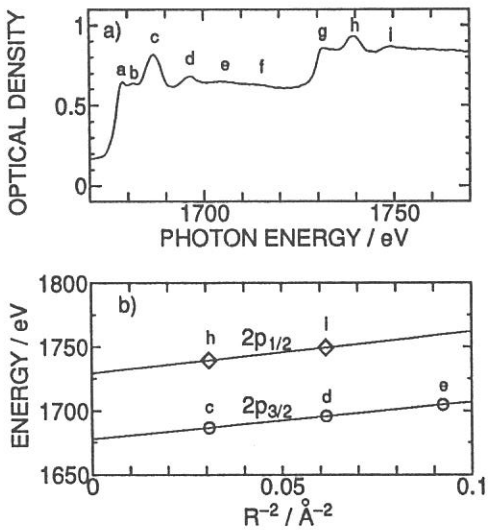

Figure 3. Kr *L*-edge XANES spectrum and correlation plot between energy and R^{-2}.

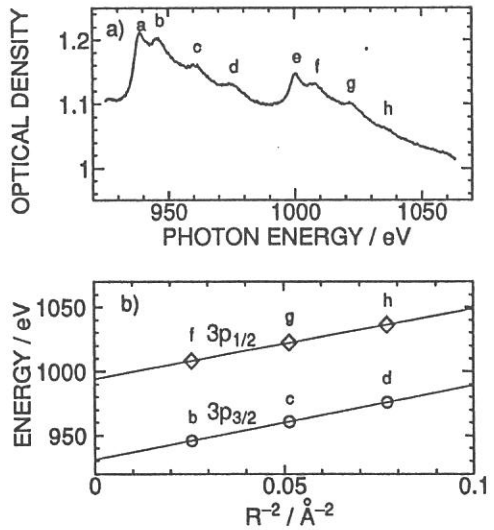

Figure 4. Xe *M*-edge XANES spectrum and correlation plot between energy and R^{-2}.

References

1) M. Kasray, M. E. Fleet, G.M. Bancroft, K. H. Tan and J. M. Chen, Phys. Rev. B **43**(1991)1763.
2) C. R. Natoli, in *EXAFS and Near Edge Structure*, Vol. **27** of *Springer Series in Chemical Physics*, edited by A. Bianconi, L. Incoccia, and S. Stipcich (Springer, Berlin, 1983), p. 43.
3) A. Hiraya, K. Fukui, P-K. Tseng, T. Murata, and M. Watanabe, J. Phys. Soc. Jpn. **60**(1991)1824.

DISSOCIATION DYNAMICS OF OCS^{2+} AND OCS^{3+} STUDIED BY THE TRIPLE PHOTOELECTRON-PHOTOION-PHOTOION COINCIDENCE METHOD

Toshio MASUOKA

Department of Applied Physics, Osaka City University, Sumiyoshi, Osaka 558

The triple coincidence PEPIPICO (photoelectron-photoion-photoion coincidence) experiment has been shown to be a powerful technique to study the dynamics of dissociation of a dication into three-body fragments (two charged and one neutral particle).[1] Although Eland has studied for the case of dications, this technique provides a characterization of the three-body dissociations of multiply charged cations, such as whether the dissociation is instantaneous or involves sequential steps and further how much energies are partitioned into three fragments. The dissociations into three bodies of the doubly- and triply-charged ions of OCS are studied here by this technique with the use of synchrotron radiation in the photon energy region of 48-80 eV.

Shown in Fig. 1 is a typical PEPIPICO distribution measured at $h\nu$=80 eV and θ=55° (a pseudo magic angle) relative to the electric vector of the incident polarized light. The ordinate t_1 and the abscissa t_2 represent the time-of-flight for the lighter and heavier fragment ions produced as a pair, respectively, where the detection of electron gives a time zero. The distribution shows six islands corresponding to the coincident detection of C^++O^+, C^++S^+, S^{2+}+OC^+, O^++S^+, O^++CS^+, and OC^++S^+. The dissociation dynamics can be elucidated from the slope ($\Delta t_1/\Delta t_2$) of each island, where Δt_1 and Δt_2 are the respective spread of flight time in the t_1-t_2 plane.[1] For the two-body dissociations of

OCS^{2+} ($O^+ + CS^+$ and $OC^+ + S^+$) and OCS^{3+} ($S^{2+} + OC^+$), the slope should be equal to 1 and 0.5, respectively. The observed slope of the islands and the dissociation mechanisms are listed in Table I.

Table I. Dissociation mechanism of OCS^{2+} and OCS^{3+}.

Channel	Slope 48eV	60eV	80eV	Ref. 1	Mechanism
$C^+ + O^+$	---	0.08	0.08	---	Instantaneous three body dissociation of OCS^{3+}, C^+ is a spectator.
$C^+ + S^+$	0.46	0.46	0.43	0.52	Sequential dissociation $OCS^{2+} \rightarrow OC^+ + S^+$, $OC^+ \rightarrow O + C^+$ with $U_2 = 0$.
$S^{2+} + OC^+$	---	---	0.39	---	Two body dissociation of OCS^{3+}
$O^+ + S^+$	---	0.97	0.90	1.11	Instantaneous three body dissociation of OCS^{2+}, C is a spectator.
$O^+ + CS^+$	0.92	1.03	0.98	0.96	Two body dissociation
$OC^+ + S^+$	0.97	0.99	0.96	0.98	Two body dissociation

Reference
1) J. H. D. Eland, Mol. Phys. 61, 725 (1987).

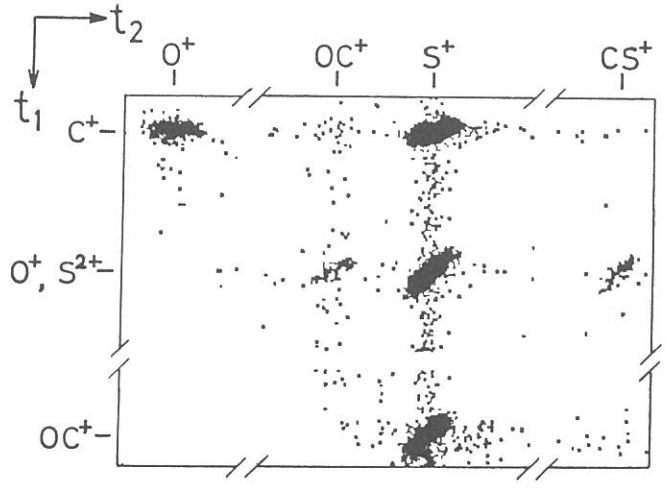

FIG. 1. Photoelectron-photoion-photoion-coincidence distribution in the t_1-t_2 plane for the charge-separating reactions of OCS^{2+} and OCS^{3+}.

SINGLE, DOUBLE, AND TRIPLE PHOTOIONIZATION CROSS SECTIONS OF OCS AND IONIC FRAGMENTATION OF OCS^+, OCS^{2+}, AND OCS^{3+}

Toshio MASUOKA and Hiroyuki DOI

Department of Applied Physics, Osaka City University, Sumiyoshi, Osaka 558

Single, double, and triple photoionization processes of carbonyl sulfide (OCS) have been studied in the photon energy region of 20-100 eV by use of time-of-flight mass spectrometry and the photoion-photoion coincidence (PIPICO) method together with synchrotron radiation. The single (σ^+), double (σ^{2+}), and triple (σ^{3+}) photoionization cross sections of OCS are determined in which the double photoionization cross section is found to be considerably large at $h\nu$=60 eV. The result gives a ratio σ^{2+}/σ^+ of 0.38, in contrast to previous observations for other molecules (SO_2 and CH_4). The ratio of double to single and that of triple to single photoionization are shown in Fig. 1. It is emphasized that the double photoionization cross sections reported in Fig. 1 include both the dissociative and nondissociative processes of the precursor OCS^{2+} and that this is the first observation of σ^{2+} including both processes. The ratio is in close agreement with that for the isoelectronic zinc atom.

Ion branching ratios and the partial cross sections for the individual ions produced from the parent OCS^+ and OCS^{2+} ions are also obtained. High-lying electronic states of the precursors OCS^+ and OCS^{2+} are newly observed.

The dissociation ratios of the singly and doubly charged parent ions are shown in Fig. 2. It is interesting to note that the both dissociation ratios reach an asymptotic value very close

to 0.9 at about 40 eV for OCS^+ and at about 55 eV for OCS^{2+}. The ground state of OCS^+, $X^2\Pi$, and that of OCS^{2+}, $X^2\Sigma^-$, are known to be nondissociative. If only these ground states are the source for the (meta)stable OCS^+ and OCS^{2+}, the dissociation ratios should increase at high photon energies. Obviously, the results in Fig. 2 provide an evidence for the presence of the bound electronic states of OCS^+ and OCS^{2+} at high photon energies and/or autoionization of the high-lying electronic states to the ground states of OCS^+ and OCS^{2+}.

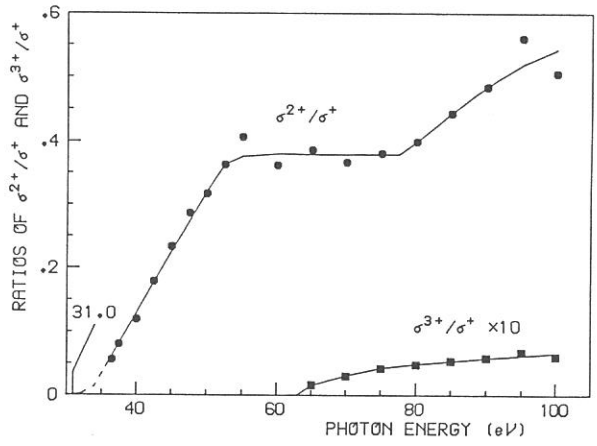

FIG. 1. Double (σ^{2+}) and triple (σ^{3+}) photoionization cross sections relative to single (σ^+) photoionization cross section of OCS.

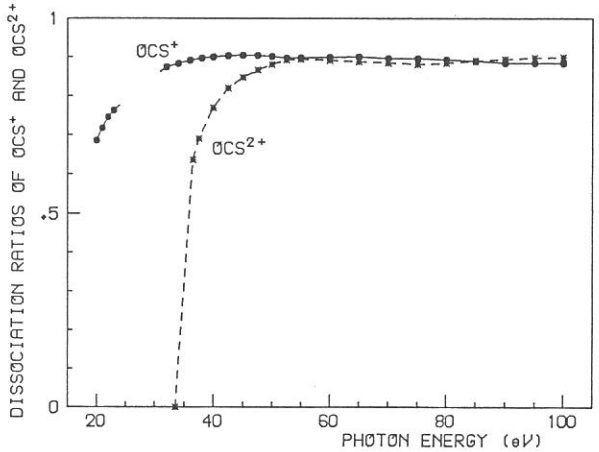

FIG. 2. Dissociation ratios of the precursors OCS^+ and OCS^{2+}.

STORAGE AND LIFETIME MEASUREMENTS OF MULTIPLY CHARGED Xe IONS PRODUCED BY SYNCHROTRON RADIATION

Makoto SAKURAI, Tsuguhisa SEKIOKA†, Masahiro KIMURA‡, Hitoshi YAMAOKA§, Takao KOJIMA§, Michitaka TERASAWA†, Yohko AWAYA§, Koichi KITAZAWA¶ and Shunsuke OHTANI¶

National Institute for Fusion Science, Nagoya 464-01
†Faculty of Engineering, Himeji Institute of Technology, Himeji 671-22
‡Faculty of Science, Osaka University, Toyonaka 560
§The Institute of Physical and Chemical Research, Wako 351-01
¶The University of Electro-Communications, Chofu 182

Spectroscopic research on multiply charged ions using several kinds of ion traps has been proposed, stimulated by the results on high-resolution spectroscopy of singly charged ions using ion traps coupled with laser technique. Charge state distribution of trapped ions produced by synchrotron radiation has been measured, and successive photoionization of ions in the trap was observed. In the ion storage of multiply charged ions, however, there are some technical difficulties compared to the case of singly charged ions. The limited lifetime of stored ions due to large rate of charge transfer process is one of the problems. In order to store enough number of ions with longer lifetime, it is necessary to have more intense photon flux and reduce background gas pressure.

We have developed the techniques for trapping and probing multiply charged ions produced through photoionization using synchrotron radiation. Undulator radiation from the BL3A1 beamline was used for the production of Xe multiply charged ions.

The experimental chamber comprises an rf ion trap, a time-of-flight (TOF) mass spectrometer and a gas handling system. The driving field for the confinement of ions consists of ac potential V_{ac} of frequency Ω and dc potential V_{dc}. The rf field of high voltage more than 200V with the frequency range 0.8-1.7 MHz covers the trapping conditions for Xe^{2+}-Xe^{8+}. The storage of ions was probed by extracting the ions from the trap, and the lifetime of trapped ions was measured from the storage time dependence of the amount of extracted ions.

Figure 1 shows a TOF spectrum of Xe multiply charged ions which were produced by the irradiation of SR and confined in the ion trap. The extraction pulses of 100V were applied for ~3μs with a period of 100ms while SR was continuously irradiated the trapping center. The Xe^{3+} ions are possibly created by the third harmonic of undulator radiation (~108 eV) since the ionization energy of Xe^{3+} is 65.4 eV. The peak height of each charge state depends on not only the cross section of photoionization and charge transfer process but the trapping efficiency. The lifetime of trapped ions was measured from the variation of the ion signal after the irradiation. SR was

turned on and off using light chopper. Figure 2 shows the variation of the amount of trapped Xe^{3+} ions with storage time for various Xe pressures. Xenon gases were ionized for 2.5s and created ions were stored with the trap condition for Xe^{3+}. It is evident that ion signal decreases more rapidly for higher Xe gas pressure. The lifetime of Xe^{3+} was limited less than 1s due to the charge transfer process with residual gases.

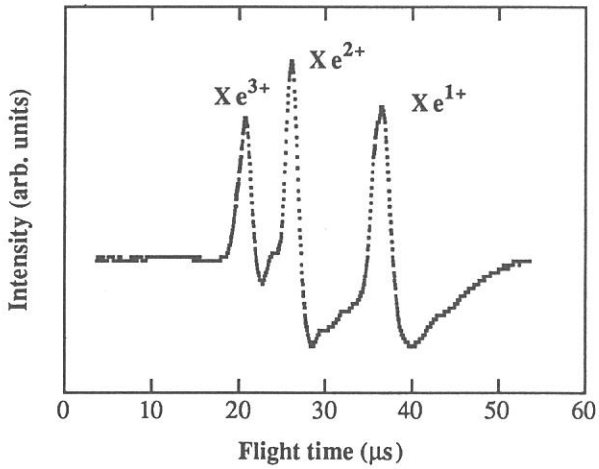

Fig. 1. Time-of-flight spectra of Xe multiply charged ions extracted from the rf ion trap. The trapping condition was for Xe^{2+}. Ambient pressure of Xe gas was $8x10^{-7}$ Pa.

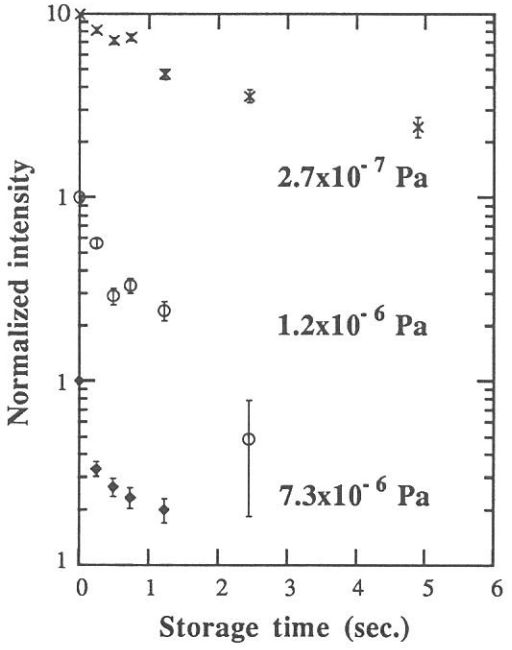

Fig. 2. Decay of the stored ions vs storage time for various ambient Xe pressure.

DIFFRACTION EFFICIENCY MEASUREMENTS OF SiC GRATINGS IN THE SOFT X-RAY REGION

Eiji ISHIGURO, Makoto SAKURAI†, Kazuo SANO‡, Masaru KOEDA‡, Tetsuya NAGANO‡ and Koujun YAMASHITA§

Department of Applied Physics, Osaka City University, Osaka 558
†National Institute for Fusion Science, Nagoya 464-01
‡Optical Devices Department, Shimadzu Corporation, Kyoto 604
§The Institute of Space and Astronautical Science, Sagamihara 229

SiC is an excellent mirror material for high power synchrotron radiation optics in the soft X-ray region, because of the extreme thermal resistance and super smooth surface. SiC Laminar gratings have been fabricated by using holographic technique and reactive ion-beam etching. We measured diffraction efficiencies of SiC laminar gratings using monochromatized synchrotron radiation of UVSOR in the wavelength range of 2-12nm. The experiment was carried out at the calibration beam line of NIFS (BL5B).

Figure 1 shows an output spectrum of the plane grating monochromator of BL5B with an combination of gratings and mirrors for the shortest wavelength region measured with an electron multiplier (photo-cathode : BeCu). The scattered light is negligible at 2nm or longer and a K-edge structure of oxygen around 2.4nm is clearly observed. Since the PGM was designed to cover a wavelength range of 1.8 ~ 120 nm, the initial requirement is fulfilled at length. The SiC gratings fabricated have 500 and 1200/mm grooves. The reflectivities of the gratings were measured over the scattering angle range which covers several diffraction orders by scanning a detector for various incident angles.

Figure 2 shows an angular distribution of a diffracted light obtained for a monochromatic light of 3nm incident at the grazing angle of 1°. The diffraction efficiency of the first order light (m=1) is 2%. It is noticed that a small peak at the scattering angle of 4.2°, which is due to light of 1.5nm induced as the second order in the incident light of 3nm, is well resolved in the spectrum. Figure 3 shows diffraction efficiencies of the grating with 1200/mm grooves, groove depth of 7.5nm and RMS roughness of 0.34nm. The diffraction efficiencies of the -1st to 5th orders are shown as a function of the grazing angle for various wavelengths between 0.834 to 12nm. For 0.834nm, Al-Kα emission from a X-ray tube was used. The maximum values measured for the efficiency in the +1st order exist between 4.7 to 9.4%.

It should be noted that in the region above 6nm the best value of the efficiency may be available at a grazing angle larger than 5° as being expected from the efficiency curves. The efficiency for the second order is approximately 10% of the first order.

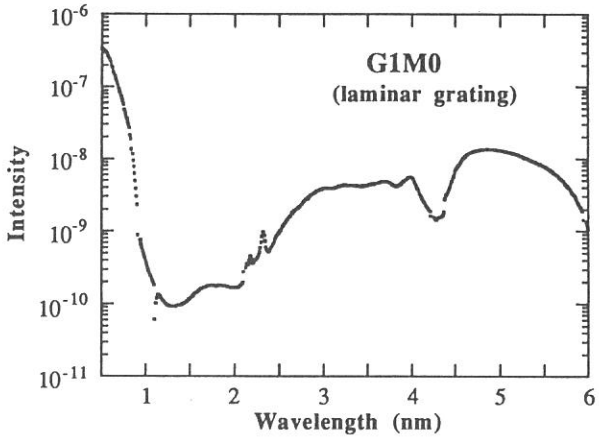

Fig. 1. Output spectrum of PGM.

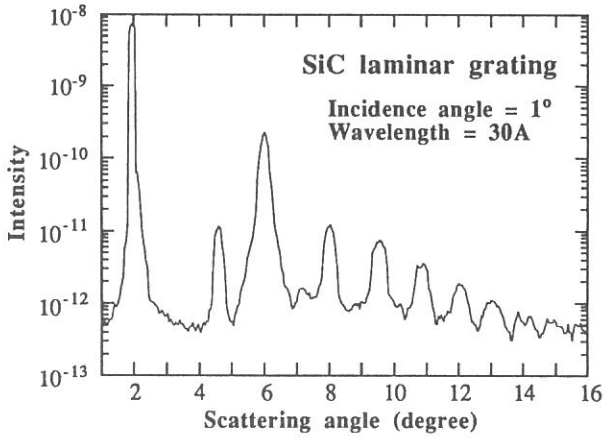

Fig. 2. Angular distribution of diffracted light by a SiC grating.

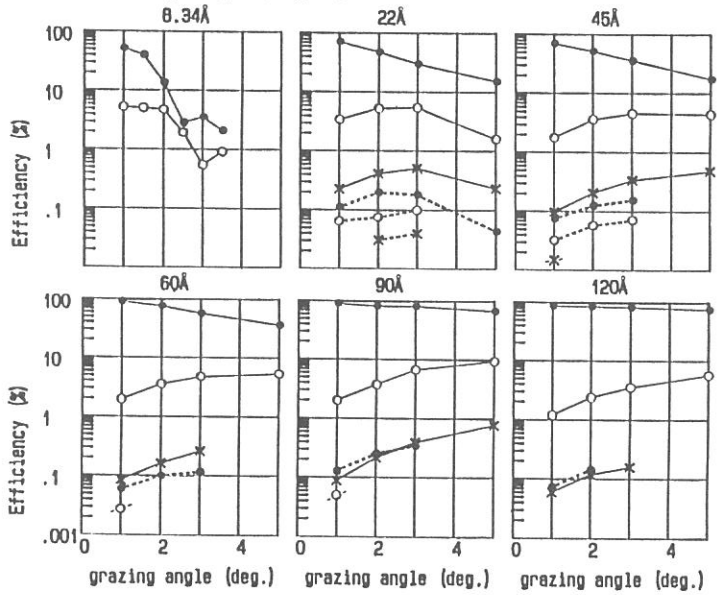

Fig. 3. Diffraction efficiency of SiC grating for the -1st to 5th order as a function of the grazing angle for various wavelengths between 0.834 to 12 nm. A combination of a mark and a line indicates the spectral order m: △ for m = -1, —●— for m = 0, —○— for m = 1, —×— for m = 2, --●-- for m = 3, --○-- for m = 4 and --×-- for m = 5.

SULFUR 1S X-RAY ABSORPTION NEAR EDGE STRUCTURE (XANES) OF DILUTED MAGNETIC SEMICONDUCTOR (DMS) $Zn_{1-x}Mn_xS$.

W.F. Pong,* P.K. Tseng,*[1] K.T. Wu,[1] R.A. Mayanovic,[2] B.A. Bunker,[2] A. Hiraya,[3] M. Watanabe.[3]

Phys. Dept. Tamkang U., Tamsui, Taiwan, Natl. Taiwan U., Taipei, Taiwan,[1] U. of Notre Dame, IN., USA,[2] Institute for Molecular Science, Okazaki, Japan.[3]

I INTRODUCTIONS

A wide variety of tetrahedrally bonded semiconductors having the chemical formula $A_{1-x}B_xC$ have been studied in recent years including the Mn-based II-VI ternary alloys of diluted magnetic semiconductor (DMS) $Zn_{1-x}Mn_xS$. Extensive studies[1] have revealed that DMS exhibit unique electric, magnetic and optical properties, attributed to the short-range exchange interactions between the spins of the Mn^{+2} ions and between the Mn^{+2} ions and group VI anion sp band electrons. Larson et al.[2] have calculated the Mn^{+2} d-d and Mn^{+2} d-anion sp exchange mechanism in $Zn_{1-x}Mn_xS$ and another DMS alloys. Using a generalized Anderson Hamiltonian and perturbation theory, they find that the Mn^{+2} d-d exchange integral J is antiferromagnetic for both Mn^{+2} nearest-neighbot (J_{NN}) and next-nearest-neighbor (J_{NNN}) interactions, and that J_{NN} is predominant larger than J_{NNN}. Furthermore, due to the Mn^{+2} 3d-orbital lies below the top of anion p-orbital valence band and contributes significantly within the valence band, the exchange integral J^{v}_{sp-d} and the superexchange integral J_{dd} being proportional to V_{pd}^{2} and V_{pd}^{4}, respectively, (where V_{pd} is the hybridization energy between the Mn^{+2} 3d and local anion p-orbital valence electron). In this paper, we present our x-ray absorption near-edge structure (XANES) spectra for the sulfur K-edge $Zn_{1-x}Mn_xS$ alloys. For p-d hybridization the main density of states modification, XANES spectra at sulfur K-edge, is also expected to be seen for the final sulfur p-states and reflects sulfur p in unoccupied states mixing of mainly Mn ions character.

II MEASUREMENTS

Sulfur K-edge XANES spectra of $Zn_{1-x}Mn_xS$ (the sample having x=0.05, 0.10, 0.20, 0.30, 0.50, 0.60, and ZnS) were performed at the Ultraviolet Synchrotron Orbital Radiation (UVSOR), Institute for Molecular Science Okazaki, using the beam line 7A with an electron-beam energy of 750 Mev and a maximum storied current of 200 mA. The measurements were made in total electron yield mode using an electron multiplyer detector and at a base pressure of $\sim 5 \cdot 10^{-8}$ torr. Data were collected using a Ge(111) double-crystal monochromator. The photon energy was calibrated from the M_5-edge (2.220 KeV) of a Au-photocathode.

III EXPERIMENTAL RESULTS

Fig. 1 shows the sulfur K-edge XANES spectra of $Zn_{1-x}Mn_xS$. After pre-edge background subtraction, the spectra have been normalized to the threshold energy. The spectra have vigorous fine structure up to at least 20 eV above the threshold, which is related to sulfur 3p hybridize in states of prominently Mn 3d band as well as may mixing with the Mn 4(s,p) and Zn 4s states. In the case of $Zn_{1-x}Mn_xS$ samples, the Mn ions lie in a general tetrahedral environment (T_d symmetry group), therefore, the effect of the crystal field is to split the Mn 3d↑ (filled) and 3d↓ (empty) levels, giving a stabilized doublet level, e (Γ_{12}), of lower energy than the undistorted 3d orbitals, and less stable triplet levels, t_2 (Γ_{15}), of higher energy, respectively. The 3p levels of sulfur have the Γ_{15} symmetry. Thus, there is no p-d hybridization for the Mn e↑ and e↓ between them. On the other hand, the p-d hybridization appreciable between sulfur 3p levels (↑ and ↓) and Mn t_2 (↑ and ↓) due to the same symmetry. At present, we consider the

origin of the prominent peaks I in Fig. 1, which are alike among the different Mn concentration in the series of DMS samples. The absorption maximum can be assigned to dipole-selection transition to higher-energy vacant states of sulfur 3p character in bonds with insensibly Mn e↓ character. Additional, the increase of the intensity, between peak II and peak III with Mn concentration, is related to the strong p-d hybridization between sulfur 3p bonds and unoccupied Mn t_2↓ character. As see in Fig. 2, the spread area between absorption maximum and peak III are become extensive with increasing Mn concentration, which significantly indicate that the degree of p-d hybridization increase as a function of x. This experimental results suggest that the exchange integral J does depend on x in DMS. Due to the lack of electronic band structure of $Zn_{1-x}Mn_xS$, the peaks IV and extended area of peaks V presumably correspond to sulfur p level mixing with the cation Mn 4(s,p) and Zn 4s states. The future theoretical study should be done to confirm these fine structure.

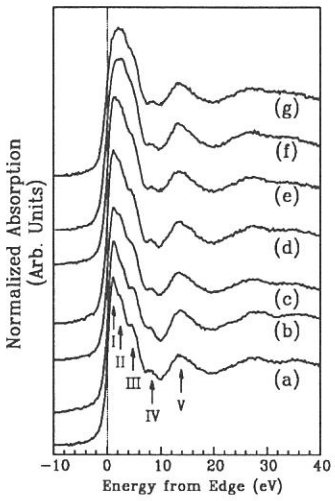

Fig. 1. Normalized S K near-edge absorption for $Zn_{1-x}Mn_xS$ samples. (a) ZnS (b) x=0.05 (c) x=0.1 (d) x=0.2 (e) x=0.3 (f) x=0.5 (g) x=0.6. The energy zero corresponds to 2472.5 eV.

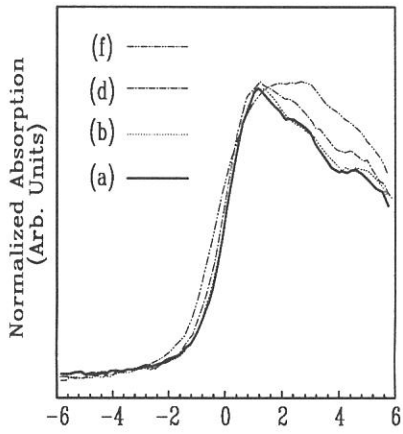

Fig. 2. Normalized S K near edge absorption for $Zn_{1-x}Mn_xS$ samples. (a) ZnS (b) x=0.05 (d) x=0.2 (f) x=0.5. The energy zero corresponds to 2472.5 eV.

1*Semiconductors and semimetals* Vol. 25, Diluted Magnetic Semiconductors, edited by J.K. Furdyna and J. Kossut, (Academic Press, New York, 1988).

2B.E. Larson, K.C. Hass, H. Ehrenreich, and A.E. Carlsso, Solid State Commun. **56**, 347 (1985); K.C. Hass, B.E. Larson, H. Ehrenreich, and A.E. Carlsso, J. Magn. Magn. Mater. **54-57**, 1283 (1986).

* Supported by the NSC, Taiwan, under grand No. NSC81-0208-M-032-13.

SYNCHROTRON RADIATION-EXCITED ETCHING REACTIONS OF POLYCRYSTALLINE SiC

Haruhiko OHASHI*, , Kosuke SHOBATAKE*,**
Eiji ISHIGURO*,*** and Akira YOSHIDA***

**Institute for Molecular Science, Myodaiji, Okazaki 444 Japan*
***Toyohashi University of Technology, Tenpaku, Toyohashi 440 Japan*
****Osaka City University, Sumiyoshi, Osaka 558 Japan*

SiC is an important semiconductor material with a wide band gap, and is also expected to be used as a thermal resisting optical element for high brightness synchrotron radiation sources to be constructed in the future. However since SiC is a very hard material and chemically very stable, its fabrication is difficult and thus synchrotron radiation was used to etch it.

Wavelength dependence of synchrotron radiation (SR)-excited etching of SiC surfaces are studied to clarify the mechanisms of the etching processes. Several experimental schemes were employed in which pressure dependence of the etching rates was measured for and SiC in the atmosphere of SF_6. We have proposed a simple reaction model for the SR-excited etching of insulator surface that the excitation of the outermost layer is important and leads to reaction with a unit probability.

EXPERIMENTAL Synchrotron radiation from the bending magnet (BL8A) was used for the SR-excited etching experiments. SR was irradiated upon the β-SiC(220) surface in SF_6 as a function of SF_6 pressure at room temperature.

RESULTS The SR-excited etching of the β-SiC(220) surface with a resist pattern of 1.0 μm line and space width (500 lines/mm) was carried out at room temperature using SF_6 gas as an etchant. The micrograph of the etched SiC surface after removing a resist is shown in Fig. 1.

The etched depth was determined as the averaged value for the β-SiC(220) surface. Fig. 2 shows the etch rate against the SF_6 pressure. One finds that the etch rate increases with pressure below 0.1 Torr, peaks at around 0.15 Torr, and then decreases at higher pressures. From these results one may conclude that in the low pressure region (below 0.1 Torr) the etching reaction rate is limited by F atom supply. The similar trend was observed in the SR-excited etching of SiO_2 surface with SF_6 gas. However at the pressures higher than 0.15 Torr the rate

seems to be limited by the photon intensity irradiated upon surface.

The dashed and solid curves in Fig. 2 are the calculated transparent light intensities irradiated upon the sample for photons in the whole wavelength region and in the region 30 - 44 Å corresponding to C(1S) excitation, respectively. They are normalized to the maximum etch rate (0.0077Å/mA·min) obtained from the experiment. The actual photon number for the former is about 10 times larger than the one in the C(1s) excitation region.

Another point to be noted is that *the etch rate for SiC is lower by at least a factor of ten than that for SiO_2 etching with SF_6 which value was measured at about 0.1Å/mA·min.* Why is the quantum yield for the etching reaction of β-SiC ten times smaller than that for SiO_2? Furthermore since the diamond surface was not successfully etched by SR-excited etching with SF_6, C atoms must be harder to be removed and thus the etching reaction is promoted by inner core excitation with SR, while Si atoms may be spontaneously etched in the presence of the F atoms.

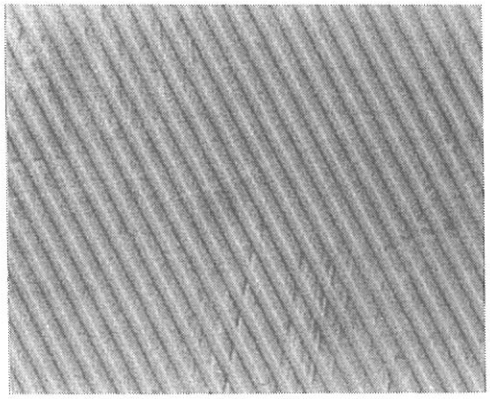

Fig. 1
Micrograph of the SR-excited β-SiC(220) surface. SF_6 pressure was 0.5 Torr.

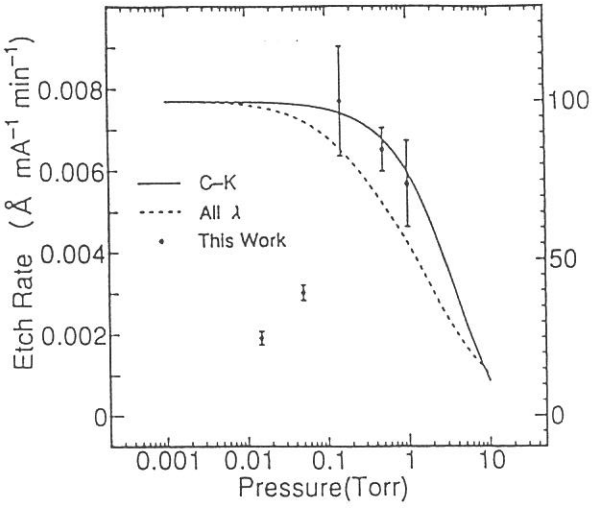

Fig. 2.
Etch rate of β-SiC(220) against SF_6 pressure. Solid circles represent experimental results. See the text for explanations.

Mg K-EDGE XAFS STUDIES ON Mn-ADDED Na/MgO

Sadao HASEGAWA[a], Masahiko MOROOKA[a], Tetsuya SHISHIDO[a],
Hisao YOSHIDA[b], Tsunehiro TANAKA[b] and Satohiro YOSHIDA[b]

a Department of Chemistry, Tokyo Gakugei University,Koganei, Tokyo 184
b Department of Hydrocarbon Chemistry, Faculty of Engineering, Kyoto University, Kyoto 606

<INTRODUCTION> We previously reported that the surface O_2^- or OOH^- on manganese dioxide ($MnO_{2-x}\cdot nH_2O$) acts as oxidation sites for iso-propanol[1] and surface Mn^{4+} species is found on Mn cation added Na/MgO and is converted to surface Mn^{2+} by degassing.[2] Thus, manganese oxide is useful catalysts for oxygen related reaction. While, G. Zhang et al. reported that Na doped MgO increase surface basicity in order to occur more strong dispersion of charge density of Mg and O.[3]

In the present study, surface electronic structure of Na and/or Mn loaded MgO catalysts have been investigated by XAFS.

<EXPERIMENTAL> Mn ion loaded MgO were prepared by doping on MgO with aqueous solution of Mn nitrate for MnN/MgO catalysts or ethanol solution of Mn acetylacetonate for MnA/MgO catalysts. Na loaded MgO were prepared by doping on MgO with ethanol solution of metal sodium. Na and Mn loaded MgO (Na/Mn/MgO) were prepared by doping on Na/MgO with ethanol solution of Mn acetylacetonate. After drying at 383K for 12h, samples were calcined at 1073K for 1h in air. Mg K-edge absorption spectra of the catalysts were measured at BL-7A soft X-ray beam line with UVSOR facilities. A beryl two-crystal monochrometer was used.

<RESULTS AND DISCUSSION> Figure 1 shows Mg K-edge XANES pattern of Mn/MgO, Na/MgO, and Na/Mn/MgO catalysts calcined at 1073K. The peak at 1310eV of photon energy is due to 1s-3p transition, the peak intensity is expected to reflect the distribution of unoccupied 3p orbital for Mg. The intensity of peak at 1310eV and at 1318eV are denoted P1 and P2,respectively. Table 1 shows the intensity ratio of Mg K-edge absorption spectra at 1310eV and 1318eV of photon energy (P1/P2). The intensity ratio is MnA/MgO < MnN/MgO < Na/MgO < Mn/Na/MgO. The intensity of XANES spectrum at 1310eV was decreased

with the doping of Mn ion on MgO powder, however the intensity increase with the doping of Na ion on Mn/MgO. While, H. Tsuji et al. reported that the intensity of XANES spectrum at 1310eV was increased with the doping of Na ion (Na from aqueous solution of NaOH or $NaNO^3$) to MgO powder.[4] Our results in this investigation suggest that the population of 3p orbital changed by doping Na and Mn to MgO. The electron density of 3p in Mg atom is decreased with existence of Na atom on MgO and it is increased with Mn atom on MgO.

<Reference> 1 S. Hasegawa, K. Yasuda, T. Mase, T. Kawaguchi, J. Catal., 46, 125 (1977); 2 H. Suzuka, S. Hasegawa, T. Tanaka, G. Zhang, H. Hattori, Surface Science,221, L769 (1989); 3 G. Zhang ,T. Tanaka ,T. Yamaguchi ,H. Hattori ,K. Tanabe, J. Phys. Chem., 94, 506 (1990); 4 H. Tsuji, T. Hisazaki, T. Tanaka, H. Hattori, UVSOR ACTIVITY REPORT 1990,83 (1990)

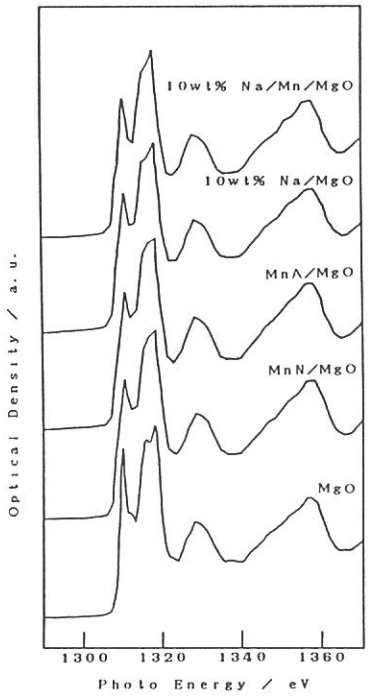

Fig. 1 XANES pattern of MgO, Mn/MgO, Na/MgO, Na/Mn/MgO calcined at 1073K Mn/Mg=0.01

	Intensity ratio P1/P2
MgO	0.885
MnN/MgO	0.721
MnA/MgO	0.708
10wt% Na/MgO	0.737
10wt% Na/Mn/MgO	0.746

Table. 1 The intensity ratio of Mg K-edge absorption spectra at 1310eV and 1318eV of photon energy

Photoelectron spectroscopic study of decay process of Cs 5p-excited states in CsCl

Masao Kamada, Yasuo Fujii,* and Kazutoshi Fukui+

Institute for Molecular Science, Okazaki 444
*Osaka City University, Osaka 558
+Fukui University, Fukui 910

Recently so-called Auger-free luminescence has been observed in insulators having a valence-to-conduction band gap larger than the energy difference between valence band and inner core levels.[1] The luminescence, for example, in CsCl is simply understood in terms of the radiative decay of Cs 5p-excited states without competition of Auger process. However, there are several questions to be solved: (1) Why the energy position of the luminescence is slightly different from the energy difference between the valence band and the inner core levels ? (2) Does the shape of the luminescence agree with the density of states of the valence band or not ? (3) Why the exciton peaks do not appear in the excitation spectrum of the luminescence ? (4) Is the radiative decay the dominant decay process of the Cs 5p-excited states ? The purpose of the present study is to solve these questions, and to see the non-radiative decay process by using photoelectron spectroscopy.

The photoelectron experiments were carried out at BL6A2 of UVSOR facility. The photoelectrons from CsCl evaporated thin films were analysed with using a cylindrical-retarding field analyzer. The plane grating monochromator with changeable focusing mirrors was used to obtain the monochromatic exciting lights with less amounts of higher order components. The absorption and reflective spectra were also measured at BL7B with a 1-m Seya-Namioka type monochromator. These spectra agreed well with those reported previously.[2,3]

Figure 1 shows the energy distribution curve (EDC) of CsCl excited with 23 eV. The valence band, Cs $5p_{3/2}$, and Cs $5p_{1/2}$ levels are observed at 13.4, 7.5, and 5.7 eV, respectively. The gross feature of the EDC agrees with the previous results

obtained by Smith and Pong,[4] who used a cylindrical collector and a discharge source. Figure 2 shows the constant-initial-state (CIS) spectra with the various initial states in the valence band. As seen in this figure, there is the enhancement of the valence band intensity at about 13.1 eV, which corresponds to the excitation photon energy of the Cs 5p-core exciton. This indicates that the Cs 5p-core exciton decays non-radiatively with the energy being transferred to the valence electrons. Moreover, it should be noted that the resonant enhancement is more remarkable in the CIS spectra with the higher initial binding energy. We suppose that the higher binding energy part in the valence band involves Cs-components more than the lower binding energy part does, or Cs 5p-core exciton relaxes before its non-radiative decay. Futher investigations are under way and the results will be reported in near future.

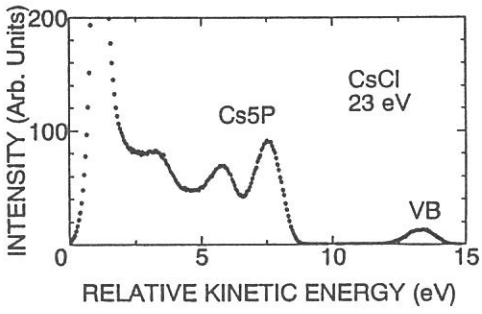

Fig. 1. EDC of CsCl

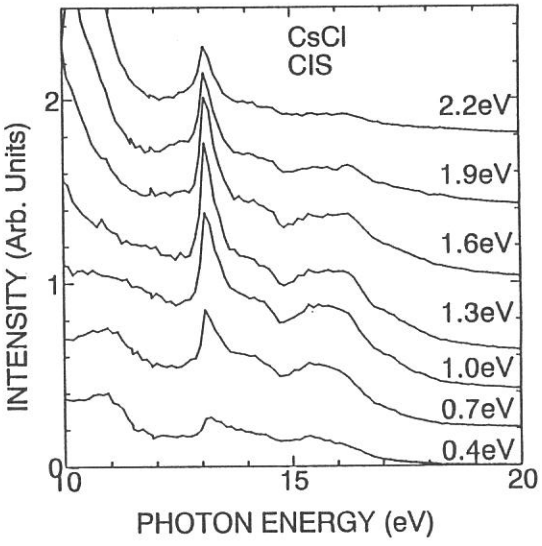

Fig. 2. CIS spectra of CsCl

References

1) S. Kubota, M. Itoh, J. Ruan(Gen), S. Sakuragi and S. Hashimoto, Phys. Rev. Lett. **60** (1988) 2319.
2) G. W. Rubloff, Phys. Rev. B **5** (1972) 662.
3) H. Saito, S. Saito, R. Onaka, and B. Ikeo, J. Phys. Soc. Jpn. **24** (1968) 1095.
4) J. A. Smith and W. Pong, Phys. Rev. B **12** (1975) 5931.

X-RAY CHARACTERISTICS OF PLATINUM-CARBON MULTILAYERS

Koujun YAMASHITA, Takashi SUZUKI, Gyanendra S. LODHA,
Isamu HATSUKADE* Shin-ichiro TAKAHAMA** and Masayuki OHTANI***

Institute of Space and Astronautical Science, Sagamihara 229
*Department of Electronic Engineering, Miyazaki University, Miyazaki 889-21
**Department of Physics, Osaka University, Toyonaka 560
***NIKON Corporation, Shinagawa, Tokyo 140

Platinum-Carbon(Pt/C) multilayers are useful to apply to grazing incidence reflectors in 1-10keV region, which have high reflectivity with small number of layer pairs. Moreover Pt/C overcoated with 100A thick Pt makes it possible to extend the sensitive energy region or glancing angle without degrading the total reflection obtained by a single layer mirror. The characterization of these multilayers was carried out in 1.7-4keV region by using double crystal monochrometer with InSb crystal on BL-7A. The method of reflectivity measurement is mentioned in ref.(1).

Reflectivities of Au(300A), Pt(300A), Pt/C(2d=104A, N=10) and Pt/C(2d=108A, N=10)+Pt(100A) against X-ray energies by changing the incidence angle to the reflecting surface are shown in Fig.1(a), (b), (c) and (d), respectively. These mirrors were fabricated on superpolished quartz and float glass by an electron beam deposition method in ultra-high vacuum. They show discontinuous reflectivities at M-absorption edge, 2.2keV for Au and 2.1keV for Pt. The reflectivity of Pt mirror are a bit higher than that of Au mirror at the same incidence angle. The total reflection of Pt/C multilayer is lower than that of other mirrors, since the thickness of Pt is too thin compared to the penetration depth of incident X-rays. However it shows higher

refletivity at large angle corresponding to the Bragg condition. Pt/C+Pt is a combination of total and Bragg reflection, which shows the highest reflectivity. Its Bragg reflectivity is lower than that of Pt/C due to the absorption of top layer of Pt(100A).

(1) K. Yamashita et al., UVSOR Activity Report 1989, p.92.

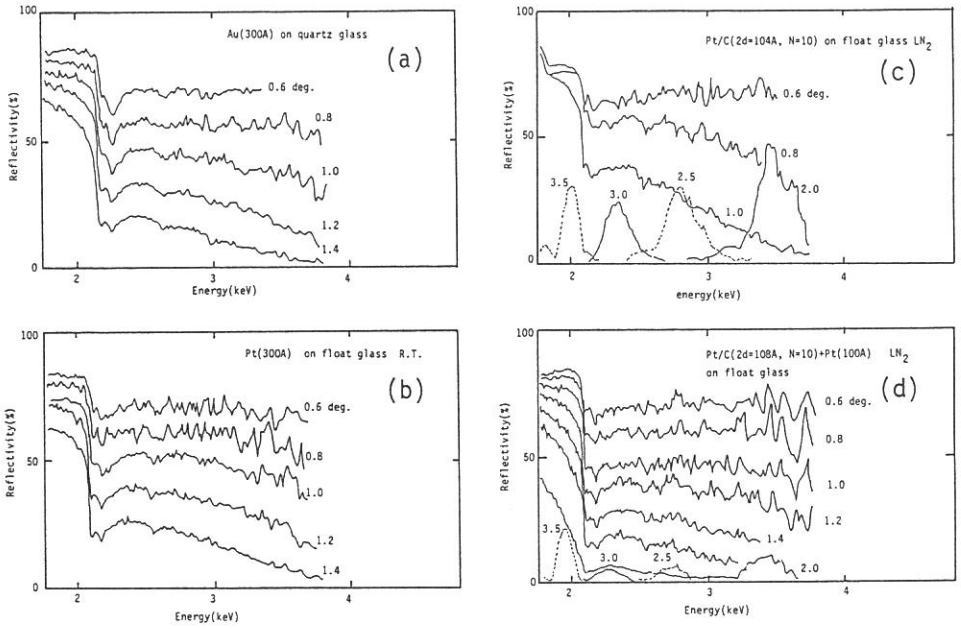

Fig. 1 X-ray reflectivity vs. energies. Incidence angle is written on each curve. (a) Au(300A), (b) Pt(300A), (c) Pt/C(2d=104A, N=10) and (d) Pt/C(2d=108A, N=10)+Pt(100A)

Temperature Dependence of Sputtering of Na atoms from Na-Halides Irradiated with Undulator Radiation

Sayumi Hirose and Masao Kamada
Institute for Molecular Science, Myodaiji, Okazaki 444

Bombardment of solids by energetic electron- or photon-beams causes the ejection of constituent species from the surface. However, most previous studies of electron- or photon-induced sputtering have been limited primarily to ionized species and ground-state species, while few groups have studied the sputtering of excited species.[1] We have studied the sputtering of excited-state alkali atoms from alkali-halides.[2] In this report we will present the temperature dependence of sputtered alkali atoms to get a better understanding of the sputtering mechanism of excited-state alkali atoms from alkali-halides.

Experiments were performed at the BL-3A1 of UVSOR facility. Undulator radiation was used as an exciting light source. Aluminum filters were inserted between the undulator and samples to eliminate visible and higher energy photons. Single crystals were cleaved with a knife edge in sample chamber, of which base pressure was about 2×10^{-7} Pa. Excited-state Na atoms were measured by observing emission spectra, while ground-state Na atoms were detected with the Quadrupole Mass Spectrometer. Sample temperatures were monitored with an Alumel vs Chromel thermocouple attached on the surface of a dummy sample.

Emission spectra of Na-halides are composed of the atomic emission (so-called Na D-line) due to the transition from desorbed excited-state Na atoms and broad band. The intensity of Na D-line is stronger in NaF than in NaCl, and is too weak to be observed in NaBr and NaI. This tendency is in good agreement with the production efficiency of halogen defects, which increases in the order of NaI to NaF, in accordance with Rabin-Klick parameters.[3] While the photon-induced sputtering of ground-state Na atoms from Na-halides decreases in the order of NaI to NaF.

Figure 1 shows temperature dependences of the sputtering yield of ground-state (open circle) and excited-state (solid circle) Na atoms from NaCl under excitation with undulator radiation of 36 eV. Sputtering of ground-state Na atoms begins around 300 K and increases with increasing the temperature. This

dependence agrees with sputtering of Cl atoms. This can not be explained with the idea that Na atoms evaporate thermally from the crystal surface. Kanzaki et al.[4] have observed temperature dependence of neutrals from alkali-halides, and proposed that the diffusion of Vk-center plays important roles in the temperature dependence of ground-state atoms. The present temperature dependence of the sputtering yield of ground-state Na atoms from NaCl can be understood in terms of diffusion of Vk-center. On the other hand, temperature dependence of the Na D-line intensity from NaCl shows a maximum at 303 K and decreases with increasing the temperature. Temperature dependences of excited-state and ground-state Na atoms are obviously opposite to each other. Thus, the sputtering mechanisms of excited-state and ground-state Na atoms are different from each other. We suppose that the sputtering of excited-state Na atoms is caused by surface defects different from Vk-center.In other words, it is supposed that the sputtering of excited-state Na atoms is closely related to the lattice instability due to electronic excitation in the surface layer.

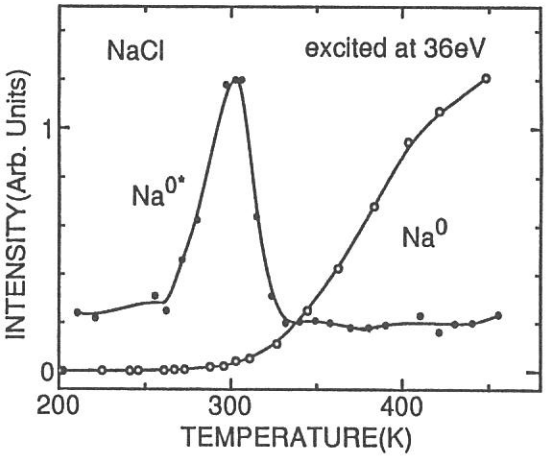

Fig.1 Temperature dependences of the sputtering yield of ground-state (open circle) and excited-state (solid circle) Na atoms from NaCl NaCl crystal was excited with undulator radiation of 36 eV through an aluminum filter.

References

1) Desorption Induced by Electronic Transitions (DIET IV), edited by G. Betz and P. Varga (Springer, Berlin, 1990).
2) S. Hirose and M. Kamada, J. Phy. Soc. Jpn, 60, 4376, (1991)
3) H. Rabin and C. C. Klick, Phys. Rev. 117, 1005 (1960)
4) H. Kanzaki and T. Mori, Phys. Rev. B29, 3573 (1984)

VUV-EXCITED DEPOSITION OF AMORPHOUS SILICON FILMS

Akira YOSHIDA, Haruhiko OHASHI and Yasuhiro IWANO

Toyohashi University of Technology
Tempaku,Toyohashi,441

In the usual photo-CVD (Chemical Vapor Deposition) system, the exciting light is introduced into a chamber through an optical window such as CaF_2 and MgF_2. However, the light intensity is decreased by the absorption of the window materials, and the deposited films on the window make the growth rate decrease. The light with short wavelength is more suitable for the decomposition of the usual source gases in the photo-CVD. The VUV light without any window is a more desirable light source. In this study, we report the deposition of amorphous silicon films by using synchrotron radiation.

The VUV light from synchrotron radiation was used as a light source through no filter or window. Source gases were pure disilane (Si_2H_4) or monosilane (SiH_4), and introduced into the reaction chamber. The pressure in the chamber was fixed at 0.1 and 0.2 Torr during the deposition. The light from SR was irradiated perpendicularly to the surface of the substrates on the sample holder in the chamber. The substrate temperature was varied from room temperature up to 250 ℃. During the growth of the films, a positive electric field was applied to some samples so that positive ions were accelerated toward the substrate.

Fig.1 shows the growth rate of the deposited films. The rate of deposition decreased with increasing the substrate temperature, and increased with increase of the gas pressure. From the Arrhenius plot of the growth rate in Fig.2, the apparent activation energy was negative, and several tens of meV. The films contained a large number of hydrogen atoms bonded to silicon atoms, as shown in Fig.3. The hydrogen content was deduced from infrared absorption coefficients, and decreased with increase of the substrate temperature. The optical gap also showed a similar behavior (Fig.4), corresponding to the hydrogen content in the films. The growth rate was greatly enhanced with the applied electric field, but the hydrogen content was independent of the applied electric field. Although the detailed kinetics is not yet clarified, the deposited layers grow by inter-

action of adsorbed molecules with active species, probably positive ions in the gas phase.

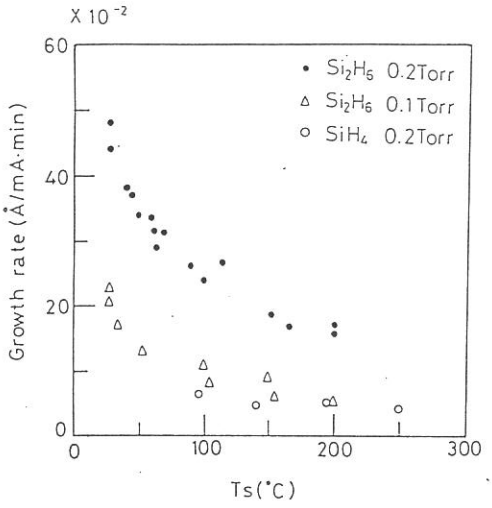

Fig.1

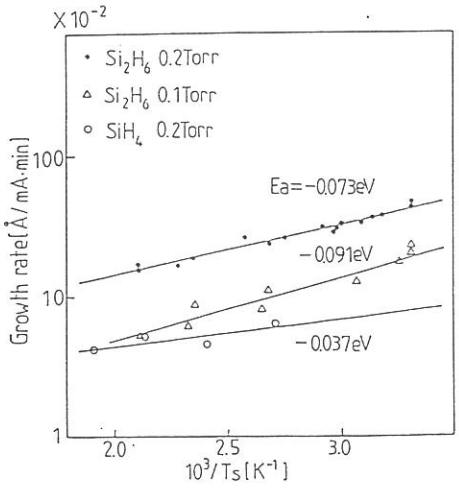

Fig.2

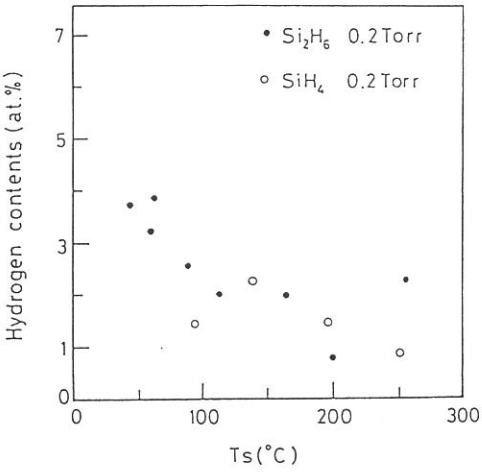

Fig.3

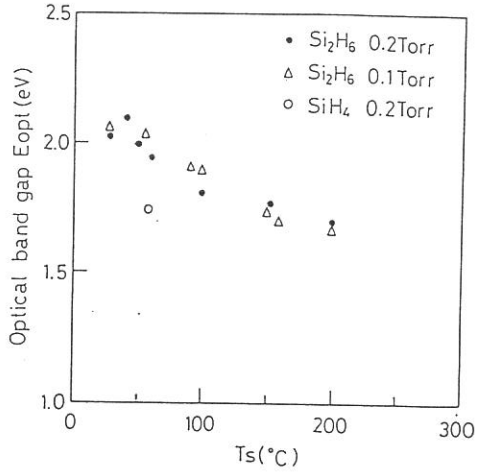

Fig.4

LUMINESCENCE OF HIGH-TEMPERATURE SUPERCONDUCTOR SINGLE CRYSTALS CLEAVED IN ULTRA-HIGH VACUUM.

V.G.Stankevitch, N.Yu.Svechnikov, K.V.Kaznacheev, M.Kamada,[1] S.Tanaka,[1] S.Hirose,[1] R.Kink,[2] G.A.Emel'chenko,[3] S.G.Karabachev,[4] Th.Wolf,[5] H.Berger,[6] and F.Levy[6]

I.V.Kurchatov Institute of Atomic Energy, Moscow 123182, CIS.
[1]Institute for Molecular Science, UVSOR, Okazaki 444, Japan.
[2]Institute of Physics, Tartu 202400, Estonia.
[3]Institute of Solid State Physics, Chernogolovka 142432, CIS.
[4]Moscow Institute of Steel and Alloys, Moscow, 117936, CIS.
[5]Kernforschungszentrum Karlsruhe, Institut fur Technische Physik, D-7500, Karlsruhe, Germany.
[6]Institut de Physique Appliquee, Ecole Polytechnique Federale, CH-1015, Lausanne, Swiss.

This work continues a series of our investigations of electronic structures and luminescence properties of high temperature superconductors (HTSC) (Refs 1-3). Results on luminescence investigations of various HTSC single crystals are presented in this paper.

We performed the experiments at the BL3A1 beam line of the UVSOR facility. An undulator radiation with a photon energy of 30eV was incident onto a sample via a 1-mm diaphragm. An aluminium filter of 1500 Å allowed to cut off a background of visible light from the bending section of the electron-storage ring. The experimental curves shown in the figure 1 were obtained under the same experimental conditions and normalized to a maximum intensity.

The first three curves (1-3) correspond to emission spectra of crystals based on yttrium. The curve 1 corresponds to a crystal grown by technique of slow cooling of the melt, employing the $BaCuO_2$-CuO eutectics. Both curves 2 and 3 correspond to $YBa_2Cu_3O_{7-x}$ single crystals grown from a BaO-CuO self flux in a Al_2O_3 crucible. The curves 4 and 5 correspond to emission spectra of bismuth-based crystals. The $Bi_2Sr_2CaCu_2O_{8+x}$ crystal (curve 4) was grown by the arc-melt method without a crucible. The crystal corresponding to curve

5 was additionally doped with lead ($Bi_{2-z}Pb_zSr_2CaCu_2O_{8+x}$).

As it follows from Fig. 1, the freshly cleaved bismuth crystals of different fabrications and contents possess the same blue luminescence as HTSCs based on yttrium. The structure of HTSC crystals based on yttrium and bismuth shows a Cu-O plane to be the single common element of these structures. Similarity of luminescence spectra of both systems suggests an idea that the localization of excitations occurs in this Cu-O plane and that an oxygen quasi-molecule emission is bound up to oxygen in a Cu-O plane. However further investigations are required to check up this idea, since the luminescence centers of the weakly-bound oxygen molecule type may localize at another place in a crystal lattice, giving a rather similar emission.

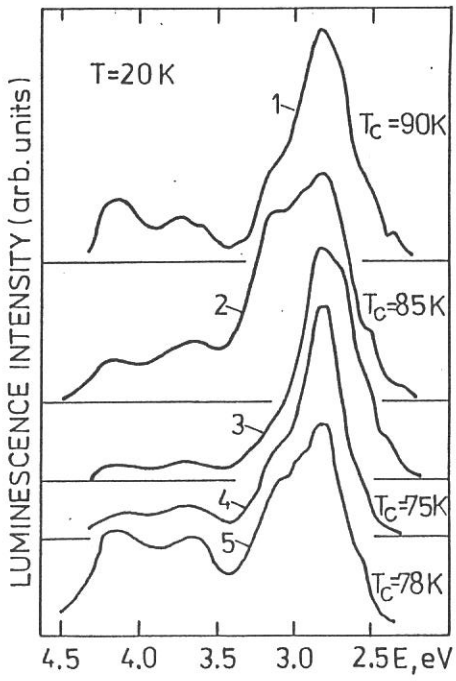

Fig.1. The luminescence spectra of various HTSC single crystals after cleaving in a ultra-high vacuum at 20K under excitation of 30 eV: $YBa_2Cu_3O_{7-x}$ (curve 1); $YBa_2Cu_{3-z}Al_zO_{7-x}$ (with a 2%-admixture of Al_2O_3 from the crucible), cleaved parallel to the [ab] plane (curve 2) and cleaved perpendicular to the [ab] plane (curve 3); $Bi_2Sr_2CaCu_2O_{8+x}$ (curve 4) and $Bi_{2-z}Pb_zSr_2CaCu_2O_{8+x}$ (curve 5). The curves 1,4,and 5 are obtained for crystals, cleaved in the [ab] plane.

References

1). V.G.Stankevitch, N.Yu.Svechnikov, K.V.Kaznacheev, R.Kink et al., JETP Lett., 47 (1988) 321. In Russian.

2). V.G.Stankevitch, N.Yu.Svechnikov, K.V.Kaznacheev, R.Kink et al., Nucl. Instr. Meth. A282 (1989) 684.

3). V.G.Stankevitch, N.Yu.Svechnikov, K.V.Kaznacheev, R.Kink et al., Journ. Lumin. 48 & 49 (1991) 845.

VACUUM UV FLUORESCENCE MEASUREMENTS OF EXCITED Rg_N AND Rg_N-Cl_2 CLUSTERS BY SMA SPECTROSCOPY

Kiyohiko TABAYASHI, Atsunari HIRAYA, and Kosuke SHOBATAKE

Institute for Molecular Science, Myodaiji, Okazaki 444

A Spectrometric Multi-channel Analyzer (SMA) equipped with an MCP intensified CCD detector has been installed in BL2A system to measure dispersed radiation/fluorescence from energized gaseous species formed from UV photo-excited/induced processes. It has been first applied to vacuum UV photochemical studies of Rg_N and Rg_N-Cl_2 clusters and complexes using McPherson 218 Monochromator for UV/VUV fluorescence analyses.

Figure 1 shows a sample fluorescence spectrum from Xe_N^* clusters (average size N ~200), generated by free jet expansion of Xe gas and excited with monochromatized SOR light. Although the emission was analyzed with low spectral resolution (~3 nm) under selective excitation of Xe_N cluster band[1] at 148.2 nm, free-exciton (FE) emission in the resonant region and Stokes-shifted broad band emission of self-trapped exciton (STE) can be clearly seen. A relatively long-red tail of FE band is also indicative of a superimposition with phonon-coupled sidebands. The present results show the direct evidence that the same excitation and radiative relaxation mechanisms as in solid crystals are applicable in Xe_N clusters with $200 < N < 1000$.

Reference

[1] K. Tabayashi, A. Hiraya, and K. Shobatake, **UVSOR** Activity Report 1990, **18**, 23 (1991).

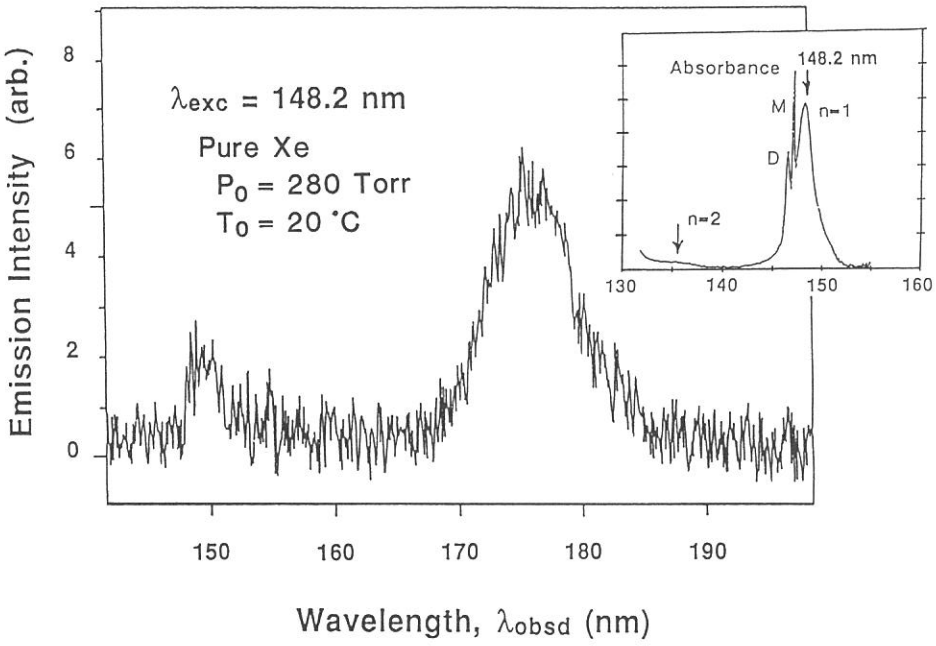

Figure 1.
VUV emission spectrum observed from excited Xe_N^* clusters. Photons are accumulated for 30 sec. Spectral resolution of SMA system is 3nm. Inset shows the cluster band excited at 148.2 nm. Stagnation conditions: P_0 = 280 Torr and T_0 = 20°C.

ELECTRON-ION RECOMBINATION IN PHOTOIONIZATION PROCESS OF ANTHRACENE DOPED IN NONPOLAR SOLVENT

Nobuhiko OHMORI, Kazumichi NAKAGAWA, Kazuie KIMURA*, Arisato EJIRI+ and Aiko KIMURA

Physics Division, Faculty of Education, Kobe University, Tsurukabuto, Nada-Ku, Kobe 657, Japan
*The Institute of Physical and Chemical Research(RIKEN), Wako, Saitama 351, Japan
+Department of Pure and Applied Sciences, University of Tokyo, 3-8-1 Komaba, Meguro-Ku, Tokyo 153, Japan

The Onsager theory is known to be very successful for understanding of electron-ion recombination in a variety of nonpolar systems with low electron mobility[1] such as liquid hydrocarbons, anthracene crystals and amorphous semiconductors. Recently it was found that the Onsager theory fails to reproduce the electric field dependence of photocurrent yield in high-electron-mobility liquids such as liquid methane[2]. Here we reported the electric field dependence of photocurrent yield of anthracene doped in 2,2,4-trimethylpentane (TMP) as a first step of our project to study the evolution of recombination process from Onsager-type to non-Onsager-type in supercritical fluids.

Experiment was performed at the BL-1B of UVSOR. Small amount of anthracene was put into a photoionization cell with a pair of parallel plate electrodes with a gap of about 1.65 mm. After evacuation of the cell, TMP was transferred into the cell on a vacuum line. Concentration of anthracene was estimated to be about 0.2 ppm from absorption spectra. Light beam from a 1 m Seya-Namioka monochromator with bandwidth of about 1 nm was introduced between the electrodes and produced photocurrent was measured by a Keithley 617 electrometer. Intensity of transmitted light was measured by a sodium-salicylated photomultiplier tube. Signal T of this photomultiplier tube was used as an intensity of incident light to normalize the photocurrent i. Figure 1 shows values of i/T (relative values of photocurrent yield) at 185 nm vs. applied electric field E. In order to check the reproducibility of data, measurements were made first from lower electric field to higher field and secondly from higher field to lower field. Experimental error estimated by this procedure was within the area of the drawn points in the figure.

Obtained result was analyzed according to the Onsager theory at low electric field; $i(E)=i(0)(1+AE)$, where $i(E)$ is photocurrent at field of E.

A is determined with the dielectric constant C of TMP and temperature T; $A=e^3/2Ck^2T^2$. This value is 5.605×10^{-5} cm/V at 299 K for TMP (C=1.93). The solid line in Fig. 1 is the best fit line for points at higher than 2×10^3 V/cm. The value of i(0) was determined by extrapolation of this line to E=0. A dotted curve in the figure shows the result of calculation with the Onsager theory. As seen from the figure, experimental data cannot be reproduce by the Onsager theory. This result is not consistent with the result by Tweeten and Lipsky[3], in which experiment the Onsager theory was successful for wide range of electric field and photon energy. In their experiment, the concentration is higher than our case by about 10^3 and incident light intensity was monitored by measuring the fluorescence of anthracene. Refinement of our experiment is under contemplation.

Authors would like to thank professor H. Inokuchi for encouragement. This work was supported the Joint Studies Program of the Institute for Molecular Science (1989-1992) Nos. 1-E535, 1-E833, 2-A806 and 3-H508.

References: [1]B.S.Yakovlev and L.V.Lukin, Advances in Chem.Phys. 60(1985) 99. [2]Y.Nakamura et.al.,Proc.26th Symp. on Radiation Chemistry, Osaka, 1983,p.48. [3]D.W.Tweeten and S.Lipsky,J.Phys.Chem.93(1989)2683.

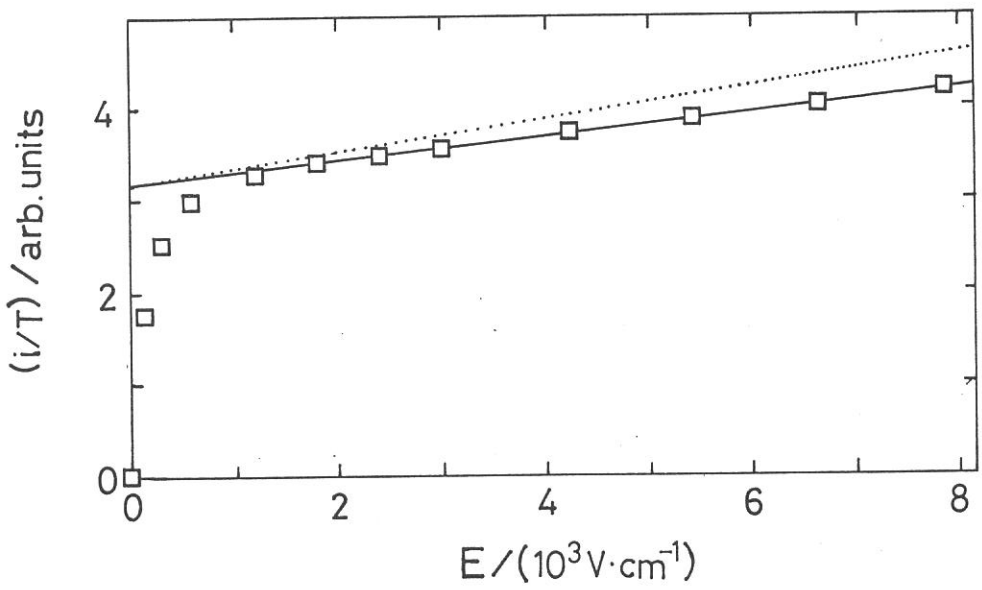

Fig. 1. Photocurrent i normalized by transmitted light intensity T at 185 nm of anthracene doped in 2,2,4-trimethylpentane vs. electric field E at 299 K. (□):Experimental values, dotted line: Onsager theory (see text).

DENSITY DEPENDENCE OF STRUCTURES IN PHOTOCURRENT SPECTRA OF ANTHRACENE DOPED IN SUPERCRITICAL XENON FLUIDS

Kazumichi NAKAGAWA, Arisato EJIRI*, Kazuie KIMURA+, Ken'ichiro TANAKA#, Deti Nurdiawati, Nobuhiko OHMORI, and Aiko KIMURA

Physics Division, Faculty of Education, Kobe University, Tsurukabuto, Nada-Ku, Kobe 657, Japan
+The Institute of Physical and Chemical research(RIKEN), Wako, Saitama 351, Japan
*Department of Pure and Applied Sciences, University of Tokyo, 3-8-1 Komaba, Meguro-Ku, Tokyo 153, Japan
#Photon Factory, National Laboratory for High Energy Physics(KEK), Oho, Tsukuba 305, Japan

Several peaks or shoulders are found in photocurrent spectra of anthracene doped in nonpolar media such as nonpolar hydrocarbon liquids[1] or supercritical xenon[2]. As origin of these structures, three candidates are suggested; (1)Due to anthracene molecular Rydberg states with no energy shift from gas to condensed phase (Holroyd et. al.[1]), (2)Due to vibrational states of anthracene ion (Tweeten and Lipsky[3]), and (3)Due to higher Rydberg states (Nakagawa et. al.[2]). Among them the model by Holroyd may be easy to be examined in terms of density effect of photocurrent peaks by changing the fluid density. We performed this experiment at BL-1B of UVSOR at the first time in 1988[2]. It was repeated again this time with a smaller increment of density changing. In this note we report results obtained from this experiment at BL-1B of UVSOR together with results from another experiment at BL-12A of KEK-PF, in which experiment the model by Holroyd was checked by measuring the pressure-induced energy shift of Rydberg transitions with band width of 0.1 nm.

Fig. 1 shows energies of photocurrent peaks (□ and △) and absorption peaks (⊙) which were assigned as Rydberg transitions of anthracene measured as a function of xenon density N at 300 K. Following results are seen from the figure,

1. Density-induced energy shift was clearly observed for absorption peaks at 6.255, 6.252 and 6.535 eV for N=0 which were tentatively assigned by Koch et. al.[4] as Rydberg transitions of anthracene. This result seems to be a counter-evidence against the model by Holroyd[1].
2. Density-induced energy shift was observed also for photocurrent peaks. The shift are red shift.
3. Magnitude of energy shift per unit change of density are larger in

an order of;

IONIZATION POTENTIAL > ABSORPTION PEAKS > PHOTOCURRENT PEAKS.

The model(2) by Tweeten and Lipsky seems to be difficult to meet the result 2 because photocurrent peaks due to vibrational states should shift parallel with the onset of photocurrent. The model(3) by us have a difficulty to explain the result 3 because energy shift of higher Rydberg transitions should be the same with the shift in ionization potential. At the present time, a new model is to be expected.

Authors would like to thank professor H. Inokuchi for encouragement. This work was supported by the Joint Studies Program (1990-1991) of the Institute for Molecular Science No. 2-A806 and the Joint Studies Program of the National Laboratory of High Energy Physics No. 90-136.

References: [1]R.A.Holroyd et.al.,J.Phys.Chem.88(1984)744. [2]K.Nakagawa et.al.,Chem.Phys.Lett.41(1989)278. [3]D.W.Tweeten and Lipsky,J.Phys.Chem. 93(1989)2683. [4]E.E.Koch et.al.,Chem.Phys.Lett.21(1973)501.

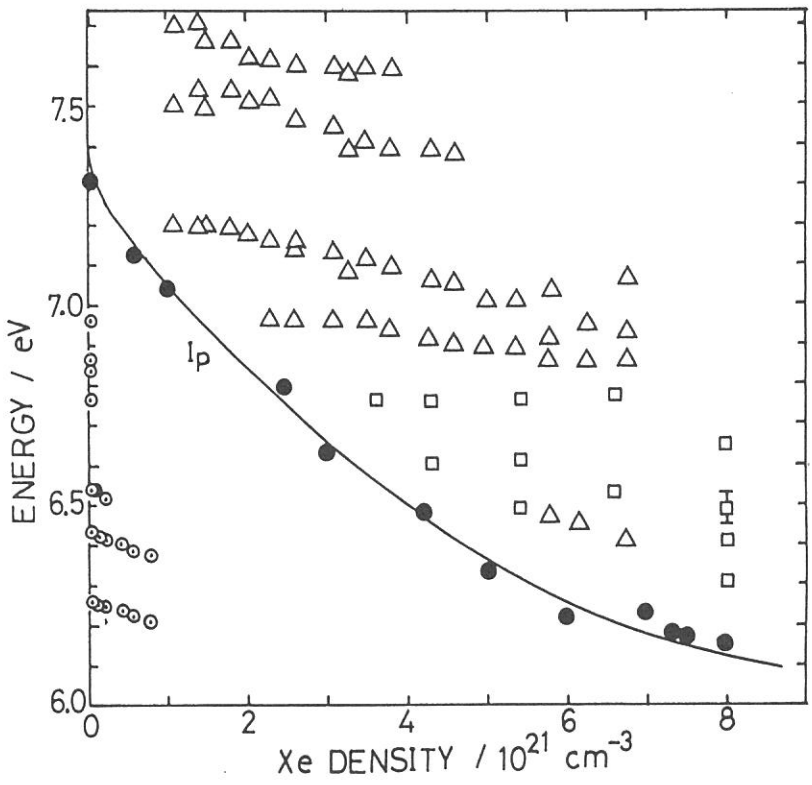

Figure 1. Energy positions of photocurrent peaks (△ and □), Rydberg transitions (⊙) and ionization potential (●) of anthracene doped in supercritical xenon as a function of xenon density.

Si-$L_{3,2}$ Absorption in Polysilanes and a Polysiloxane

M. WATANABE,[1] K. SEKI,[2] K. FUKUI,[3]
E. ISHIGURO[4] AND J. YAMAZAKI[1]

[1] *UVSOR, Institute for Molecular Science, Okazaki 444*
[2] *Department of Chemistry, Nagoya University, Nagoya 464*
[3] *Department of Electrical and Electromics Engineering, Fukui University, Fukui 910*
[4] *Department of Applied Physics, Osaka City University, Osaka 558*

The Si-$L_{3,2}$ absorption have been studied on poly(dimethylsilane) PDMeSi, poly(methylpropylsilane) PMePrSi, poly(methylphenylsilane) PDMeΦSi, and poly(dimethylsiloxane) PDMeSiO by the total photoelectron yield spectroscopy at room temperature. The results are shown in the Figure 1. The Si-$L_{3,2}$ absorption rises around 101 eV in the three polysilanes. The spin-orbit pair of the spectral structure is not clear. In the polysilanes, the spectral feature of PDMeSi is quite similar to that of PMePrSi, but very different from that of PDMeΦSi. The tentative assignment is as follows. The shoulder A and peak B in polysilanes may be attributed to the transitions from Si $2p$ level to the empty state of side group. The intensities of the shoulder A and the peak B of the PDMeΦSi are larger than those of the PDMeSi and PMePrSi. This fact is probably due to the difference in the number of atoms in alkyl and phenyl groups and due to the contribution of π^* state of phenyl group. The peak D in PDMeSi, PMePrSi and PDMeΦSi may be attributed to the transition from Si $2p$ level to Si $4s$ or $4d$ orbits located on the main chain. The Si-$L_{3,2}$ absorptions rise around 104 eV in the polysiloxane, while around 101 eV in the polysilanes. This may be due to the fact that the electron

negativity of oxygen is larger than that of silicon so that the ionic charactor is larger in the polysiloxane than in the polysilane.

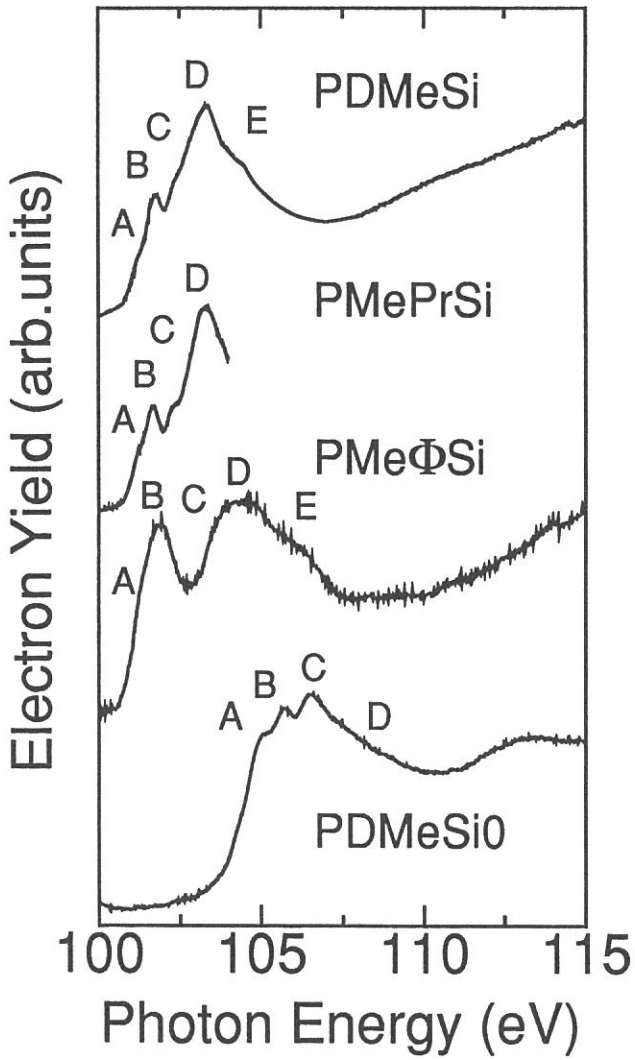

Fig. 1 Total photoelectron yield spectra of poly(dimethylsilane) PDMeSi, poly-(methylpropylsilane) PMePrSi, poly(methylphenylsilane) PDMeΦSi and poly-(dimethylsiloxane) PDMeSiO.

Formation of Photostimulated Luminescence Center in BaFBr:Eu^{2+} Single Crystal by Synchrotron Radiation

Yasuo Iwabuchi, Nobufumi Mori, Terumi Matsuda
Tadaoki, Mitani1), Shigeo Shionoya2)

Fuji Photo Film Co.,Ltd., Technology Development Center, Miyanodai, Kaisei, Kanagawa ,258 Japan
1)Institute for Molecular Science, Myodaiji, Okazaki,444 Japan
2)Tokyo Engineering University, Department of Electronics, Hachioji, Tokyo,192 Japan

The Imaging Plate (IP) which is made of BaFX:Eu^{2+}(X=Br,I) phosphor is widely used as two dimensional image detector in medical[1], biological, and physical fields[2,3] because the phosphor shows excellent photostimulated luminescence (PSL) properties such as wide dynamic range and high sensitivity for various radiation such as x-rays, and ß-rays. In order to investigate the physical model of the PSL of BaFBr:Eu^{2+} single crystal, optical measurements around exciton energy region were performed by using synchrotron radiation.

BaFBr:Eu^{2+} single crystals were grown by the horizontal Bridgman method in a graphite boat. The measurements using vacuum ultra violet (VUV) light were performed at Ultraviolet Synchrotron Orbit Radiation Facility Institute for Molecular Science. The monochromatic VUV photon beam in 3~12eV was obtained from the 750MeV electron storage ring through a 1m Seya-Namioka monochromator installed at the beam line BL-7B.

The PSL center formation spectra were measured as follows. The samples were irradiated by chopped He-Ne laser at 10 Hz (633nm:NEC) as the VUV light was continuously scanned, and detected the signal of Eu^{2+} luminescence which was synchronized with chopped He-Ne laser excitation by using lock-

in amplifier. The electric vector E of the excitation light was always perpendicular to the c-axis of the single crystal.

Figure 1 shows PSL center formation spectra of the BaFBr:Eu^{2+} (500ppm) single crystal at LNT. It is seen that there are two peaks at 7.0 and 7.7 eV due to spin-orbit splitting of the valence band formed in the ground 4p state of Br- .[4] PSL centers are created efficiently at the energies of exciton. In addition, a shoulder like structure is observed at 6.6eV in the PSL center formation spectra . As to this structure at the low energy side of the exciton, two origins are considered. One is due to the ionization of Eu^{2+} and another is the Eu^{2+} bound exciton. In order to clarify the origin of this structure, we intend to measure the Eu^{2+} concentration dependence on this structure in PSL formation and photoconductivity spectra.

Reference

[1] M.Sonoda, M.Takano, J.Miyahara and H.Kato, Radiology 148 (1983) 833

[2] Y.Amemiya, K.Wakabayashi, H.Tanaka, Y.Ueno and J.Miyahara, Science 237 (1987) 164

[3] Y.Amemiya and J.Miyahara, Nature 336 (1988) 89

[4] E.Nicklaus, Phys. Stat. Sol.(a) 53 (1979) 217

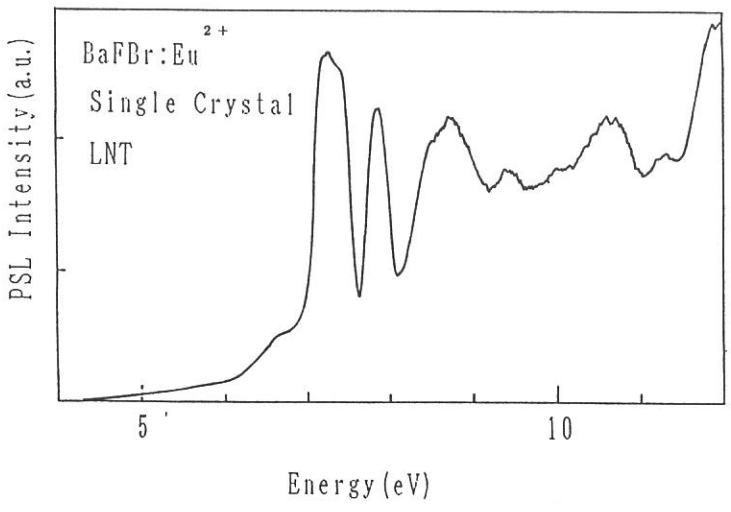

Figure 1 PSL center formation spectra in BaFBr:Eu^{2+} (500ppm) single crystal at LNT.

TRANSMISSION SPECTRA OF BLACK PHOSPHORUS DUE TO THE B1u LATTICE VIBRATION

Takao NANBA and Ichimin SHIROTANI*

Department of Physics, Faculty of Science, Kobe University, Rokkodai 1-1, Nada-ku, Kobe 657.

** Department of Engineering, Muroran Institute of Technology, mizumoto, Muroran 050, Hokkaido*

The transmission spectrum of black phosphorus single crystal in the far infrared region was measured at 300 K using the UVSOR. Intense absorption band was observed at 132 cm-1 at room temperature in the configuration of the linearly polarized incident light whose electric vector is parallel to the *x*-axis of the crystal as shown in Fig. 1 (in the present paper, this configuration is denoted as *E//x*). On the other hand, in the configuration of *E//y*, the absorption disappeared.

Such anisotropic character in the optical properties of the black phosphorus originates from its crystal structure. Black phosphorus is a semiconductor with a narrow-band gap of about 0.3 eV. The crystal is composed of puckered layers of atoms and belongs to an orthorhombic crystal structure(D_{2h}^{16}). The structure of the puckered layer is schematically drawn in Fig. 2*a* with a cartesian coordinate. According to the its crystal symmetry, an infrared active phonon mode, i.e. B_{1u} mode, exists in the far infrared region [1]. Although black phosphorus possesses no permanent dipole moment because the four atoms in the primitive unit cell are the same , definite dipole moment can be induced by the atomic displacement according to the B_{1u} phonon mode. The induced dipole moment due to the B_{1u} mode is directed along the *x*-axis of the crystal as shown in Fig. 2*b*. Observed intense absorption can be attributed to the excitation of the B_{1u} phonon mode and confirmed the theoretical consideration on the mechanism of the induced dipole moment due to the B_{1u} phonon mode.

Secondary peak also was observed at about 143 cm^{-1} which intensity was about one tenth of the main peak. It may be attributed to two phonon absorption due to the anharmonicity of the lattice vibration.

Reference

[1] C. Kaneta and A. Morita: J. Phys. Soc. Jpn. 55(1986) 1224.

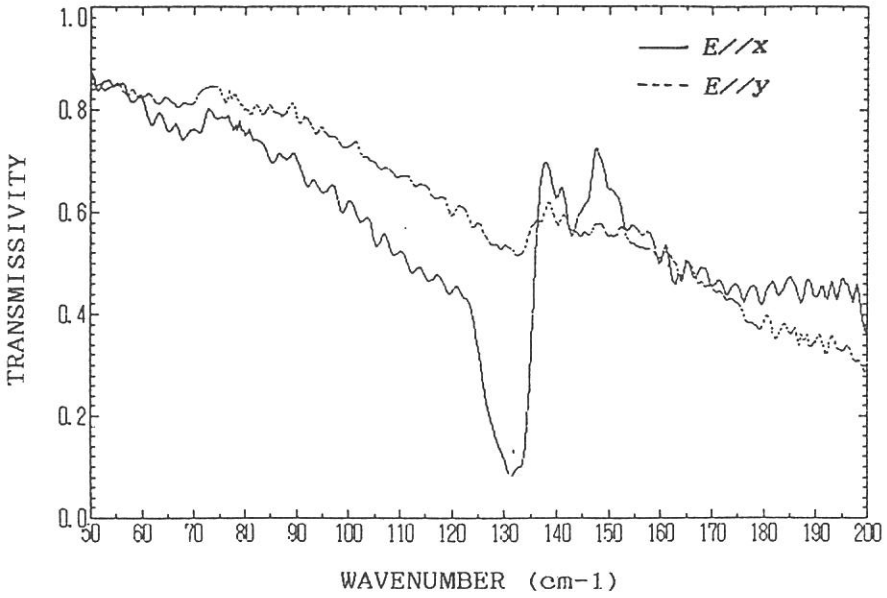

Fig. 1 Transmission spectrum of a black phosphorus single crystal at room temperature. Solid curve coresponds to the configuration of *E//x* and dashed one to the *E//y*.

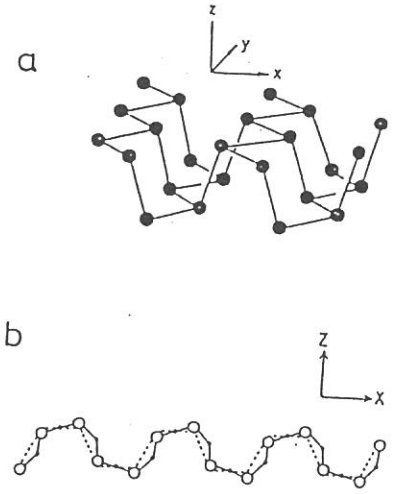

Fig. 2 (*a*) The structure of a single puckered layer of black phosphorus with a Cartesian coordinate. (*b*) Schematic representation of the atomic displacement according to the B_{1u} mode projected to the *xz*-plane.

INFRARED ABSORPTION OF SMALL NaCl CRYSTAL AND ITS PRESSURE DEPENDENCE

Takao NANBA, Mitsuhiro MOTOKAWA and Takashi MATSUYA

Department of Physics, Faculty of Science, Kobe University, Rokkodai 1-1, Nada-ku, Kobe 657

The absorption spectrum of small NaCl crystal embedded in a transparent medium (apiezon grease-N) in the far- infrared region and its pressure (P) dependence was measured at room temperature. At P=0, an intense and broad absorption band was observed at 183 cm^{-1}. The absorption curve is drawn by a dashed line in Fig. 1*a* in comparison with that of an evaporated thin NaCl film of which thickness was 1.2 μm (solid line). The absorption of the thin film at 164 cm^{-1} is due to the bulk TO-phonon mode.

According to the continuum theory [1] which describes an infrared absorption of spherical particles which are spatially isolated each other in a nonabsorbing medium, as the size of the absorbing particle becomes much smaller than the wavelength of an incident light, a "surface phonon" mode occurs at the position between the TO-(ω_T) and the LO-phonon frequency(ω_L). The frequency(ω_s) is approximately given by the following equation

$$\varepsilon(\omega_s) = -2\varepsilon_m .$$

Here, ε is the dielectric function of the material comprising the sphere and ε_m the dielectric constant of the surrounding medium of the absorbing sphere. The intense absorption of small NaCl particle at 183 cm^{-1} ascribes to the surface phonon mode.

The pressure dependence of the absorption spectrum of the small NaCl particle and the thin film of NaCl was measured by using the diamond anvil cell system installed at the BL6A1 of the UVSOR. The result at P= 0.8 GPa is shown in Fig. 1*b*. The amount of the peak energy shift of the surface phonon mode from the energy at P=0 was found to be smaller than the peak energy shift of the bulk phonon. Such difference of the peak energy shifts under pressure between the surface phonon mode and the bulk phonon can be seen clearly in Fig. 2 which plots the peak energies of the surface and the bulk phonon modes as function of the applied pressure to the sample. The different pressure dependence of the phonon energy shifts between the surface and the bulk mode can be understand the extended continuum theory.

Reference

[1] L. Genzel and T. P. Martin: Surface Science **34**(1973)33.

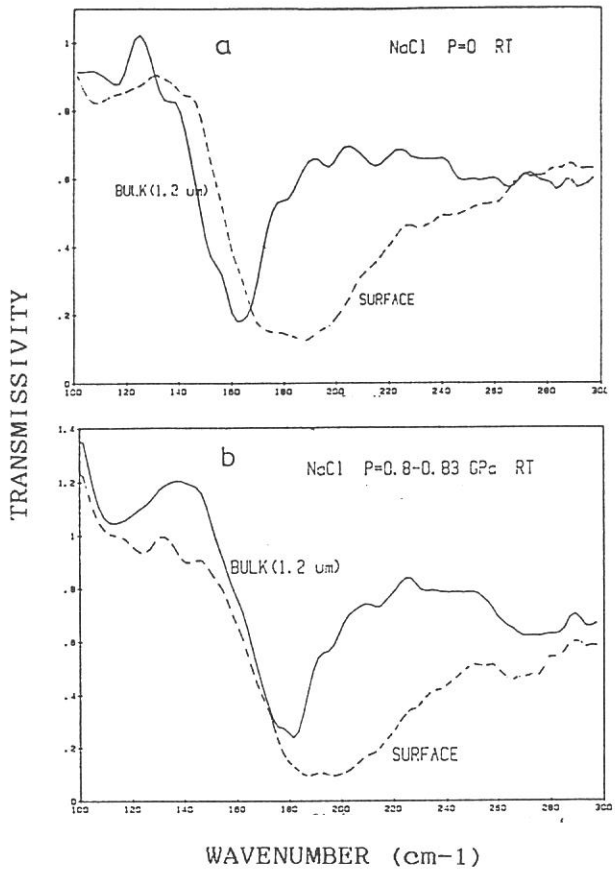

Fig. 1 shows (*a*) transmission spectra of the small NaCl crystals embedded in grease (dashed curve) and the thin film (solid curve) of NaCl at P=0. The size of the small particle was several μm in average and the thickness of the evaporated film was 1.2 μm, and (*b*) those at P=0.8 GPa.

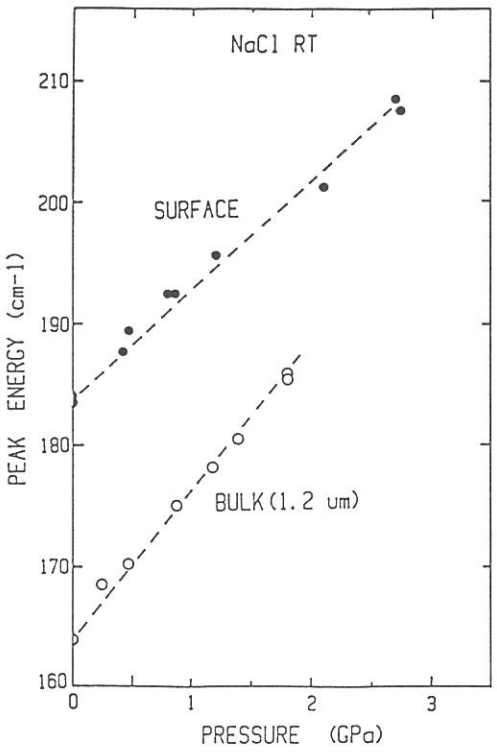

Fig. 2 shows the peak positions of the surface phonon mode and the bulk phonon as function of the applied pressure to the sample.

EMISSION SPECTRA AND DECAY CURVES FOR AUGER-FREE LUMINESCENCE (CROSS-LUMINESCENCE) FROM $CsCl_{1-x}Br_x$ MIXED CRYSTALS

Shinzou KUBOTA, Yoshihiko NUNOYA, Jian-zhi RUAN(GEN)
and Satoshi Hashimoto*
Rikkyo University, Nishi-Ikebukuro 3 Tokyo 171
* Kyoto University of Education, Fushimi-ku, Kyoto 612

The experiment was carried out by using a 1-m Seya-Namioka monochromator at BL7B beam line of UVSOR. The experimental set up is similar to that described in Ref. 1. By using 5.632 MHz UVSOR single bunch, the energy resolved luminescence photons were detected by an MCP photomultiplier with a single-photon-counting method. The output pulses from this photomultiplier were used to start a time-to-amplitude converter, while UVSOR rf signals were used as stop pulses. The output from the time-to-amplitude converter is fed into the pulse height analyzer where the decay curve is accumulated. The emission spectra were obtained by counting the total number of pulses of the energy resolved decay curves for different energies of luminescence photons under the condition of the constant number of incident exciting photons.

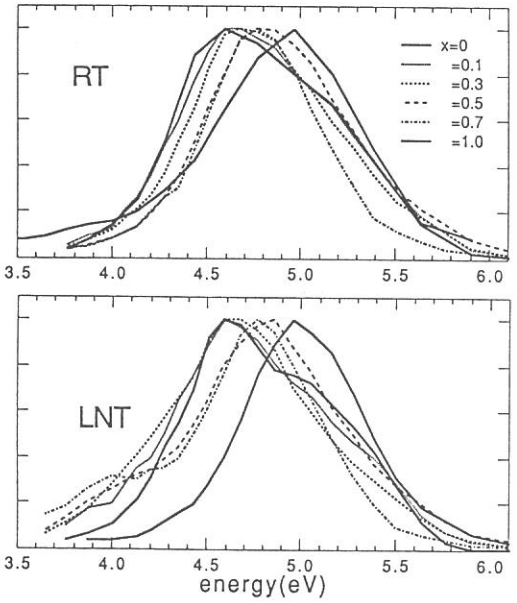

Fig. 1. The emission spectra of the fast component of Auger-free luminescence from $CsCl_{1-x}Br_x$ crystals at room temperature and liquid nitrogen temperature. The energy of incident photons is 15.3 eV.

Figure 1 shows emission spectra for the Auger-free luminescence from $CsCl_{1-x}Br_x$ crystals at room temperature and liquid nitrogen temperature. The measured decay curves are shown in Fig.2. The emission spectra were normalized at the peak values. The decay time for CsBr at liquid nitrogen temperature is 1.1 ns, which is longer than that at room temperature. It is observed that the luminescence intensity for CsBr at liquid nitrogen temperature is about 100 times larger than that at room temperature. The most outstanding feature for the decay curves from $CsCl_{1-x}Br_x$ crystals of $0 \leq x \leq 0.5$ is that the decay curve does not show a single exponential decay. This behavior is more pronounced at liquid nitrogen temperature. For $0.5 \leq x \leq 1$, the luminescence intensity decays more rapidly with increasing x. One

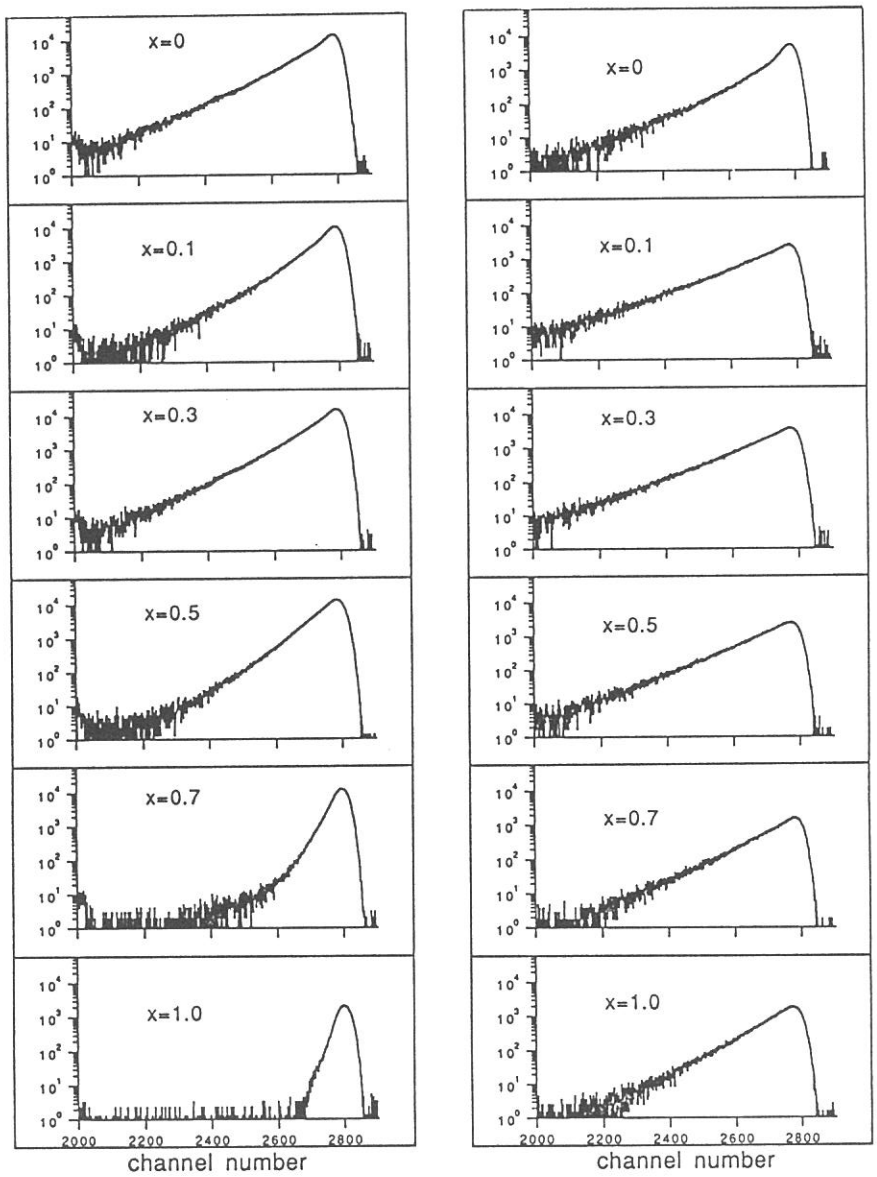

Fig. 2. The decay curves for Auger-free luminescence from $CsCl_{1-x}Br_x$ crystals at room temperature (left) and liquid nitrogen temperature (right). The energy of incident photons is 15.3 eV. One channel corresponds to 14 ps.

possible explanation for the non-exponential decay is that the Cs^+ 5p outermost core holes produced by incident photons near to the surface relax non-radiatively more rapidly than those in the bulk. [2)]

References

1. S. Kubota et al. Phys. Rev. Lett. 60 (1988)239.
2. S. Kubota et al. J. Lum. 48 & 49 (1991)589.

EXCITON INITIATED DESORPTION OF METASTABLE ATOMS FROM THE SURFACE OF SOLID Ne

Ichiro Arakawa, Daniel Eduardo Weibel*, Akira Hoshino,
Takato Hirayama, and Makoto Sakurai+
Department of Physics, Gakushuin University, Mejiro, Toshima, Tokyo 171
+ *National Institute for Fusion Science, Huro, Chikusa, Nagoya 464-01*
* *Present address: Department of Physical Chemistry, University of Cordoba, Argentina*

Photo-stimulated desorption of Ne metastables from the surface of solid Ne was studied by using synchrotron radiation light as a state-selective excitation source. Kinetic energy distributions of desorbed metastable species were obtained by time-of-flight(TOF) measurement. The sample, solid Ne condensed on a copper substrate, was prepared in an ultra-high vacuum (< 10^{-8} Pa) system installed on BL5B. It is indispensable for the purpose of the present study to keep a sample surface clean. Monochromatized SR-light was chopped to pulse beam by a rotating disc with ten slits on the peripheral. The pulse duration was 16 μs and the recurring cycle was 250 Hz typically. Desorbed particles were detected by a secondary electron multiplier (Ceratron, Murata Corp.) which had a sufficient sensitivity for excited neutrals of Ne. The flight length, that is the distance between the target and the entrance of the Ceratron, was 155 mm. As we measured desorbed particles with the flight time between 20 to 1000 μs, the detectable particles were two metastable species of Ne excited neutrals: $^3P_2$ (16.619 eV of the excitation energy and 24.4 s of the life time) and $^3P_0$ (16.716 eV and 430 s)[1]. The details of the time-of-flight (TOF) measurement have been given elsewhere[2].

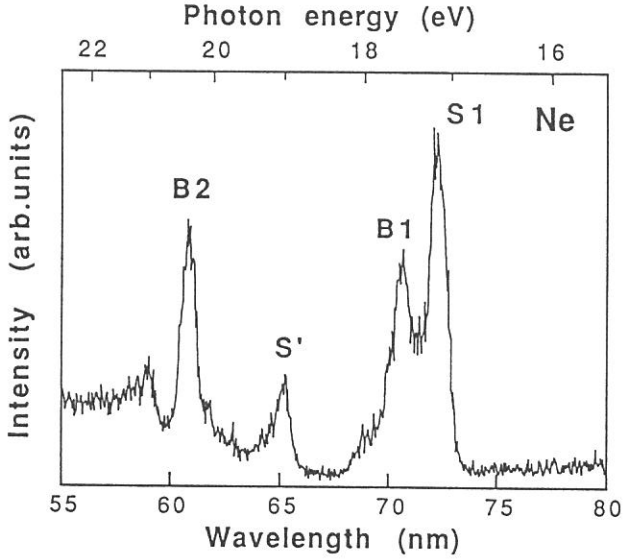

Fig. 1. Desorption yield of Ne metastables as a function of an excitation photon energy.

The relation between the yield of the Ne metastables and the wavelength of SR-light is shown in Fig. 1. The photon energies at the peaks in the spectrum coincide with the excitation energies of the excitons obtained by Saile and Koch[3]; S1: the first order surface exciton, B1 and B2: the first and the second order bulk exciton, respectively, S': a free exciton in $2p^5 3p$ state which is allowed at the surface because of the reduced symmetry[4]. Thus the close correlation between the desorption yield of Ne metastables and the excitation of excitons are clearly shown here as previously shown for the case of Ar[5]. The four TOF spectra obtained by exciting S1, B1, S', and B2 excitons are shown in Fig. 2. Several characteristic features observed in these spectra can be pointed out;

1. The higher kinetic energy peak (peak A) by S' and B2 excitation.
2. The shift of the kinetic energy of the slower metastable from 0.17 eV (peak B) by S1 and B1 excitation to 0.23 eV (peak C) by S' and B2 excitation.
3. Broad peaks or tails (peak D) by B1 and B2 excitation.

On examination of the dependence of the desorption yields and the kinetic energy distributions on the excitation of surface and bulk excitons, two groups of metastables which were desorbed by "cavity-ejection" and "excimer-dissociation" mechanisms were identified in the TOF spectra[6].

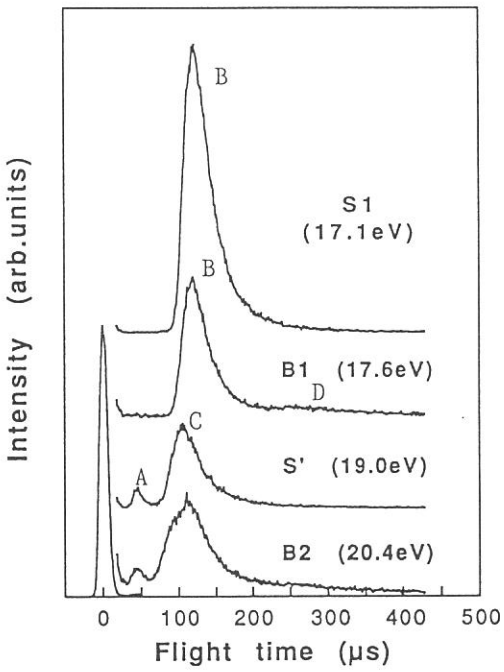

Fig. 2. Time-of-flight spectra of Ne metastables at the photon energies of 17.1(S1), 17.6(B1), 19.0(S'), and 20.4 eV(B2).

1) N. E. Small-Warren and L. Y. Chow Chiu: Phys. Rev. A 11 (1975) 1777.

2) M. Sakurai, T. Hirayama and I. Arakawa: Vacuum 41 (1990) 217.

3) V. Saile and E.E. Koch: Phys. Rev. B 20 (1979) 784.

4) K. Inoue, H. Sakamoto, and H. Kanzaki: Solid State Commun. 49 (1984) 191.

5) I. Arakawa and M. Sakurai: *DIET IV*(Springer, 1990) p.246.

6) I. Arakawa et al.: Jpn. J. Appl. Phys. to be submitted.

EFFECT OF TEMPERATURE ON THE LUMINESCENCE OF HEAVY MEROMYOSIN

Mieko TANIGUCHI, Sinya KATO and Norio WATANABE

Department of Physics, Faculty of Science, Nagoya University, Nagoya 464-01

The luminescence properties of heavy meromyosin (HMM) have been investigated using synchrotron radiation from UVSOR. The fluorescence and phosphorescence spectra of tryptophan residues in HMM were measured over wide temperature ranges (80 - 300^{0} K). A cryostat chamber was connected to a 1 m Seya-Namioka monochromator in BL7B beam line with LiF window. A quartz vessel containing HMM powder was placed in a metallic sample holder. The temperature of the samples was measured by a copper-constantan thermocouple. Fluorescence decay times were also measured by the time-correlated single photon counting system under the single bunch operation. Figure 1-1 shows the excitation spectrum of HMM powder at 145 K, when emitted at 330 nm. The spectrum has four bands peaking at 235, 275, 290 and 298 nm. The spectral profile did not change with temperature. Figure 2 shows the luminescence spectra at various temperatures, when excited at 295 nm. The emission spectra at room temperature show a fluorescence band peaking at 330 nm. The emissions of various temperature ranges show the short-wavelength fluorescence ($\lambda \sim 330$ nm) from buried tryptophan residues. When the temperature was lowered from room temperature to near that of 200 K at 2~3 X 10^{-7} torr, two phosphorescence bands peaking at 415 nm and 438nm appeared. Plots of $\ln I_{0}/\ln I_{max}$ versus 1/T gave two different slopes. The results suggest a temperature-dependent conformational transition in some tryptophan residues in HMM.

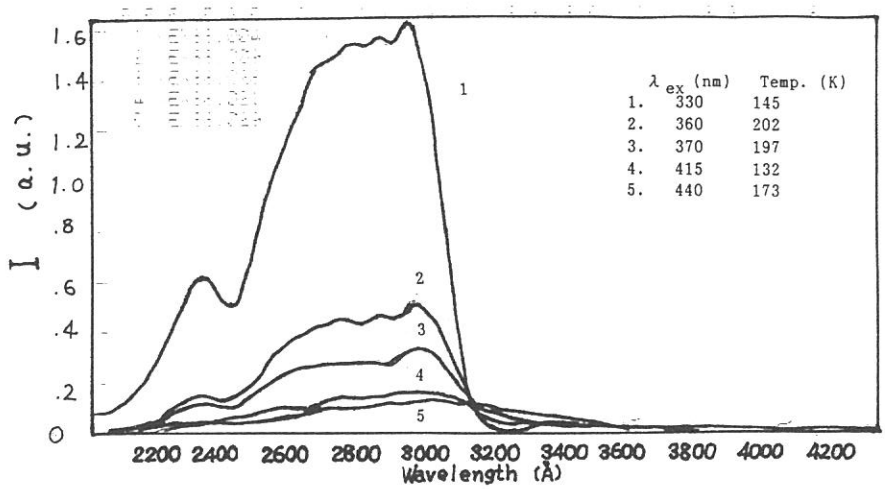

Fig. 1 The excitation spectrum of HMM powder at various temperatures.

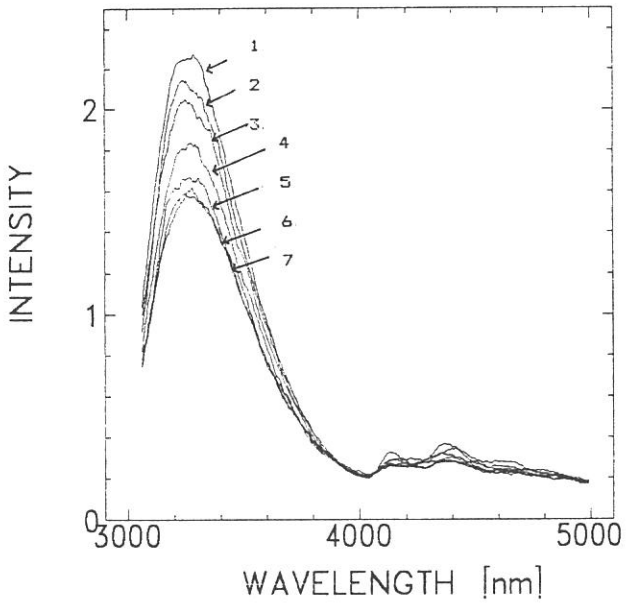

Fig. 2 Total emission spectra of HMM powder at various temperatures. Excitation at 295 nm.

Temperatures : 1) 128 K, 2) 140 K, 3) 148 K, 4)156 K, 5) 166 K, 6) 175 K and 7) 182 K.

KINETIC-ENERGY RELEASE IN THE DISSOCIATIVE DOUBLE PHOTOIONIZATION OF NO

Toshio MASUOKA and Kyouichi MIYAZAKI

Department of Applied Physics, Osaka City University, Sumiyoshi, Osaka 558

One interesting aspect in the study of the dissociative double ionization of molecules is the determination of kinetic-energy release distributions (KERDs) in the fragmentation of AB^{2+}. The KERD reflects the energy differences between the repulsive part of the potential surface of AB^{2+} in the Franck-Condon region, and the dissociation limits corresponding to the various internal energies shared by the fragment ions.

In the present study, the KERDs of fragment ions produced in the dissociative double photoionization of NO have been studied in the photon energy region of 40-110 eV by use of synchrotron radiation and the photoion-photoion coincidence (PIPICO) method. The most probable KERDs are determined for the N^++O^+ channel of NO^{2+} as a function of the excitation photon energy. This was accomplished by analyzing the spectral profile of the PIPICO peaks measured at the pseudo magic angle ($\sim$55°), which minimizes any effect of the anisotropic angular distributions of the fragment ions.

Fig. 1 shows the KERDs obtained at $h\nu$=50 and 110 eV. The AKER as a function of the excitation photon energy was also obtained. Apparently, the KERD and AKER increase very much as the excitation energy increases. This means that the high-lying electronic states of NO^{2+} result in more excited N^+ and/or O^+ with larger kinetic energies than those resulting from the low-lying states. Qualitatively, this is the natural consequence of

an increased Coulomb repulsion because the shielding of positive core charges weakens when two inner-valence electrons are ejected as compared to the ejection of two outer-valence or one inner-valence and one outer-valence electrons. The nearly continuous KERDs derived for the direct double photoionization from valence orbitals will be discussed elsewhere, in relation to the electronic states of NO^{2+}.

In order to obtain the dissociative double photoionization threshold (=39.1±0.3 eV), the number of N^++O^+ coincidences are plotted in Fig. 2 as a function of the photon energy. This signal was corrected for the variation of the excitation photon energy as measured from the photoemission of a CuBe cathode.

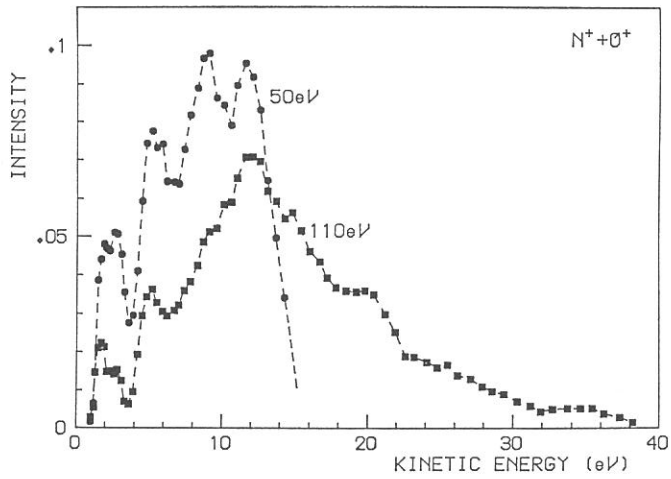

Fig. 1. Kinetic-energy release distributions of N^++O^+ at excitation energies of 50 and 110 eV.

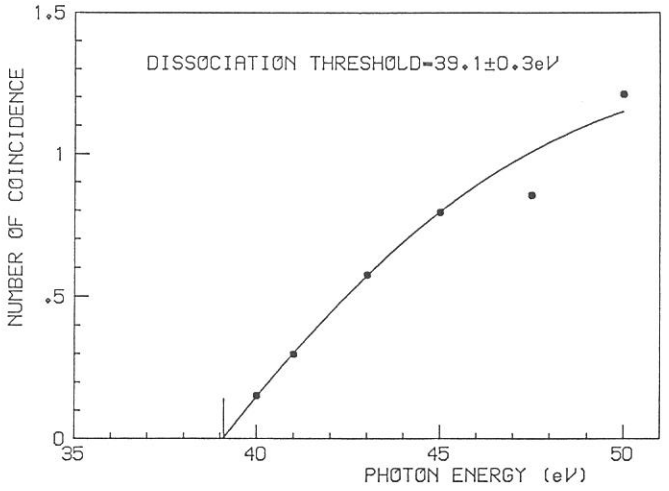

Fig. 2. Number of N^++ O^+ coincidences as a function of excitation energy.

Low-temperature Growth of ZnTe by Synchrotron Radiation Irradiated Metalorganic Chemical Vapor Deposition

Hiroshi OGAWA, Mitsuhiro NISHIO and Makoto IKEJIRI

Department of Electronic Engineering, Faculty of Science and Engineering, Saga University, 1 Honjo, Saga 840, Japan

ZnTe is promising for applications to optoelectronic devices. Hence, it is important to obtain high quality ZnTe layer. The low temperature growth is one of the important factors required to realize the high quality layer. Accordingly, much effort should be made to grow the ZnTe layer at reduced temperature. The synchrotron radiation (SR) irradiated metalorganic chemical vapor deposition (MOCVD) technique seems to be very useful for lowering the growth temperature, since SR can easily dissociat the source organometallics.

In this report, we describe the growth of ZnTe layer on GaAs substrate by the new SR-assisted MOCVD procedure which may bring out the ideal ALE process.

Figure 1 shows typical time sequences of the source gas flow and SR irradiation, which describe the new SR-assisted MOCVD procedure. Here, SR used for the excitation has a wavelength above 120nm. In this procedure, the source gases of DETe and DEZn are separately introduced into a growth chamber by switching the valves, and SR is irradiated onto the substrate by opening the gate valve gradually after the growth chamber was evacuated up to a vacuum of about 10^{-7} Torr. In typical growth condition, the amount of the transported source is $\sim 0.2\mu$ mol/cycle for DETe or DEZn, and the substrate temperature is ~ 200℃.

Figures 2(a) and 2(b) show respectively the ESCA data and RHEED picture of the grown layer. The layer is composed of Zn and Te atoms. The RHEED pattern represents the streak one, indicating that the layer is the single crystal with smooth surface. The thickness of the layer is estimated to be around 100 Å. Thus we have succeeded in the low-temperature growth of the ZnTe epit axial filmwith good quality by the new growth procedure.

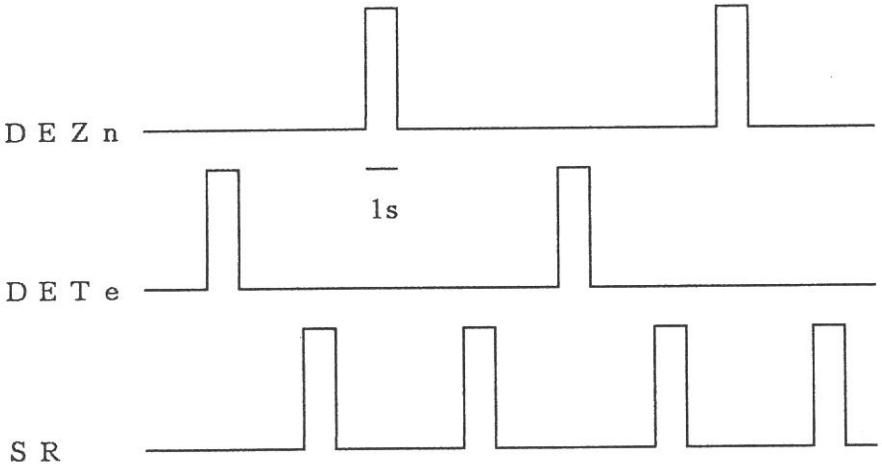

Fig. 1. typical time sequences of the source gas flow and SR irradiation.

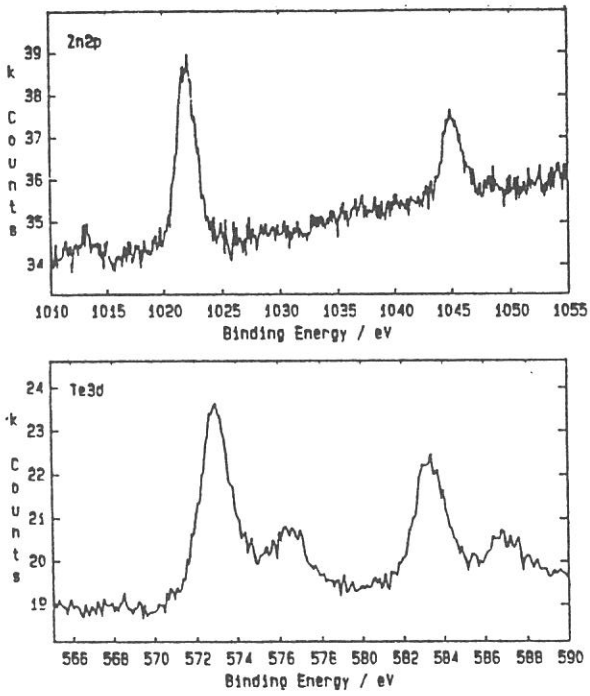

(a)

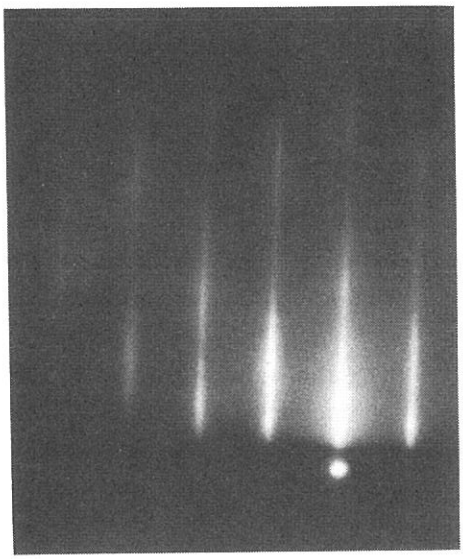

(b)

Fig. 2. (a)the ESCA data and (b)RHEED picture of the typical grown layer.

VUV Reflection Spectra of $NaNO_2$

Masaaki ASHIDA, Osamu OHTA, Masao KAMADA*,
Makoto WATANABE* and Riso KATO

Department of Physics, Kyoto University, Kyoto 606
**Institute for Molecular Science, Myodaiji, Okazaki 444*

Sodium nitrite is a well-known ferroelectrics, which undergoes order-disorder phase transition at 163.5 ° C. There have been few studies on the higher electronic states.[1] In this paper, we report VUV reflection spectra of $NaNO_2$ single crystal studied with synchrotron radiation from UVSOR.

The measurement has been made at 28K with a Seya-Namioka monochromator installed at the beam line 1B. $NaNO_2$ has an orthorhombic structure and shows strong optical anisotropy. Therefore samples were prepared by cutting out of crystal blocks along the crystallographic axes. We measured polarized reflection spectra for each crystal axis ($E \parallel$ a,b and c), using the good polarization property of SR. The absolute value of the reflectivity is determined by fitting the observed value to that calculated by already-known refractive indices in visible region.[2] Fig. 1 shows the absorption spectra of $NaNO_2$ obtained by the Kramers-Kronig transformation of the reflection spectra.

Referring to McEwen's molecular orbital calculation of NO_2^- molecule, [3] we can assign the general feature of spectra below 9eV to the intramolecular transition. The strong absorption band near 6eV with $E \parallel c$ polarization corresponds to $^1A_1 \rightarrow {}^1B_2$ ($\pi \rightarrow \pi^*$) transition in the molecule. In this absorption band we find vibronic structure, which has an interval of about 1000cm^{-1}. (See Fig. 2.) This structure is caused by the coupling between the electronic excited state ($^1B_2$) and the totally symmetric stretching vibration (ν_1) of NO_2^-. Vibronic lines in this band are not separated so clearly, in contrast to the discrete vibronic lines of the lowest singlet absorption.[4] The fact may suggest that the strength of the electron-phonon interaction of the former is larger than that of the latter. The hump near 8.5eV with $E \parallel b$ polarization corresponds to $^1A_1 \rightarrow {}^1A_1$ transition.

The absorption above 9eV are likely assigned to charge transfer transition, which were studied by absorption measurement of the evaporated thin films by Yamashita *et al.*[1] It is noteworthy that there is some resemblance between polarization dependent K-XANES in $NaNO_2$ crystal observed by Murata *et al.*[5] and the present spectra. Further investigation is necessary to discuss the relation between the XANES and the VUV spectra.

References

1) H. Yamashita and R. Kato : J. Phys. Soc. Jpn. **29**(1970)1557.

2) S. Hirotsu, T. Yanagi and S. Sawada : J. Phys. Soc. Jpn. **25**(1968)799.

3) K. L. McEwen : J. Chem. Phys. **34**(1961)547.

4) H. Kawaura, Y. Kawaguchi and R. Kato : J. Phys. Soc. Jpn. **57**(1988)3613.

5) T. Murata, S. Naoe and R. Kato : Read at the Sectional Meeting of Phys. Soc. Jpn., Kagoshima, October, 1989, 5a-A-11.

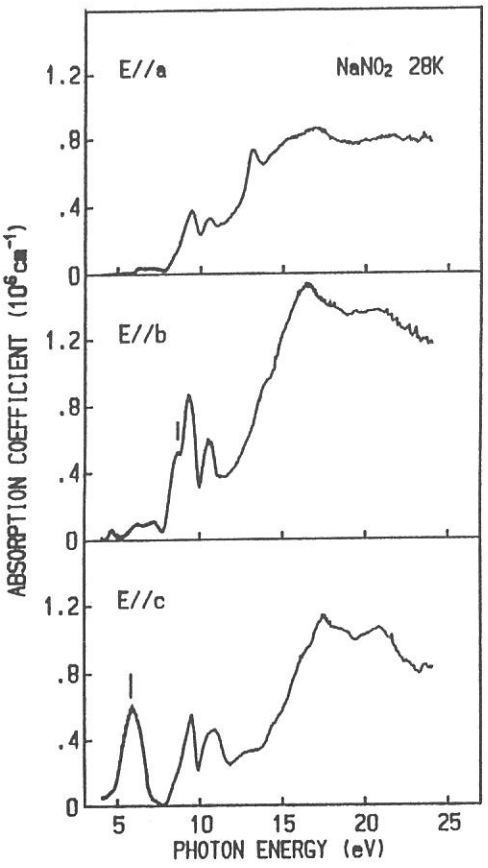

Fig. 1

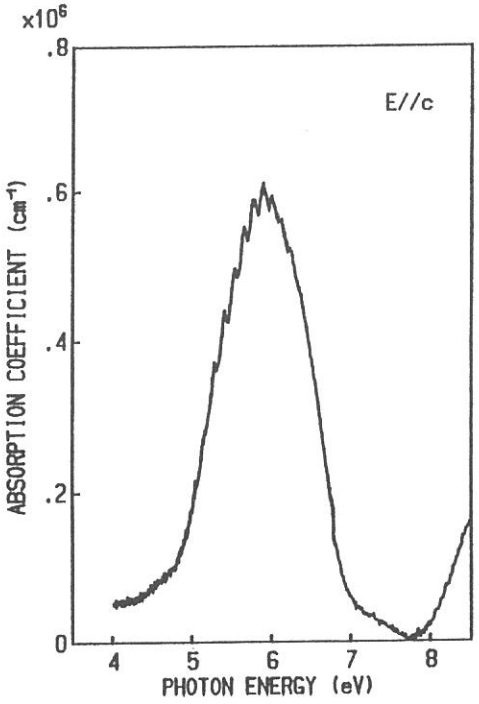

Fig. 2

Core level shifts of K atoms adsorbed on the Si surfaces

Shin-ichiro TANAKA and Masao KAMADA

Institute for Molecular Science, Myodaiji, Okazaki, 444

Adsorption of alkali metals on semiconductor surfaces, particularly on the Si surfaces, has been the subject of extensive studies for these years. One of the most controversial issues is whether alkali atoms on the Si surfaces are ionic or neutral in nature: The classical picture suggested by Langmuir is that alkali metals are ionic in the low coverage region, while they become neutral (metallic) with the increase of the coverage due to the charge transfer between alkali atoms and the substrate. Recently, Ishida et. al. proposed the new picture that alkali metals are covalently bonded to the substrate in any coverage region, and charge distribution occur in the atomic radius of alkali metals. In this work, energy shifts of 3p semicore-levels of K atoms were monitored as a function of coverage on the Si(100)(2X1) and Si(111)(7X7) surfaces at room temperature using PhotoElectron Spectroscopy (PES).

The experiments were carried out by the use of the grasshopper monochromator at BL2B1. The experimental chamber (base pressure of 5 X 10^{-11} Torr) was equipped with a LEED optics, a double-pass CMA for PES with a coaxial electron gun for AES, and an ion gun, etc. Samples were Si(111) and Si(100) wafers [B-doped, ~10Ωcm], both of which were mounted on the sample holder such that an in situ comparison of the two surfaces can be made by merely a rotation. Samples were cleaned by several cycles of Ar^+ bombardment and annealing, and then checked by the use of LEED and AES. Potassium was deposited from a SAES getter source. The pressure was less than 2 X 10^{-10} Torr during the deposition after a sufficient degas. The temperature of the samples was increased to about 350K during the deposition, which was higher than the desorption temperature of the bulk K, thus, only the chemisorbed K atoms (monolayer at most) will be discussed in the following.

Figs. 1 and 2 show the K-3p emission recorded after various K deposition on the Si(100)(2X1) and Si(111)(7X7) surfaces, respectively. The photon energy was 150 eV, and the overall resolution was 0.3 eV. Spectra were normalized and subtracted by the use of spectra for the clean surface. Peaks are broad and asymmetric (the $p_{3/2}$-$p_{1/2}$ spin-orbit splitting is not resolved). Dotted lines are guides for changes of peak positions. The binding energies vary with the amount of K atoms, and are plotted in Figs. 3 and 4 for Si(100) and Si(111), respectively, as a function of the peak heights normalized by the saturated one, which approximately represent the fractional coverage of K atoms.

For the Si(100)(2X1) surface (Fig. 3), K-3p binding energy is nearly constant at lower coverages, suggesting the dispersive adsorption in a single site, and shifts to lower binding energy at higher coverages. Total amount of the decrease is about 0.25 eV. According to the classical model by Langmuir, K atoms are changed from ionic to neutral with the increase of the coverage, thus, the large core-level shifts (chemical shifts) are expected due to the charge transfer. However, the shift of 0.25 eV for the Si(100)/K system is too small for such a transition, hence, the classical picture is ruled out. It is noted that we observed the 2p core-level emission with the photon of 130 eV and found that the surface component shifted to lower binding energies by about 0.2 eV after the deposition of K atoms. This shift is much smaller compare to that for the case of, for example, Ca on Si surface (1.2 eV) where the charge is transferred from Ca to Si. Thus, for the Si(100)(2X1)/K system, it is considered that the charge transfer is little and that K-Si bond is not ionic but covalent in nature in any coverage region.

For the Si(111)(7X7) surface (Fig. 4), the behavior of the K-3p emission is significantly different from that for Si(100)/K. There are two different regimes of adsorption behavior: K-3p binding energies shift by 0.5 eV toward higher binding energy

at lower coverages and then shift by 0.9 eV toward lower binding energy at higher coverages. This indicates that the adsorbed species at lower coverages are different in nature from those at higher coverages. This is consistent with the observation by STM: Hashizume et. al. observed the STM images for the Si(111)(7X7)/K system and found that the images of K atoms on Si(111) are dark (suggesting the ionic bonding) at lower coverages while they are bright (suggesting the covalent bonding) at higher coverages. Thus, the different behavior of the K-3p shifts at lower coverages from that at higher coverages is considered to be due to the change of the nature of adsorbed K atoms depending on the coverage. This is very different from the case for Si(100).

The core-level shifts toward lower binding energy with the increase of the coverage of alkali atoms have been observed on metal surfaces (ex. 0.7 eV for W(110)/K), and is considered to be related through a Born-Haber cycle to the decrease of the adsorption enthalpy due to the adsorbate-adsorbate repulsion. This is reasonable because the average K-K distance become small at higher coverages. However, the shifts towards higher binding energy with the increase of the coverage of alkali atoms, observed at lower coverages for Si(111)/K, have not been reported on other surfaces to our knowledge. More studies may be needed in order to understand the origin of this shift.

In summary, K-3p core-level shifts depending on the coverage were studied on the Si(100)(2X1) and Si(111)(7X7) surfaces, and it was shown that the behavior of the adsorption of K atoms on two surfaces are very different.

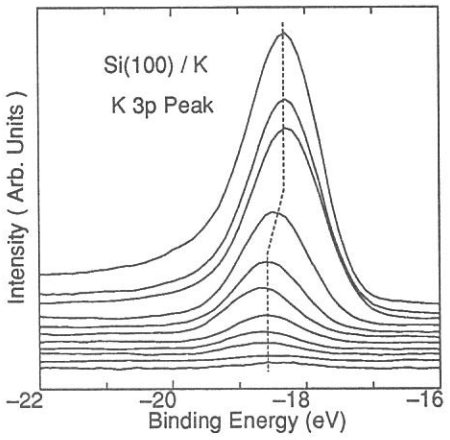

Fig. 1

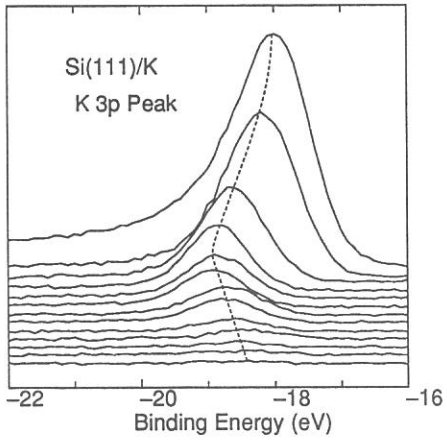

Fig. 2

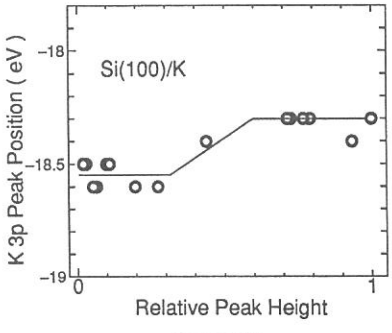

Fig. 3

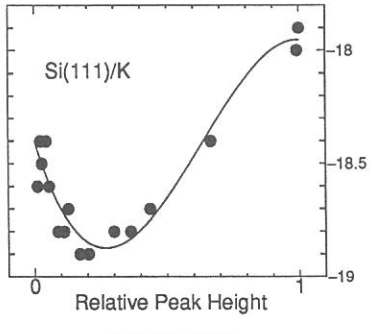

Fig. 4

Krypton *L*-Absorption and Xenon *M*-absorption Spectra in Gas and Solid Phases

Atsunari HIRAYA and Makoto WATANABE

Institute for Molecular Science, Myodaiji, Okazaki 444

Krypton *L*-absorption and xenon *M*-absorption spectra were measured in both gas and solid phases. Measurements were carried out at BL1A equipped with a focusing pre-mirror and a double crystal monochromator. Pairs of beryl crystals and W/B_4C multilayers were used as the dispersing elements. Solid samples were deposited on an Al foil (0.8 μm) supported at the cold end of a He cryostat. For the measurements of gaseous samples a gas cell with organic-polymer windows was used.

Figure 1 shows the *L*-absorption spectra of solid and gaseous krypton in 1650 - 2000 eV region. In the gas phase spectrum, peaks of the $L_{1,2,3}$ edges are observed at 1928.4, 1733.9, and 1680.9 eV, respectively. About 12.5 eV above the L_2 and L_3 edges, two peaks are observed (1746.2 and 1693.8 eV). These two peaks may be attributed to the "delayed transition" into resonantly localized continuum *d* states which are caused by the outer shallow minimum in the effective radial potential. In the solid the first peaks of the $L_{1,2,3}$ edges are observed at 1926.0, 1731.7, and 1678.6 eV, respectively. The L_2 and L_3 show almost similar XANES, while the L_1 edge exhibits only one post-edge peak at 1937.0 eV.

Figure 2 shows the *M*-absorption spectra of solid and gaseous xenon in 620 ~ 1280 eV region using W/B_4C multilayers. Higher resolution spectra were also measured above 900 eV using beryl crystals. In the gas phase, the M_1 to M_5 edges are observed at 1147.8, 1001.0, 939.7, 701.4, and 688.5 eV, respectively. In the solid the first peaks of these edges were observed at 1146.9, 1000.1, 938.8, 700.8, and 687.6 eV, respectively. The M_2 and M_3 show almost the similar XANES pattern, while the M_1 shows no or very weak post-edge structure. Although the XANES of the M_4 and M_5 are not resolved into each component, their pattern is different from that of the M_2 and M_3. Details of the XANES of Kr $L_{2,3}$ and Xe $M_{2,3}$ are given in the following report.

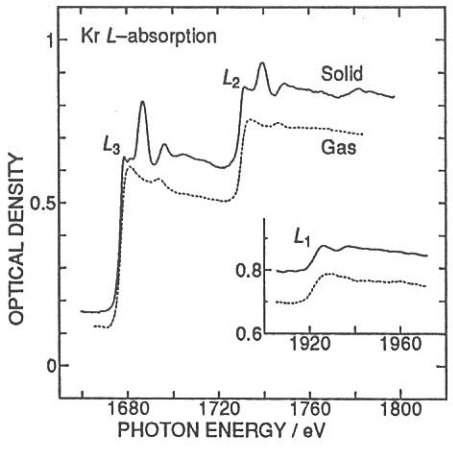

Figure 1. $L_{2,3}$-absorption spectra in gaseous and solid krypton. Inset shows the L_1 region in the same scale as for the $L_{2,3}$ region.

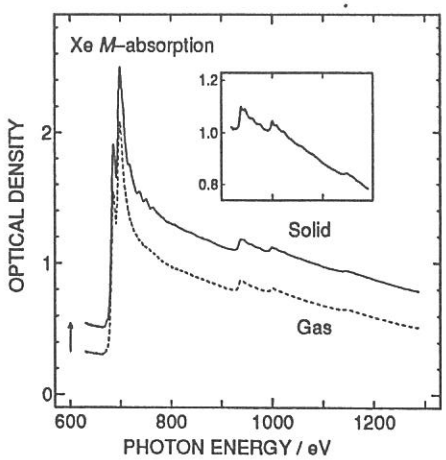

Figure 2. *M*-absorption spectra in gaseous and solid xenon. Inset shows the higher resolution spectrum in solid. The curve for solid is raised by 0.2.

Polarized Reflection Spectra of Quasi-One-Dimensional Halogen-Bridged Bi-nuclear Platinum Complexes.

Yoshiki Wada, *Masahiro Yamashita, and **Koshiro Toriumi

National institute for Research in Inorganic Material.
*College of General Education, Nagoya University.
**Faculty of Science, Himeji Institute for Technology.

Halogen-bridged bi-nuclear platinum complexes have linear-chain structures of bi-nuclear platinum ions and halogen ions (X=Cl, Br, and I) as X^{-}-Pt^{3+}-Pt^{3+}-X^{-}--Pt^{2+}-Pt^{2+}--X^{-}-Pt^{3+}-Pt^{3+}-X^{-}--Pt^{2+}-Pt^{2+}[1]. These complexes also have one-dimensional electron systems which consist of electrons in δ^* (d_z2-d_z2) orbitals of Pt-Pt ions. In order to elucidate the electronic structures of the ground and the photo-excited states of the complexes, polarized reflection spectra of $(NH_4)_4[Pt_2(pop)_4][Pt_2(pop)_4Cl_2]$ have been measured in the wavelength range from near IR to VUV.

Polarized Reflection spectra of $(NH_4)_4[Pt_2(pop)_4][Pt_2(pop)_4Cl_2]$ parallel (solid line) and perpendicular (broken line) to the chain axis at room temperature are shown in Fig. 1. Structures indicated by A, B, and C are polarized parallel to the chain axis. Structures indicated by D, E and F are polarized perpendicular to the chain axis. Structures are also seen in both polarizations in the energy range 8 eV - 15 eV. However, the polarization of these structures are not clear.

The structures A, B, and C may be assigned to the CT-excitation from a Pt^{2+}-Pt^{2+} ion to the neighboring Pt^{3+}-Pt^{3+} ions, an intramolecular electron excitation from the δ^* orbital of a Pt^{2+}-Pt^{2+} ion to a higher energy state of the same ion, the CT-excitation from the p_z orbital of a Cl^{-} ion to the δ^* orbital of the neighboring Pt-Pt ion, respectively. Considering the polarizations and the energy positions, D and E may be due to the CT-excitations from ligand phosphorus atoms to $d_{x^2-y^2}$ orbitals of Pt^{2+}-Pt^{2+} and Pt^{3+}-Pt^{3+} ions.

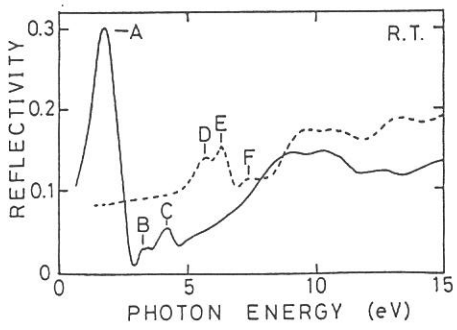

Fig 1. Reflection Spectra of $(NH_4)_4[Pt_2(pop)_4][Pt_2(pop)_4Cl_2]$

1) M.Yamashita and K.Toriumi, Inorg.Chimi.Acta, 178, 143(1990).

OXYGEN DEFICIENT DEFECTS IN SYNTHETIC SILICA GLASSES IDENTIFIED WITH VACUUM ULTRAVIOLET ABSORPTION

Hiroshi KAWAZOE, Shigetoshi HAYASHI* and Tadahisa ARAHORI*

Research Laboratory of Engineering Materials,
Tokyo Institute of Technology
Nagatsuta, Midori-ku, Yokohama 227
*Fine Ceramics Research Laboratory, Advanced Technology
Research Laboratories, Sumitomo Metal Industries, Ltd.,
Sunayama, Hasaki, Kashima-gun, Ibaraki 314-02

Formation mechanisms of oxygen deficient defects in the silica glasses under a sintering process of a porous soot rod prepared by VAD method were studied by using vacuum ultrviolet absorption. Effects of the pre-sintering at 1250 ℃ under vacuum (3×10^{-3}, 0.1 or 2 Pa) prior to the full sintering at 1500℃ on the defect-formation were examined. The absorption spectra were measured with a Seya-Namioka type spectrometer attatched to the syncrotron orbital radiation fascility installed in Institute for Molecular Science, Okazaki.

Figure 1 shows VUV absorption spectra for the silica glasses pre-sintered at 1250℃ for 24h under the reduced pressures specified in the figure. A lower pressure enhances the formation of 7.6eV optical absorption band. At 2.0 Pa no absorption band was detected. The sample prepared without the pre-sintering also showed no induced optical absorption in this wavelength region. A longer pre-sintering time accelerated the formation of the optical absorption band. The band has been assigned to ≡Si-Si≡ structure. It is concluded that the pre-sinterig of VAD porous rods under vacuum enhances formation of ≡Si-Si≡ type defects.

Figure 2 shows the relation between the absorption intensities of the 7.6eV band induced in the differently pre-sintered glasses and the evaporated Cl concentrations of the respective samples. A single straight line passing through the origin was obtained. This means the evaporation of Cl is the cause of the formation of the defect, ≡Si-Si≡, under the vacuum presintering.

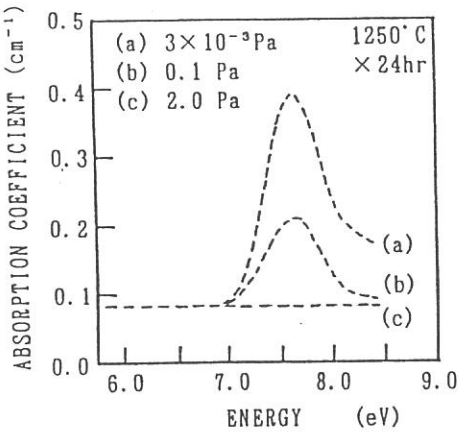

Fig.1 Absorption spectra of silica glasses calcined and sintered under a reduced pressure.

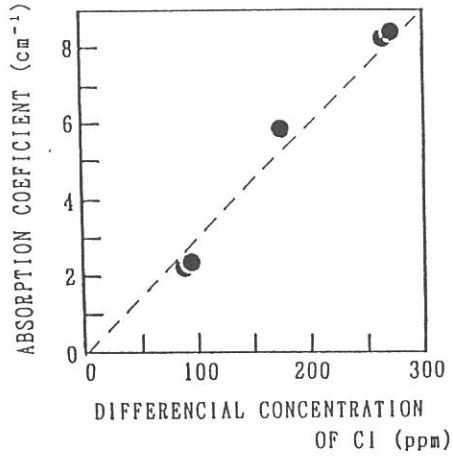

Fig.2 The relationship between decrease of chlorine and the absorption coefficient at 7.6eV.

APPENDIX

ORGANIZATION

Staff

Director

Katsumi	KIMURA	Professor

Scientific Staff

Light Source

Goro	ISOYAMA	Associate Professor
Hiroyuki	HAMA	Research Associate
Shiro	TAKANO	Research Associate

Beam Line

Makoto	WATANABE	Associate Professor
Masao	KAMADA	Associate Professor
Atsunari	HIRAYA	Research Associate
Shin-ichiro	TANAKA	Research Associate

Technical Staff

Kusuo	SAKAI	Section Chief Engineer
Osamu	MATSUDO	Unit Chief Engineer
Toshio	KINOSHITA	Engineer
Masami	HASUMOTO	Engineer
Jun-ichiro	YAMAZAKI	Engineer
Eiken	NAKAMURA	Engineer

Secretary

Yasuno	YAMAGUCHI	(~ June 1991)
Eiko	ADACHI	(June 1991 ~)

Guest Scientist

Kazuhiko	SEKI	Adjunct Associate Professor from Hiroshima Univ. (~ March 1991)
Eiji	ISHIGURO	Adjunct Associate Professor from Osaka City Univ. (April 1991 ~)
Koichiro	OBA	Visiting Research Fellow from Hamamatsu Photonics (~ March 1991)

Graduate Student

	Sayumi	HIROSE	(April 1991 ~)

Representative of Beam Lines

BL1A	Makoto	WATANABE	UVSOR
BL2A	Kosuke	SHOBATAKE	Dept. VUV Photoscience
BL2B2	Katsumi	KIMURA	Dept. VUV Photoscience
BL3B	Koichiro	MITSUKE	Dept. VUV Photoscience
BL4A	Shinri	SATO	Dept. VUV Photoscience
BL4B	Kosuke	SHOBATAKE	Dept. VUV Photoscience
BL6B	Kyuya	YAKUSHI	Dept. Molecular Assemblies
BL6A2	Masao	KAMADA	UVSOR
BL8B2	Hiroo	INOKUCHI	IMS
Others	Makoto	WATANABE	UVSOR
	Masao	KAMADA	UVSOR

Steering Committee (April 1990 - March 1992)

Katsumi	KIMURA	IMS Chairman
Jun-ichi	CHIKAWA	Himeji Inst. of Technology
Junji	FUJITA	Nat. Inst. Fusion Science
Masahiro	KOTANI	Gakushuuin Univ.
Kaizo	NAKAMURA	Okayama Univ.
Yukinori	SATO	Tohoku Univ.
Tadamasa	SHIDA	Kyoto Univ.
Shigemasa	SUGA	Osaka Univ.
Eiji	ISHIGURO	Osaka City Univ.
Keitaro	YOSHIHARA	IMS
Kyuya	YAKUSHI	IMS
Kosuke	SHOBATAKE	IMS
Norio	MORITA	IMS
Makoto	WATANABE	IMS
Goro	ISOYAMA	IMS
Masao	KAMADA	IMS

JOINT STUDIES (fiscal year 1991)

Special Project	: 3
Cooperative Research	: 27
Use of Facility	:114
Users' Meeting	: 1
Workshop on Beam Dynamics and Free Electron Lasers	: 1
Users' Time	: 40 Weeks

LIST OF PUBLICATIONS

1) "Feasibility Study for the Observation of Biological Materials in VUV Wavelength Regions. Using Zone Plates Fabricated by Electron and Ion Beam Lithographies"

   Y. Nagai, Y. Nakajima, Y. Watanabe, S. Ogura, K. Uyeda, Y. Shimanuki and H. Kihara

   X-Ray Microscopy, Instrumentation and Biological Applications, ed. by P.C. Cheng and G.J. Jan (Springer-Verlag, Berlin, 1987) p. 263.

2) "Many Body Effects in Ce 3p XAS and Ce 3p XPS of CeO_2"

   A. Bianconi, A. Clozza, T. Murata, T. Matsukawa, T. Miyahara, A. Kotani, S. Nakai and T. Mitsuishi

   Physica B **158** (1989) 389.

3) "Threshold Energy for Photogeneration of Self-Trapped Excitons in SiO_2"

   C. Itoh, K. Tanimura, N. Itoh and M. Itoh

   Phys. Rev. B **39** (1989) 11183.

4) "Negative-Ion Mass Spectrometric Study of Ion-pair Formation in the Vacuum Ultraviolet. III. $SF_6 \rightarrow F^- + SF_5^+$"

   K. Mitsuke, S. Suzuki, T. Imamura and I. Koyano

   J. Chem. Phys. 93 (1990) 8717.

5) "A Simple Cylindrical Retarding Field Energy Analyzer"

   Y. Fujii, E. Ishiguro and T. Kitada

   Jpn. J. Appl. Phys. **29** (1990) 2176.

6) "Electronic Structure of Pc_2Lu and $(PcAlF)_n$ Oriented Thin Films Using Angle Resolved Photoelectron Spectroscopy"

   M.R. Fahy, H. Fujimoto, A.J. Dann, H. Hoshi, H. Inokuchi, Y. Maruyama and M.R. Willis

   Physica Scripta **41** (1990) 550.

7) "Spectroscopic and Photoelectron-Spectroscopic Studies on Condensed Matters by Using Extreme Ultraviolet Radiation from Synchrotron"

M. Kamada

Proc. 2nd Int. Symp. on Advance Nuclear Energy Research, 1990, p. 575.

8) "Vacuum UV Microscope with Free-Standing Zone Plates at UVSOR"

H. Kihara, Y. Shimanuki, K. Kawasaki, N. Watanabe, M. Taniguchi, H. Tsuruta, Y. Nagai, Y. Watanabe and S. Ogura

X-Ray Microscopy in Biology and Medicine, ed. by K. Shinohara et. al. (Japan Sci. Soc. Press, Tokyo, 1990) p. 143.

9) "Direct Absorption Spectra of S_2 and S_3 States of Benzene Clusters"

A. Hiraya and K. Shobatake

Chem. Phys. Lett. **178** (1991) 543.

10) "Photoemission Study of an Al-Cu-Fe Icosahedral Phase"

M. Mori, S. Matsuo, T. Ishimasa, T. Matsuura, K. Kamiya, H. Inokuchi and T. Matsukawa

J. Phys. : Condens. Matter **3** (1991) 767.

11) "Photoionization Processes in Nonpolar Media : Density Effect"

K. Nakagawa

Radiat. Phys. Chem. **37** (1991) 643.

12) "Relaxed Configuration of Self-Trapped Excitons in $Na_{1-x}K_xI$ and $K_{1-x}Rb_xI$ Mixed Crystals"

M. Itoh, S. Hashimoto and N. Ohno

J. Lumin. **48 & 49** (1991) 121.

13) "Luminescence from Surface CN^- Centers Created Photochemically on Alkali Halide Crystals"

H. Nakagawa, A. Fukumoto, A. Ohnishi, K. Fukui, H. Matsumoto, M. Fujita, T. Miyanaga and M. Watanabe

J. Lumin. **48 & 49** (1991) 811.

14) "Surface Core Exciton in LiCl Studied by Photoelectron Spectroscopy"

K. Ichikawa, O. Aita, M. Kamada and K. Tsutsumi

Phys. Rev. B **43** (1991) 5063.

15) "Three Types of Emission Bands from Hetero-Nuclear Relaxed Excitons in NaBr:I, KBr:I and RbBr:I"

K. Kan'no, K. Tanaka, H. Kosaka and Y. Nakai

J. Lumin. **48 & 49** (1991) 147.

16) "Luminescence Associated with Self-Trapped Excitons in LiBr"

K. Fujiwara, S. Nagata, H. Nishimura, M. Nakayama, T. Komatsu and S. Hashimoto

J. Lumin. **48 & 49** (1991) 107.

17) "Dissociative Single, Double, and Triple Photoionization of Silicon Tetrafluoride in the Valence Shell and Silicon 2p Regions (hν = 33-133 eV)"

T. Imamura, C.E. Brion, I. Koyano, T. Ibuki and T. Masuoka

J. Chem. Phys. **94** (1991) 4936.

18) "K-Absorption Spectrum of Solid Neon"

A. Hiraya, K. Fukui, P. Tseng, T. Murata and M. Watanabe

J. Phys. Soc. Jpn. **60** (1991) 1824.

19) "Dissociative Single, Bouble, and Triple Photoionization of OCS in the Region hν = 20 - 100 eV Studied by Mass Spectrometry and the Photoion-Photoion Coincidence Method"

T. Masuoka and I. Koyano

J. Chem. Phys. **95** (1991) 909.

20) "On the Common Feature of the Optical Reflectivity in Rare-Earth Monopnictides Due to 5d Electron Screening"

Y.S. Kwon, M. Takeshige, O. Nakamura, T. Suzuki and T. Kasuya

Physica B **171** (1991) 316.

21) "Dissociative Single and Double Photoionization of CH_3F in the Region 20 - 110 eV Studied by Mass Spectrometry and the Photoion-Photoion Coincidence Method"

T. Masuoka and I. Koyano

J. Chem. Phys. **95** (1991) 1619.

22) "Fine Structures of Cd^{2+} 4d Core Excitons in $CdCl_2$-$CdBr_2$ Mixed Crystals and CdI_2 Crystal"

M. Fujita, H. Nakagawa, N. Kitagata, H. Matsumoto, T. Miyanaga, K. Fukui and M. Watanabe

J. Phys. Soc. Jpn. **60** (1991) 1792.

23) "Direct Absorption Spectra of Jet-Cooled Benzene in 130-260 nm"

A. Hiraya and K. Shobatake

J. Chem Phys. **94** (1991) 7700.

24) "Performance of the Charge-Coupled Device for Direct X-Ray Detection in the Energy Range of 1-9 keV at the Synchrotron Radiation Facility"

H. Tsunemi, S. Kawai and K. Hayashida

Jpn. J. Appl. Phys. **30** (1991) 1299.

25) "Negative-Ion Mass Spectrometric Study of Ion-Pair Formation in the Vacuum Ultraviolet. IV. $CH_4 \rightarrow H^- + CH_3^+$ and $CD_4 \rightarrow D^- + CD_3^+$"

K. Mitsuke, S. Suzuki, T. Imamura and I. Koyano

J. Chem. Phys. **94** (1991) 6003.

26) "Negative-Ion Mass Spectrometric Study of Ion-Pair Formation in the Vacuum Ultraviolet. V. $CF_4 \rightarrow F^- + CF_3^+$"

K. Mitsuke, S. Suzuki, T. Imamura and I. Koyano

J. Chem. Phys. 95 (1991) 2398.

27) "Far-Infrared Optical Constants of Liquid Acetonitrile at 238 to 343 K as Measured with a Synchrotron Radiation Source"

T. Ohba and S. Ikawa

Mol. Phys. **73** (1991) 985.

28) "Present Status of the UVSOR Light Source"

G. Isoyama

Nucl. Instr. & Meth. in Physics Research **A308** (1991) 31.

29) "Carbon K-Shell X-Ray Absorption Near-Edge Structure of Solid Co_{60}"

H. Shinohara, H. Sato, Y. Saito, K. Tohji and Y. Udagawa

Jpn. J. Appl. Phys. **30** (1991) L848.

30) "Carbon K-Edge X-Ray Absorption Near-Edge Structures of Solid C_{70}"

H. Shinohara, H. Sato, Y. Saito, K. Tohji, I. Matsuoka and Y. Udagawa

Chem. Phys. Lett. **183** (1991) 145.

31) "Anisotropic Angular Distribution of Fragment Ions in Dissociative Double Photoionization of OCS"

T. Masuoka, I. Koyano and N. Saito

Phys. Rev. A **44** (1991) 4309.

32) "Dissociative Photoionization of $Al_2(CH_3)_6$ and $Al_2(CH_3)_3Cl_3$ in the Range 40-100 eV"

S. Nagaoka, I. Koyano, T. Imamura and T. Masuoka

Appl. Organomet. Chem. **5** (1991) 269.

33) "Angle-Resolved Photoemission and Inverse Photoemission Studies of $Bi_2Sr_2Ca_{1-x}Y_xCu_2O_8$ (x=0, 0.4, 0.6)"

T. Takahashi, T. Watanabe, T. Kusunoki and H. Katayama-Yoshida

J. Phys. Chem. Solids **52** (1991) 1427.

34) "Self-Trapped Exciton Luminescence in Dilated NaI Crystals - Relaxation Process of Excitons in Alkali Halides -"

M. Itoh, S. Hashimoto and N. Ohno

J. Phys. Soc. Jpn. **60** (1991) 4357.

35) "Photon-Stimulated Desorption of Excited-State Alkali Atoms from Alkali Halides Irradiated with Undulator Radiation"

S. Hirose and M. Kamada

J. Phys. Soc. Jpn. **60** (1991) 4374.

36) "Polarized Reflection Spectra of Orthorhombic $PbCl_2$ and $PbBr_2$"

M. Fujita, H. Nakagawa, K. Fukui, H. Matsumoto, T. Miyanaga and M. Watanabe

J. Phys. Soc. Jpn. **60** (1991) 4393.

37) "Ge and Ge-L X-Ray Absorption Spectra in Some Semiconductors"

S. Naoe, K. Fukui, T. Matsukawa and T. Murata

Proc. of the 6th Int. Conf. on Xray Absorption Fine Structure, York 1990, ed. by S. Hasnain (EllisHorwood, 1991) p. 337.

38) "Structural Imperfections in Silicon Dioxide Films Identified with Vacuum Ultraviolet Optical Absorption Measurements"

K. Awazu, H. Kawazoe, Y. Saito, K. Watanabe and T. Ando

Appl. Phys. Lett. **59** (1991) 528.

39) "Characterization of Silica Glasses Sintered under Cl_2 Ambients"

K. Awazu, H. Kawazoe, K. Muta, T. Ibuki, K. Tabayashi and K. Shobatake

J. Appl. Phys. **69** (1991) 1849.

40) "Simultaneous Generation of the 7.6-eV Optical Absorption Band and F_2 Molecule in Fluorine Doped Silica Glass under Annealing"

K. Awazu, H. Kawazoe and K. Muta

J. Appl. Phys. **69** (1991) 4183.

41) "Optical Properties of Oxygen-Deficient Centers in Silica Glasses Fabricated in H_2 or Vacuum Ambient"

K. Awazu, H. Kawazoe and K. Muta

J. Appl. Phys. **70** (1991) 69.

42) "Effects of Oxidation Conditions on the Formation of Paramagnetic Centers at and near the Si/SiO_2 Interface"

K. Awazu, H. Kawazoe, T. Ando and K. Watanabe

J. Appl. Phys. **70** (1991) 2979.

43) "Anisotropy in the Electronic Structure of Polysilanes Investigated by Synchrotron-Radiation Spectroscopy"

H. Tachibana, Y. Kawabata, S. Koshihara, T. Arima, Y. Moritomo and Y. Tokura

Phys. Rev. B **44** (1991) 5487.

44) "UPS of New Type Polyacetylene"

K. Kamiya, H. Inokuchi, M. Oku, S. Hasegawa, C. Tanaka, J. Tanaka and K. Seki

Synth. Met. **41-43** (1991) 155.

45) "High-Tc Superconductor Studied with Synchrotron Radiation"

T. Takahashi

Nucl. Instr. & Methods in Phys. Reserach A303 (1991) 515.

46) "Photoemission Study of Bi System High T_c Superconductor"

T. Takahashi and T. Kusunoki

J. Advanced Science **3** (1991) 91.

47) "Photoemission Study of C_{60} and its Alkali-Metal Compounds"

T. Takahashi, T. Morikawa, S. Sato, H. Katayama-Yoshida, A. Yuyama, K. Seki, H. Fujimoto, S. Hino, S. Hasegawa, K. Kamiya, H. Inokuchi, K. Kikuchi, S. Suzuki, K. Ikemoto and Y. Achiba

Physica C **185-189** (1991) 417.

48) "Angle-Resolved Photoemission Study of $Bi_2Sr_2Ca_{1-x}Y_xCu_2O_8$ (x=0.0, 0.2, 0.4, 0.6) Single Crystals"

T. Kusunoki, T. Takahashi, S. Sato, H. Katayama-Yoshida, K. Kamiya and H. Inokuchi

Physica C **185-189** (1991) 1045.

49) "Local Structures of Metals Dispersed on Coal. 3. Na K-Edge XANES Studies on the Structure of Sodium Gasification Catalyst"

H. Yamashita, S. Yoshida and A. Tomita

Ind. Eng. Chem. Res. **30** (1991) 1651.

50) "Focusing Efficiency and Resolution of a Nickel Phase Zone Plate for Soft X-Rays"
H. Fujisaki, N. Nakagiri, H. Kihara, N. Watanabe and M. Taniguchi
Jpn. J. Appl. Phys. **30** (1991) 2943.

51) "Absorption and Fluorescence Studies of Molecules and Clusters"
K. Shobatake, A. Hiraya, K. Tabayashi and T. Ibuki
Vacuum Ultraviolet Photoionization and Photoemission of Molecules and Clusters, ed. by C.Y. Ng (World Scientific Publishing, Singapore, 1991) p. 503.

52) "Measurements of Far-Infrared Optical Constants of Liquids with a Synchrotron Radiation Source"
Y. Fujita, T. Ohba and S. Ikawa
Can. J. Chem. 69 (1991) 1745.

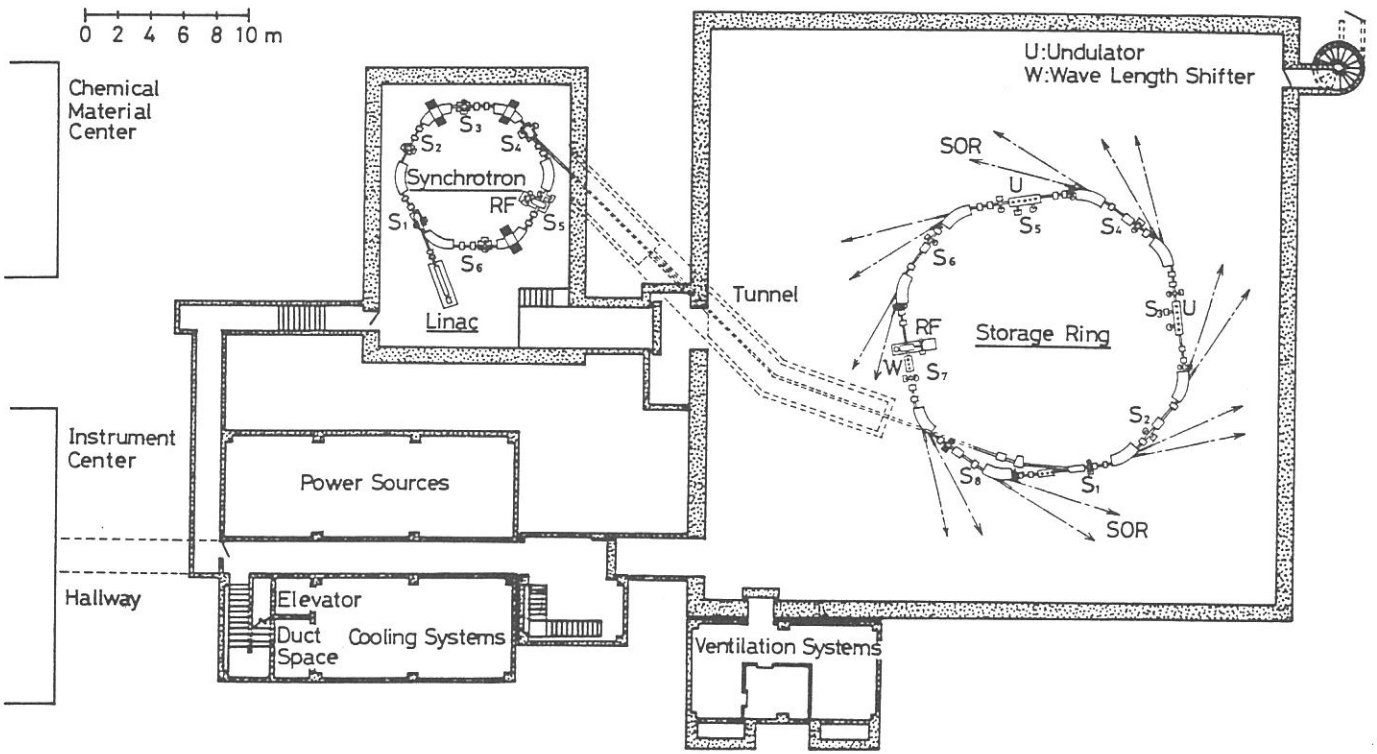

Ground plan of the basement of the UVSOR Facility

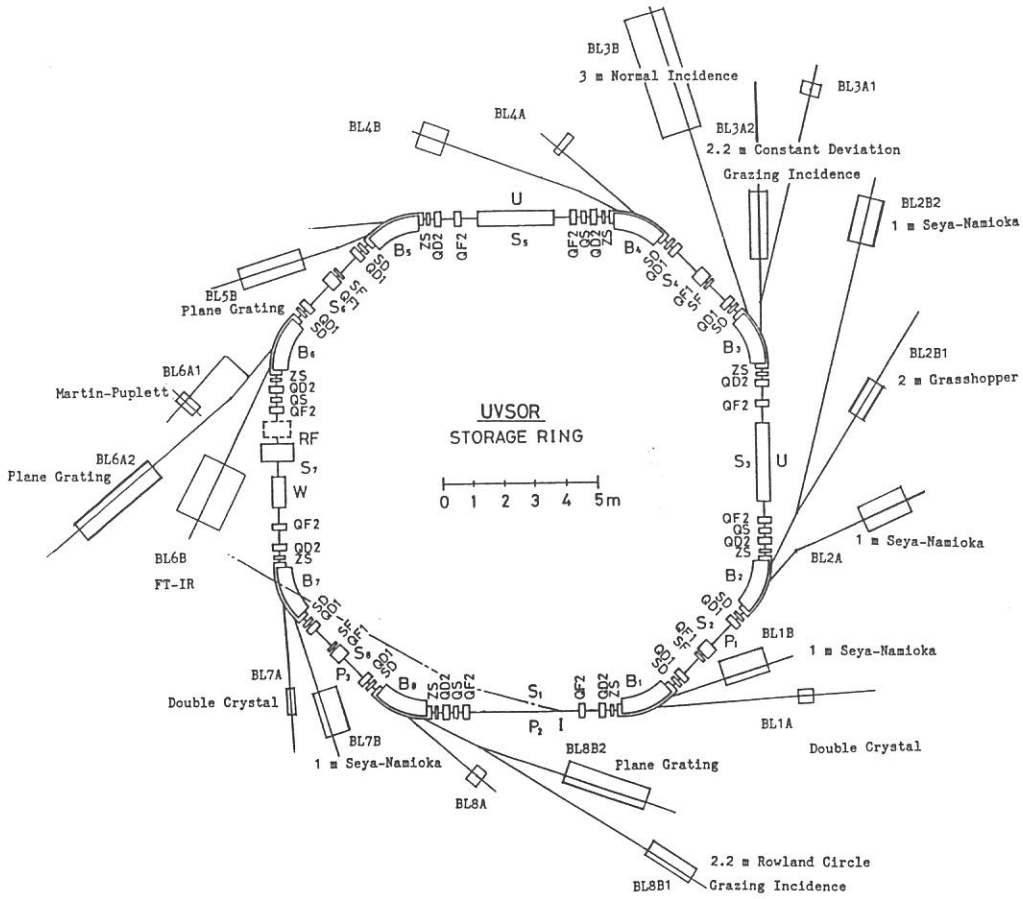

The UVSOR storage ring and the beam lines.

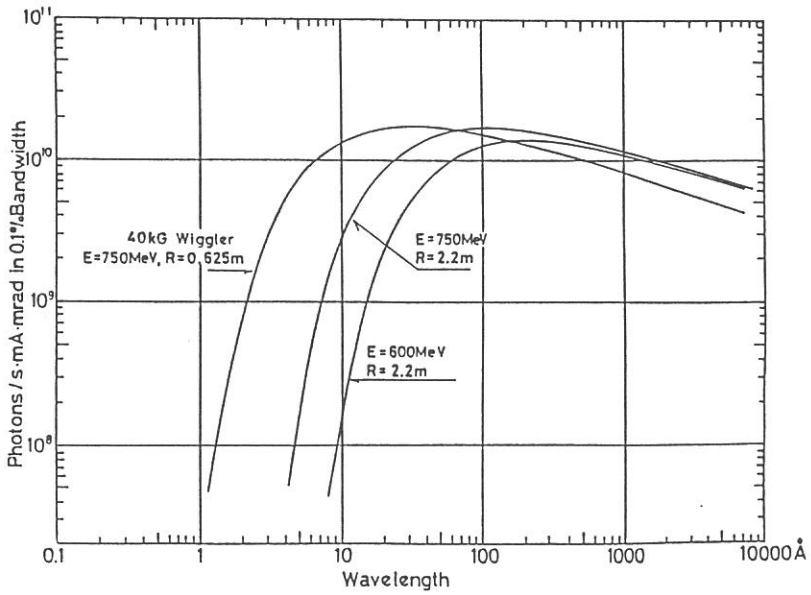

Intensity distribution of the UVSOR radiation.

Table 1. Main Parameters of the UVSOR Accelerator Complex

Linac	
Energy	E = 15 MeV
Frequency	f_{RF} = 2.856 GHz
Synchrotron	
Energy	E = 600 MeV
Beam Current	I = 32 mA
Circumference	C = 26.6 m
Superperiodicity	$N_{superperiodicity}$ = 6
Bending Radius	ρ = 1.8 m
Harmonic Number	h = 8
RF Frequency	f_{RF} = 90.115 MHz
Repetition Rate	f_{rep} = 2.6 Hz
Storage Ring	
Energy	E=750 MeV
Critical Energy of SR	ε_c = 425 eV
Beam Current (Nominal)	
Multi-Bunch	I = 200 mA
Single-Bunch	I = 50 mA
Beam Lifetime	τ = 200 min.at I=200 mA
Circumference	C = 53.2 m
Superperiodicity	$N_{superperiodicity}$ = 4
Bending Radius	ρ = 2.2 m
Betatron Wave numbers	
Horizontal	Q_x = 3.19
Vertical	Q_y = 2.22
Momentum Compaction Factor	α = 0.032
RF Frequency	f_{RF} = 90.115 MHz
RF Voltage	V_{RF} = 50 kV
Natural Emittance	
Horizontal	$\varepsilon_x = 1.15 \times 10^{-7}$ π m rad
Vertical[a)]	$\varepsilon_y = 1.15 \times 10^{-8}$ p m rad
Beam Sizes	
Horizontal	σ_x = 0.39 mm
Vertical[a)]	σ_y = 0.27 mm
Bunch Length	σ_l = 170 psec

a) 10 % coupling is assumed.

Table 2. Beam Lines at UVSOR

Beam Line	Monochromator/ Spectrometer	Wavelength Region		Acceptance Angle (mrad)		Experiment
				Horiz.	Vert.	
BL1A	Double Crystal	15 - 8 A		4	1	Solid
BL1B	1m Seya-Namioka	6500 - 300 A		60	6	Gas & Solid
BL2A	1 m Seya-Namioka	4000 - 300 A		40	6	Gas
BL2B1	2 m Grasshopper	600 - 15 A		10	1.7	Gas & Solid
BL2B2	1 m Seya-Namioka	2000 - 300 A		20	6	Gas
BL3A1	None (Filter, Mirror)		(U)	0.3	0.3	Gas & Solid
BL3A2	2.2m Constant	1000 - 100 A		10	4	Gas & Solid
	Deviation Grazing		(U)	0.3	0.3	
	Incidence					
BL3B	3 m Normal Incidence	4000 - 300 A		20	6	Gas
BL4A	None			6	6	Irradiation
BL4B	None			8.3	6	Irradiation
BL5B	Plane Grating	2000 - 20 A		10	2.2	Calibration#
BL6A1	Martin-Pupplet	5 mm - 50 μm		80	60	Solid
BL6A2	Plane Grating	6500 - 80 A		10	6	Solid
BL6B	FT-IR	200 - 1.7 μm		70	25	Solid
BL7A	Double Crystal	15 - 8 A		2	0.3	Solid
		15 - 2 A	(W)	1	0.15	Solid
BL7B	1 m Seya-Namioka	6500 - 300 A		40	8	Gas & Solid
BL8A	None (Filter)			25	8	Irradiation/
						User's Instr.
BL8B1	2.2 m Rowland Circle	440 - 20 A		10	2	Gas & Solid
	Grazing Incidence					
BL8B2	Plane Grating	6500 - 80 A		10	6	Solid

National Institute for Fusion Science

U: with an undulator, W: with a wiggler

LOCATION

Ultraviolet Synchrotron Orbital Radiation (UVSOR) Facility, Institute for Molecular Science (IMS) is located at Okazaki. Okazaki (population 300,000) is 260 km southwest of Tokyo, and can be reached by train in about 3 hours from Tokyo via New Tokaido Line (Shinkansen) and Meitetsu Line.

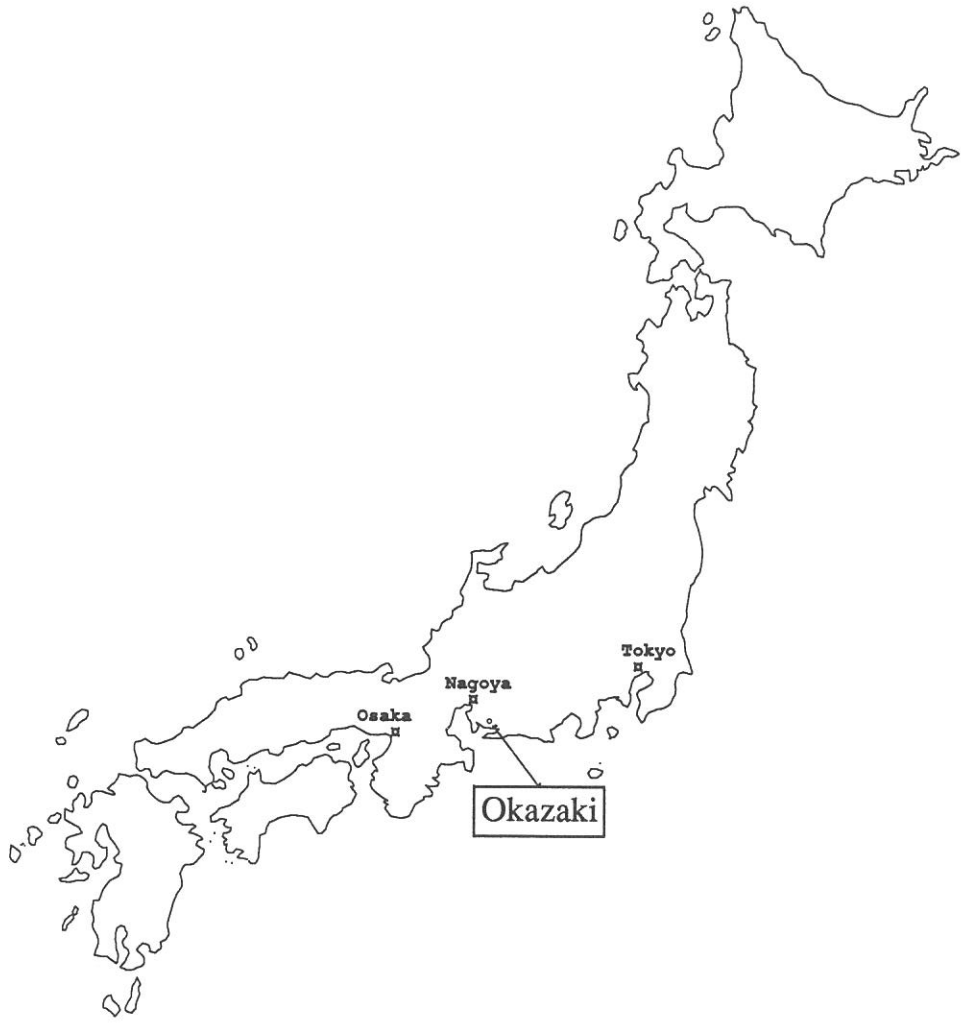

Address
UVSOR Facility, Institute for Molecular Science
Myodaiji, Okazaki 444, JAPAN

Telephone 0564-55-7402 (Secretary, UVSOR)
0564-52-6101 (UVSOR)
Fax 0564-54-7079 (UVSOR)
Telex 4537475 KOKKEN J (IMS)

Editors: H. Hama and G. Isoyama